Supplementary Information (SI) for Organic & Biomolecular Chemistry.
This journal is © The Royal Society of Chemistry 2025

Supporting information

Identification and synthesis of 4'-*ortho*-aminobenzoyl ascarosides as sex pheromones of gonochoristic *Caenorhabditis nigoni*

Célia P. Bergame[a,†], Chuanfu Dong[b,†], Siva Bandi[a], Marie-Désirée Schlemper-Scheidt[a], Sylvain Sutour[c], and Stephan H. von Reuß[a,b,c]*

	Content	Pages
Tab. S1	ESI-HR-MS/MS data of 4'-*ortho*-aminobenzoyl ascarosides	2
Fig. S1a-d	NMR spectra of *C. nigoni* JU1422 RP-C18 fractions	3 – 6
Fig. S2a-c	ESI-(–)-HR-MS/MS spectra of 4'-*ortho*-aminobenzoyl ascarosides	7 – 9
Fig. S3	ESI-(+)-HR-MS/MS spectra of 4'-*ortho*-aminobenzoyl ascarosides	10
Fig. S4a-c	EICs for *m/z* 250.1074 showing homologous AB-ascarosides	11 – 13
Fig. S5	Phylogeny of analyzed *Caenorhabditis* species	14
Fig. S6	^{1}H NMR analysis of isolated AB-asc-C5 (**6a**)	15
Fig. S7a-h	*dqf*-COSY spectra of isolated AB-asc-C5 (**6a**) and AB-asc-C6 (**6b**)	16 – 23
Fig. S8	Comparative HPLC analysis of isolated and synthetic AB-asc-C5 (**6a**)	24
Fig. S9	Comparative ^{1}H NMR analysis of isolated and synthetic AB-asc-C5 (**6a**)	25
Fig. S10	AB-asc-C5 (**6a**) retention assay with *C. nigoni* males	26
Fig. S11	AB-asc-C5 (**6a**) retention assay with *C. nigoni* females	27
Fig. S12	AB-asc-C5 (**6a**) retention assay with *C. tropicalis* hermaphrodites	28
Fig. S13-100	NMR spectra of synthetic and isolated compounds	29 – 115

Table S1a. ESI-(–)-HR-MS/MS data of 4'-*ortho*-aminobenzoyl ascarosides (AB-asc-C#, abas).

	Side chain	**$[M - H]^-$**	**calc *m/z* $[M - H]^-$**	**obs *m/z* $[M - H]^-$**	Δ (ppm)	RT [min]
§abas#5	**C3**	$C_{16}H_{20}NO_7^-$	338.1245	338.1252	-1.9	17.58
abas#11	**C4**	$C_{17}H_{22}NO_7^-$	352.1402	352.1407	-1.3	18.00
abas#9	**C5**	$C_{18}H_{24}NO_7^-$	366.1558	366.1557	0.3	18.73
abas#12	**C6**	$C_{19}H_{26}NO_7^-$	380.1715	380.1708	1.9	19.67
abas#7	**ΔC7**	$C_{20}H_{26}NO_7^-$	392.1715	392.1720	-1.3	20.53
abas#1	**C7**	$C_{20}H_{28}NO_7^-$	394.1871	394.1866	1.4	20.81
abas#13	**ΔC8**	$C_{21}H_{28}NO_7^-$	406.1871	nd		
abas#14	**C8**	$C_{21}H_{30}NO_7^-$	408.2028	408.2033	-1.2	22.14
abas#3	**ΔC9**	$C_{22}H_{30}NO_7^-$	420.2028	420.2025	0.7	22.90
abas#10	**C9**	$C_{22}H_{32}NO_7^-$	422.2184	422.2180	1.1	23.50
abas#15	**ΔC10**	$C_{23}H_{32}NO_7^-$	434.2184	434.2193	-2.0	24.29
abas#16	**C10**	$C_{23}H_{34}NO_7^-$	436.2341	436.2334	1.4	24.98
abas#17	**ΔC11**	$C_{24}H_{34}NO_7^-$	448.2341	448.2351	-2.4	25.79
abas#18	**C11**	$C_{24}H_{36}NO_7^-$	450.2497	450.2493	1.0	26.53
abas#2	**C6-MK**	$C_{19}H_{26}NO_6^-$	364.1766	nd*		
abas#6	**C6-OH**	$C_{19}H_{26}NO_6^-$	366.1922	nd*		

*: *C. nigoni* is devoid of the asc-C6-MK (ascr#2) and asc-C6-OH (ascr#6) building blocks [1].

Table S1b. ESI-(+)-HR-MS/MS data of 4'-*ortho*-aminobenzoyl ascarosides (AB-asc-C#, abas).

	Side chain	**$[M + H]^+$**	**calc *m/z* $[M + H]^+$**	**obs *m/z* $[M + H]^+$**	Δ (ppm)	RT [min]
§abas#5	**C3**	$C_{16}H_{22}NO_7^+$	340.1391	340.1388	-0.9	17.58
abas#11	**C4**	$C_{17}H_{24}NO_7^+$	354.1547	354.1541	-1.6	18.00
abas#9	**C5**	$C_{18}H_{26}NO_7^+$	368.1704	368.1707	0.8	18.73
abas#12	**C6**	$C_{19}H_{28}NO_7^+$	382.1860	382.1866	1.6	19.67
abas#7	**ΔC7**	$C_{20}H_{28}NO_7^+$	394.1860	394.1855	-1.3	20.53
abas#1	**C7**	$C_{20}H_{30}NO_7^+$	396.2017	396.2021	1.0	20.81
abas#13	**ΔC8**	$C_{21}H_{30}NO_7^+$	408.2017	nd		
abas#14	**C8**	$C_{21}H_{32}NO_7^+$	410.2173	410.2178	1.2	22.14
abas#3	**ΔC9**	$C_{22}H_{32}NO_7^+$	422.2173	422.2169	-0.9	22.90
abas#10	**C9**	$C_{22}H_{34}NO_7^+$	424.2330	424.2333	0.7	23.50
abas#15	**ΔC10**	$C_{23}H_{34}NO_7^+$	436.2330	436.2341	2.5	24.29
abas#16	**C10**	$C_{23}H_{36}NO_7^+$	438.2486	438.2482	-0.9	24.98
abas#17	**ΔC11**	$C_{24}H_{36}NO_7^+$	450.2486	450.2489	0.7	25.79
abas#18	**C11**	$C_{24}H_{38}NO_7^+$	452.2643	452.2640	-0.7	26.53
abas#2	**C6-MK**	$C_{19}H_{28}NO_6^+$	366.1911	nd*		
abas#6	**C6-OH**	$C_{19}H_{30}NO_6^+$	368.2068	nd*		

*: *C. nigoni* is devoid of the asc-C6-MK (ascr#2) and asc-C6-OH (ascr#6) building blocks [1].

[1] C. Dong, D. K. Reilly, C. Bergame, F. Dolke, J. Srinivasan, S. H. von Reuß, *J Org Chem*., 2018, **83**, 7109.

Figure S1a: *dqf*-COSY spectrum of *C. nigoni* JU1422 RP-C18 fraction eluted with 70% methanol (400 MHz, in CD_3OD).

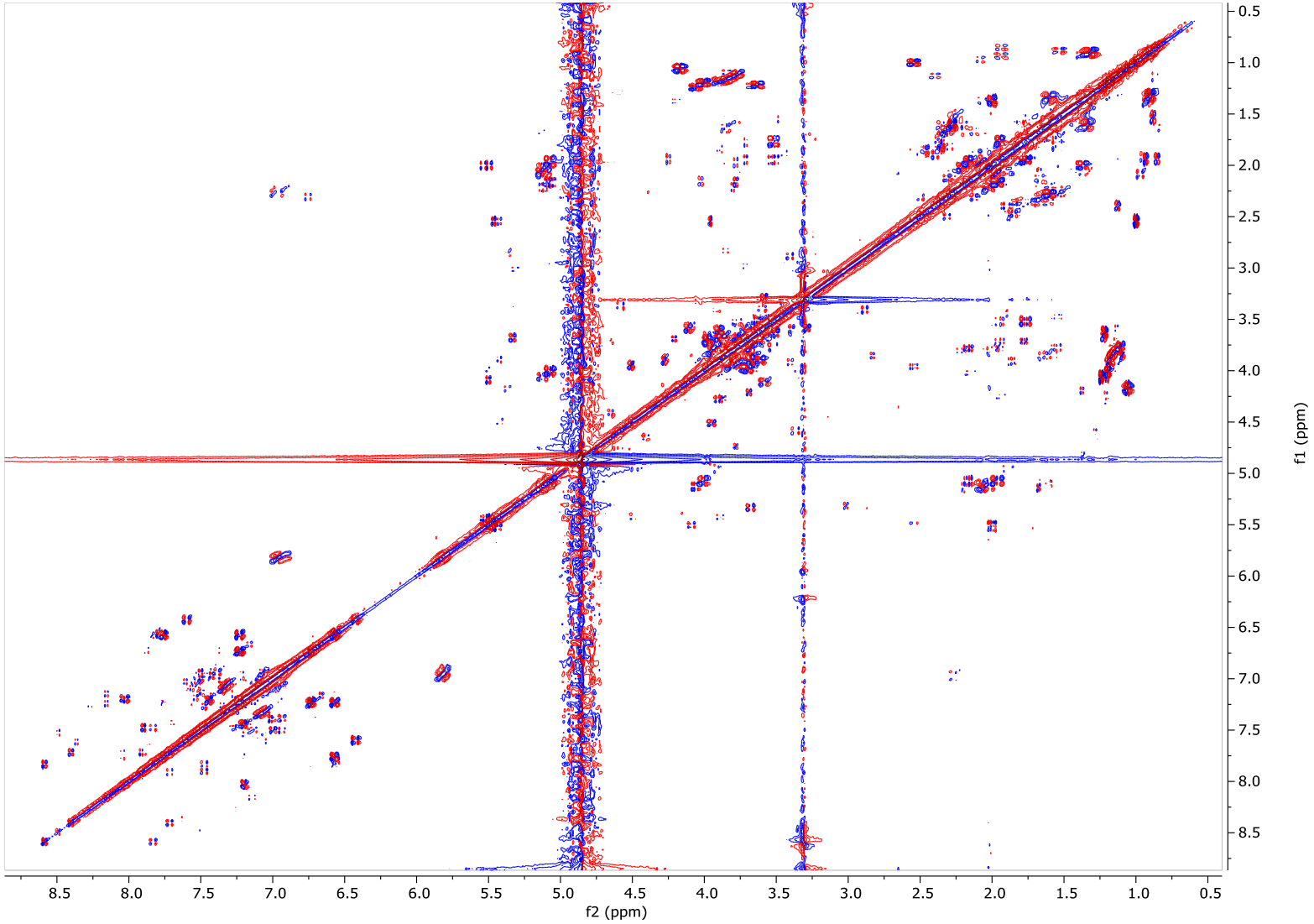

Figure S1b: Section of the *dqf*-COSY spectrum (Figure S1a) of the *C. nigoni* JU1422 RP-C18 fraction eluted with 70% methanol (400 MHz, in CD_3OD) showing signals for basic ascarosides (ascr) and 4'-substituted ascarosides (abas).

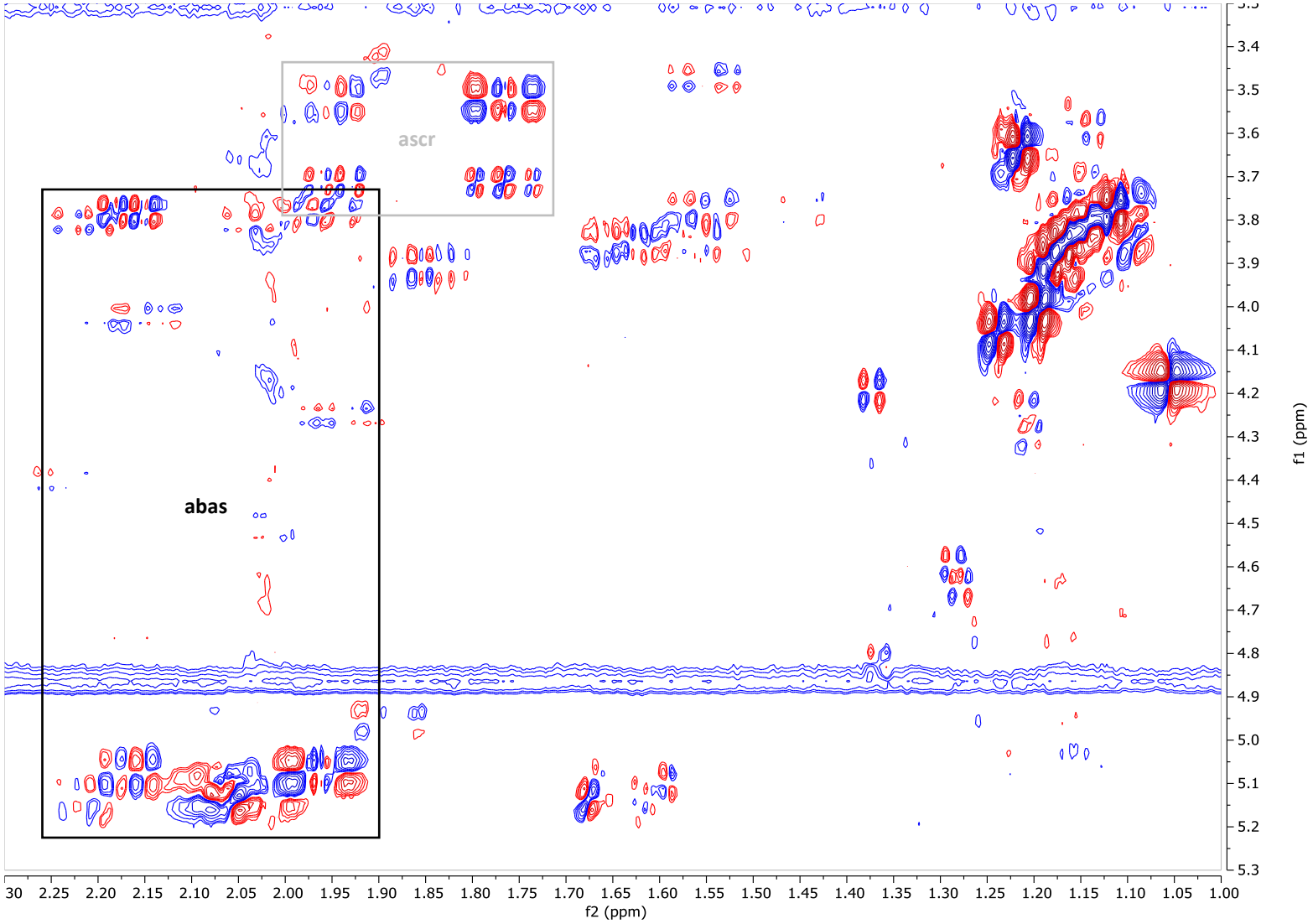

Figure S1c: Section of the *dqf*-COSY spectrum (Figure S1a) of the *C. nigoni* JU1422 RP-C18 fraction eluted with 70% methanol (400 MHz, in CD_3OD) showing signals for basic ascarosides (ascr) and 4'-substituted ascarosides (abas).

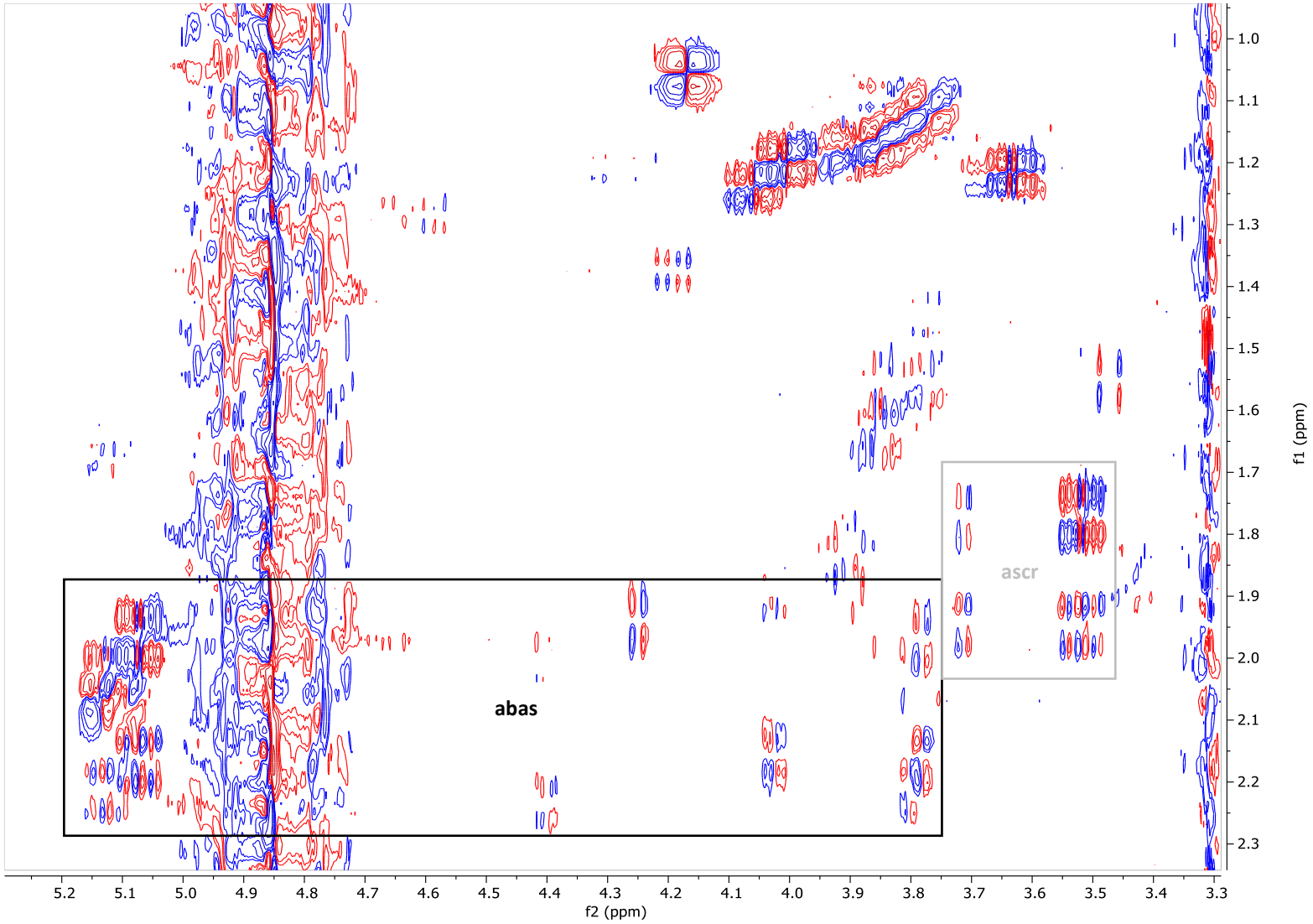

Figure S1d: Section of the *dqf*-COSY spectrum of the *C. nigoni* JU1422 RP-C18 fraction eluted with 70% methanol (400 MHz, in CD_3OD) showing signals for an *ortho*-aminobenzoyl unit.

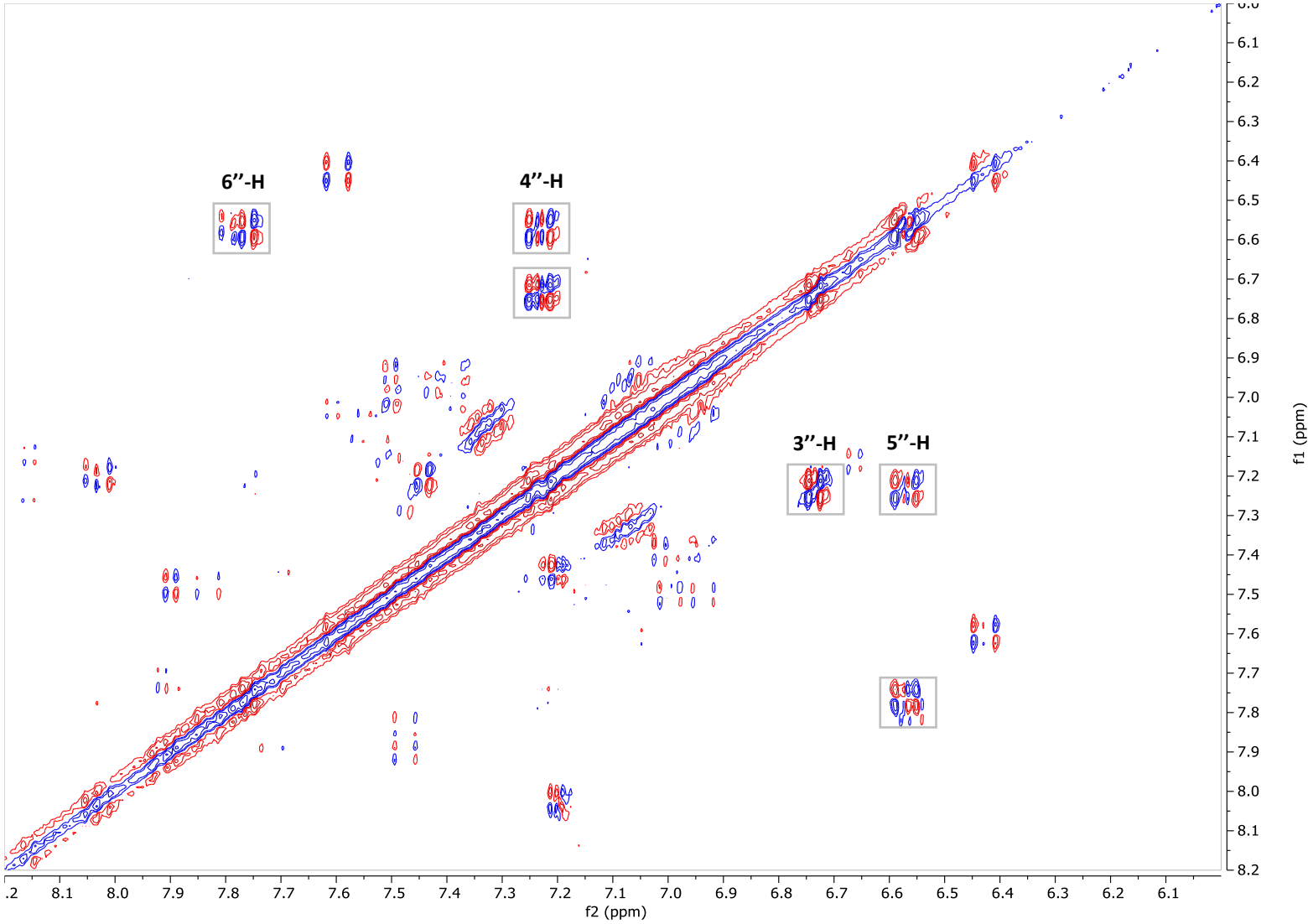

Figure S2a: ESI-(–)-HR-MS/MS spectra of 4'-*ortho*-aminobenzoyl ascarosides (AB-asc-Cx; abas).

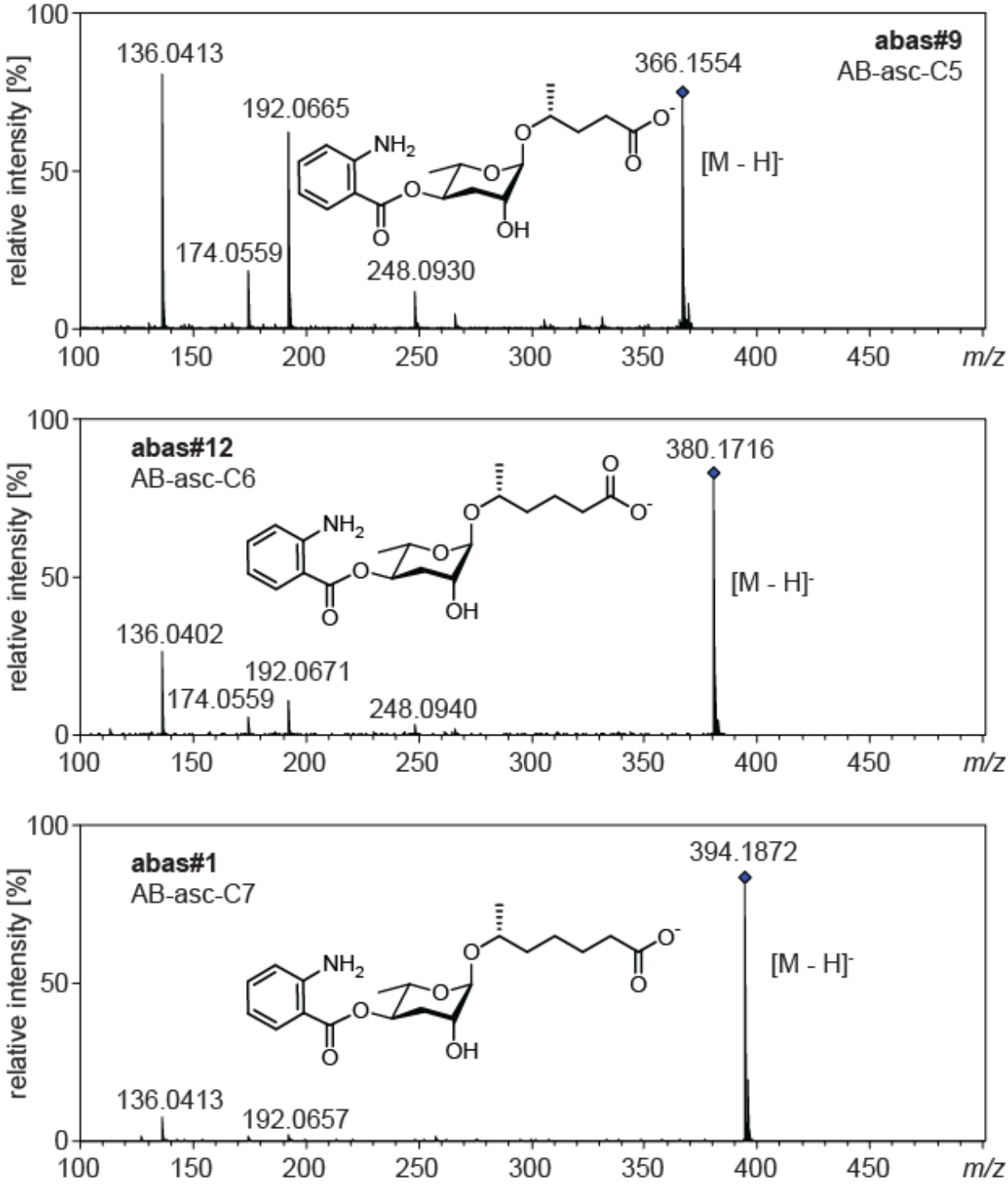

Figure S2b: ESI-(–)-HR-MS/MS spectra of 4'-*ortho*-aminobenzoyl ascarosides (AB-asc-C#; abas).

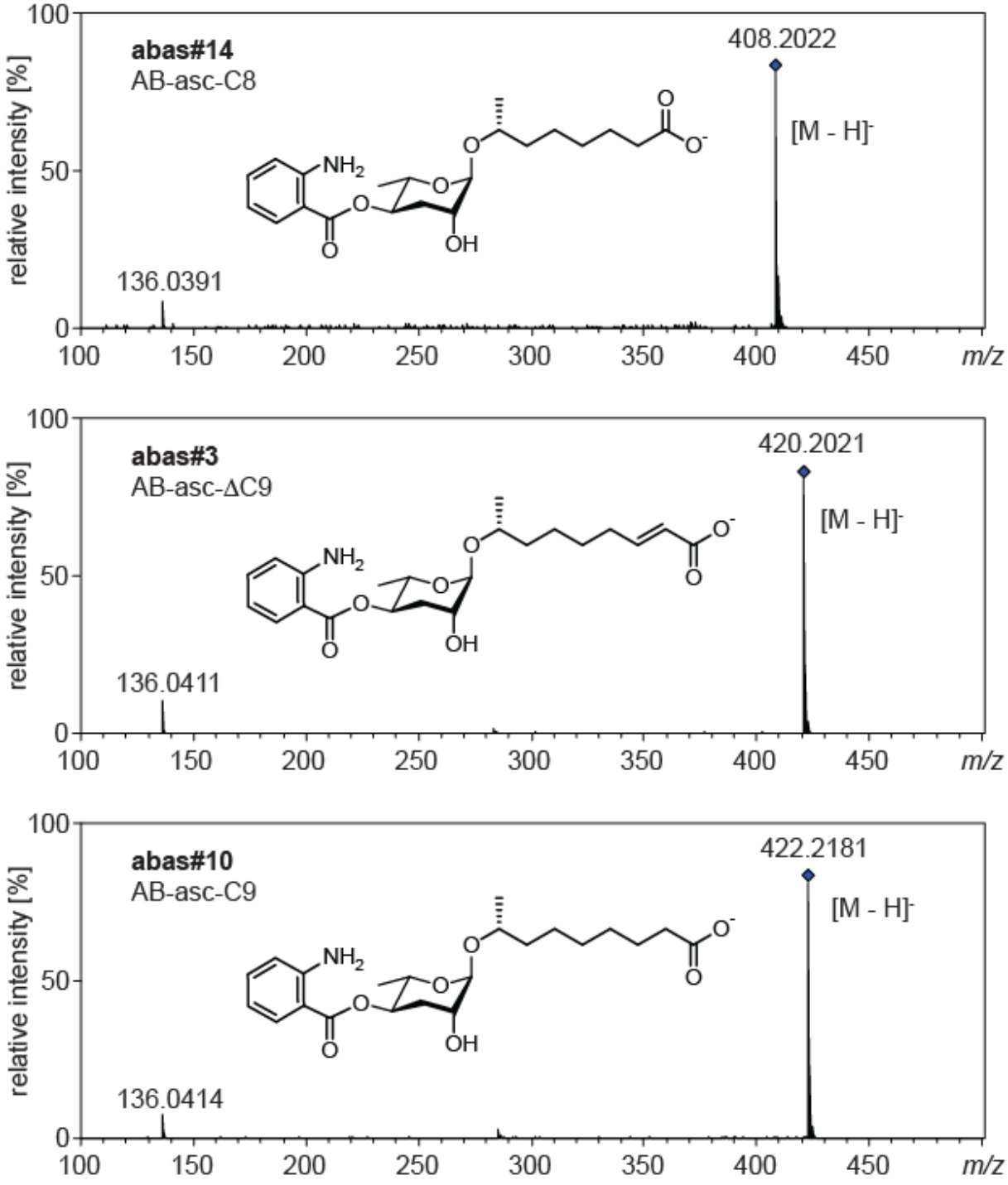

Figure S2c: ESI-(–)-HR-MS/MS spectra of 4'-*ortho*-aminobenzoyl ascarosides (AB-asc-C#; abas).

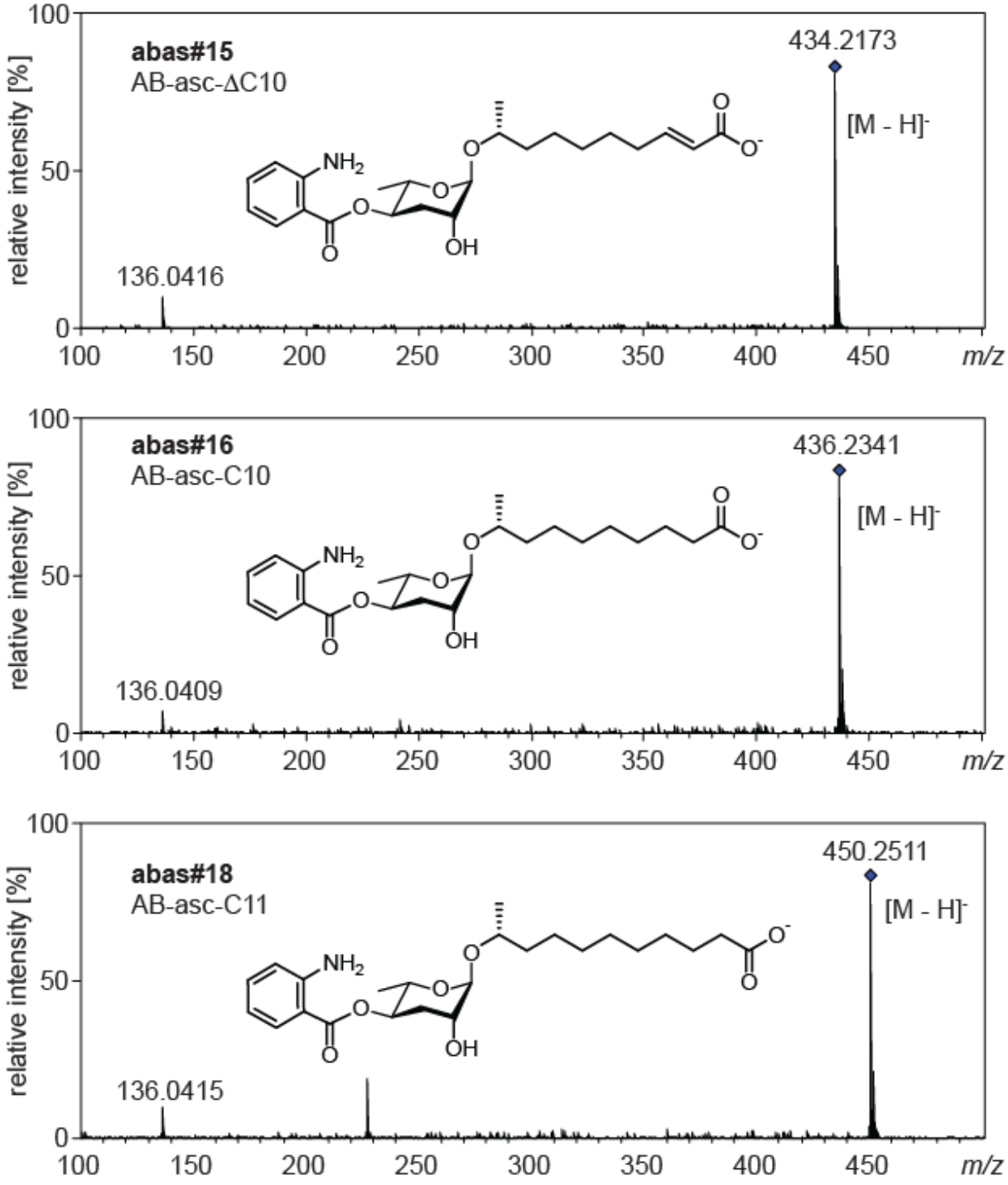

Figure S3: ESI-(+)-HR-MS (top) and MS/MS spectra (bottom) of AB-asc-C5 (**6a**, abas#9).

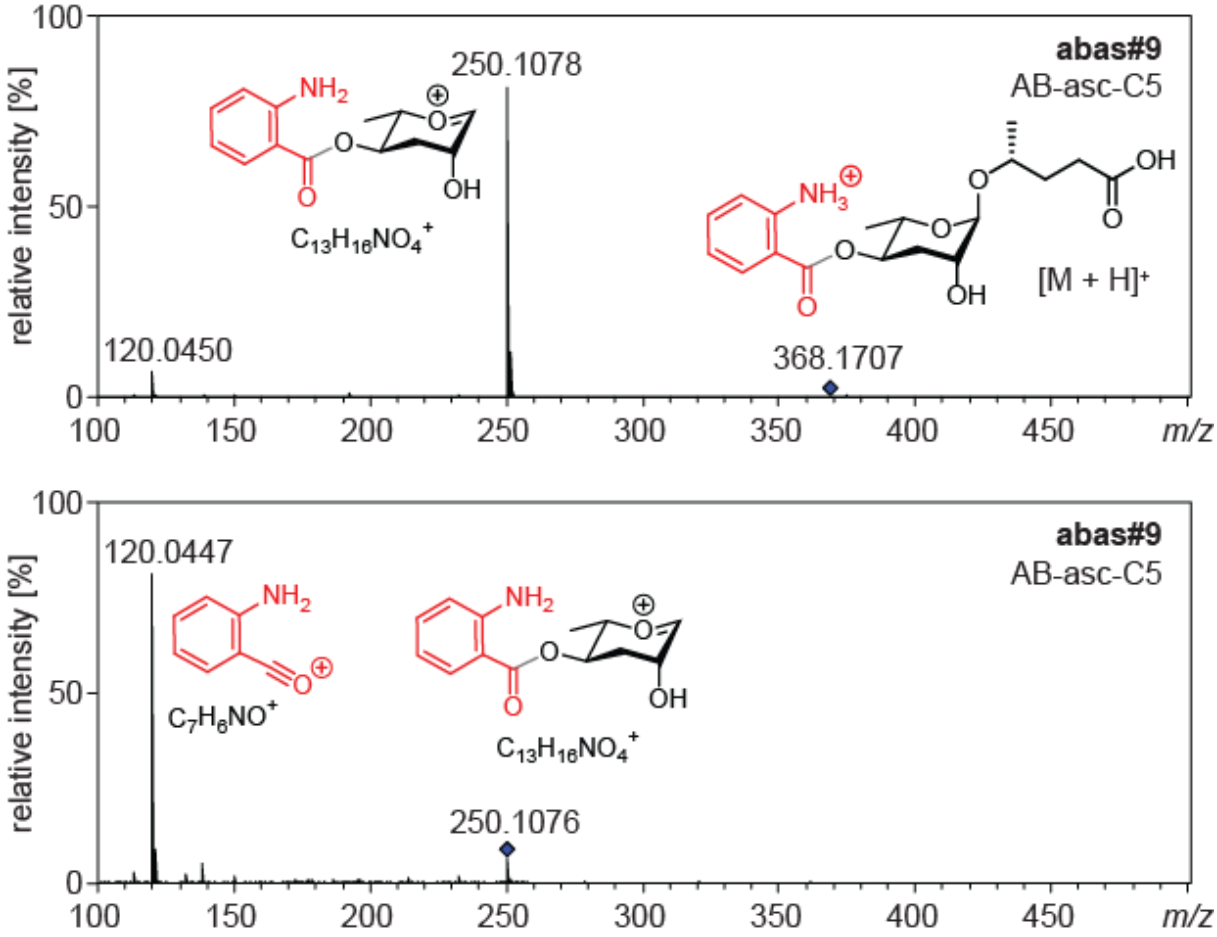

Figure S4a: Extracted ion chromatograms for *m/z* 250.1074 $[C_{13}H_{16}NO_4]^+$ showing homologous 4'-*ortho*-aminobenzoyl ascarosides (AB-asc-Cx, abas). *: 2-Methylthio-n6-isopentenyladenine at *m/z* 250.1121 $[M+H]^+$ for $C_{11}H_{16}N_5S^+$ showing fragments at *m/z* 182.0495 for $C_6H_8N_5S^+$ and 134.0461 for $C_5H_4N_5^+$.

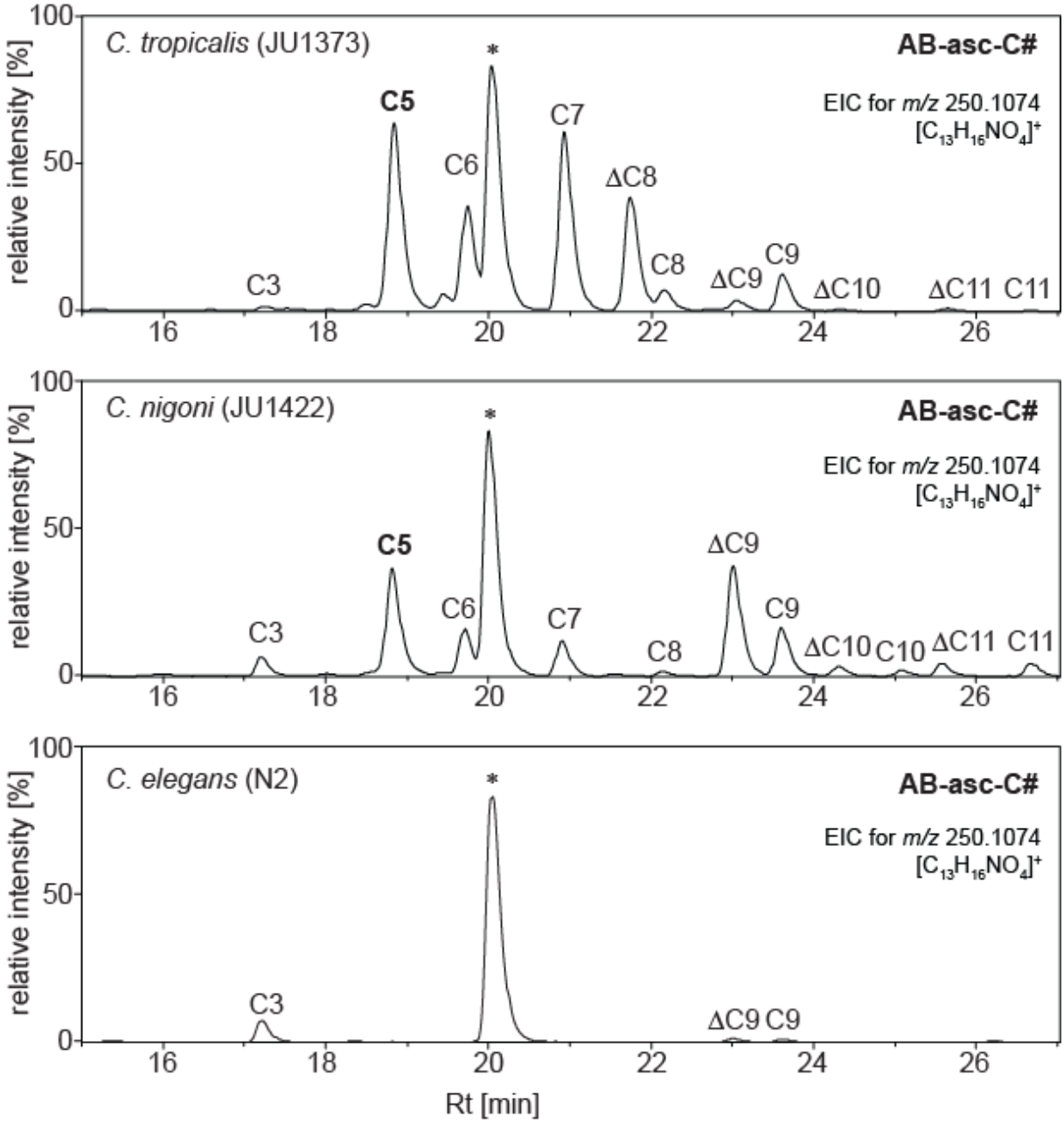

Figure S4b: Extracted ion chromatograms for *m/z* 250.1074 $[C_{13}H_{16}NO_4]^+$ showing homologous 4'-*ortho*-aminobenzoyl ascarosides (AB-asc-Cx, abas). *: 2-Methylthio-n6-isopentenyladenine at *m/z* 250.1121 $[M+H]^+$ for $C_{11}H_{16}N_5S^+$ showing fragments at *m/z* 182.0495 for $C_6H_8N_5S^+$ and 134.0461 for $C_5H_4N_5^+$.

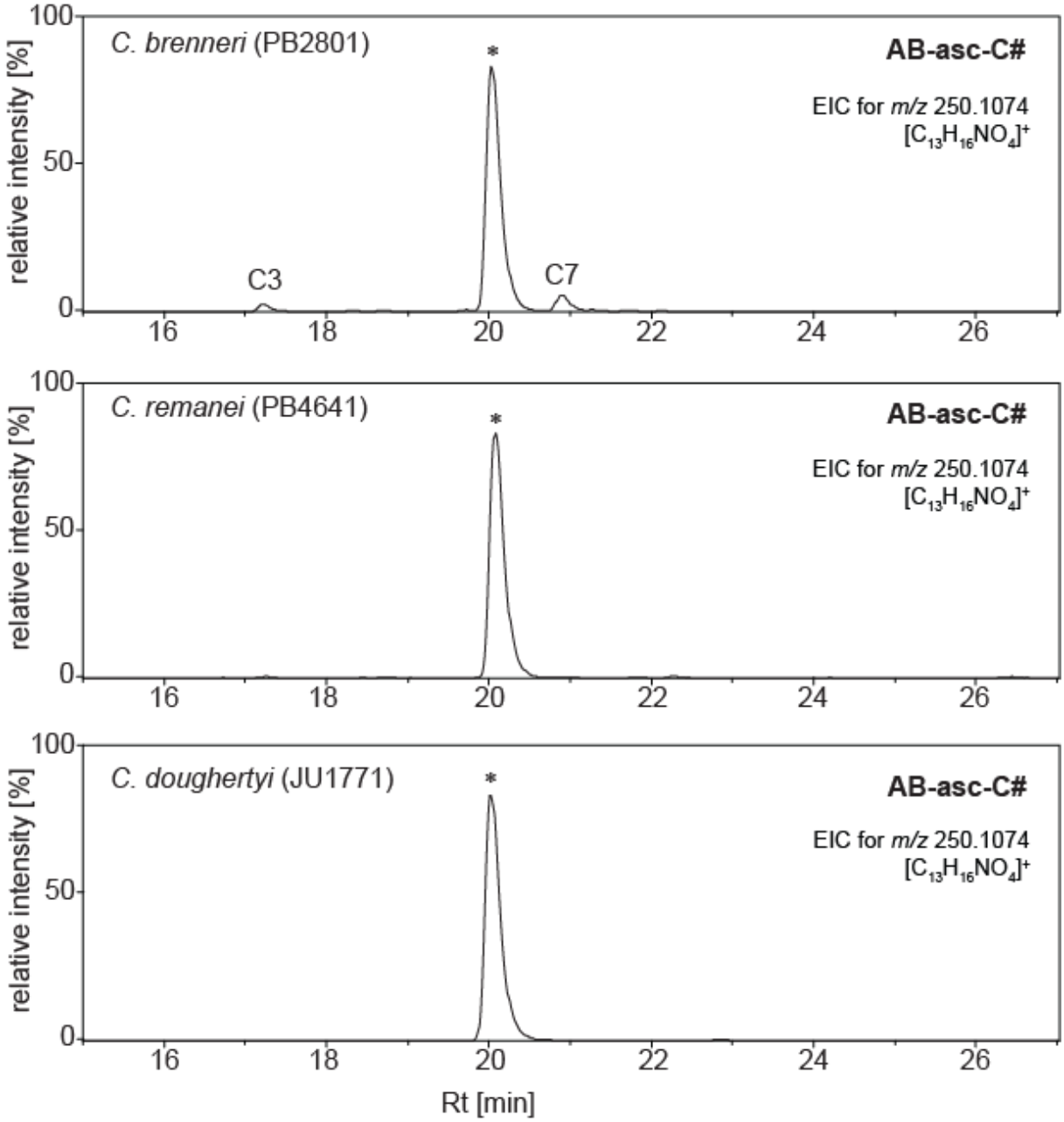

Figure S4c: Extracted ion chromatograms for *m/z* 250.1074 $[C_{13}H_{16}NO_4]^+$ showing homologous 4'-*ortho*-aminobenzoyl ascarosides (AB-asc-Cx, abas). *: 2-Methylthio-n6-isopentenyladenine at *m/z* 250.1121 $[M+H]^+$ for $C_{11}H_{16}N_5S^+$ showing fragments at *m/z* 182.0495 for $C_6H_8N_5S^+$ and 134.0461 for $C_5H_4N_5^+$.

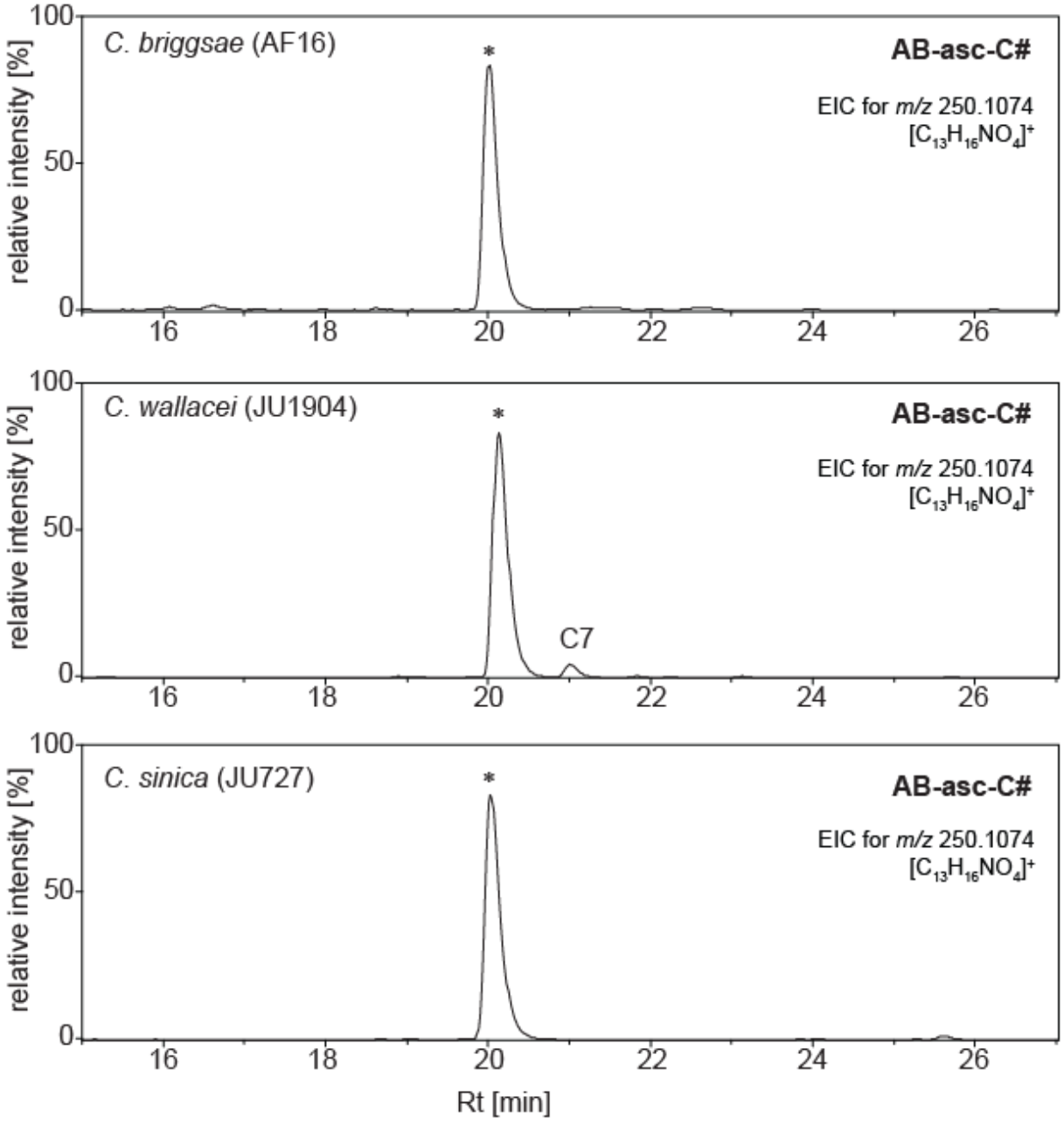

Figure S5: Phylogeny of analyzed *Caenorhabditis* species from the Elegans group [1, 2] and occurrence of homologous 4'-*ortho*-aminobenzoyl ascarosides (AB-asc-Cx, abas) as deduced from extracted ion chromatograms for *m/z* 250.1074 $[C_{13}H_{16}NO_4]^+$; androdioecious species underlined.

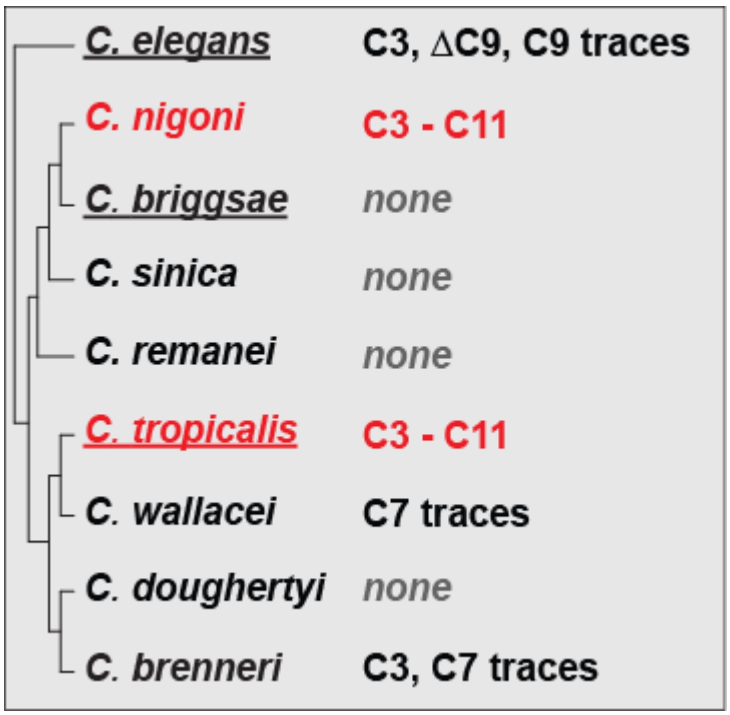

[1] K. C. Kiontke, M. A. Félix, M. Ailion, M. V. Rockman, C. Braendle, J. B. Pénigault, D. H. Fitch, *BMC Evol Biol*., 2011, **11**, 339.
[2] M. A. Félix, C. Braendle, A. D. Cutte, *PLoS One*, 2014, **9**, e94723.

Figure S6: Comparative analysis of ^{1}H NMR spectra showing (a): a mixture of AB-asc-C5 (**6a**) and asc-C11 (**1b**) isolated from *C. nigoni*, (b): AB-asc-C6 (**6b**) isolated from *C. nigoni*, and (c): synthetic asc-C11 (**1b**).

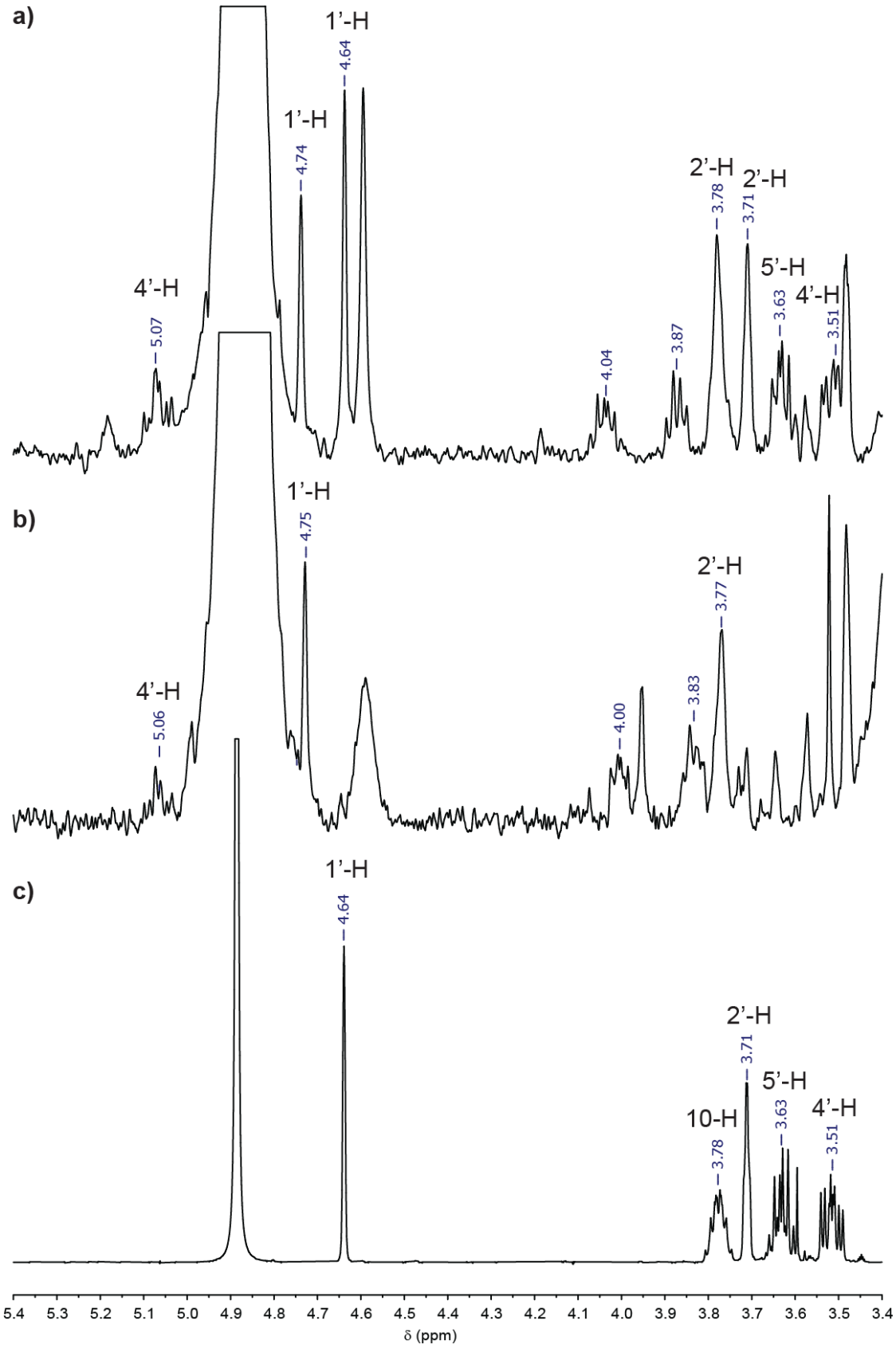

Figure S7a: Section of the *dqf*-COSY spectrum of AB-asc-C5 (**6a**, abas#9) and asc-C11 (**1b**, ascr#18) isolated from *C. nigoni*.

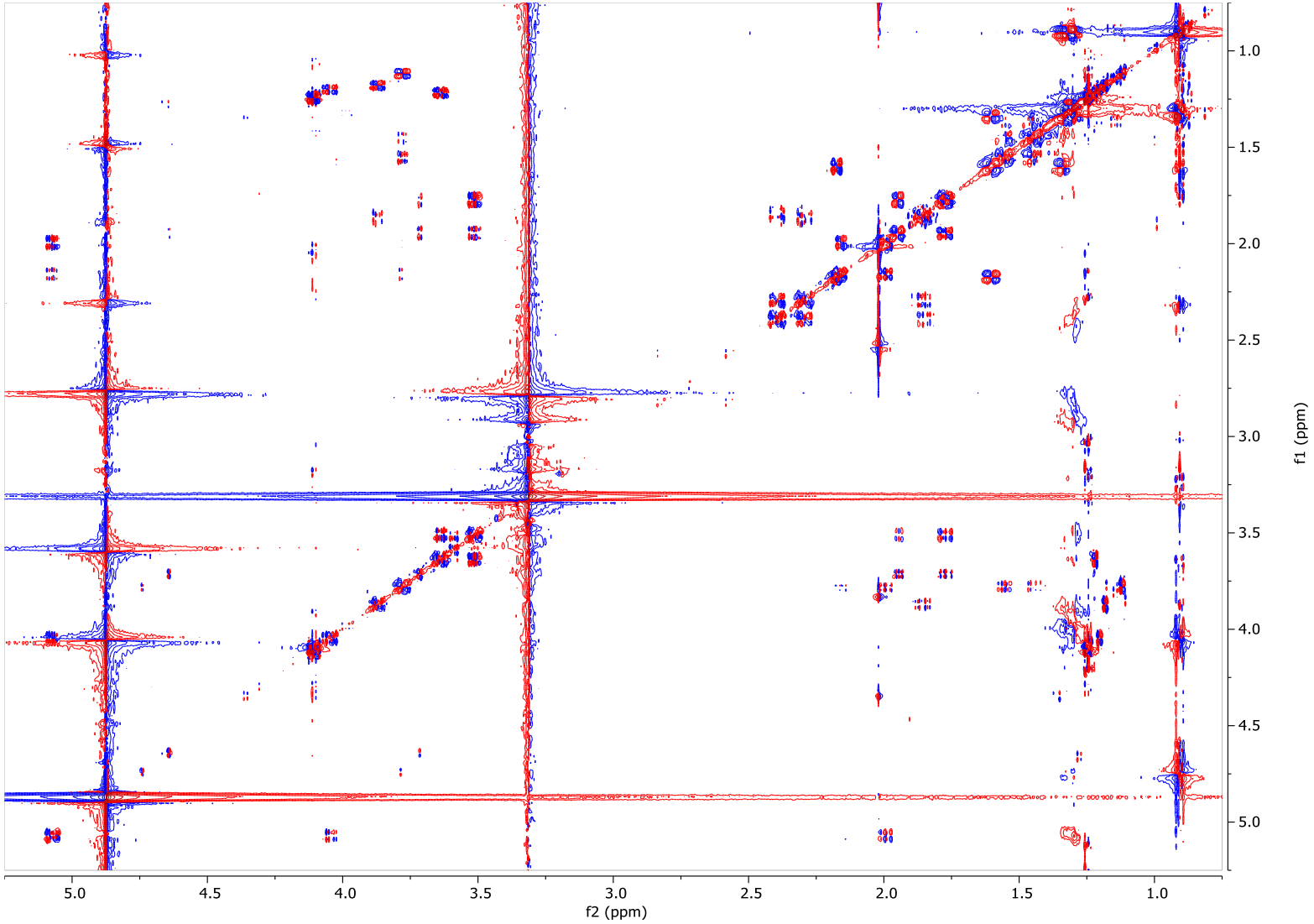

Figure S7b: Section of the *dqf*-COSY spectrum of AB-asc-C6 (**6b**, abas#12) from *C. nigoni*.

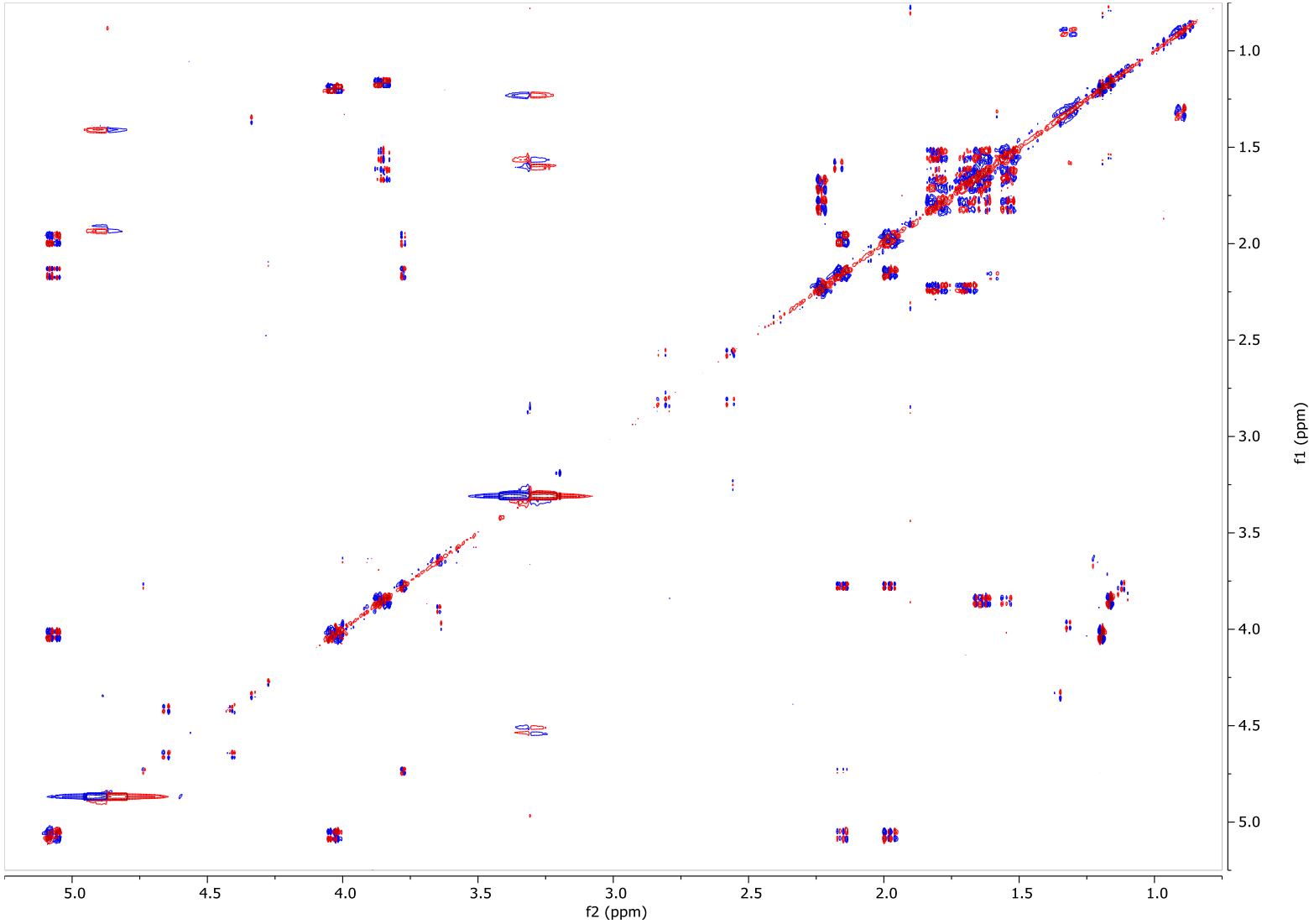

Figure S7c: Section of the *dqf*-COSY spectrum of AB-asc-C5 (**6a**, abas#9) and asc-C11 (**1b**, ascr#18) from *C. nigoni* showing signals for a 4'-substituted ascaroside.

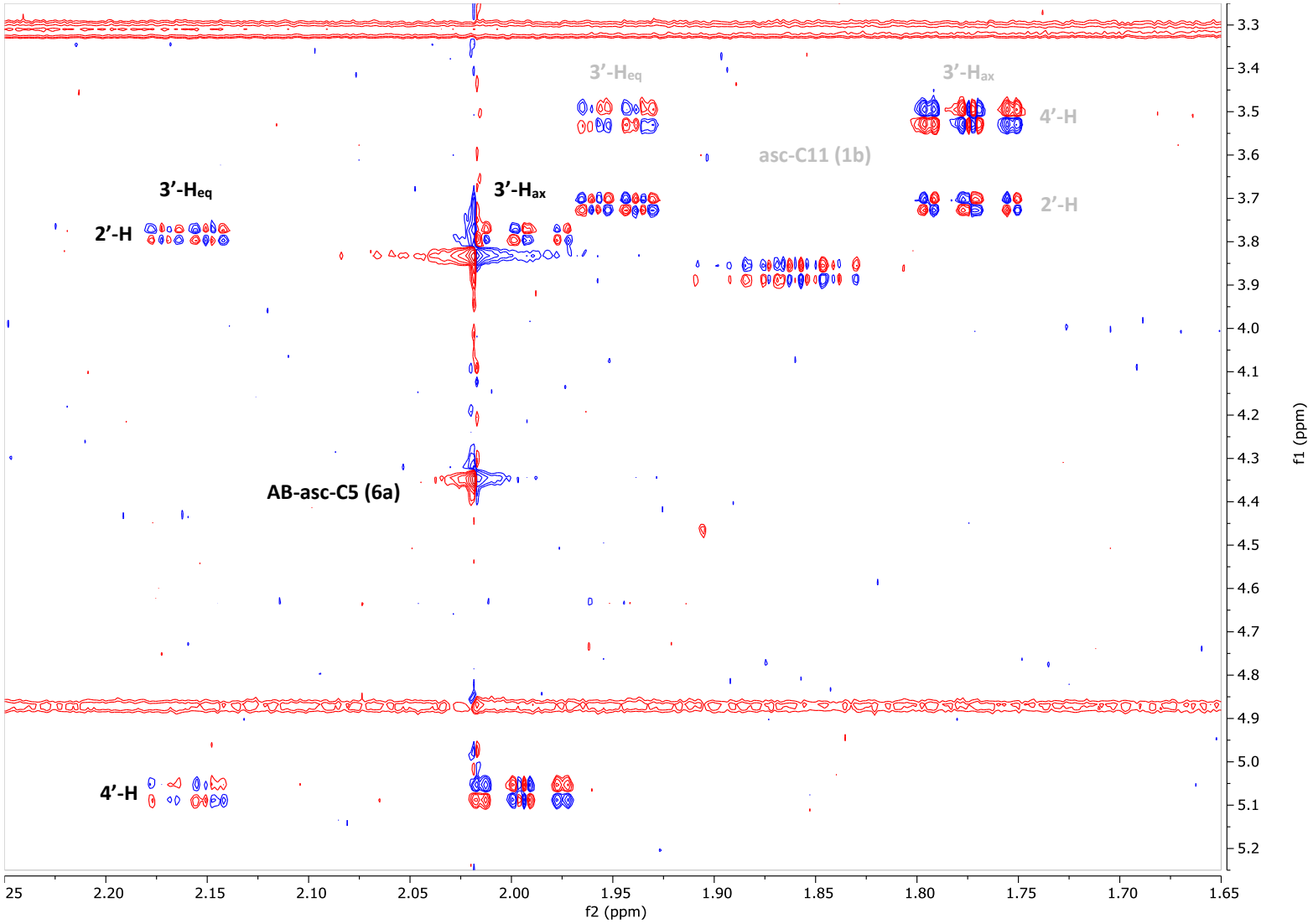

Figure S7d: Section of the *dqf*-COSY spectrum of AB-asc-C6 (**6b**, abas#12) from *C. nigoni* showing signals for a 4'-substituted ascaroside.

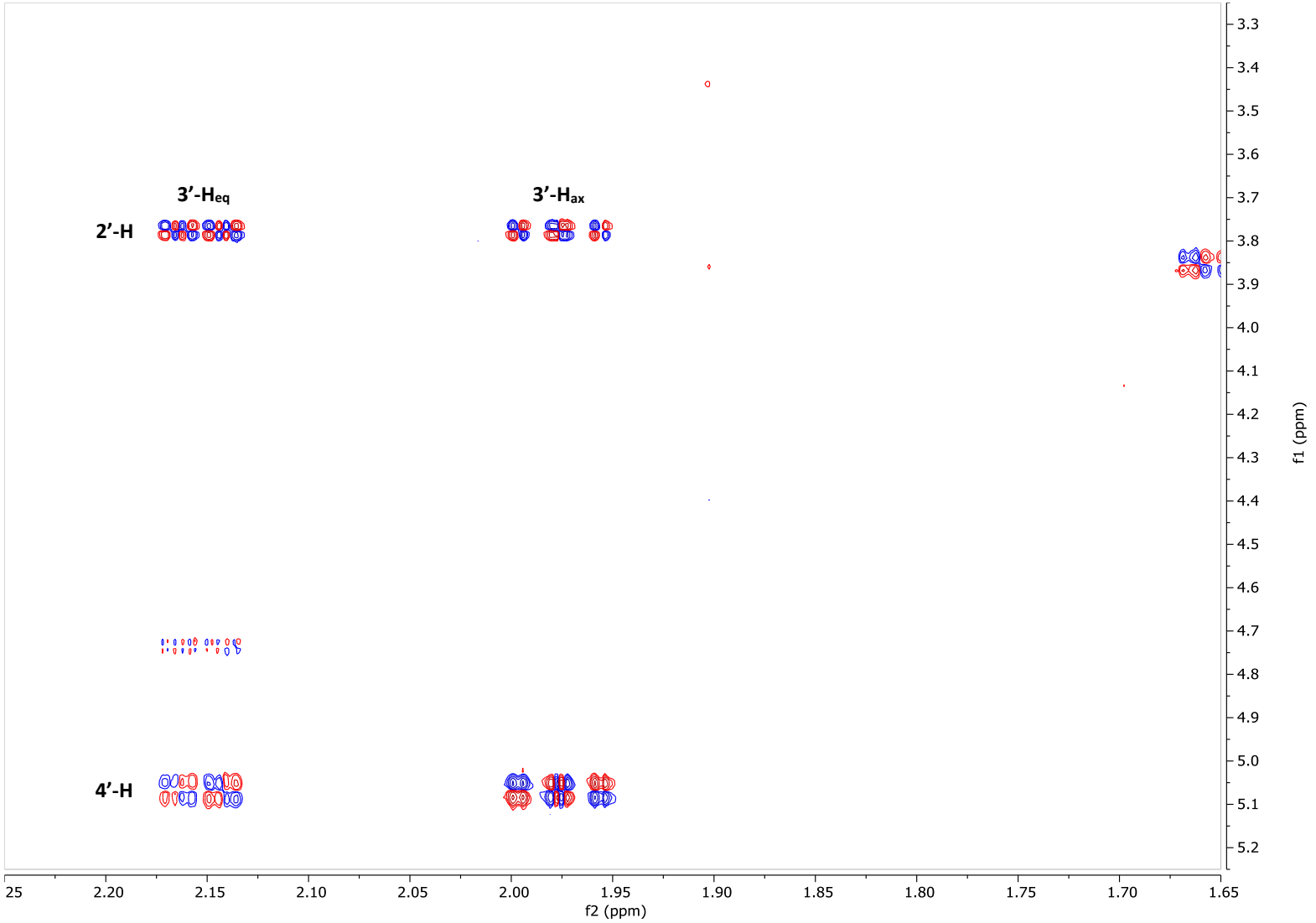

Figure S7e: Section of the *dqf*-COSY spectrum of AB-asc-C5 (**6a**, abas#9) and asc-C11 (**1b**, ascr#18) from *C. nigoni* showing signals for the C5 aglycone.

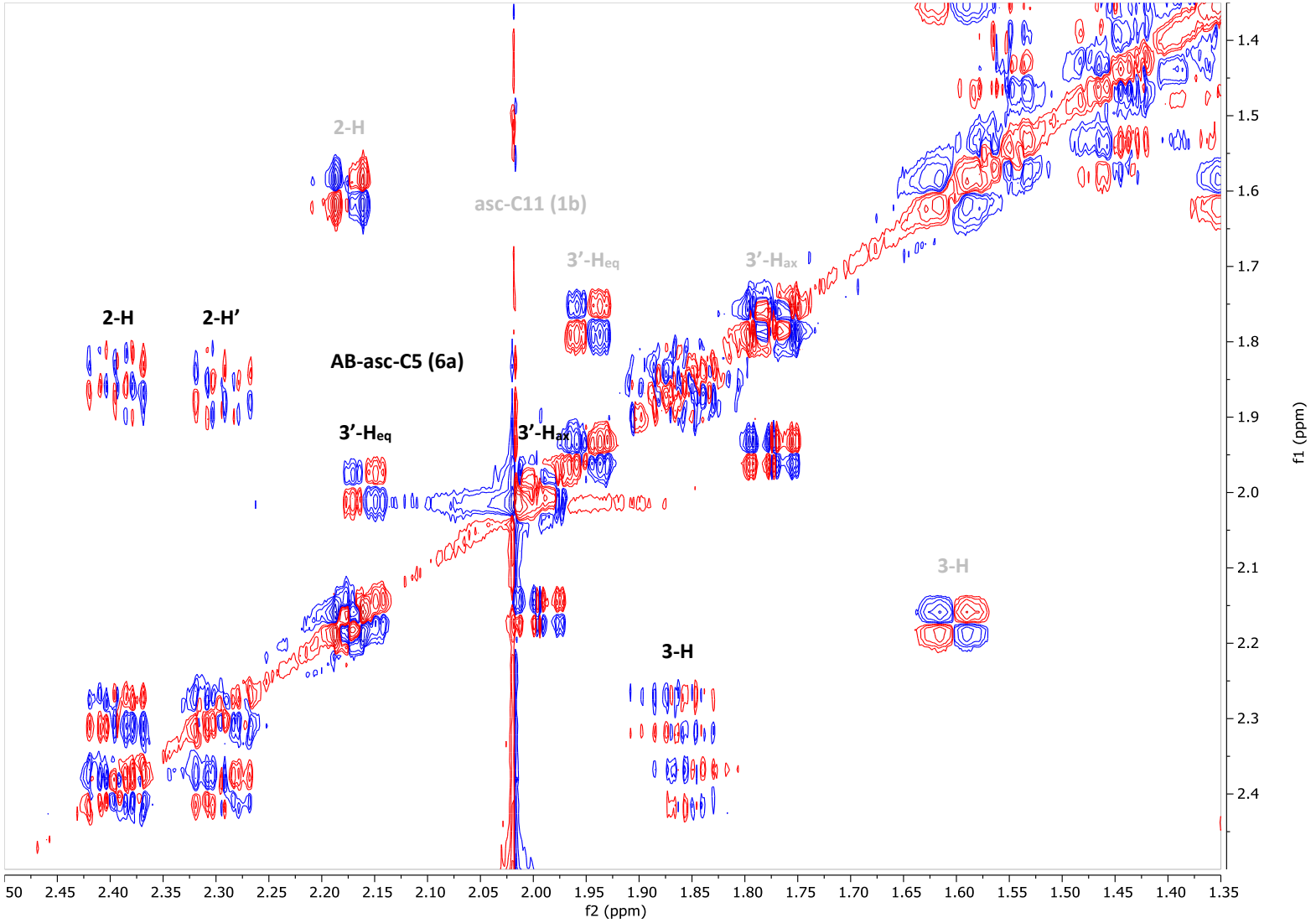

Figure S7f: Section of the *dqf*-COSY spectrum of AB-asc-C6 (**6b**) from *C. nigoni* showing signals for the C6 agylcone.

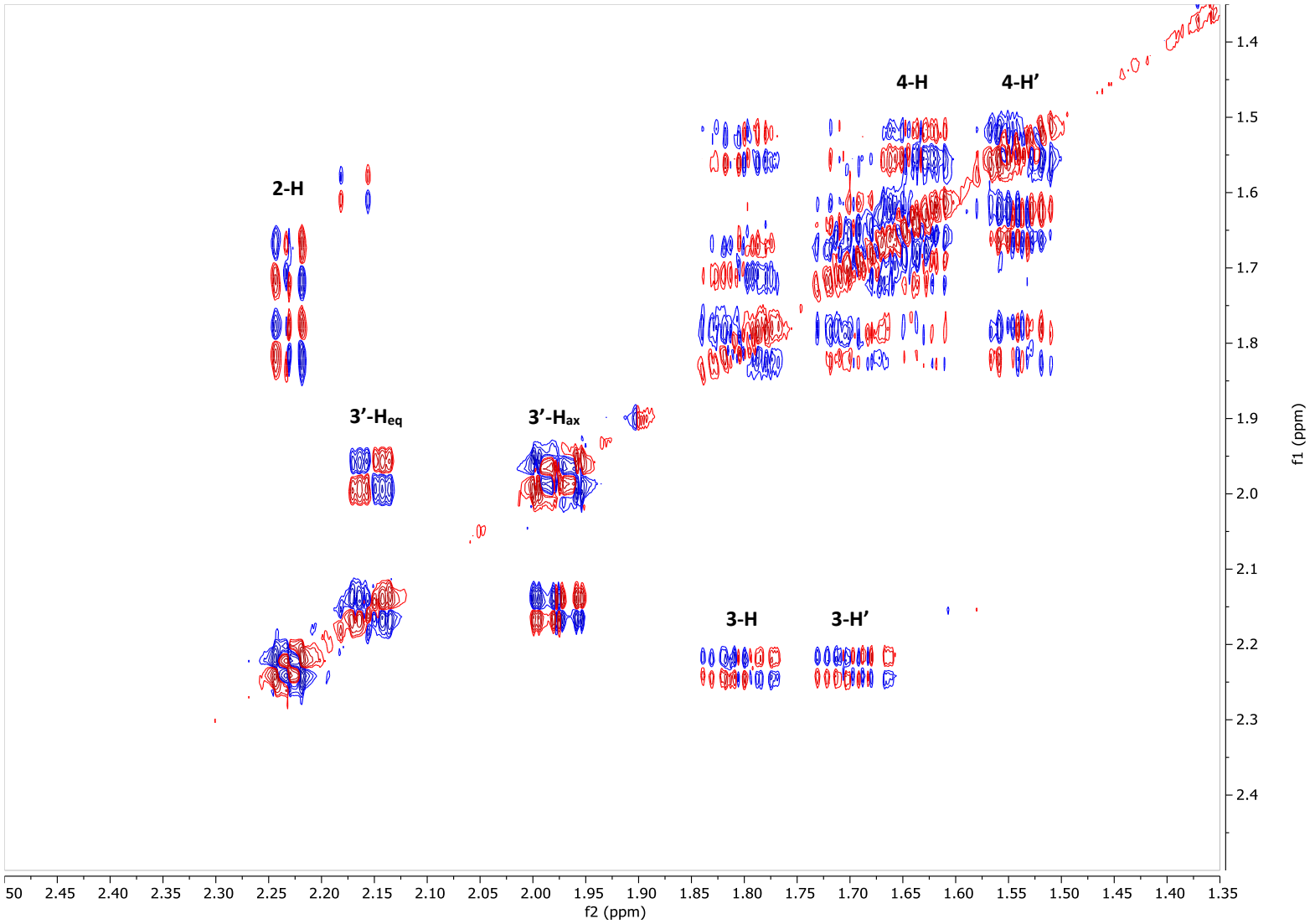

Figure S7g: Section of the *dqf*-COSY spectrum of AB-asc-C5 (**6a**) from *C. nigoni* showing signals for the *ortho*-aminobenzoyl unit.

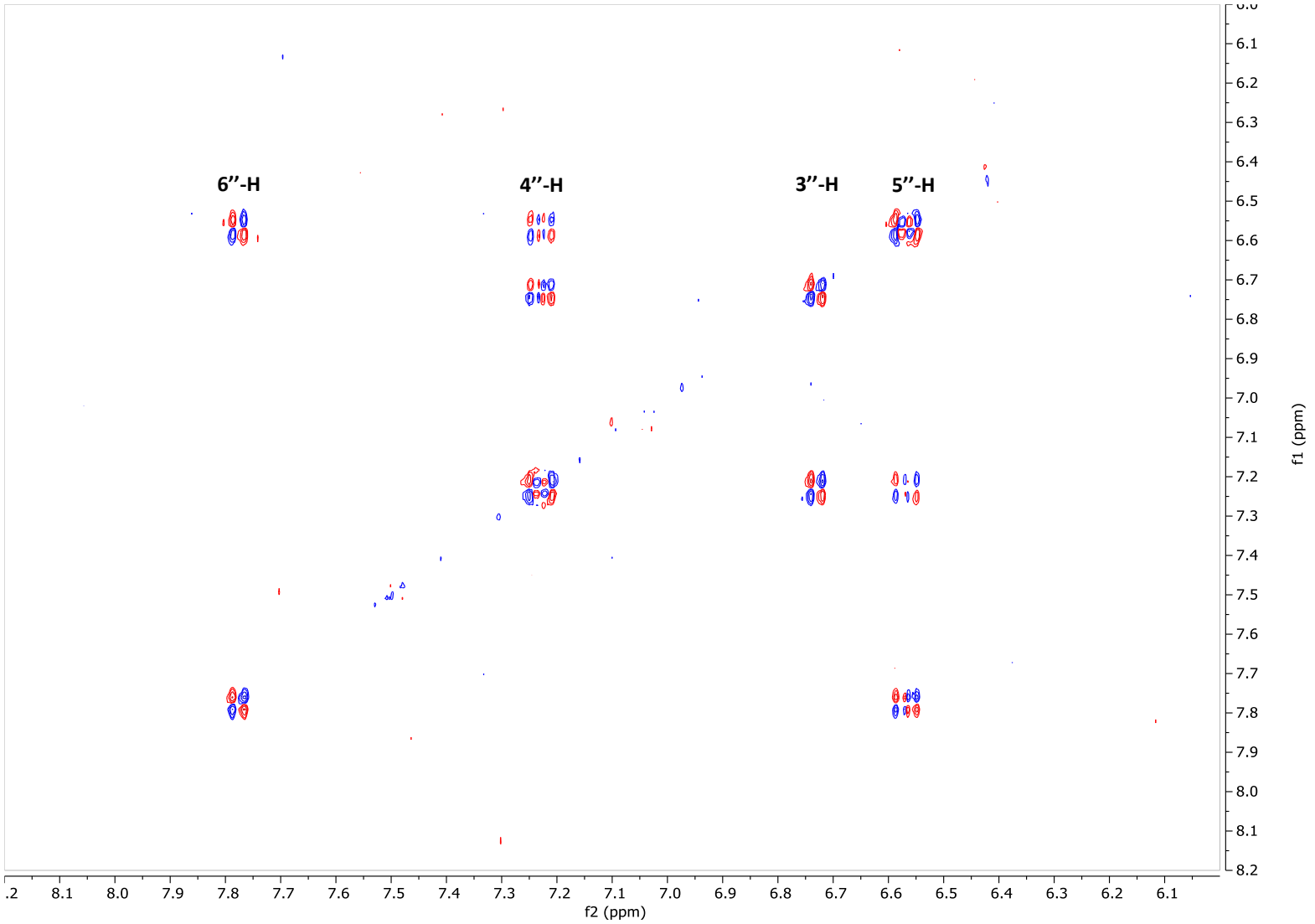

Figure S7h: Section of the *dqf*-COSY spectrum of AB-asc-C6 (**6b**) from *C. nigoni* showing signals for the *ortho*-aminobenzoyl unit.

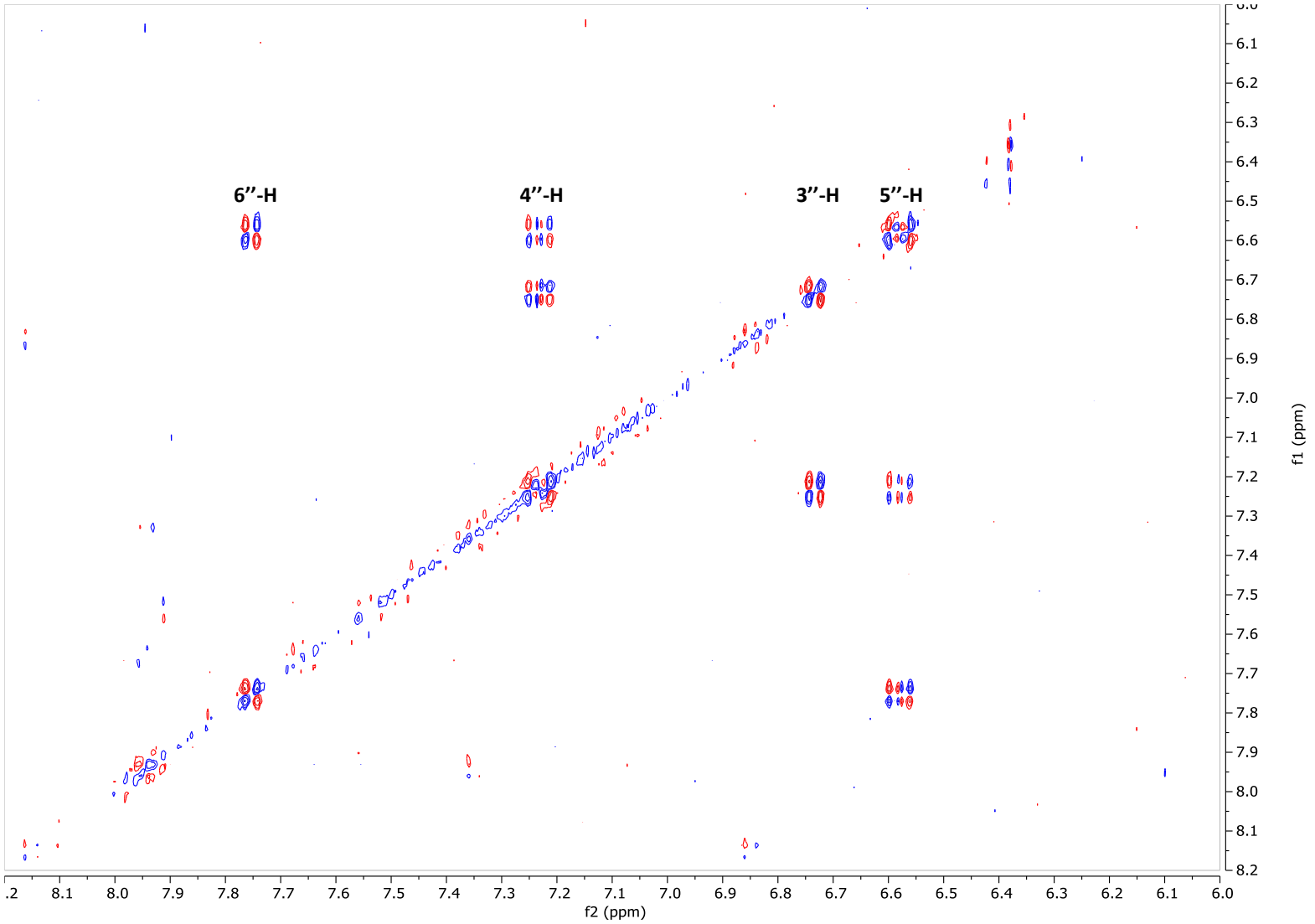

Figure S8: Comparative HPLC-ESI-(–)-HR-MS analysis of enriched AB-asc-C5 (**6a** abas#9) from *C. nigoni* and the synthetic material along with coinjection of a 1:1 mixture of the natural and the synthetic 4-AB-asc-C5.

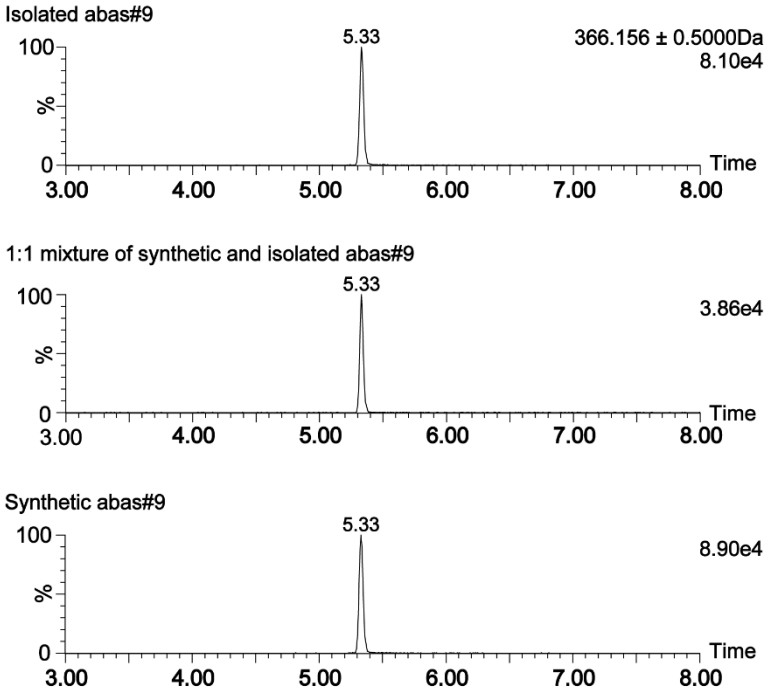

Figure S9: Comparative analysis of ^{1}H NMR (400 MHz) spectra of AB-asc-C5 (**6a**) enriched from *C. nigoni* JU1422, the synthetic AB-asc-C5 (**6a**) standard, along with a mixture of the natural and synthetic material showing their identify.

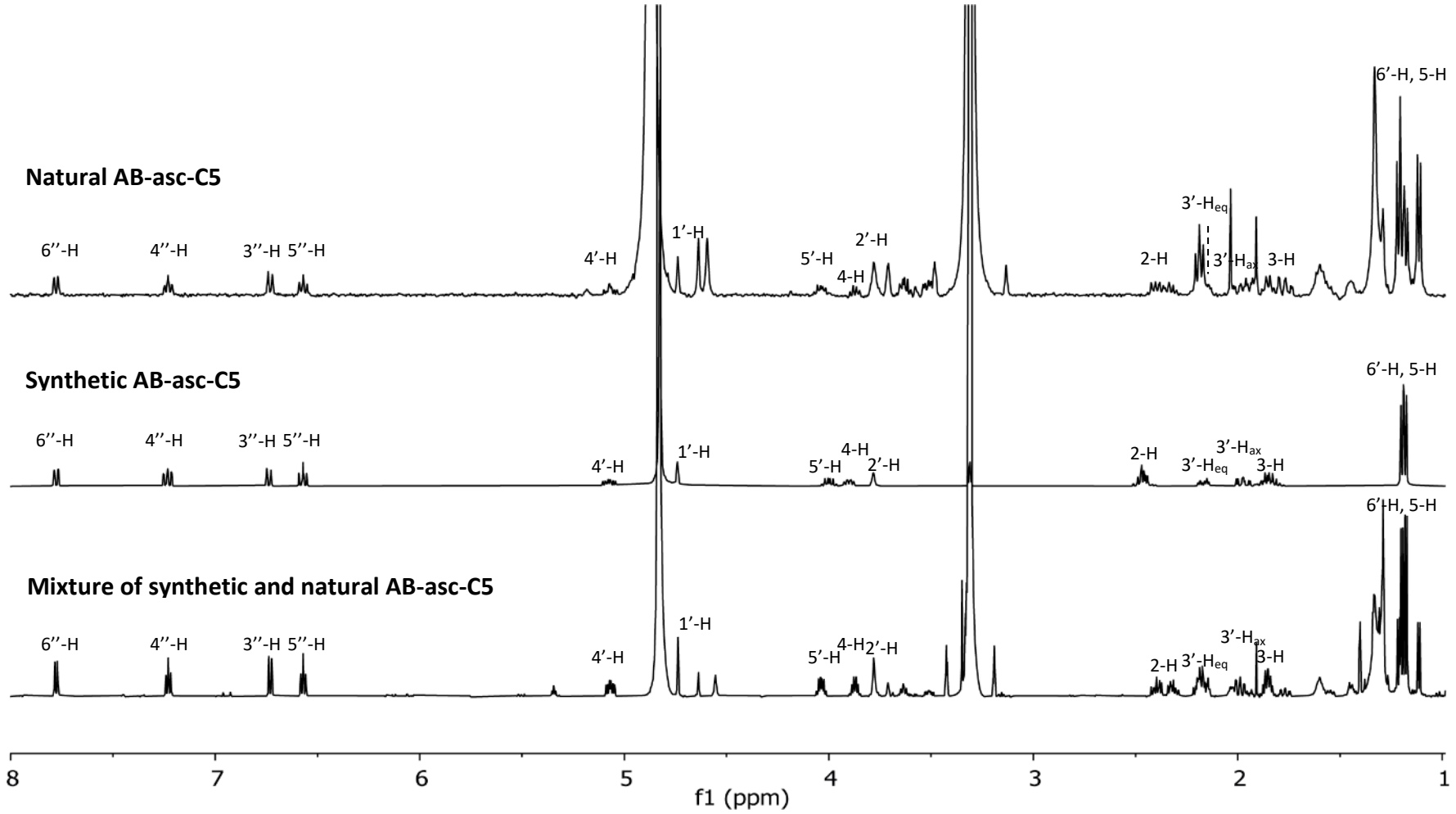

Figure S10: Retention assay with synthetic AB-asc-C5 (**6a**, abas#9) and *C. nigoni* JU1422 males**.**

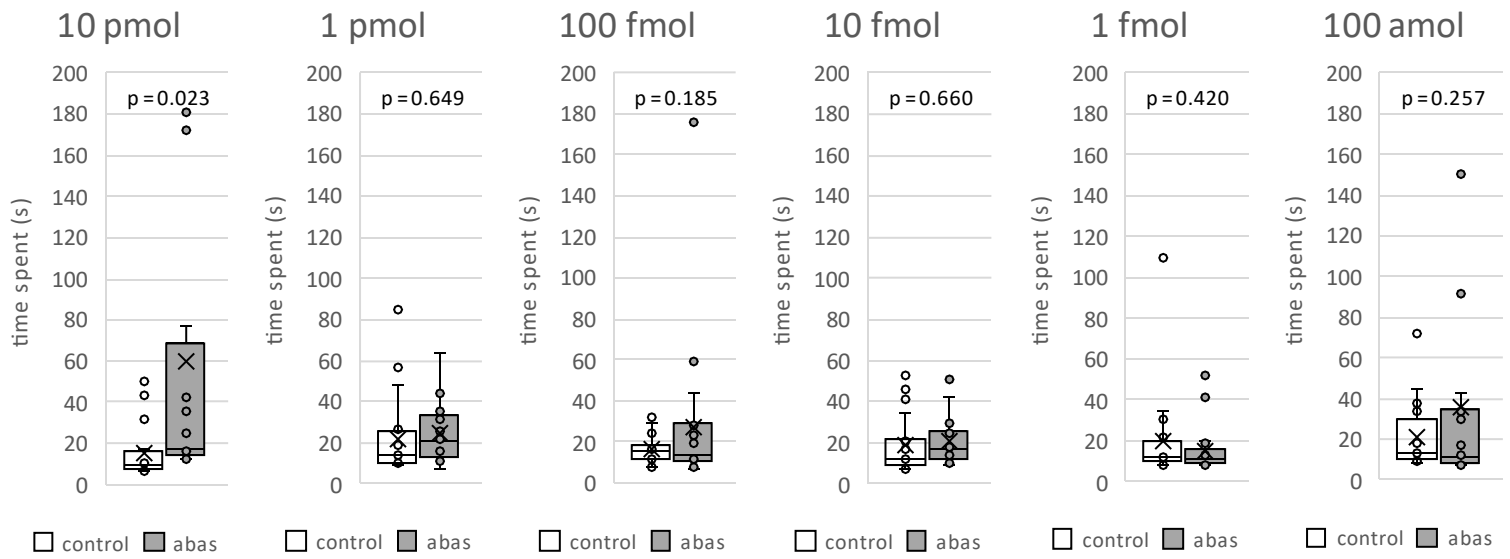

Figure S11: Retention assay with synthetic AB-asc-C5 (**6a**, abas#9) and *C. nigoni* JU1422 females**.**

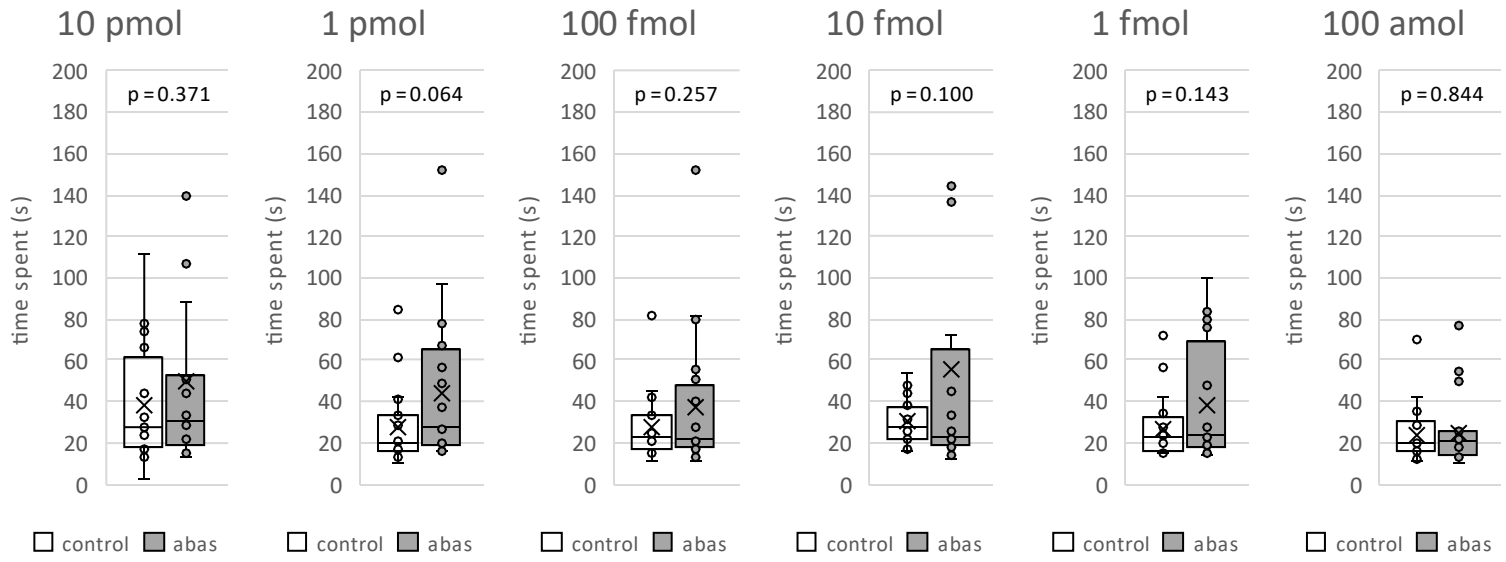

Figure S12: Retention assay with synthetic AB-asc-C5 (**6a**, abas#9) and *C. tropicalis* JU1373 hermaphrodites.

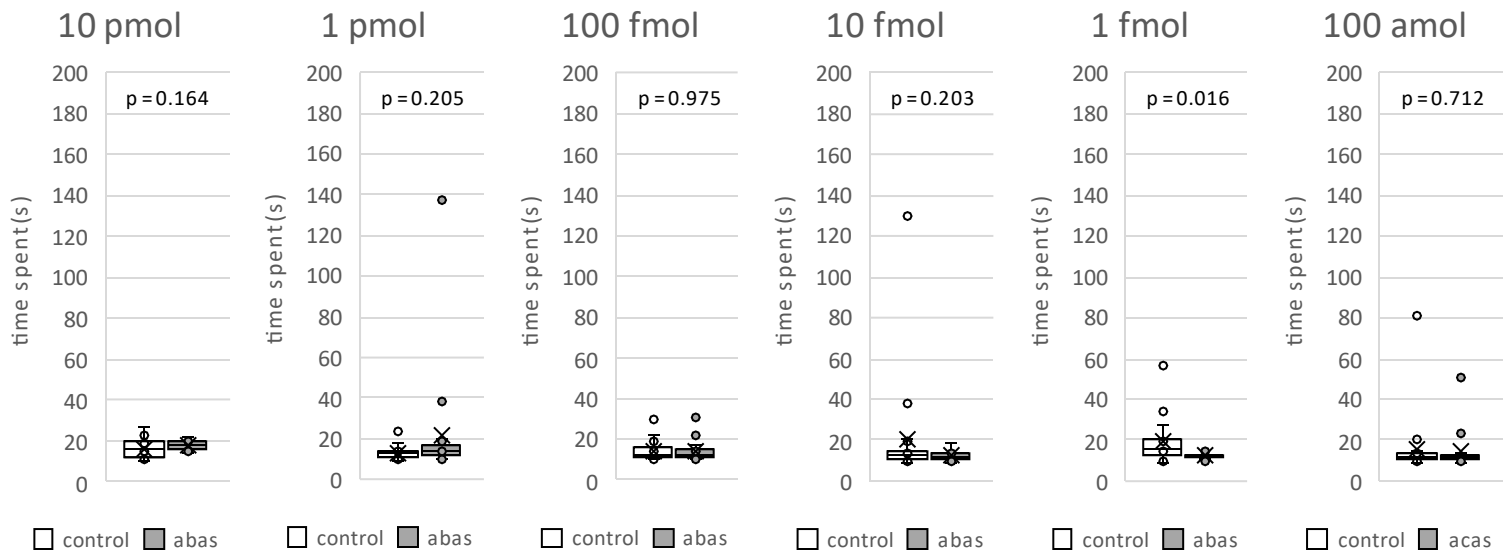

Figure S13: ^{1}H NMR (400 MHz, CD_3OD) of 1-*O*-methyl-6-deoxy-α-L-*arabino*-hexopyranoside (**8**).

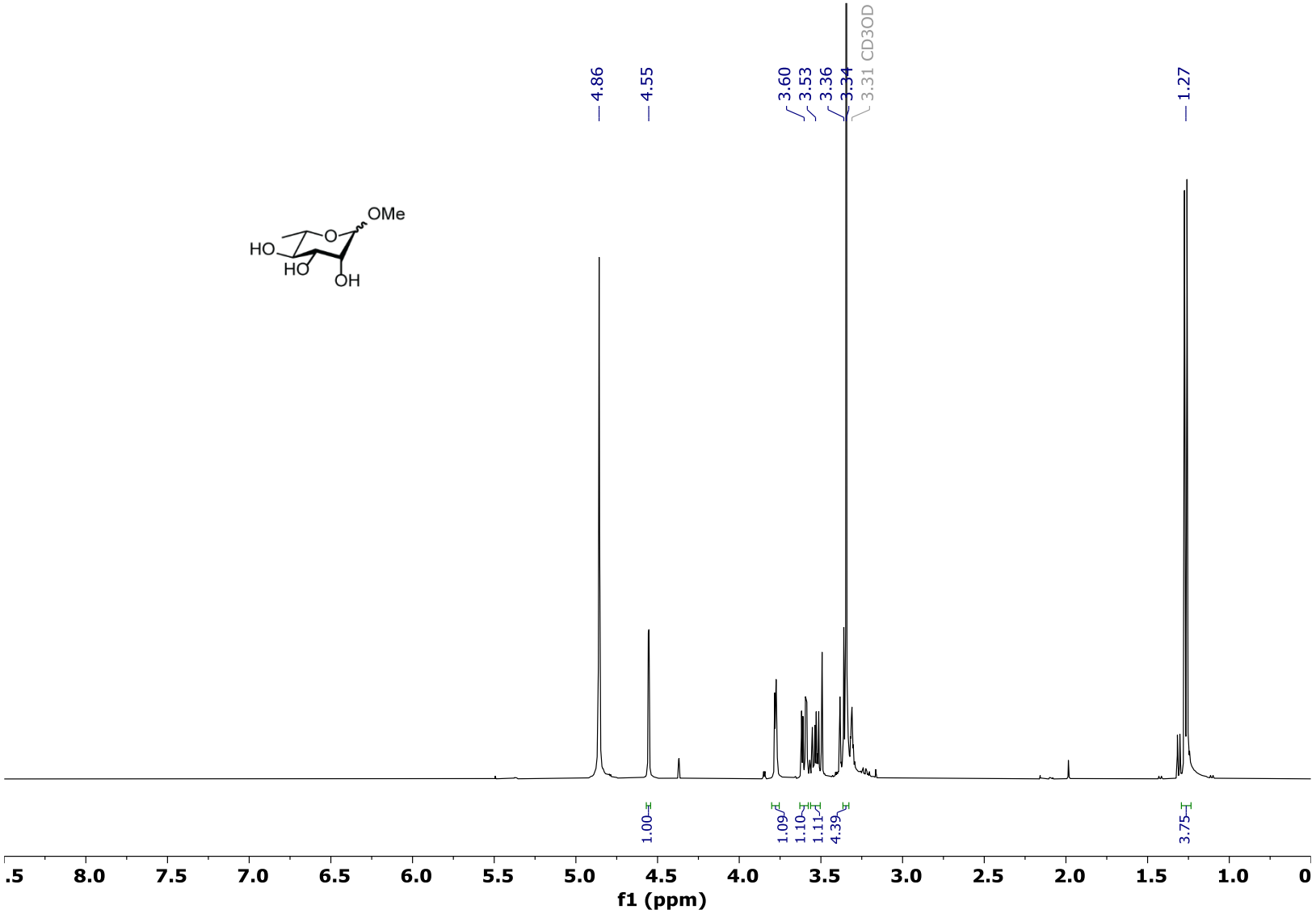

Figure S14: ^{1}H NMR (400 MHz, $CDCl_3$) of 1-*O*-methyl-6-deoxy-2,3-(*O*-isopropylidene)-α-L-*arabino*-hexopyranoside (**9**).

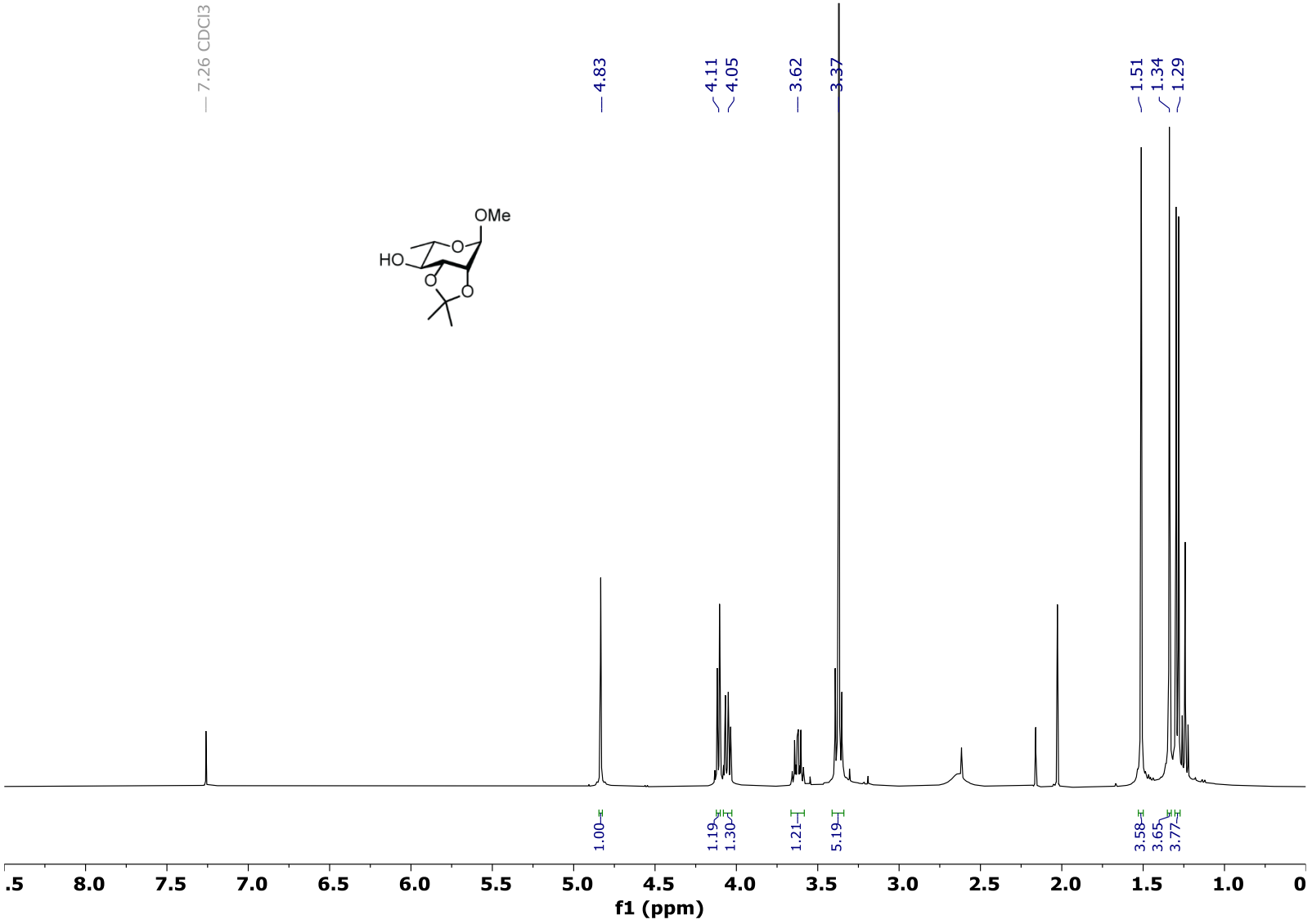

Figure S15: ^{1}H NMR (400 MHz, $CDCl_3$) of 1-*O*-methyl-6-deoxy-2,3-*O*-(isopropylidene)-4-*tert*-butyldiphenylsilyl-α-L-*arabino*-hexopyranoside (**10**).

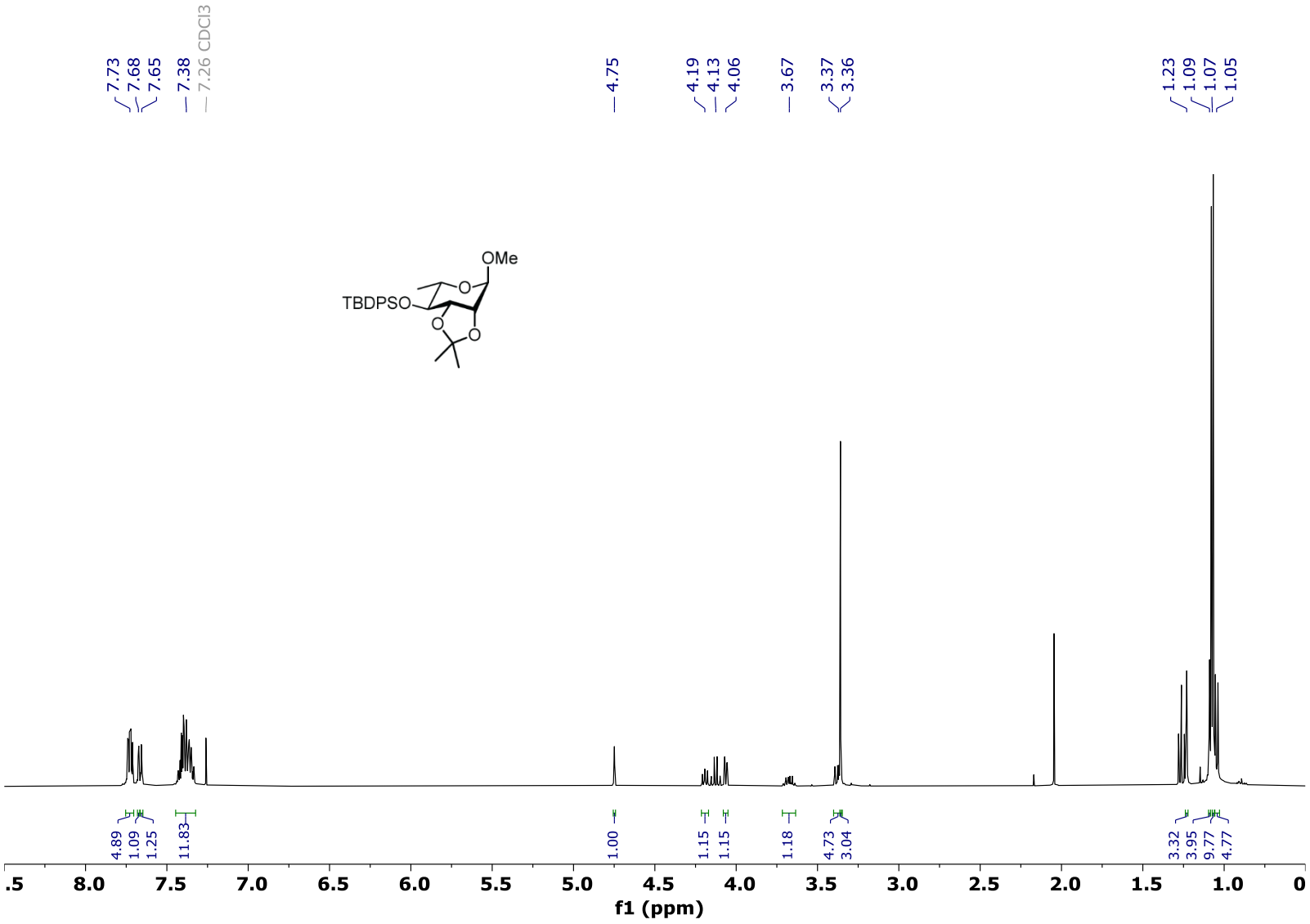

Figure S16: ^{1}H NMR (400 MHz, $CDCl_3$) of *O*-methyl-6-deoxy-4-*tert*-butyldiphenylsilyl-α-L-*arabino*-hexopyranoside (**11**).

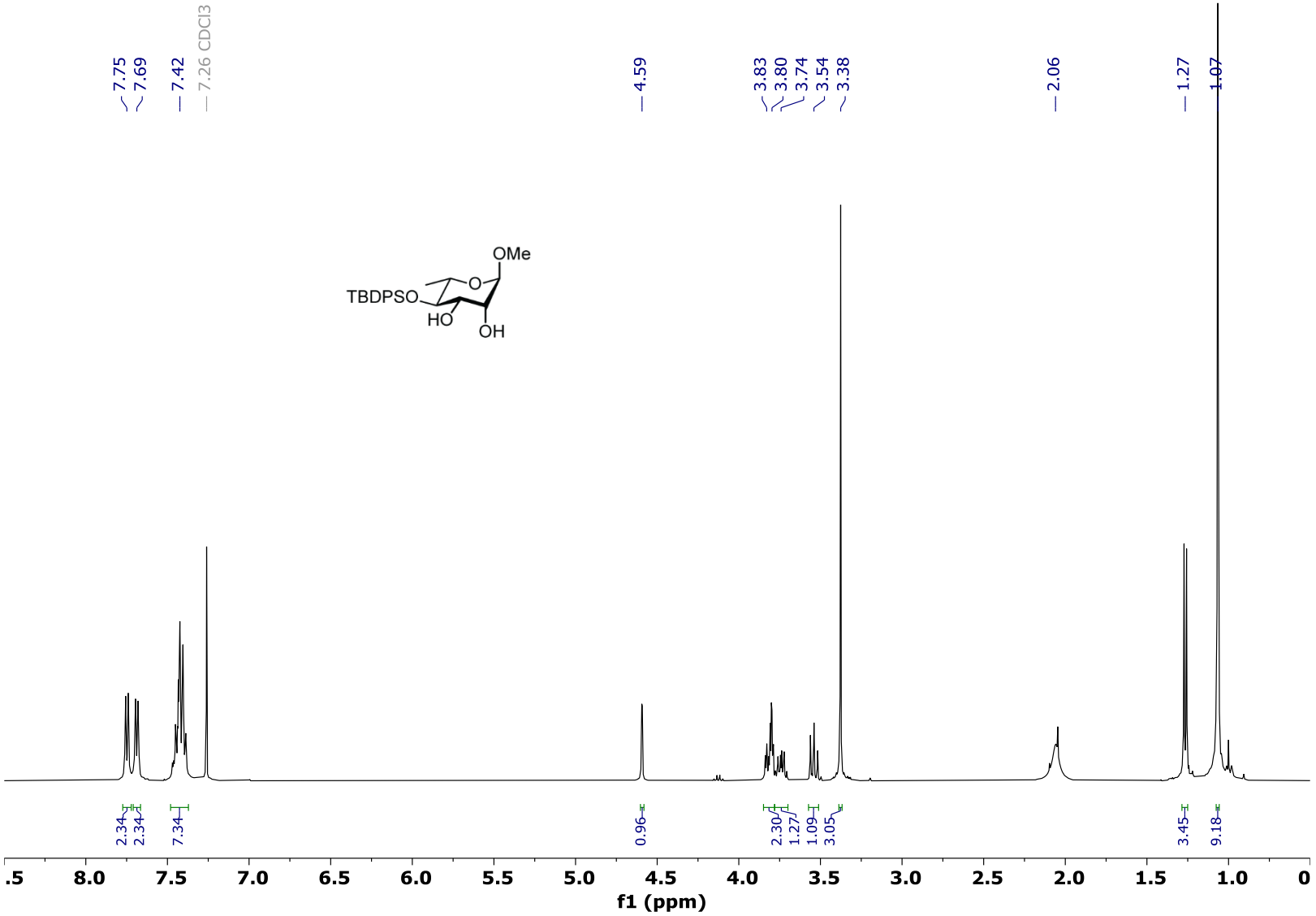

Figure S17: ^{1}H NMR (400 MHz, $CDCl_3$) 1-*O*-methyl-6-deoxy-2,3-(*O*-sulfite)-4-*tert*-butyldiphenylsilyl-α-L-*arabino*-hexopyranoside (**12**).

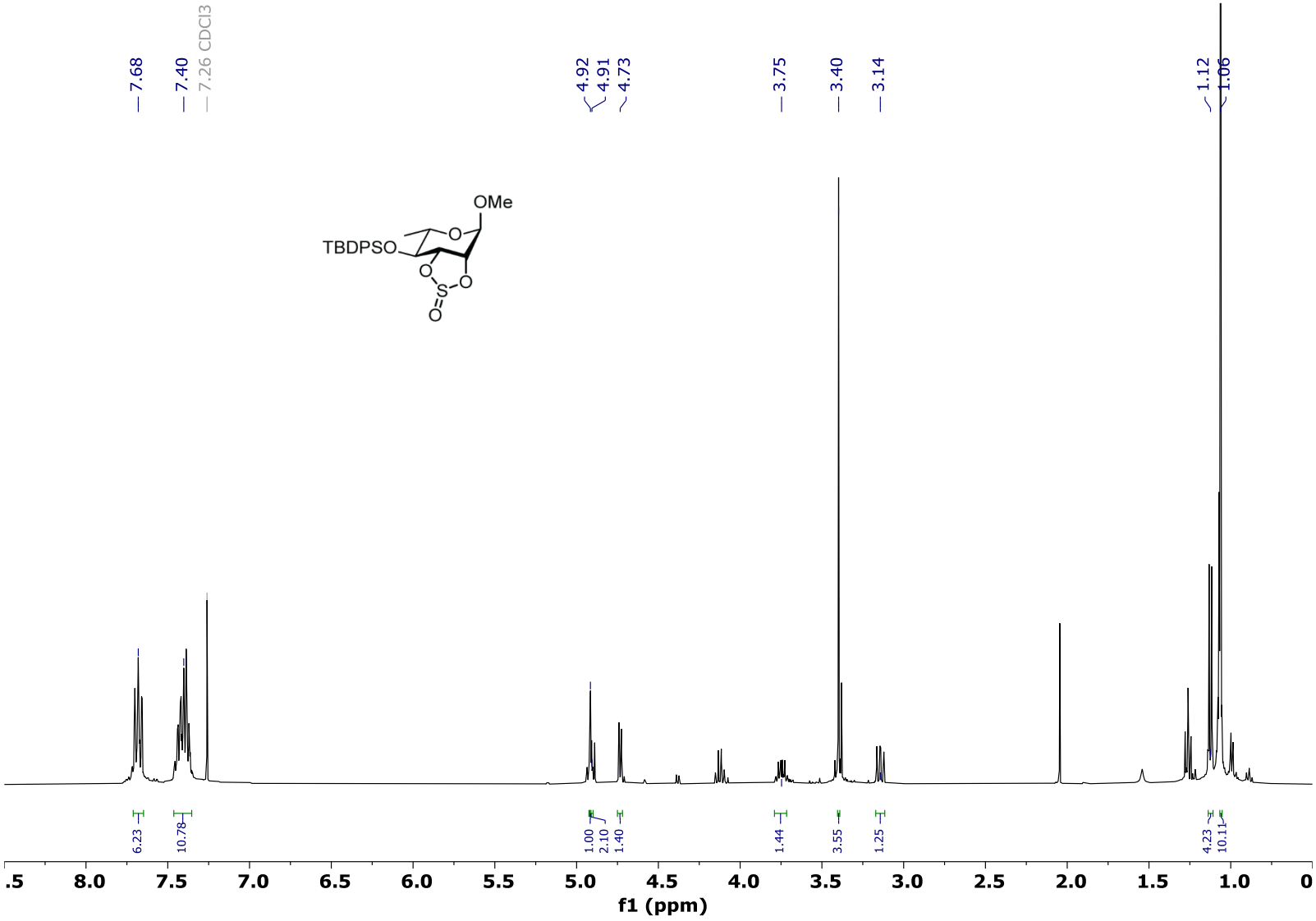

Figure S18: ^{1}H NMR (400 MHz, $CDCl_3$) 1-*O*-methyl-6-deoxy-2,3-(*O*-sulfate)-4-*tert*-butyldiphenylsilyl-α-L-*arabino*-hexopyranoside (**13**).

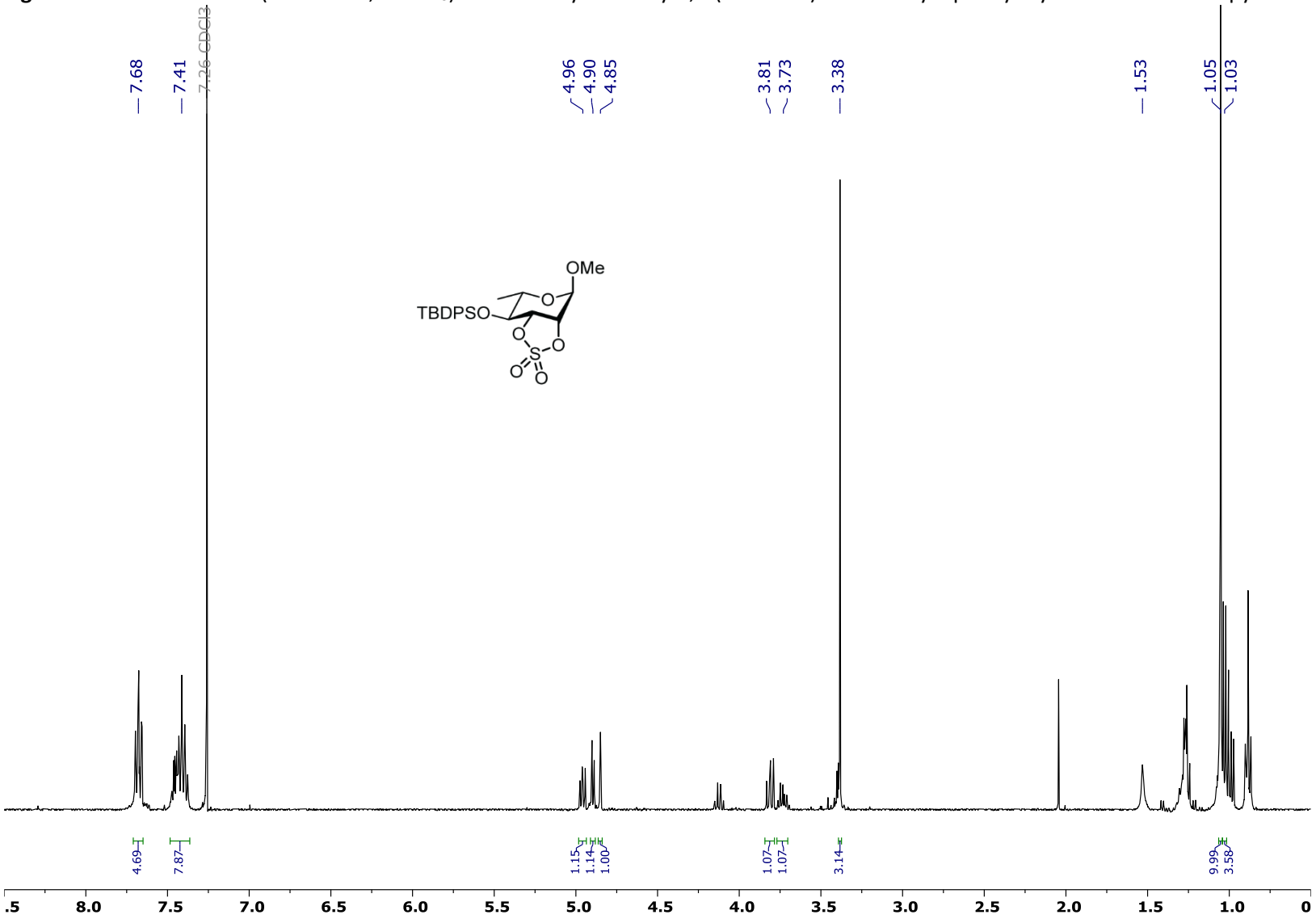

Figure S19: ^{1}H NMR (400 MHz, $CDCl_3$) of 1-*O*-methyl-4-*O*-*tert*-butyldiphenylsilyl-3,6-dideoxy-α-L-*arabino*-hexopyranoside (**14**).

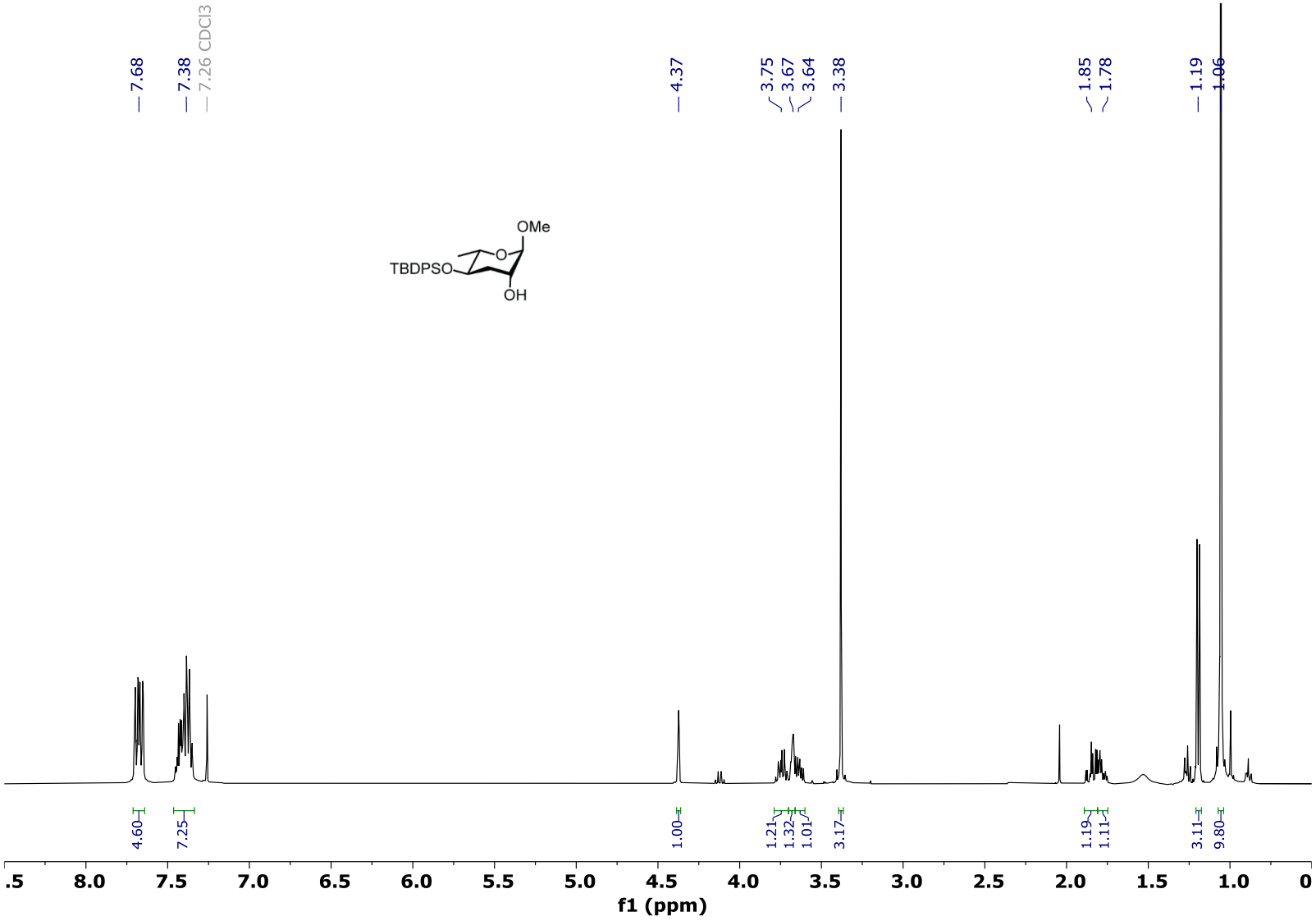

Figure S20: ^{1}H NMR (400 MHz, $CDCl_3$) of 1-*O*-methyl-2-*O*-benzoyl-4-*O*-*tert*-butyldiphenylsilyl-3,6-dideoxy-α-L-*arabino*-hexopyranoside (**15a**).

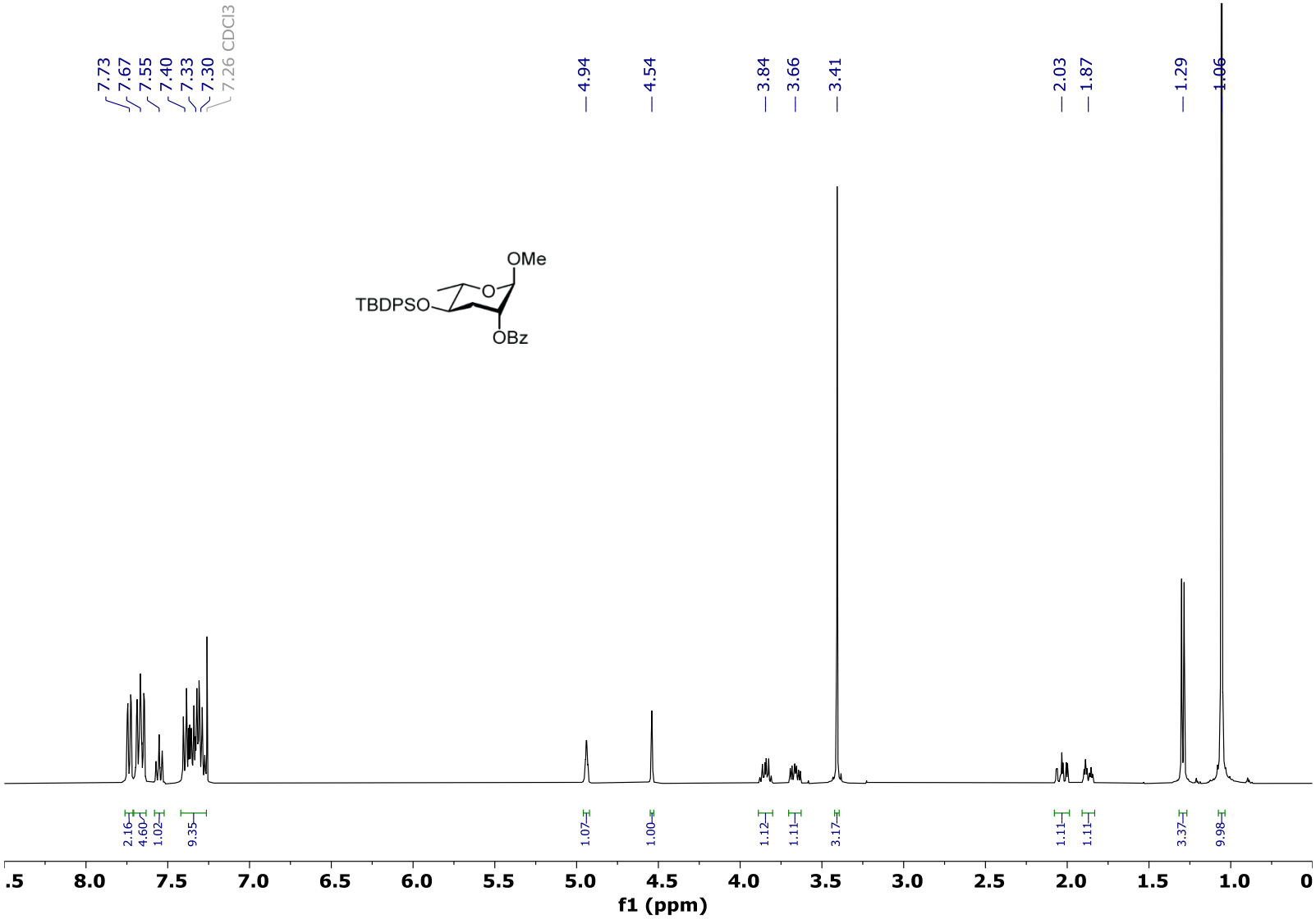

Figure S21: ^{1}H NMR (600 MHz, $CDCl_3$) of 1-*O*-methyl-2-*O*-benzoyl-4-*O*-benzyl-3,6-dideoxy-α-L-*arabino*-hexopyranoside (**15b**).

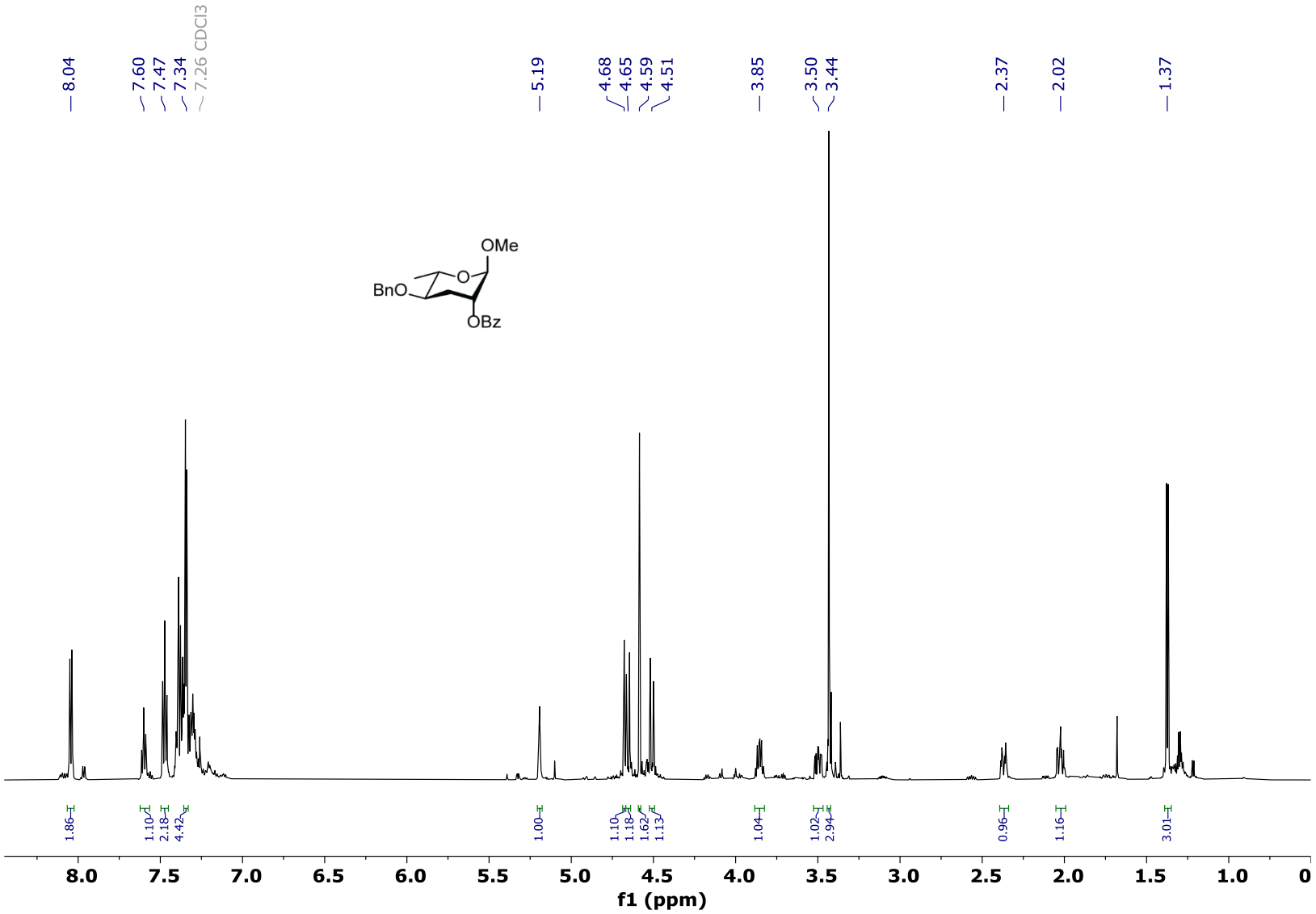

Figure S22: ^{13}C NMR (150 MHz, $CDCl_3$) of 1-*O*-methyl-2-*O*-benzoyl-4-*O*-benzyl-3,6-dideoxy-α-L-*arabino*-hexopyranoside (**15b**).

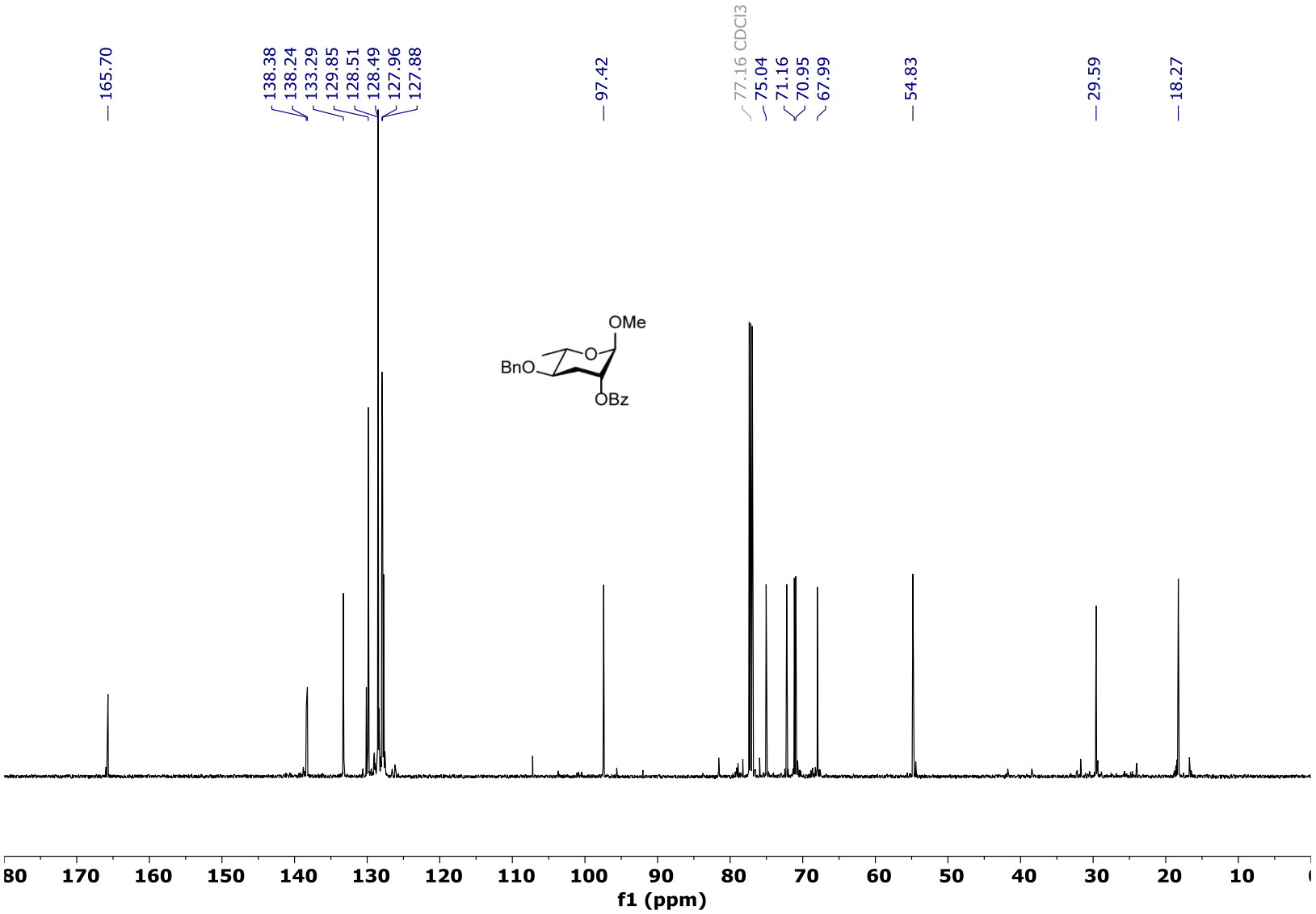

Figure S23: *dqf*-COSY (600 MHz, $CDCl_3$) of 1-*O*-methyl-2-*O*-benzoyl-4-*O*-benzyl-3,6-dideoxy-α-L-*arabino*-hexopyranoside (**15b**).

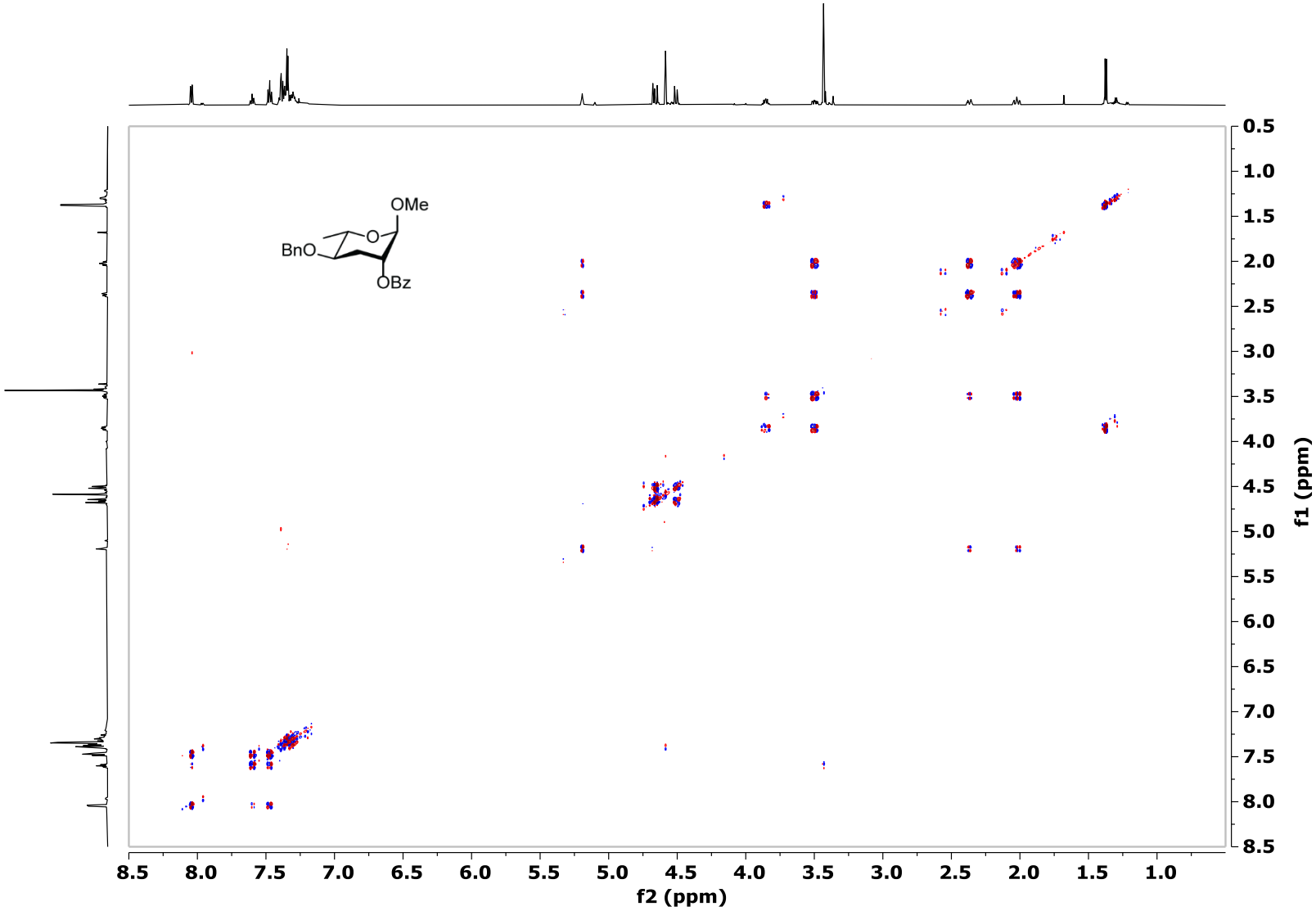

Figure S24: HSQC (600 MHz, $CDCl_3$) of 1-*O*-methyl-2-*O*-benzoyl-4-*O*-benzyl-3,6-dideoxy-α-L-*arabino*-hexopyranoside (**15b**).

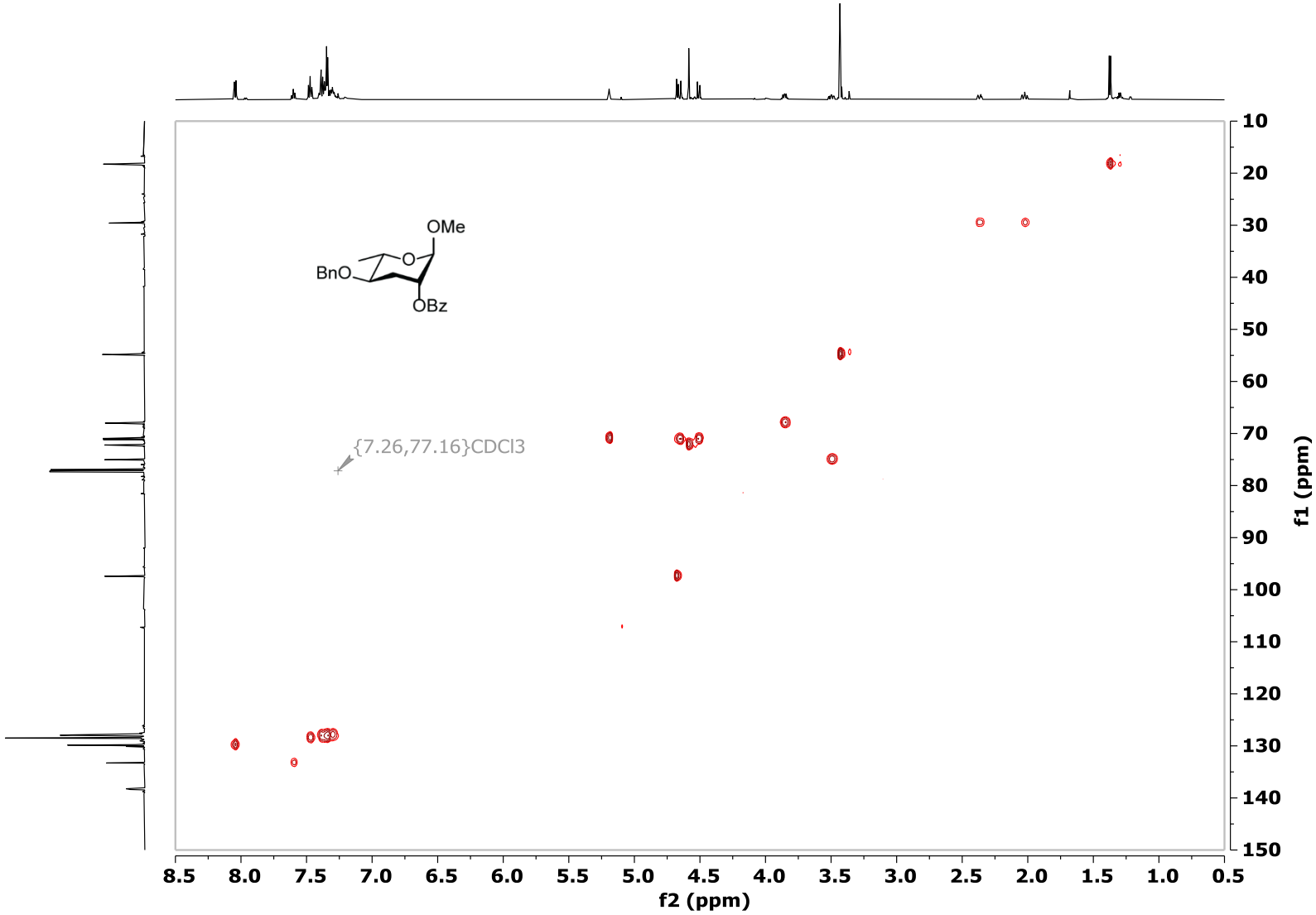

Figure S25: ^{1}H NMR (600 MHz, $CDCl_3$) of 1-*O*-methyl-2-*O*-benzoyl-4-*O*-allyl-3,6-dideoxy-α-L-*arabino*-hexopyranoside (**15c**).

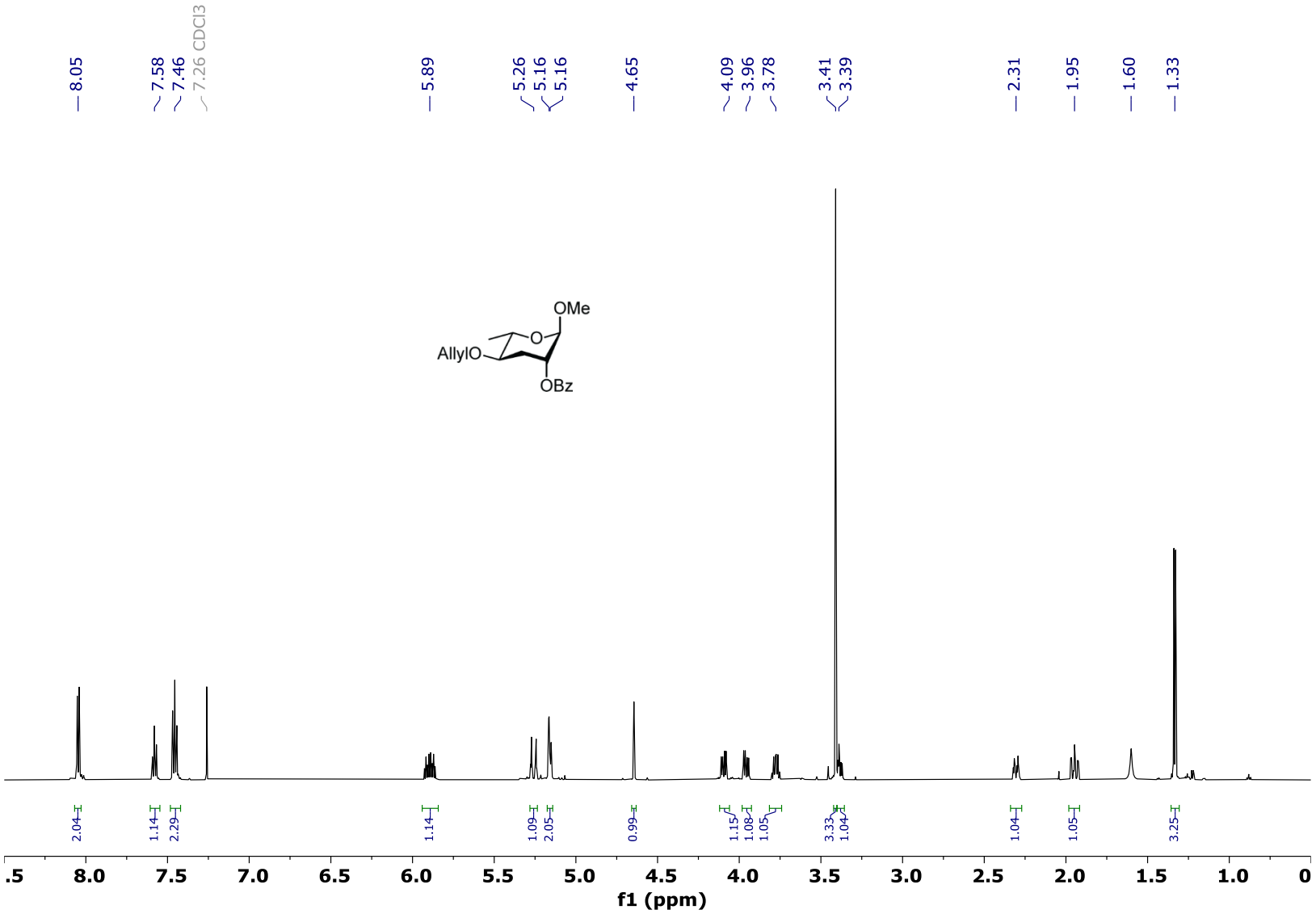

Figure S26: ^{13}C NMR (150 MHz, $CDCl_3$) of 1-*O*-methyl-2-*O*-benzoyl-4-*O*-allyl-3,6-dideoxy-α-L-*arabino*-hexopyranoside (**15c**).

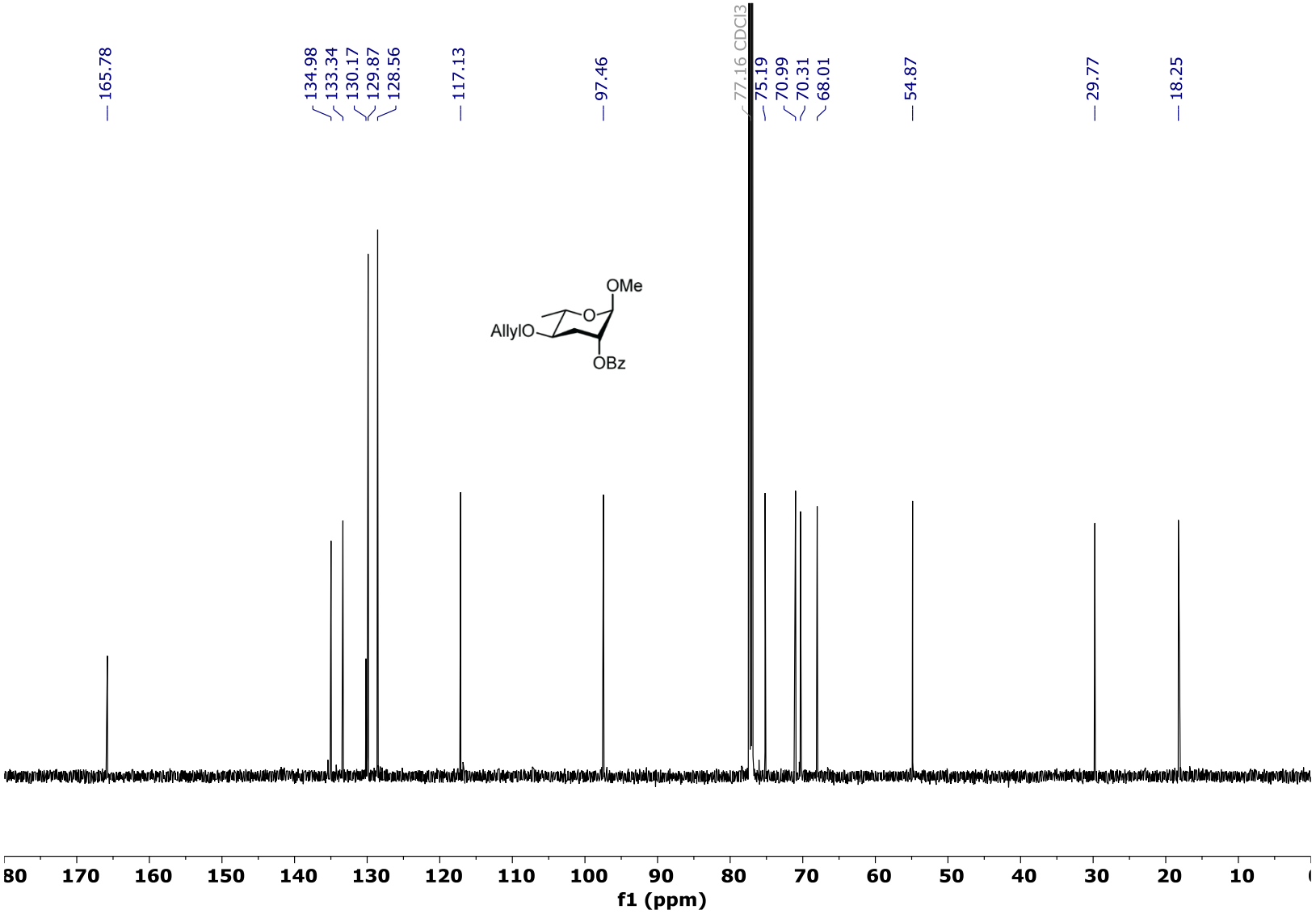

Figure S27: *dqf*-COSY (600 MHz, $CDCl_3$) of 1-*O*-methyl-2-*O*-benzoyl-4-*O*-allyl-3,6-dideoxy-α-L-*arabino*-hexopyranoside (**15c**).

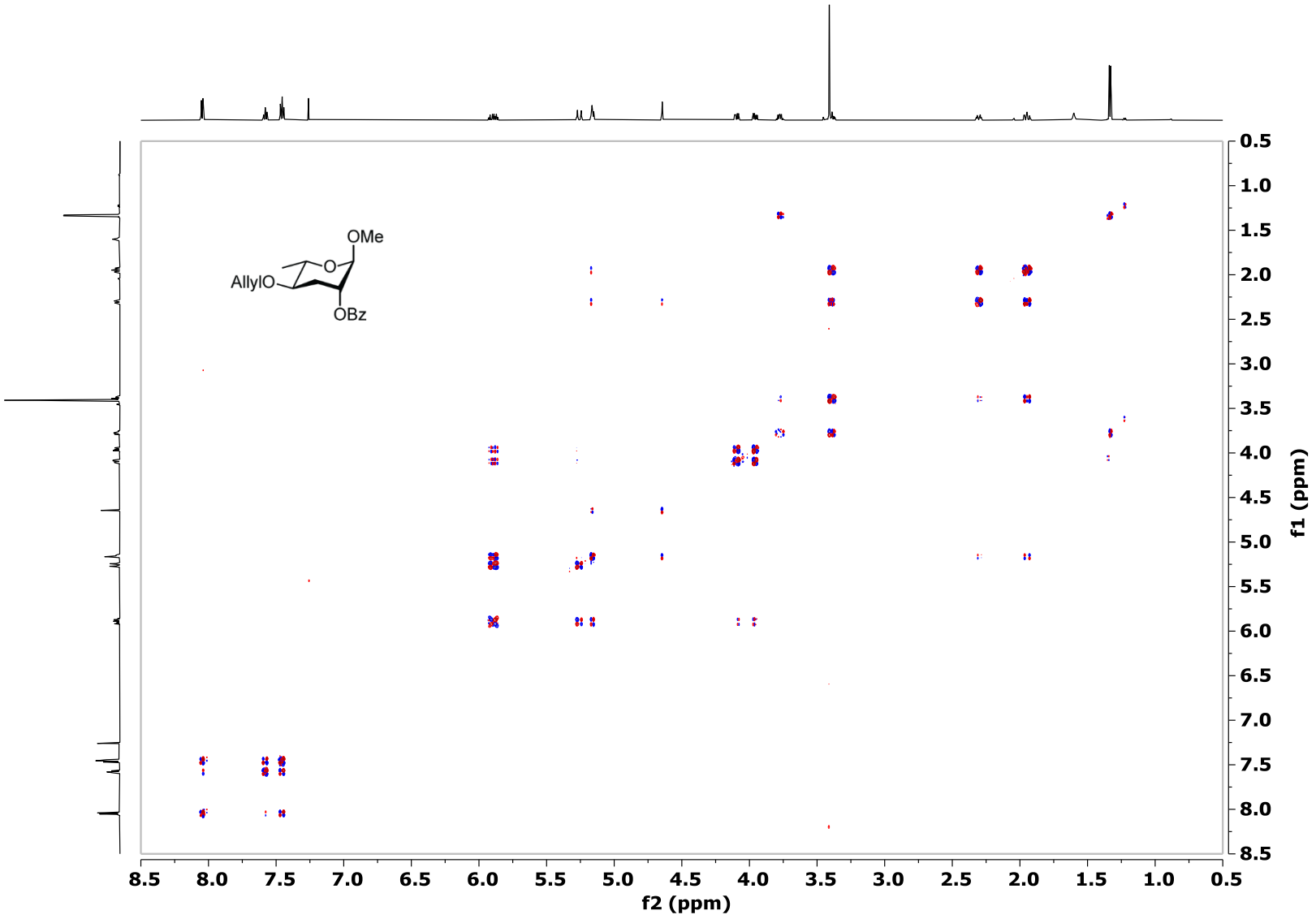

Figure S28: HSQC (600 MHz, $CDCl_3$) of 1-*O*-methyl-2-*O*-benzoyl-4-*O*-allyl-3,6-dideoxy-α-L-*arabino*-hexopyranoside (**15c**).

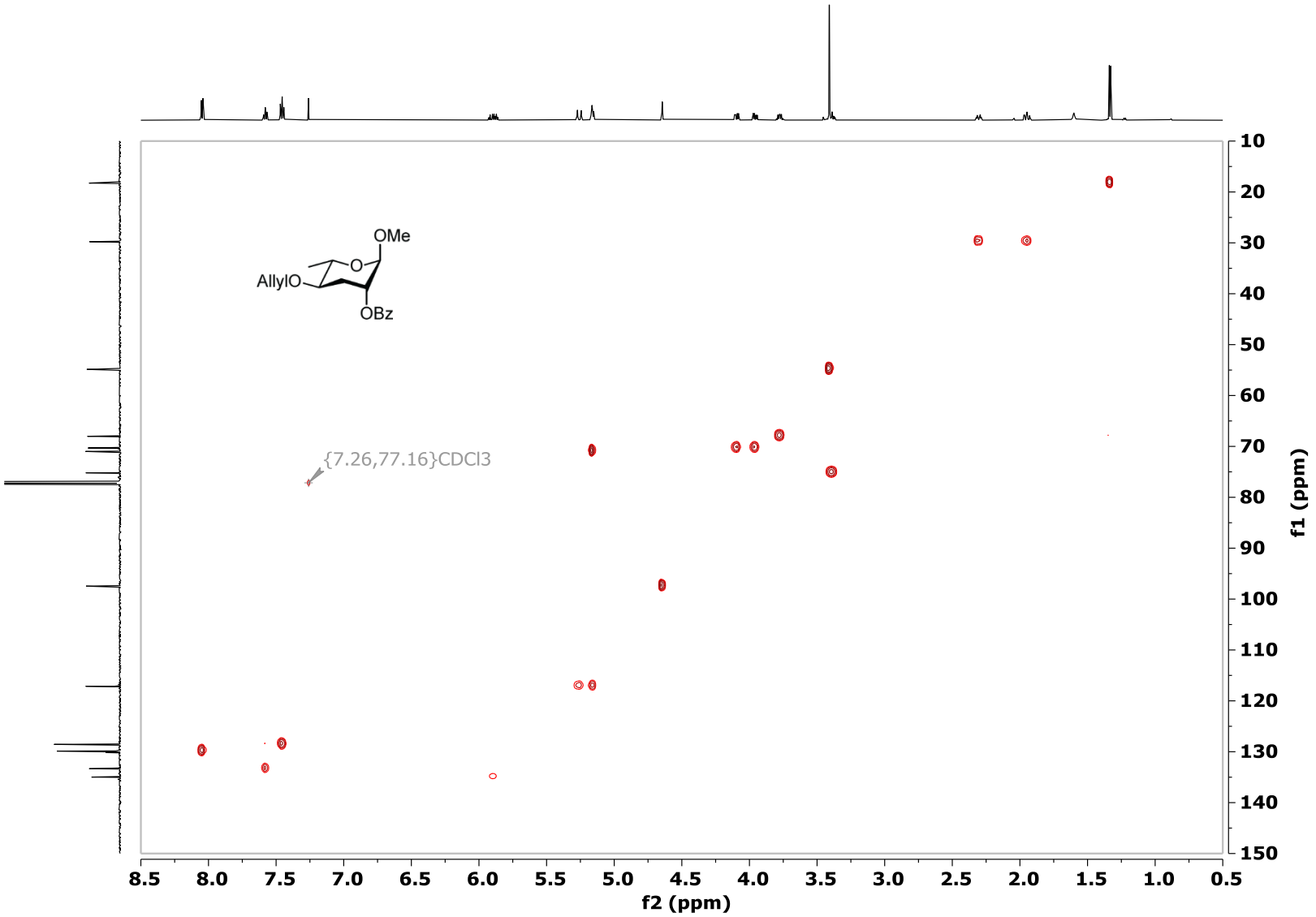

Figure S29: ^{1}H NMR (400 MHz, $CDCl_3$) of 2-*O*-benzoyl-4-*O*-*tert*-butyldiphenylsilyl-3,6-dideoxy-α-L-*arabino*-hexopyranose (**16a**).

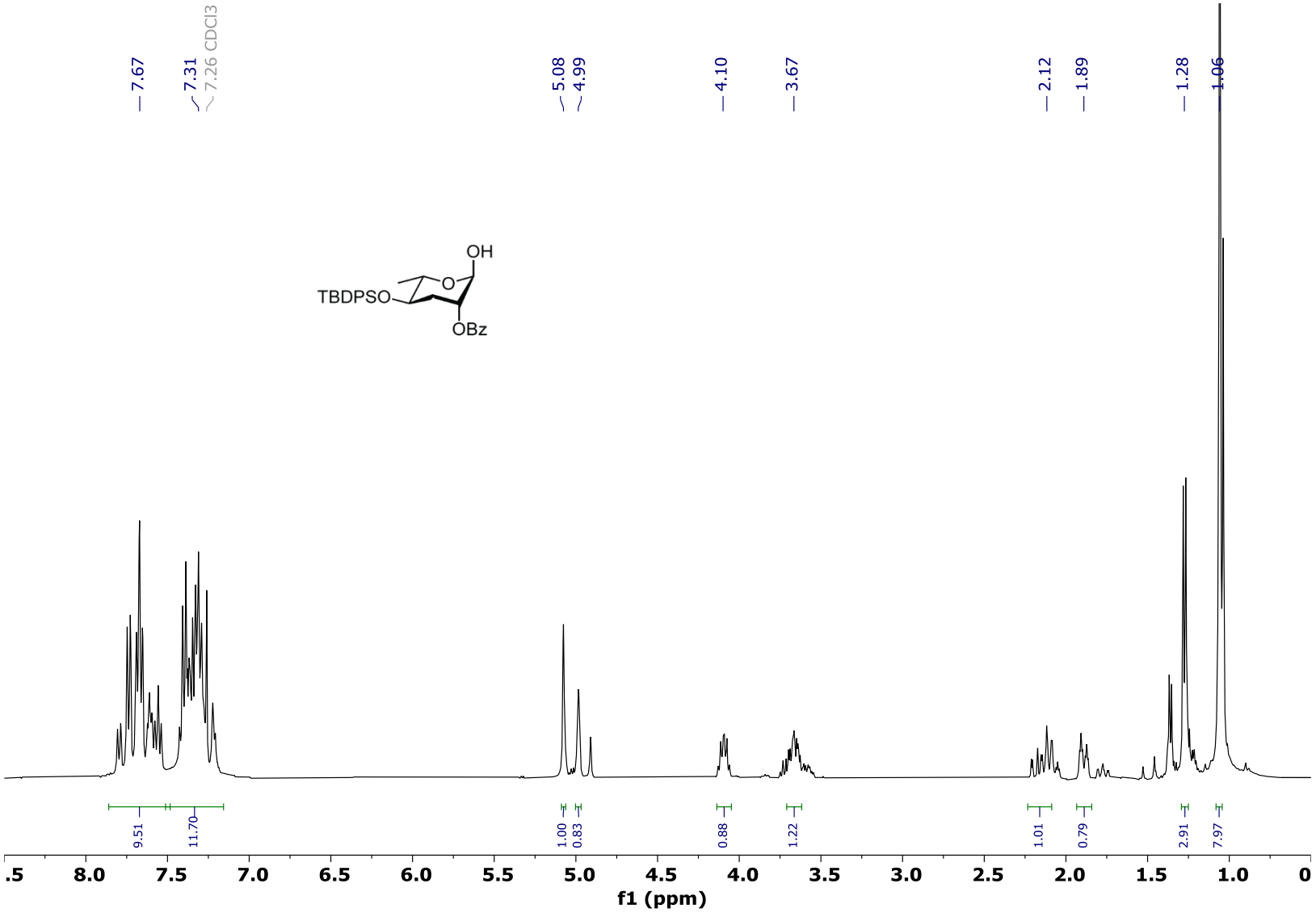

Figure S30: ^{1}H NMR (600 MHz, $CDCl_3$) of 2-*O*-benzoyl-4-*O*-benzyl 3,6-dideoxy-α-L-*arabino*-hexose (**16b**).

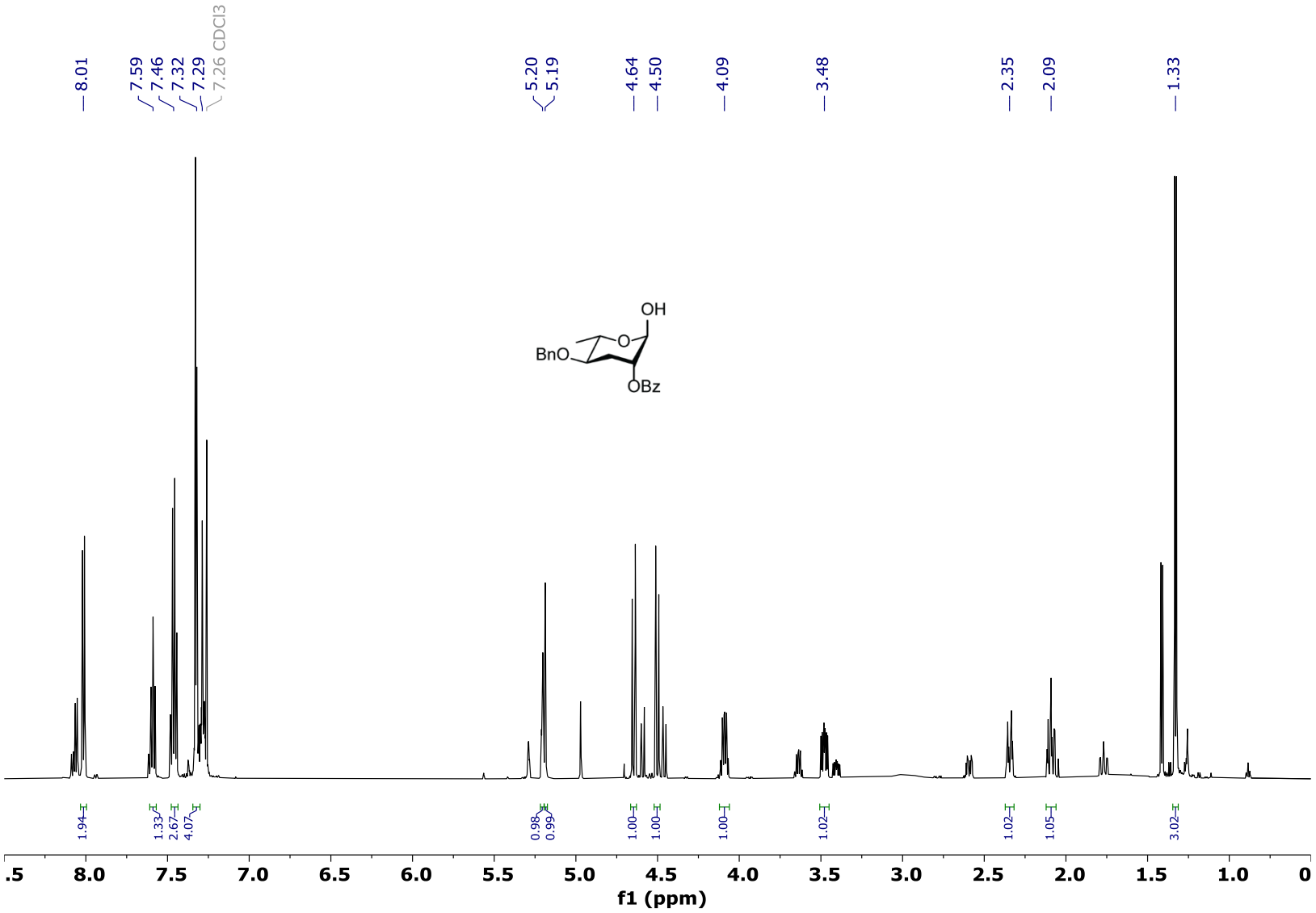

Figure S31: ^{13}C NMR (150 MHz, $CDCl_3$) of 2-*O*-benzoyl-4-*O*-benzyl 3,6-dideoxy-α-L-*arabino*-hexose (**16b**).

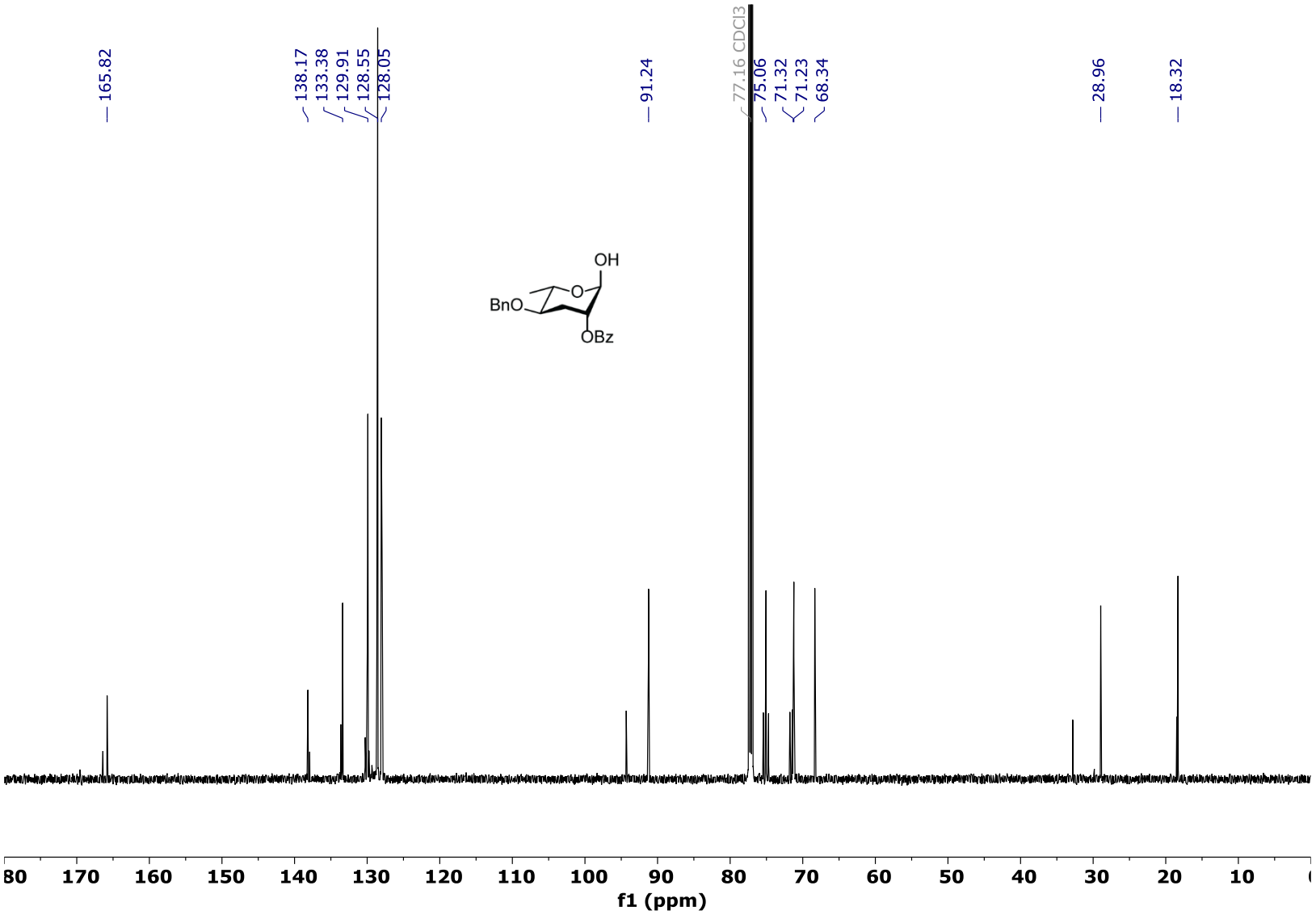

Figure S32: dqf-COSY (600 MHz, $CDCl_3$) of 2-*O*-benzoyl-4-*O*-benzyl 3,6-dideoxy-α-L-*arabino*-hexose (**16b**).

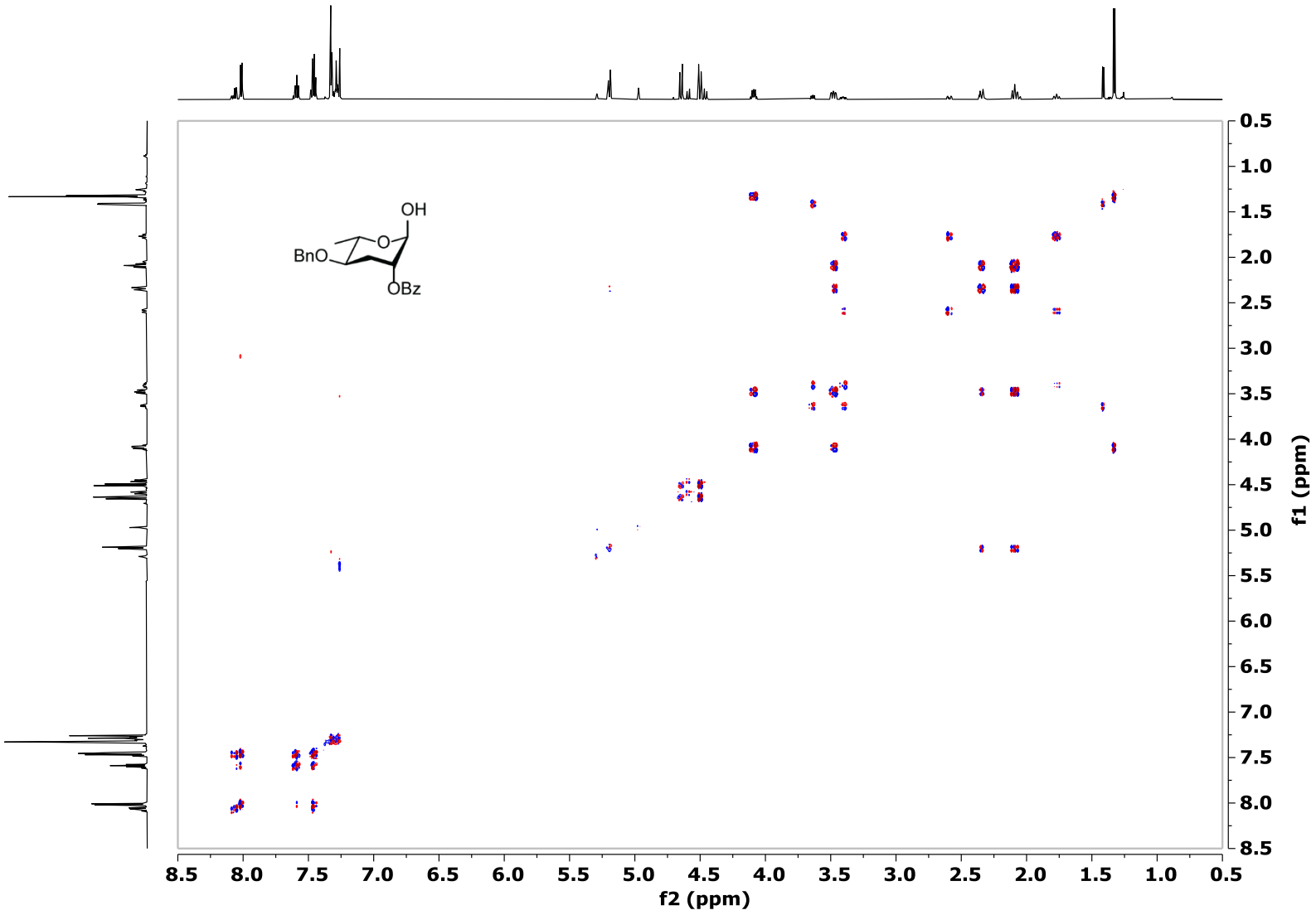

Figure S33: HSQC (600 MHz, $CDCl_3$) of 2-*O*-benzoyl-4-*O*-benzyl 3,6-dideoxy-α-L-*arabino*-hexose (**16b**).

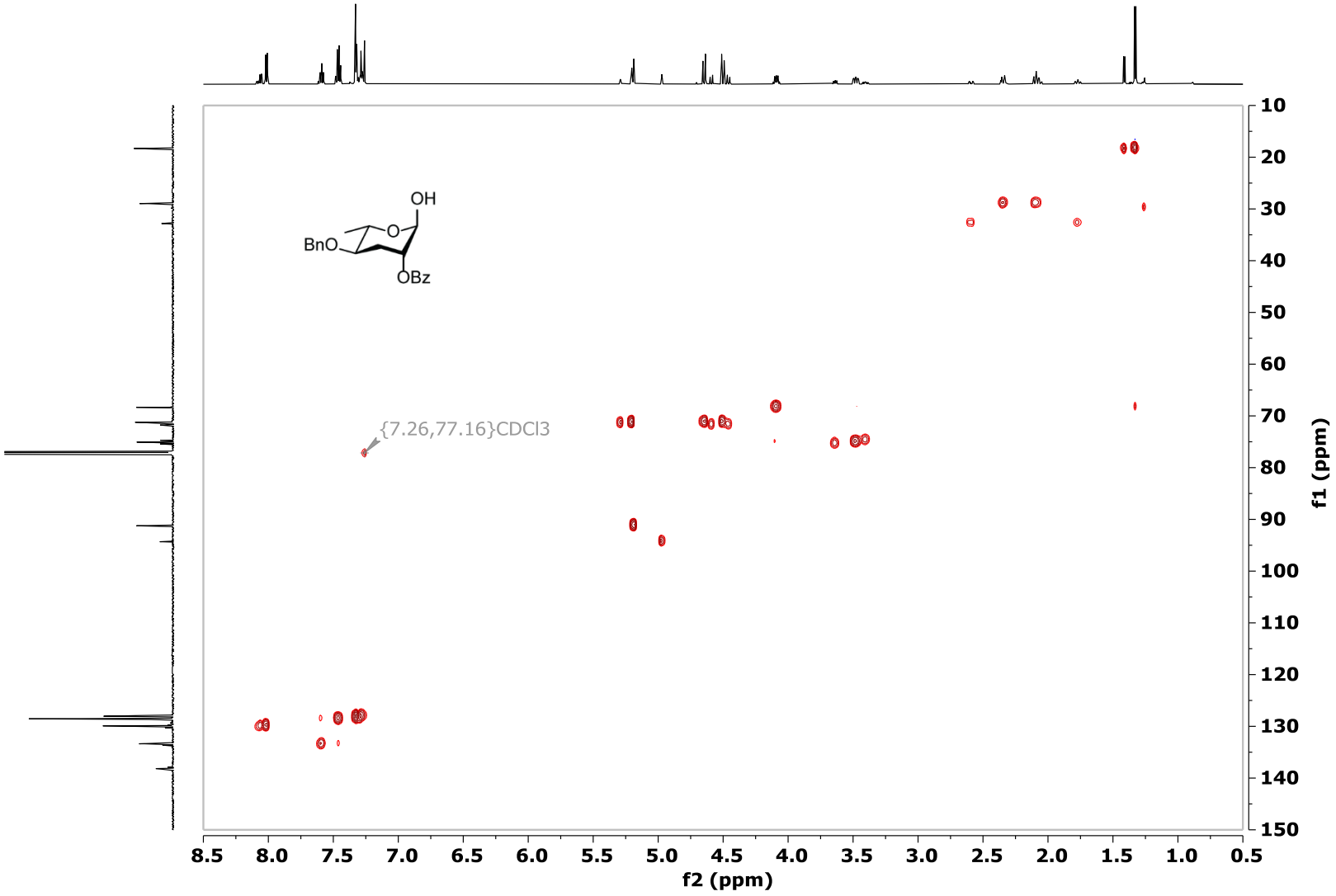

Figure S34: ^{1}H NMR (600 MHz, $CDCl_3$) of 2-*O*-benzoyl-4-*O*-allyl 3,6-dideoxy-α-L-*arabino*-hexose (**16c**).

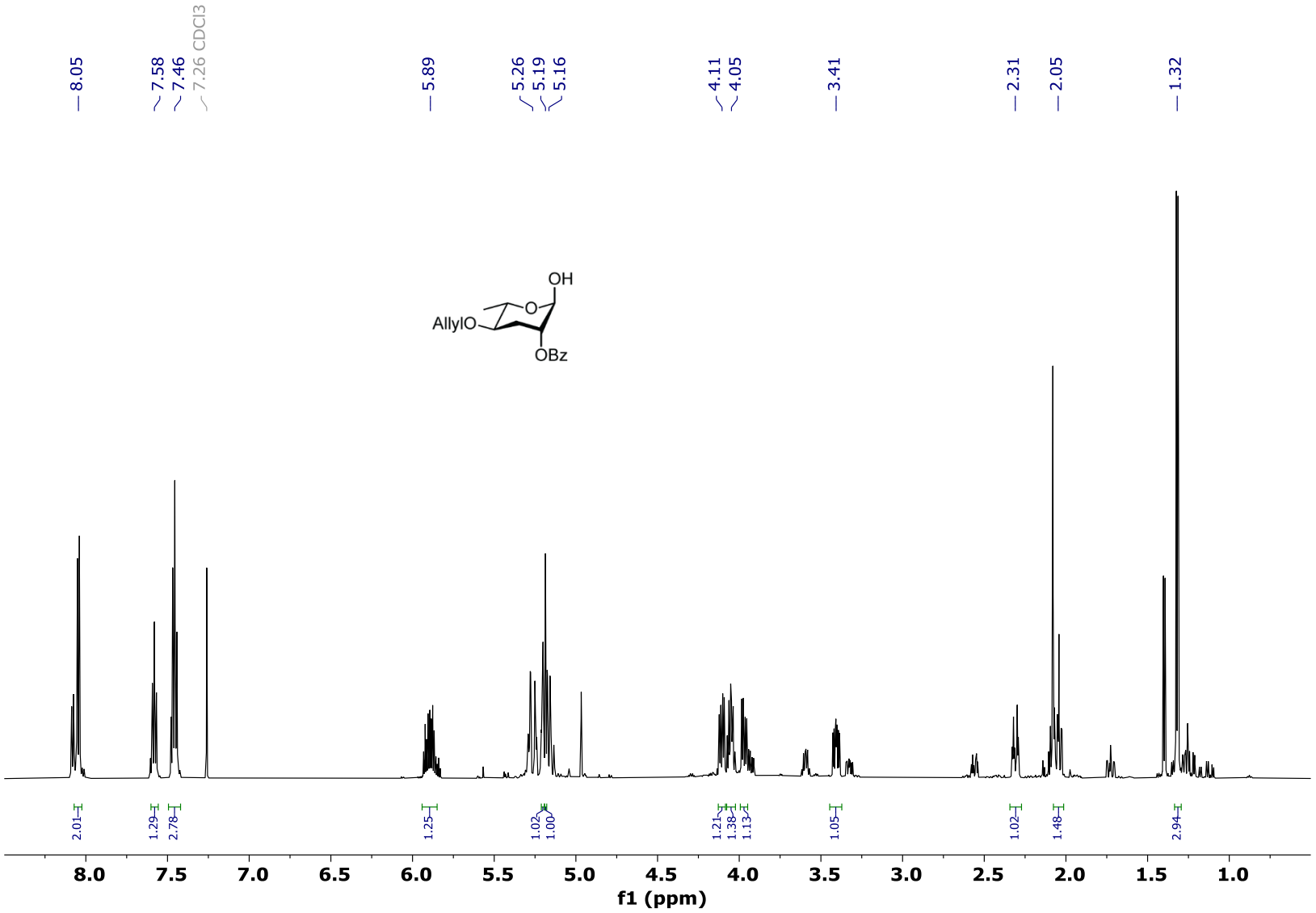

Figure S35: ^{13}C NMR (150 MHz, $CDCl_3$) of 2-*O*-benzoyl-4-*O*-allyl 3,6-dideoxy-α-L-*arabino*-hexose (**16c**).

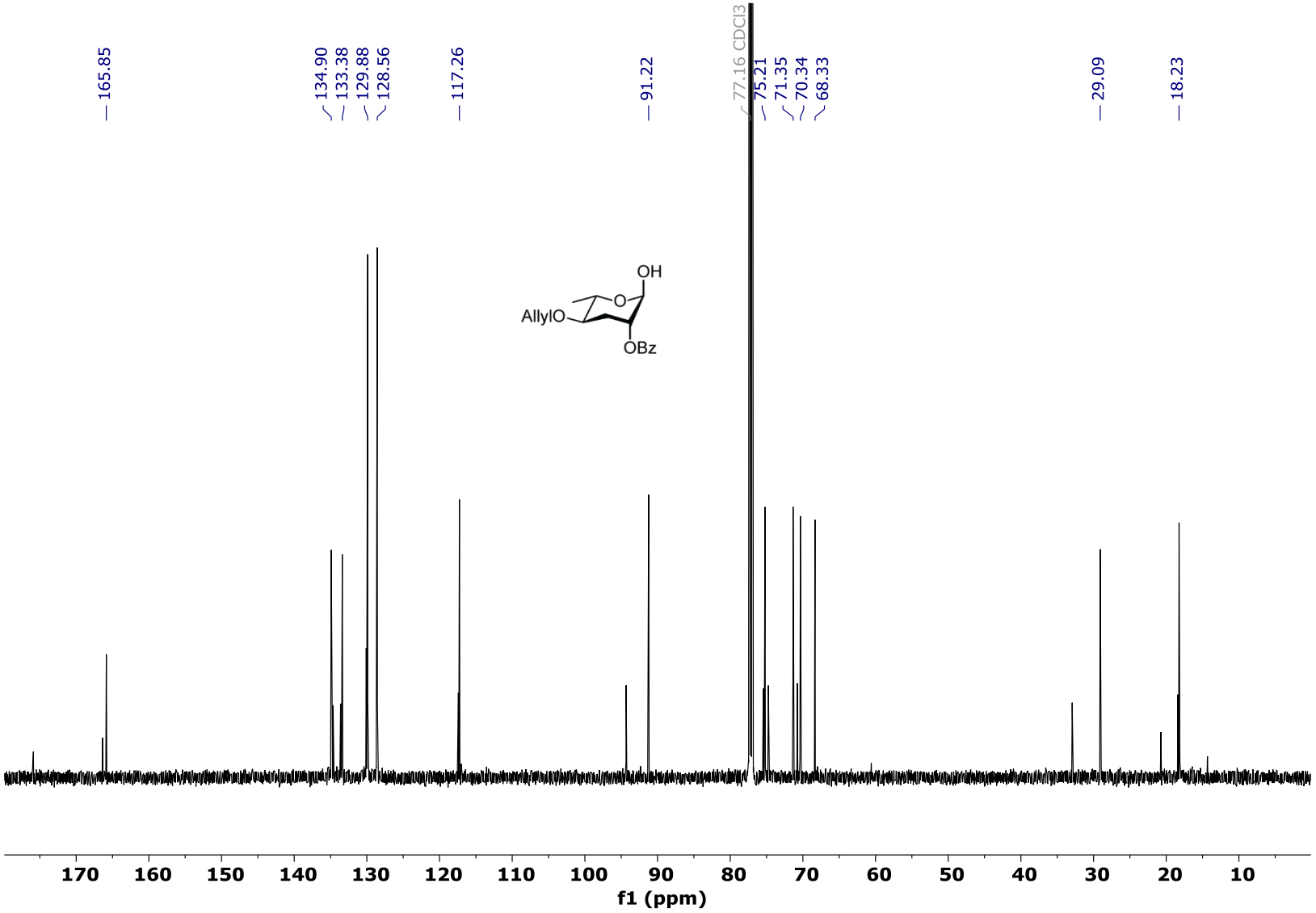

Figure S36: dqf-COSY (600 MHz, $CDCl_3$) of 2-*O*-benzoyl-4-*O*-allyl 3,6-dideoxy-α-L-*arabino*-hexose (**16c**).

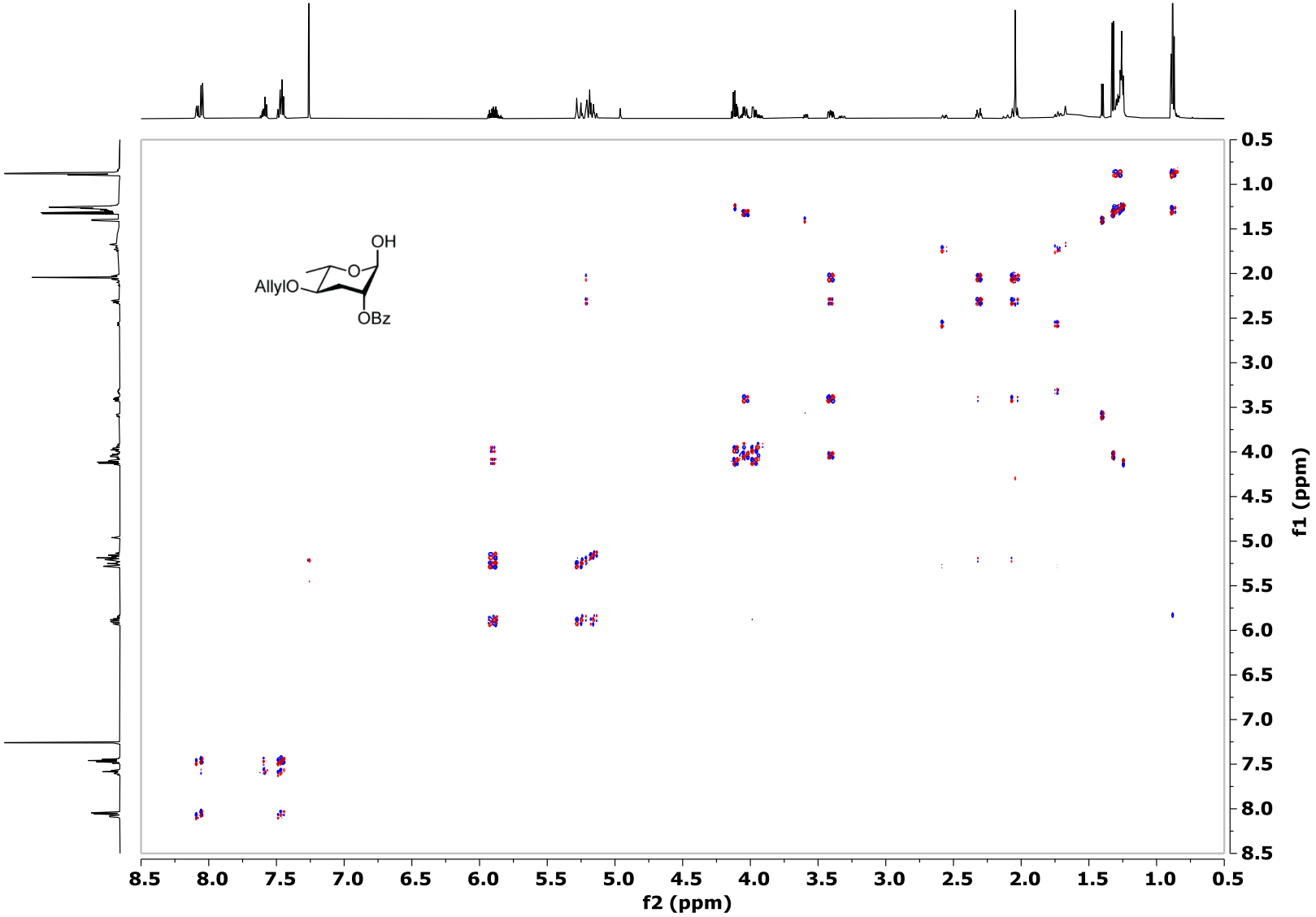

Figure S37: HSQC (600 MHz, $CDCl_3$) of 2-*O*-benzoyl-4-*O*-allyl 3,6-dideoxy-α-L-*arabino*-hexose (**16c**).

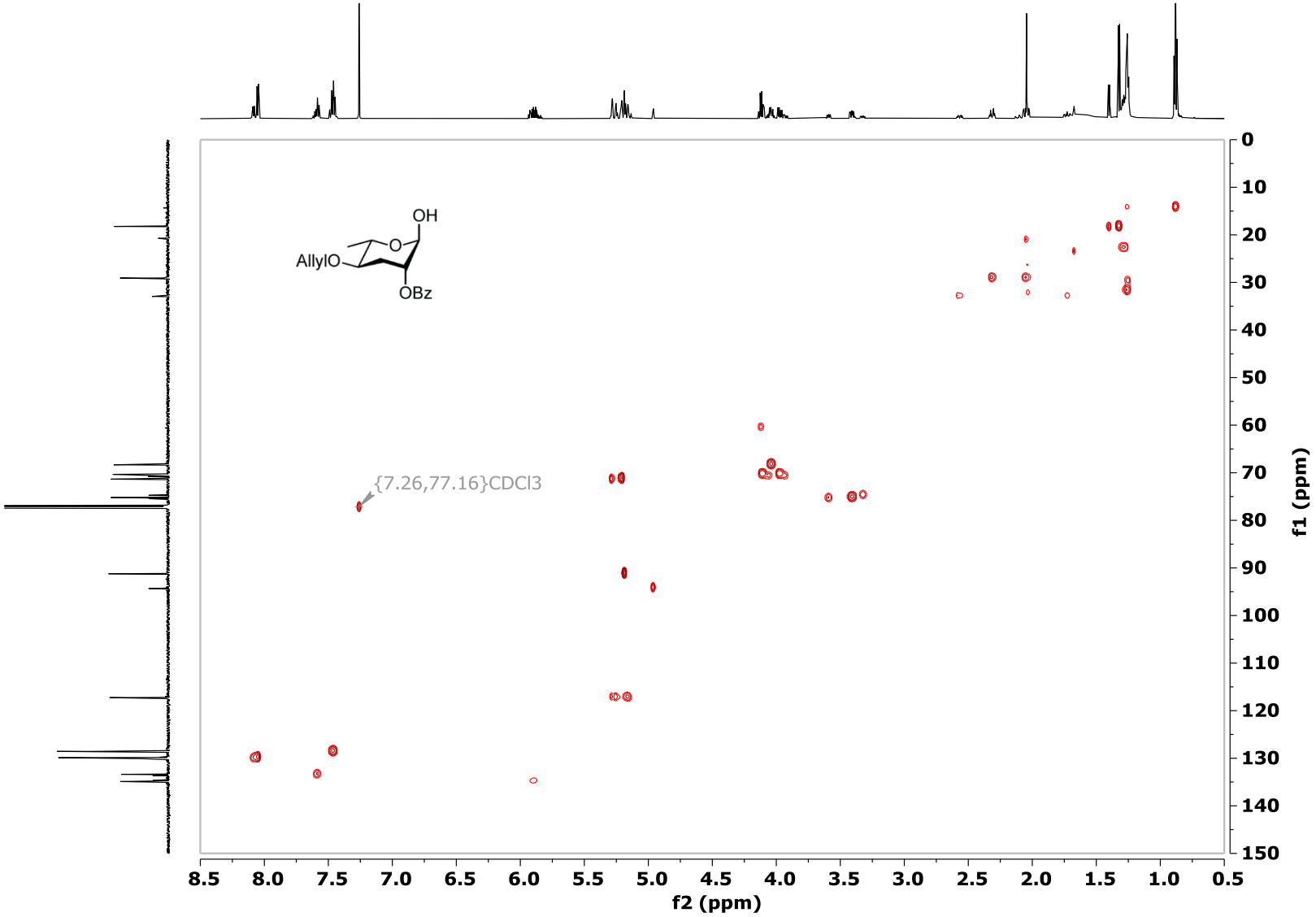

Figure S38: ^{1}H NMR (600 MHz, $CDCl_3$) of 1-*O*-methyl-6-deoxy-2,3-(*O*-benzylidene)-α-L-*arabino*-hexopyranoside (**17**).

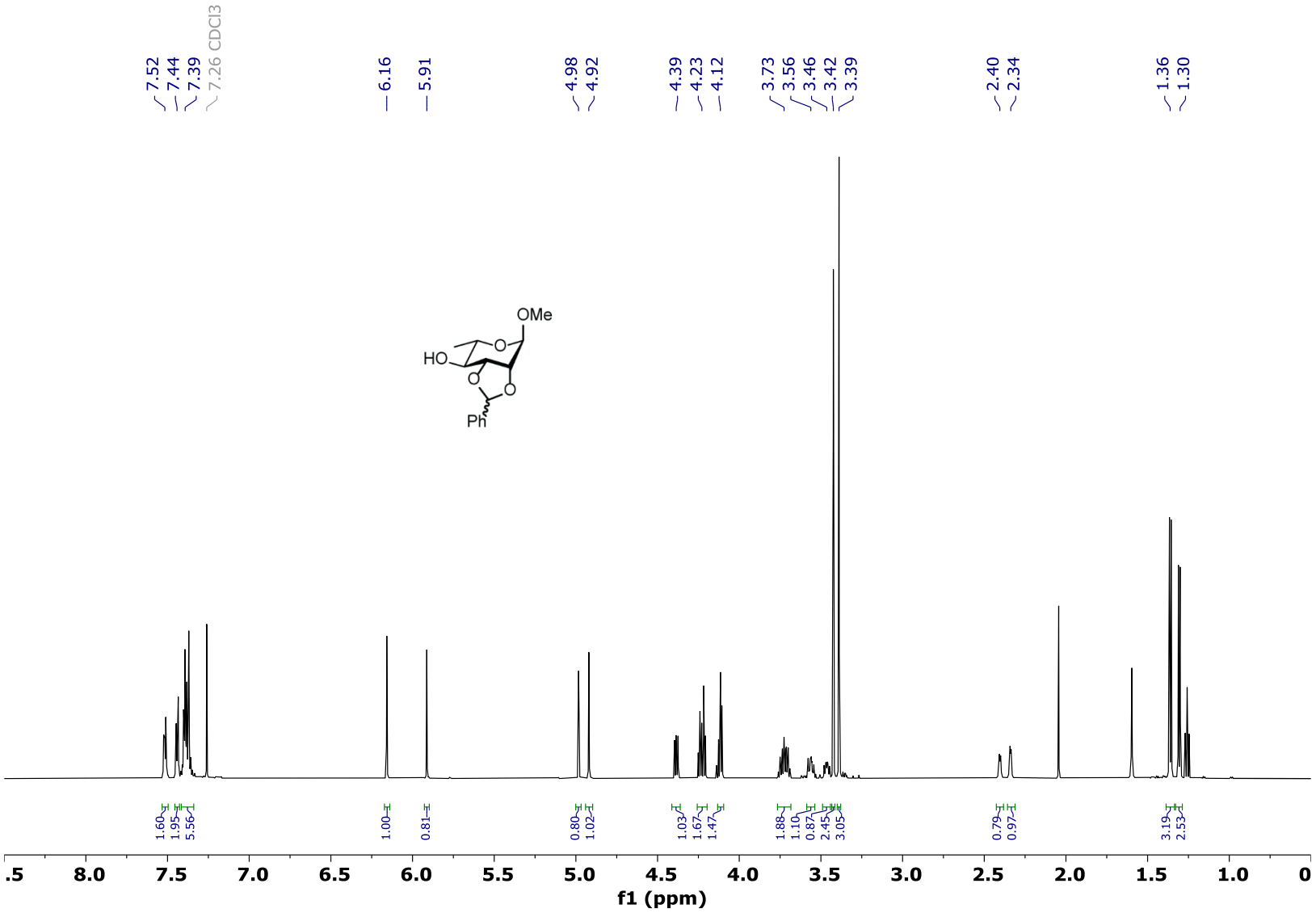

Figure S39: ^{13}C NMR (150 MHz, $CDCl_3$) of 1-*O*-methyl-6-deoxy-2,3-(*O*-benzylidene)-α-L-*arabino*-hexopyranoside (**17**).

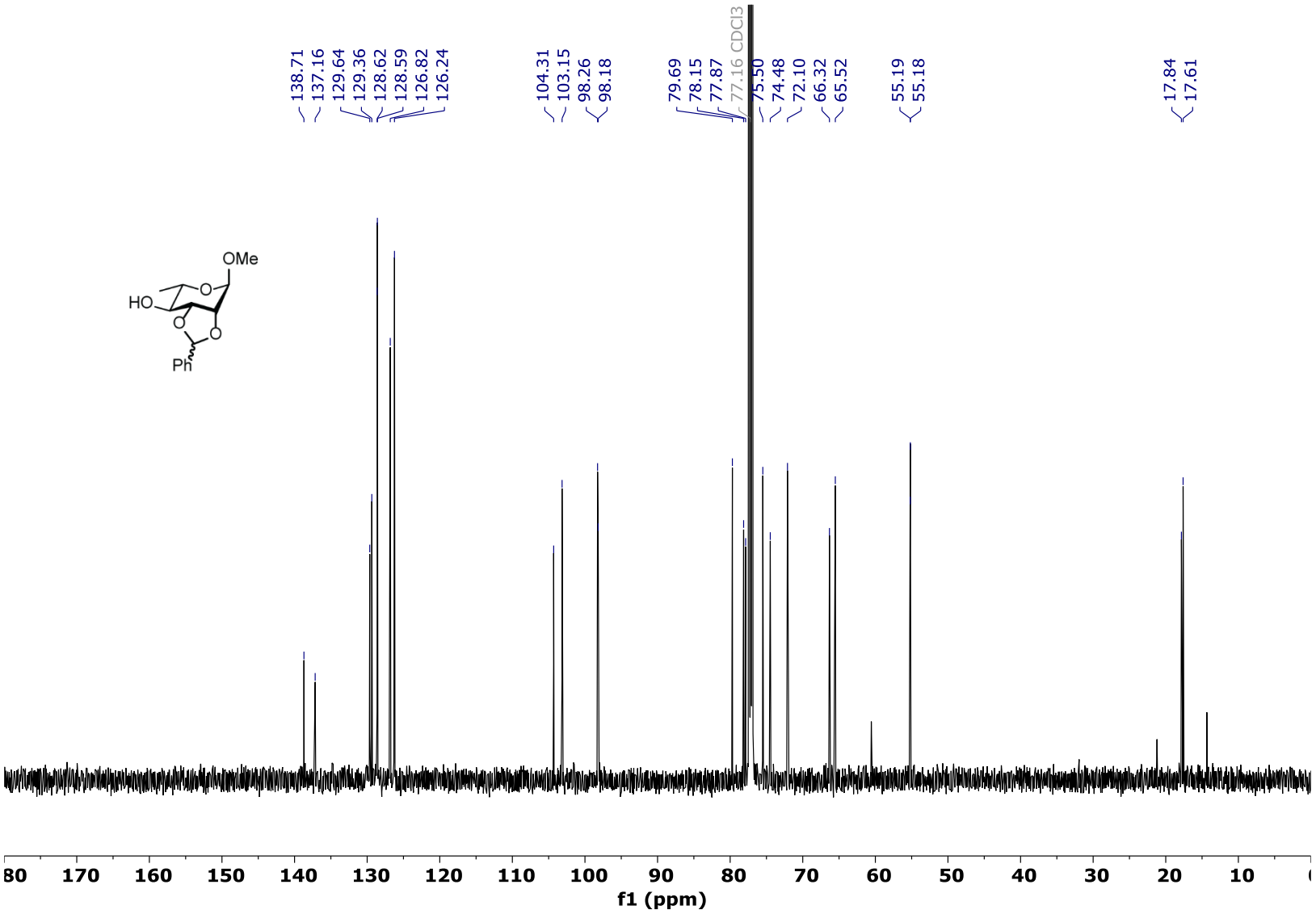

Figure S40: dqf-COSY (600 MHz, $CDCl_3$) of 1-*O*-methyl-6-deoxy-2,3-(*O*-benzylidene)-α-L-*arabino*-hexopyranoside (**17**).

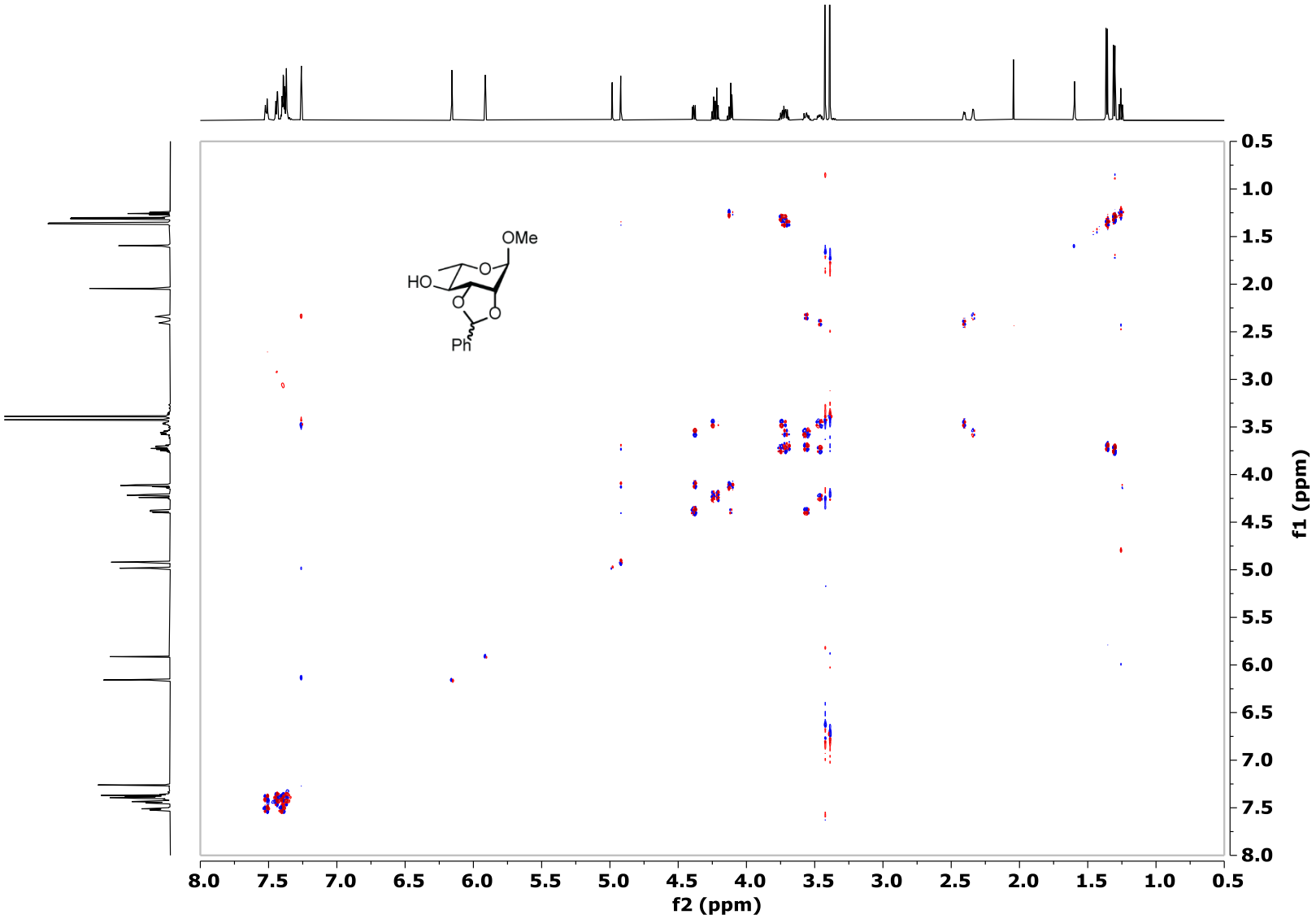

Figure S41: HSQC (600 MHz, $CDCl_3$) of 1-*O*-methyl-6-deoxy-2,3-(*O*-benzylidene)-α-L-*arabino*-hexopyranoside (**17**).

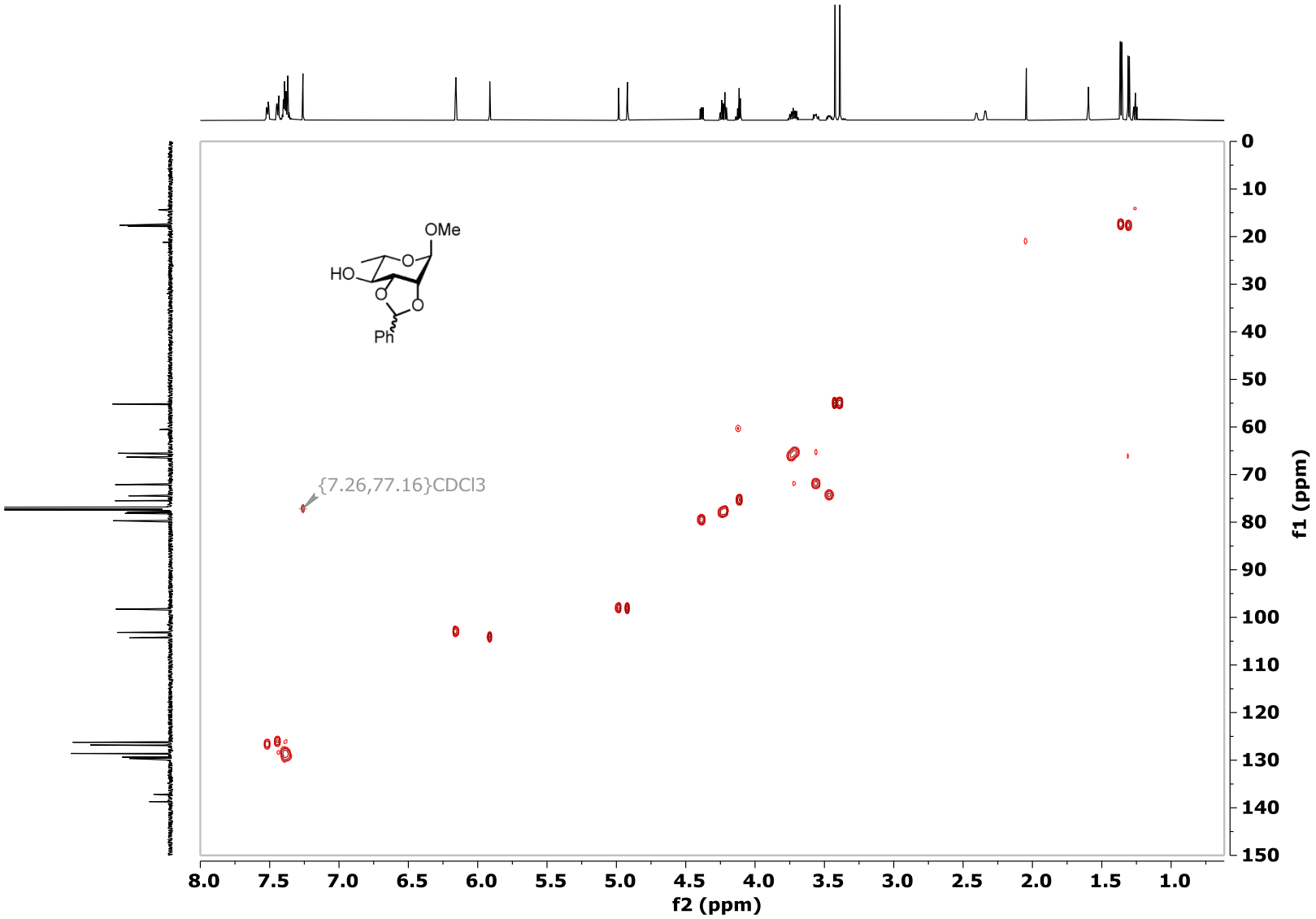

Figure S42: ^{1}H NMR (600 MHz, $CDCl_3$) of 1-*O*-methyl-2-*O*-benzoyl-3-bromo-3,6-dideoxy-*altro*-hexopyranoside (**18**).

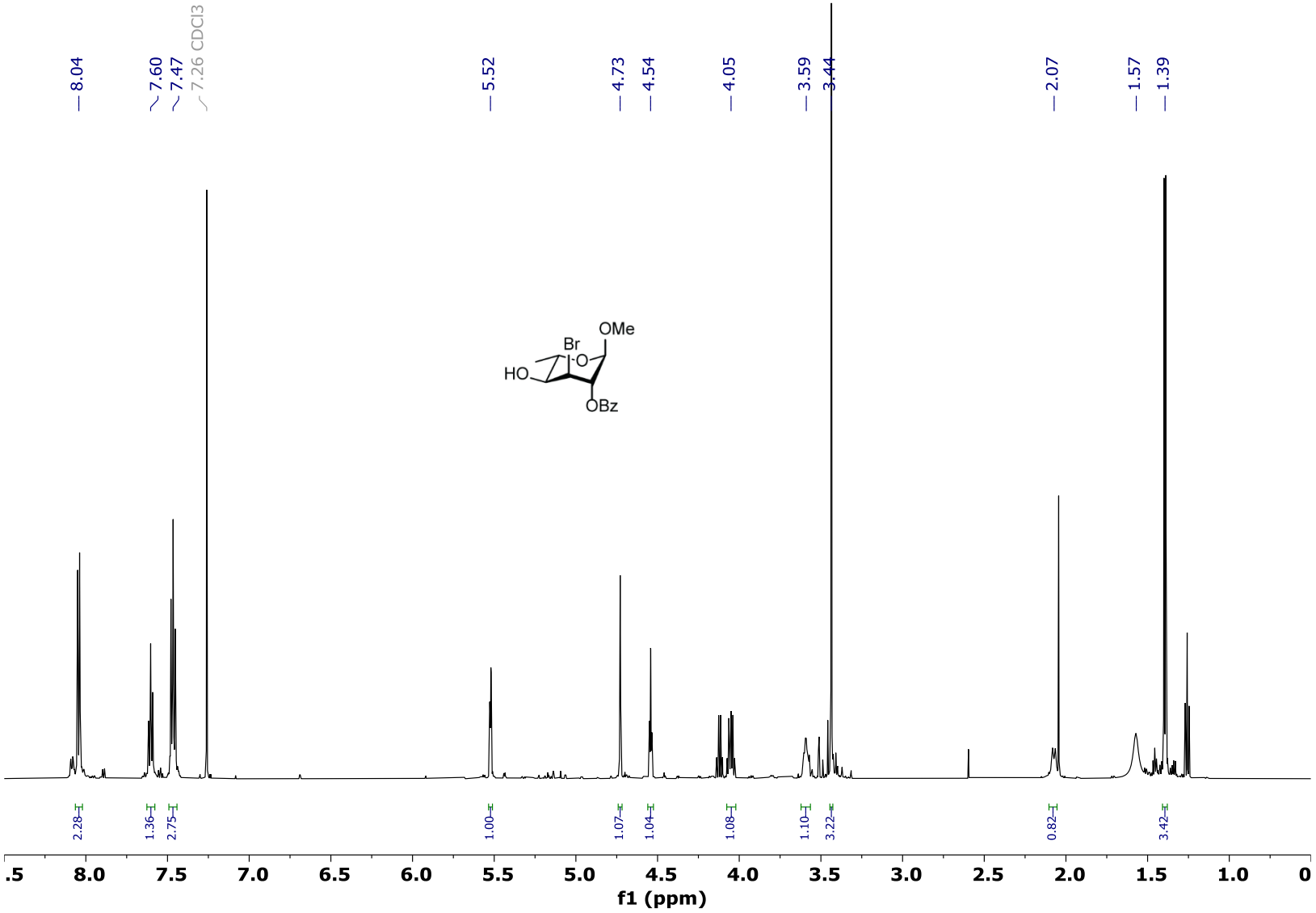

Figure S43: ^{13}C NMR (150 MHz, $CDCl_3$) of 1-*O*-methyl-2-*O*-benzoyl-3-bromo-3,6-dideoxy-*altro*-hexopyranoside (**18**).

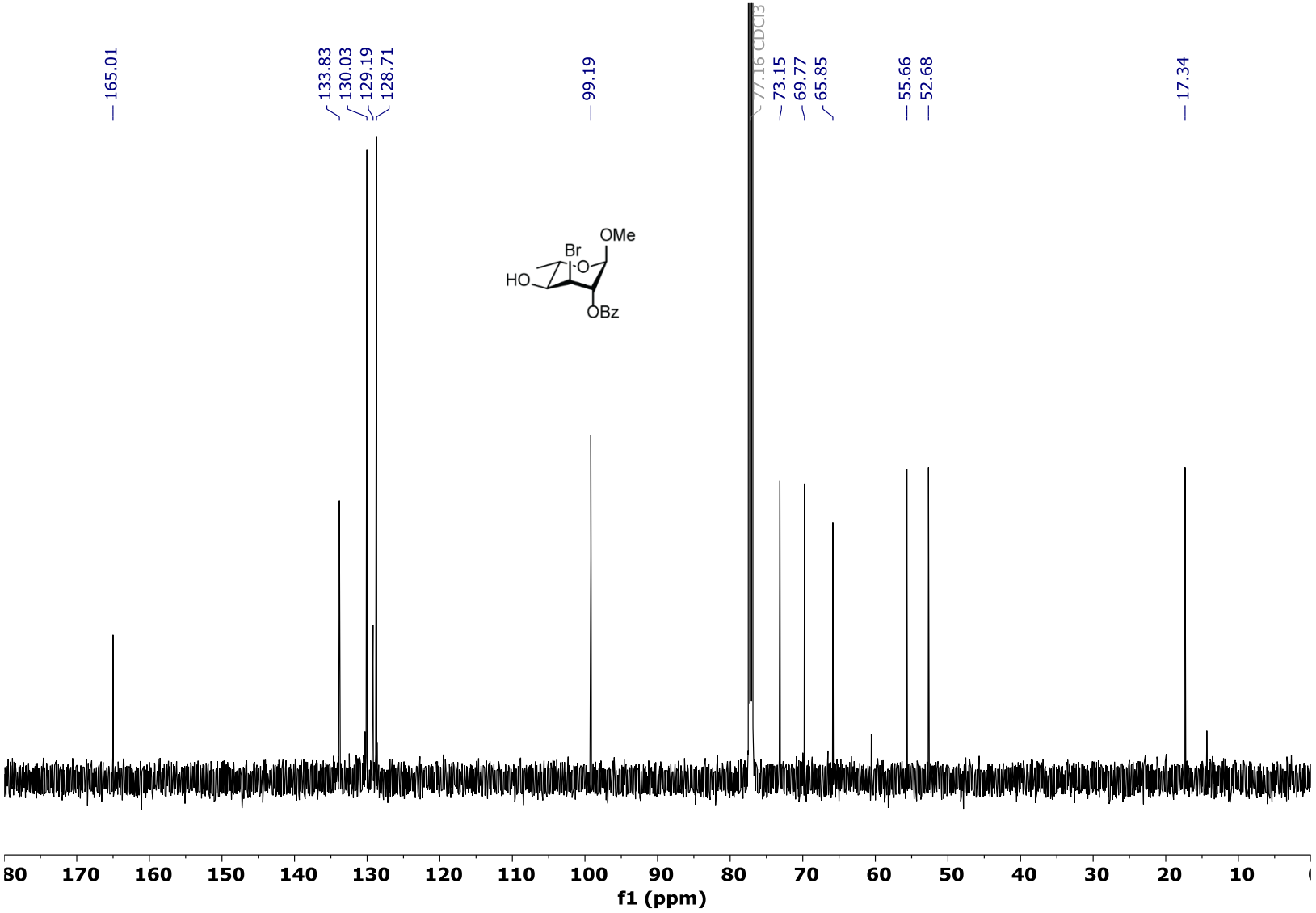

Figure S44: dqf-COSY (600 MHz, $CDCl_3$) of 1-*O*-methyl-2-*O*-benzoyl-3-bromo-3,6-dideoxy-*altro*-hexopyranoside (**18**).

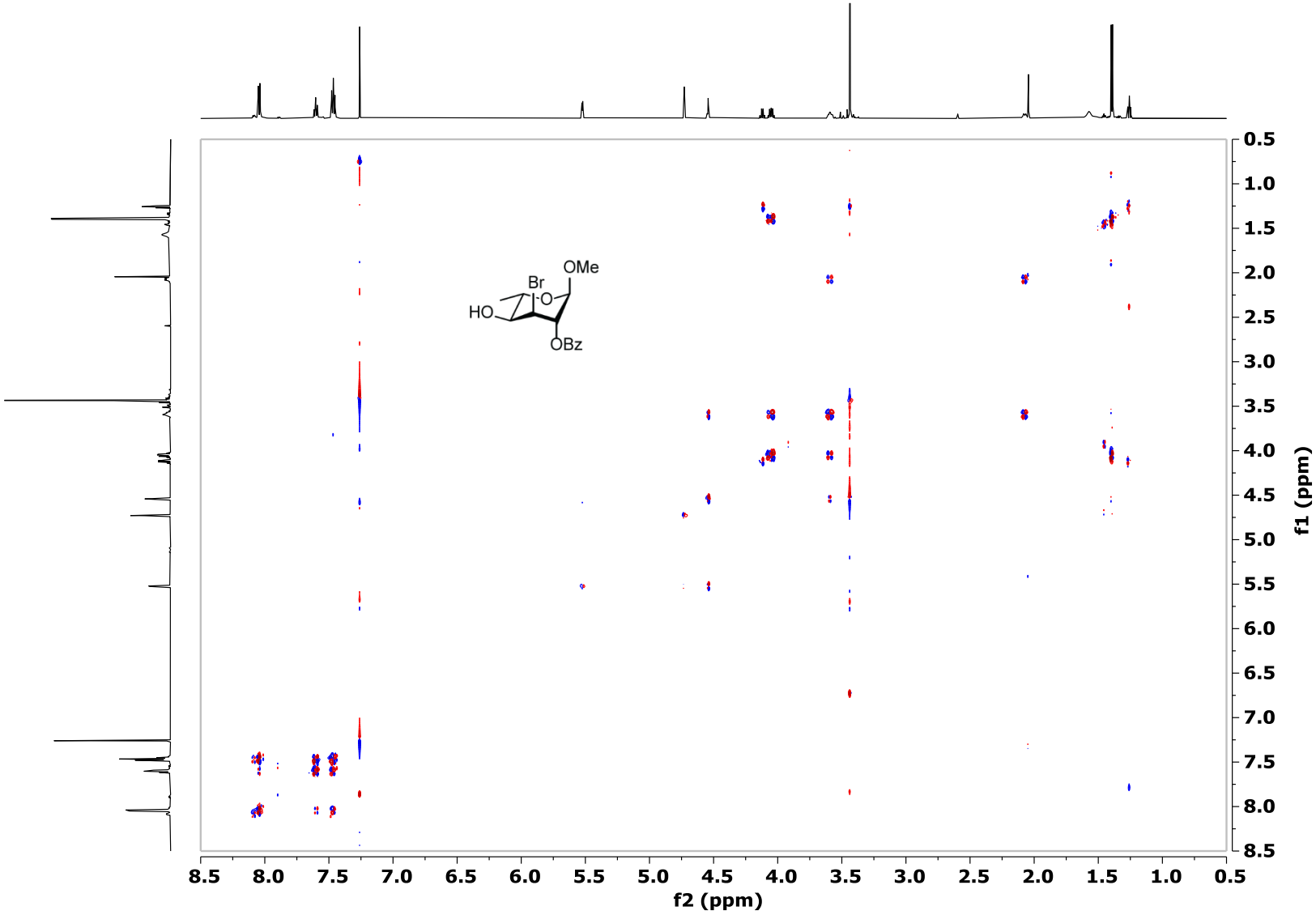

Figure S45: HSQC of (600 MHz, $CDCl_3$) of 1-*O*-methyl-2-*O*-benzoyl-3-bromo-3,6-dideoxy-*altro*-hexopyranoside (**18**).

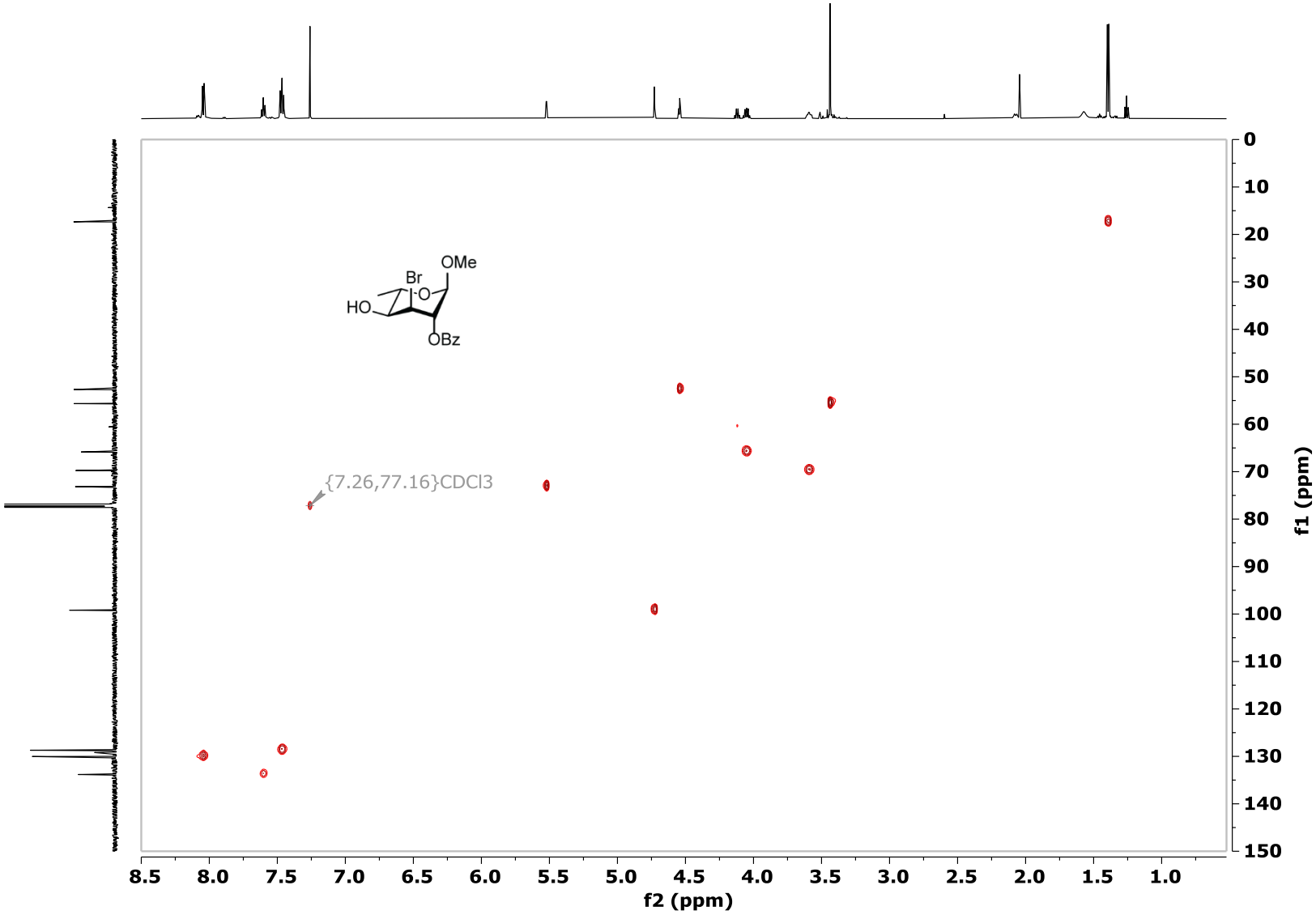

Figure S46: ^{1}H NMR (600 MHz, $CDCl_3$) of 1-*O*-methyl-2-*O*-benzoyl 3,6-dideoxy-α-L-*arabino*-hexopyranoside (**19**).

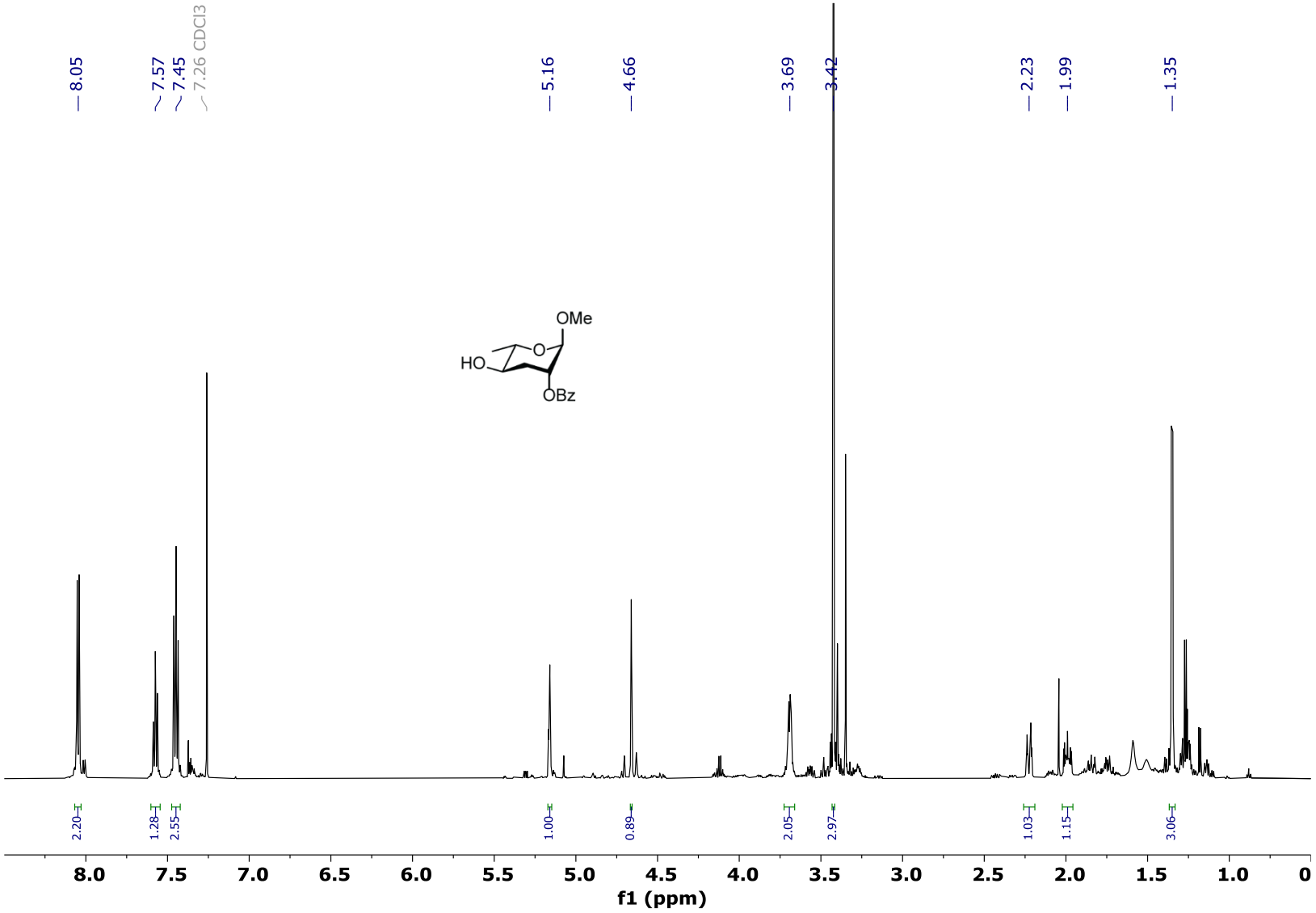

Figure S47: ^{13}C NMR (150 MHz, $CDCl_3$) of 1-*O*-methyl-2-*O*-benzoyl 3,6-dideoxy-α-L-*arabino*-hexopyranoside (**19**).

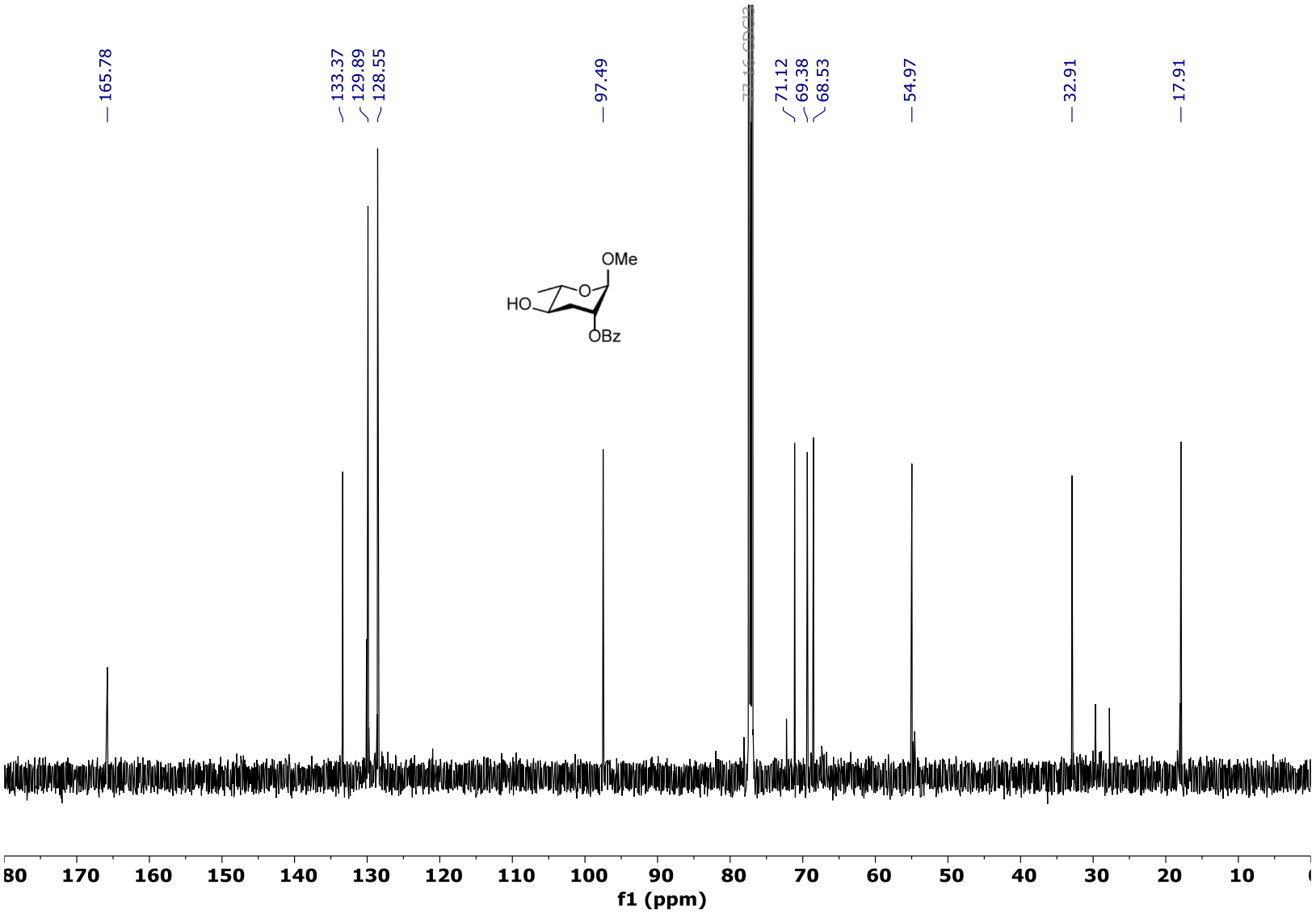

Figure S48: dqf-COSY (600 MHz, $CDCl_3$) of 1-*O*-methyl-2-*O*-benzoyl 3,6-dideoxy-α-L-*arabino*-hexopyranoside (**19**).

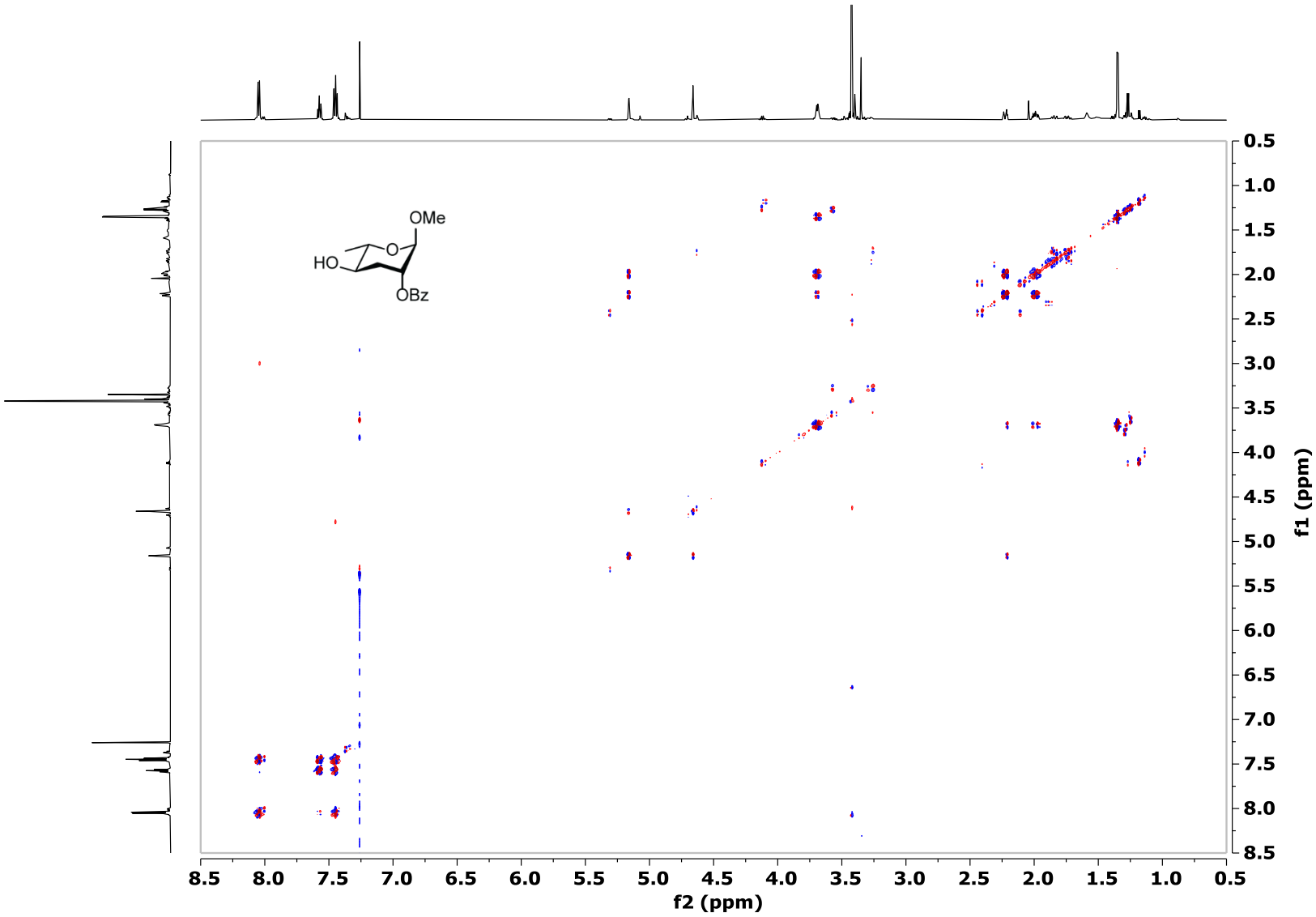

Figure S49: HSQC (600 MHz, $CDCl_3$) of 1-*O*-methyl-2-*O*-benzoyl 3,6-dideoxy-α-L-*arabino*-hexopyranoside (**19**).

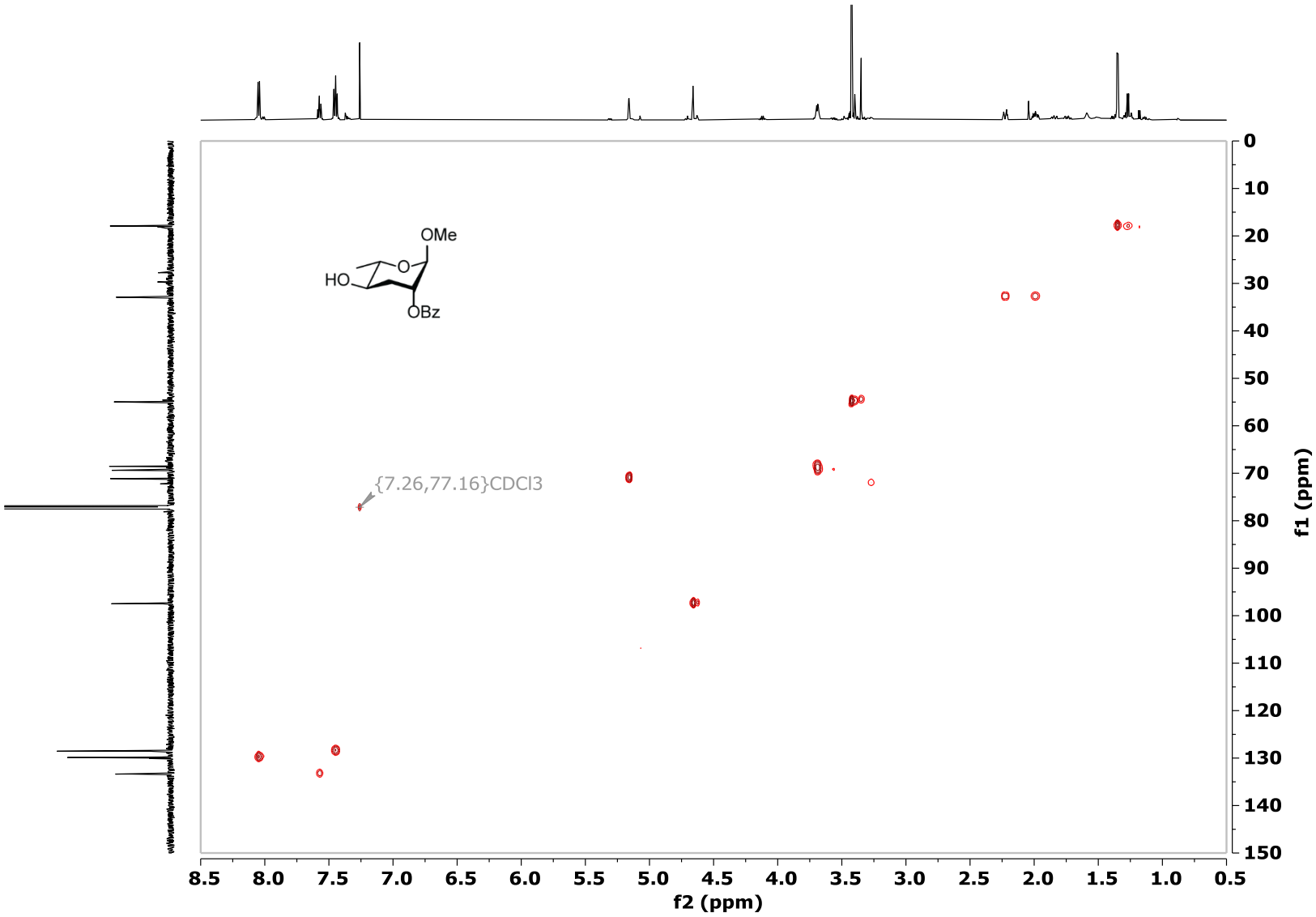

Figure S50: ^{1}H NMR (400 MHz, $CDCl_3$) of (5*R*)-5-[(2'-*O*-benzoyl-4'-*O*-*tert*-butyldiphenylsilyl-3',6'-dideoxy-α-L-*arabino*-hexopyranosyl)oxy]-1-hexene (**20**).

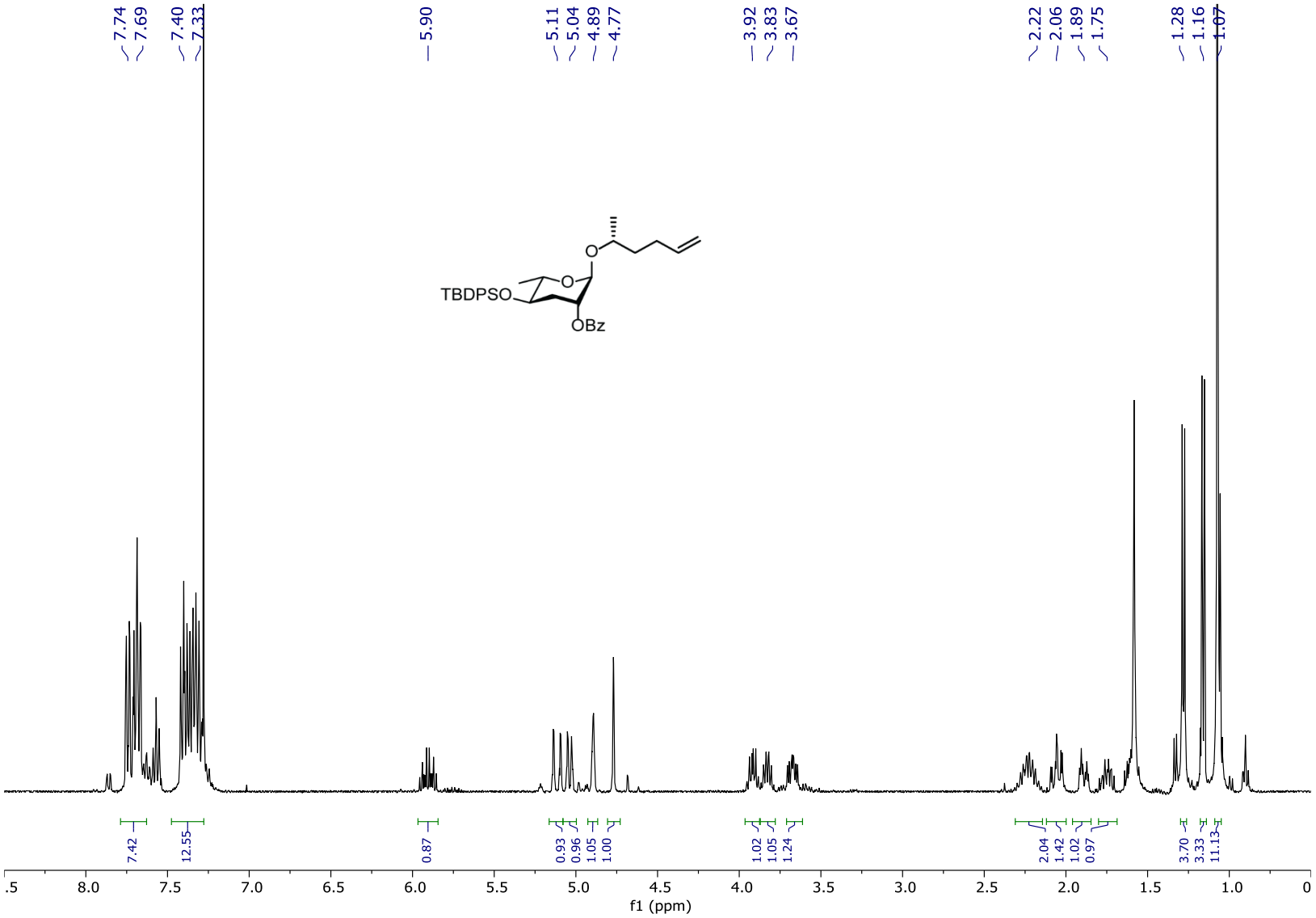

Figure S51: ^{1}H NMR (400 MHz, $CDCl_3$) of (4*R*)-4-[(2'-*O*-benzoyl-4'-*O*-*tert*-butyldiphenylsilyl-3',6'-dideoxy-L-*arabino*-hexopyranosyl)oxy]-pentanoic acid (**21**).

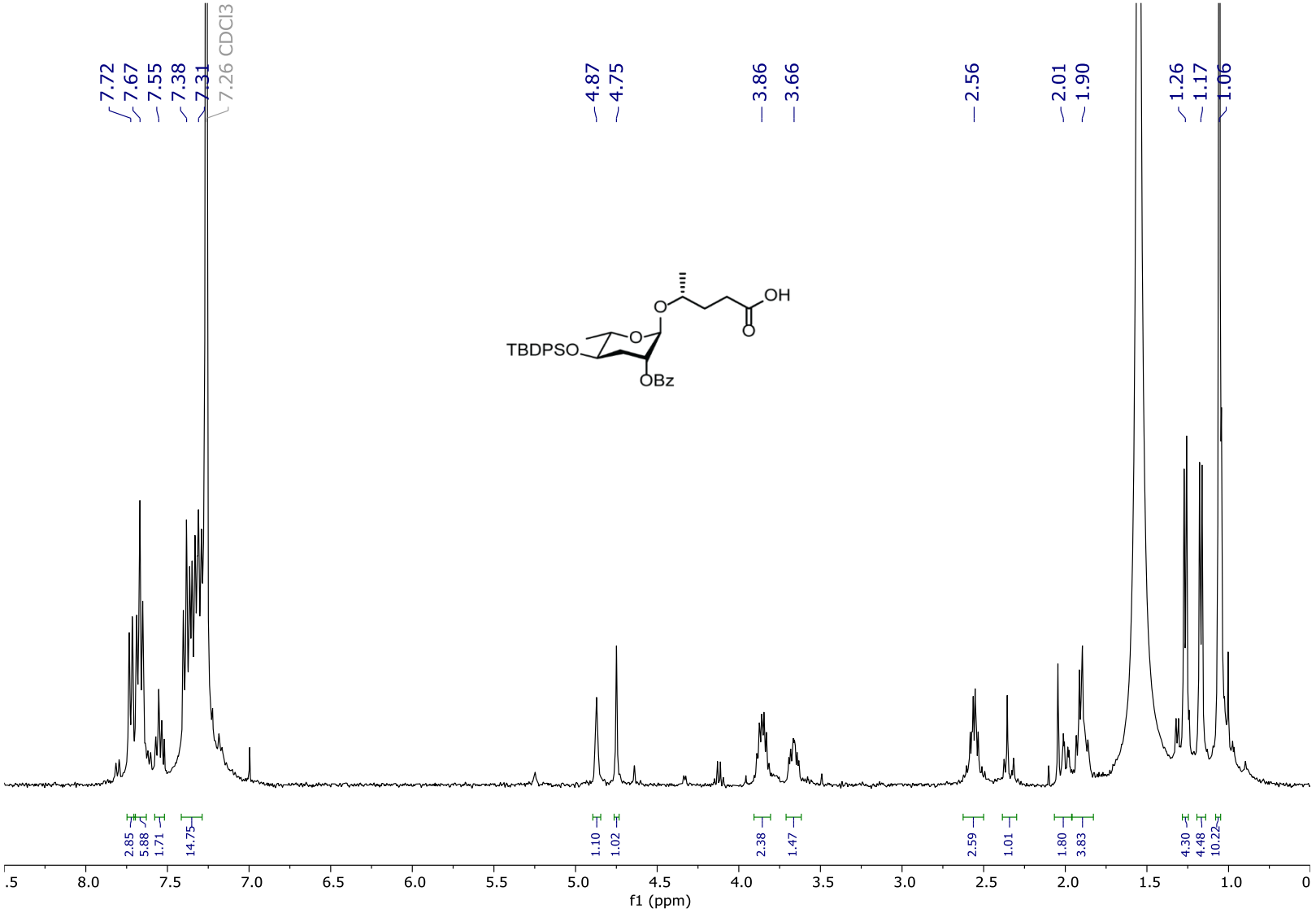

Figure S52: ^{13}C NMR (100 MHz, $CDCl_3$) of (4*R*)-4-[(2'-*O*-benzoyl-4'-*O*-*tert*-butyldiphenylsilyl-3',6'-dideoxy-L-*arabino*-hexopyranosyl)oxy]-pentanoic acid (**21**).

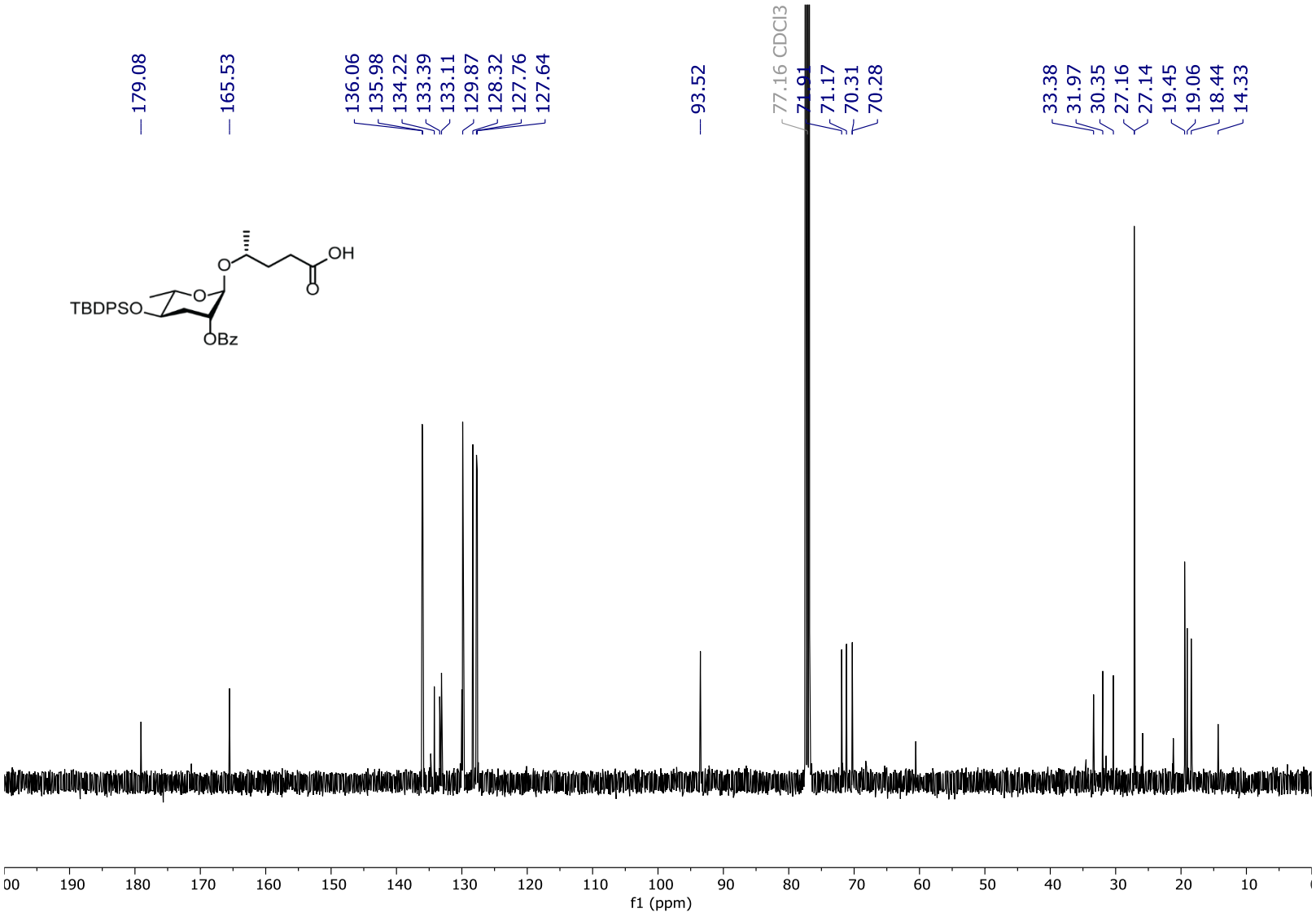

Figure S53: ^{1}H NMR (400 MHz, $CDCl_3$) of (4*R*)-4-[(4'-*O*-*tert*-butyldiphenylsilyl-3',6'-dideoxy-L-*arabino*-hexopyranosyl)oxy]-pentanoic acid (**22**).

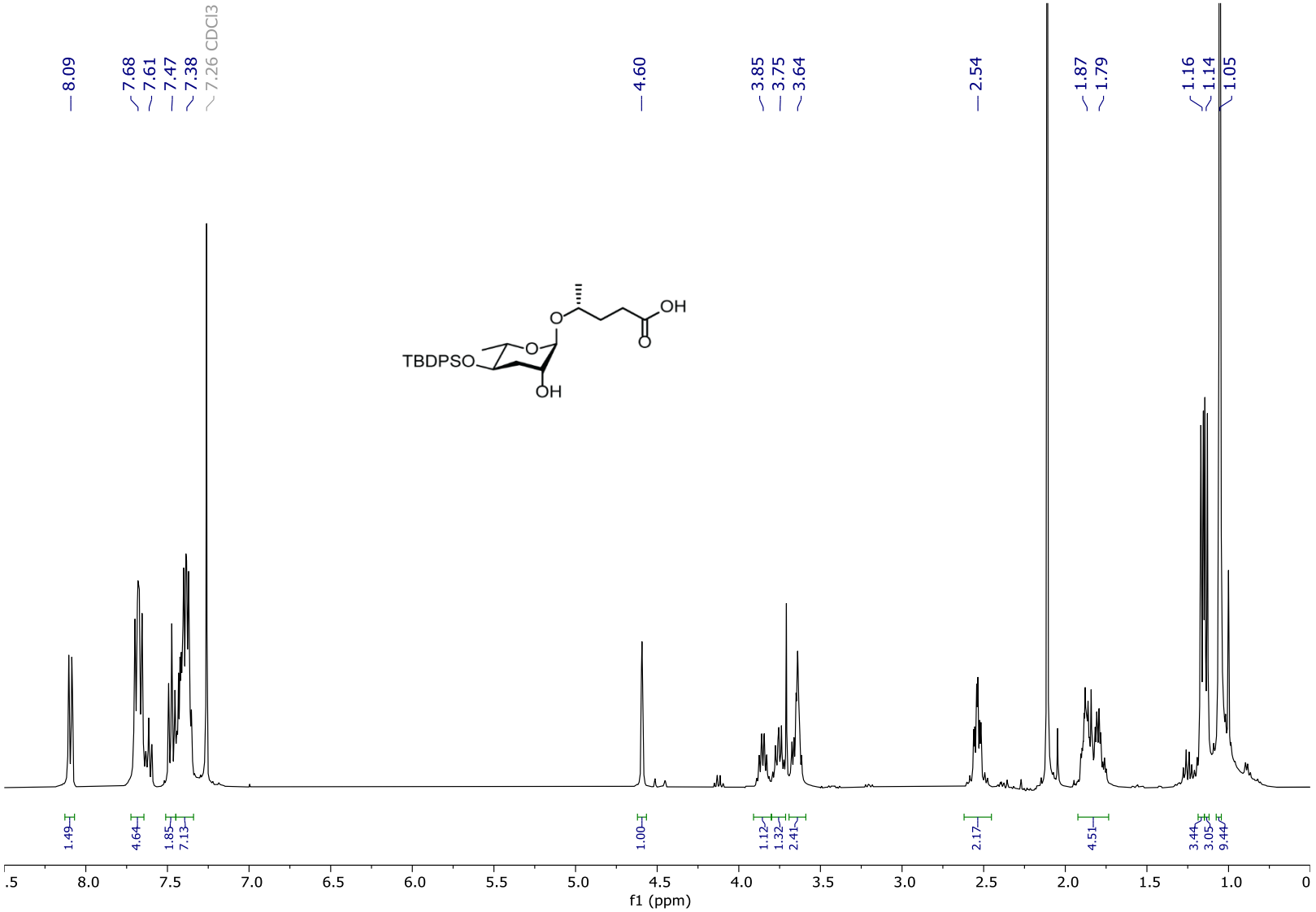

Figure S54: ^{1}H NMR (400 MHz, $CDCl_3$) of benzyl (4*R*)-4-[(2'-*O*-benzyl-4'-*O*-*tert*-butyldiphenylsilyl-3',6'-dideoxy-L-*arabino*-hexopyranosyl)oxy]-pentanoate (**23**).

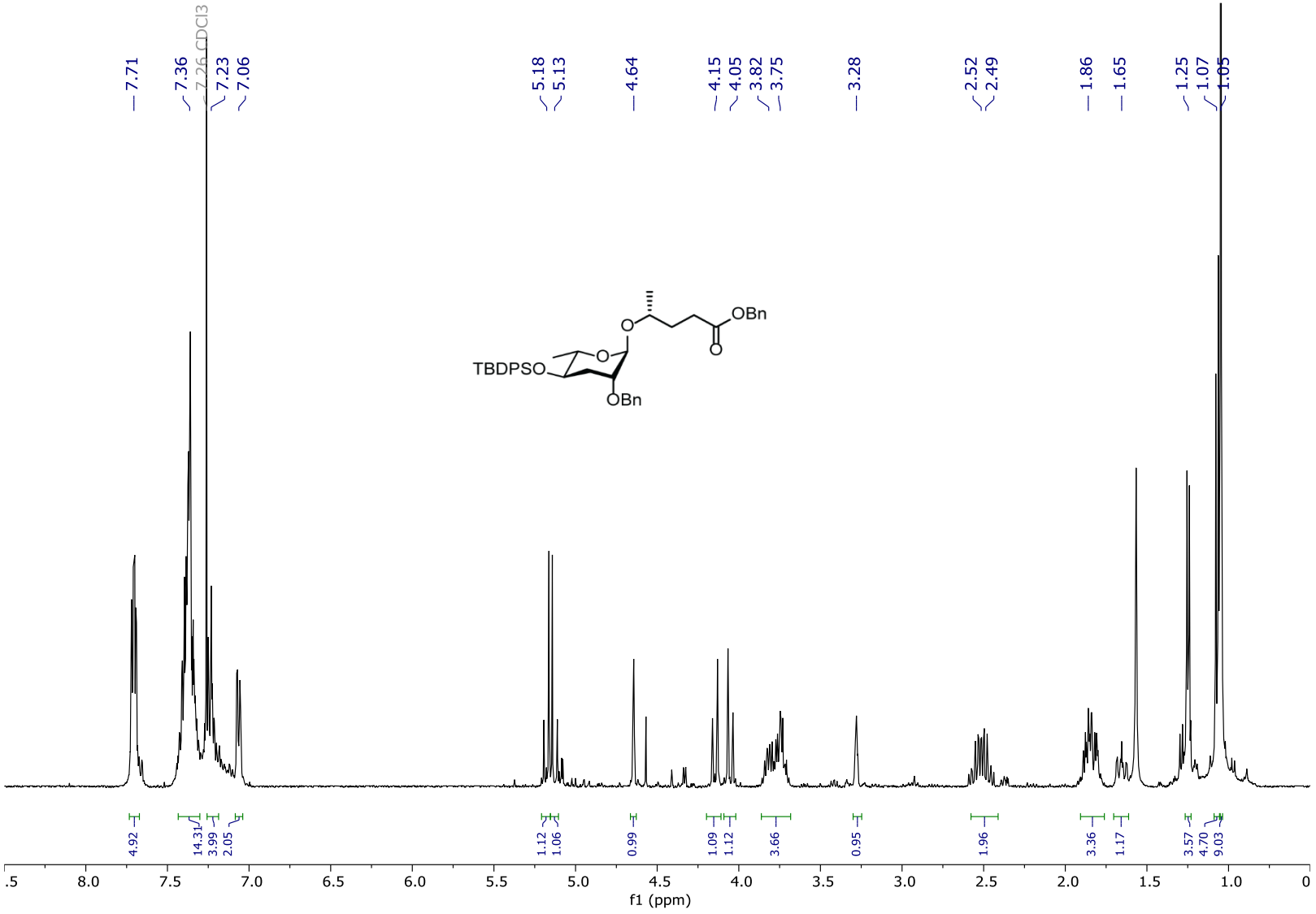

Figure S56: ^{13}C NMR (100 MHz, $CDCl_3$) of benzyl (4*R*)-4-[(2'-*O*-benzyl-4'-*O*-*tert*-butyldiphenylsilyl-3',6'-dideoxy-L-*arabino*-hexopyranosyl)oxy]-pentanoate (**23**).

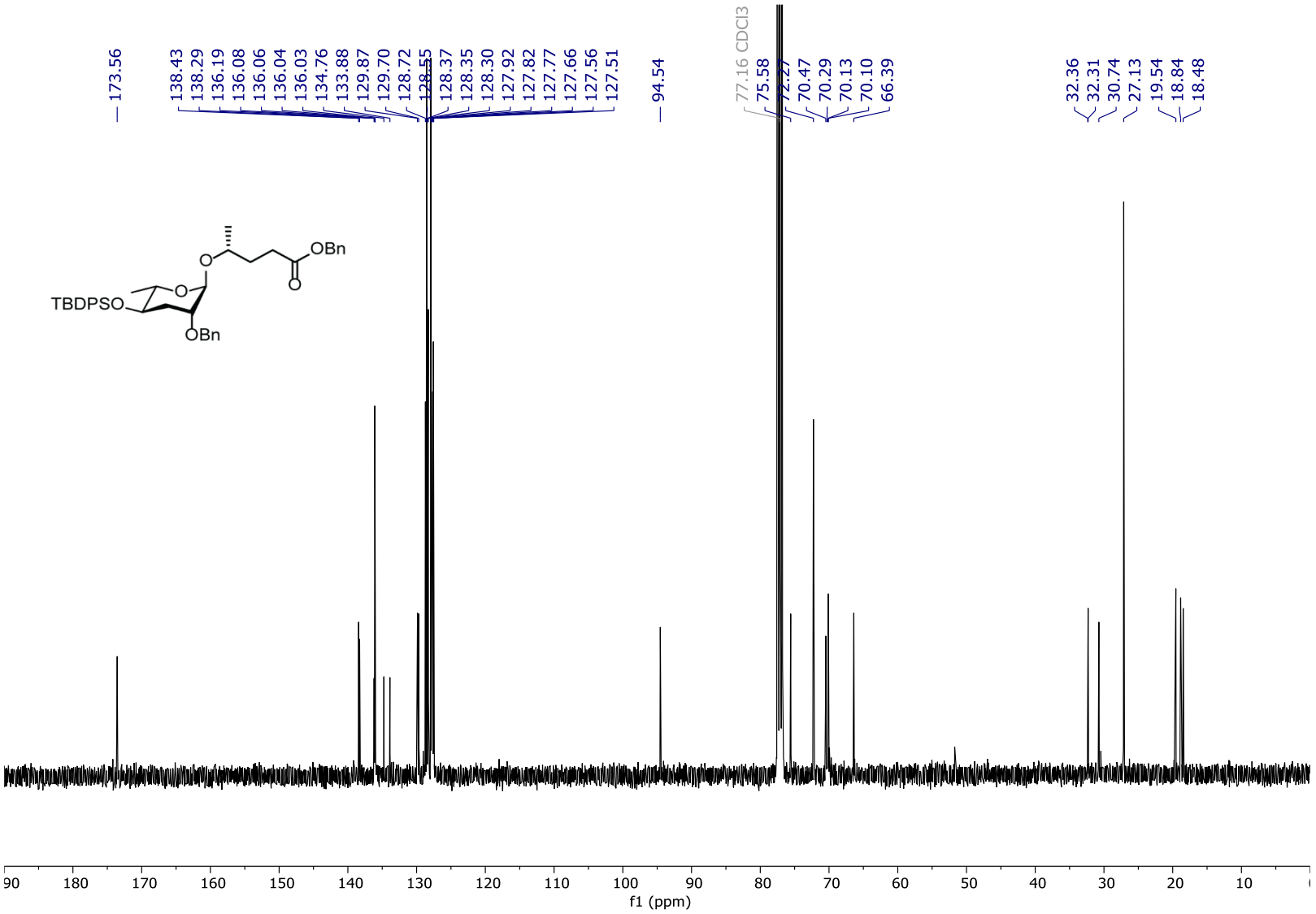

Figure S57: ^{1}H NMR (400 MHz, $CDCl_3$) of benzyl (4*R)*-4-[(2'-*O*-benzyl-3',6'-dideoxy-L-*arabino*-hexopyranosyl)oxy]-pentanoate (**24a**).

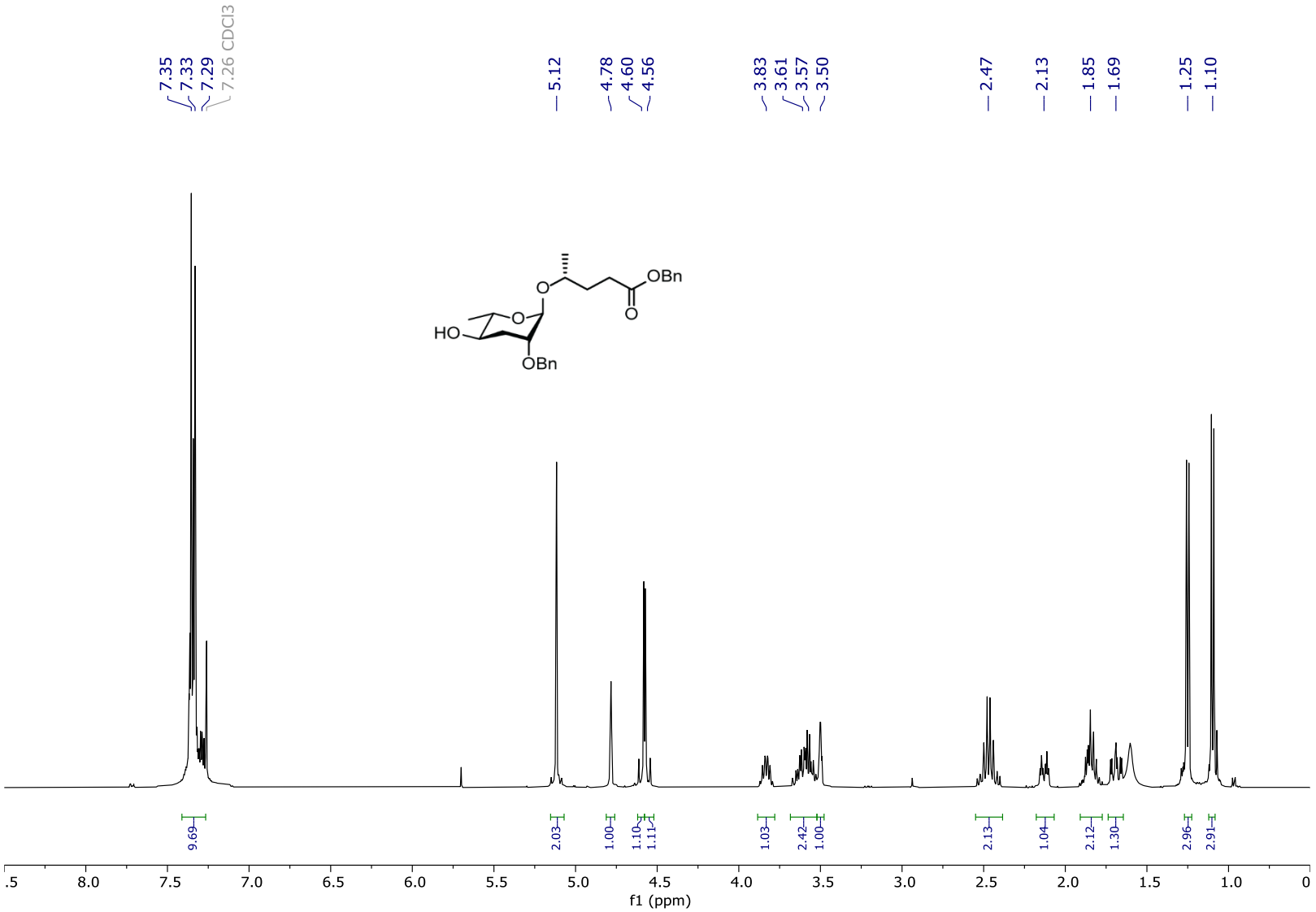

Figure S58: ^{1}H NMR (400 MHz, $CDCl_3$) of benzyl (4*R*)-4-[(2'-*O*-benzyl-3',6'-dideoxy-L-*arabino*-hexopyranosyl)oxy]-2-pentenoate (**24b**).

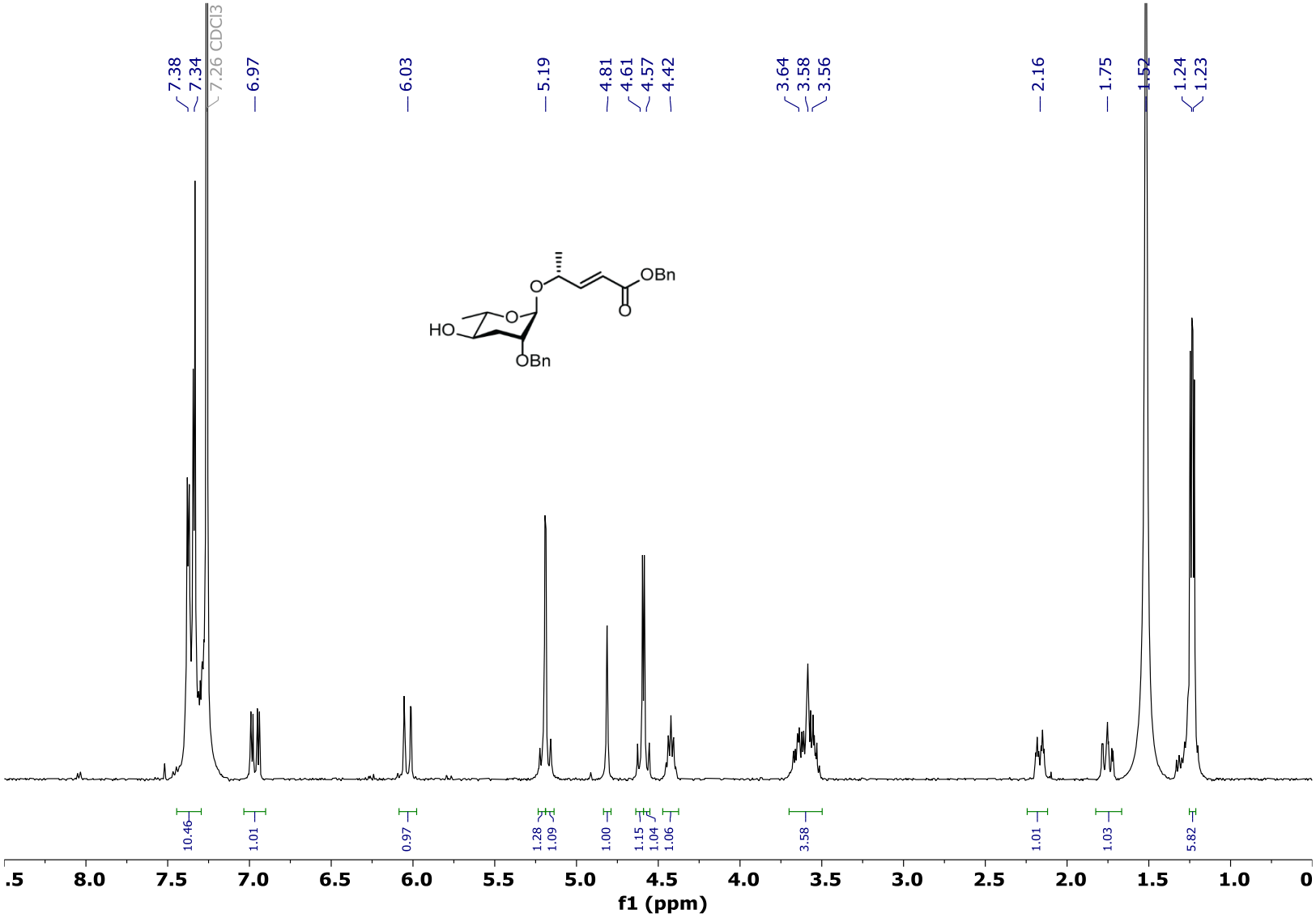

Figure S59: ^{13}C NMR (100 MHz, $CDCl_3$) of benzyl (4*R*)-4-[(2'-*O*-benzyl-3',6'-dideoxy-L-*arabino*-hexopyranosyl)oxy]-2-pentenoate (**24b**).

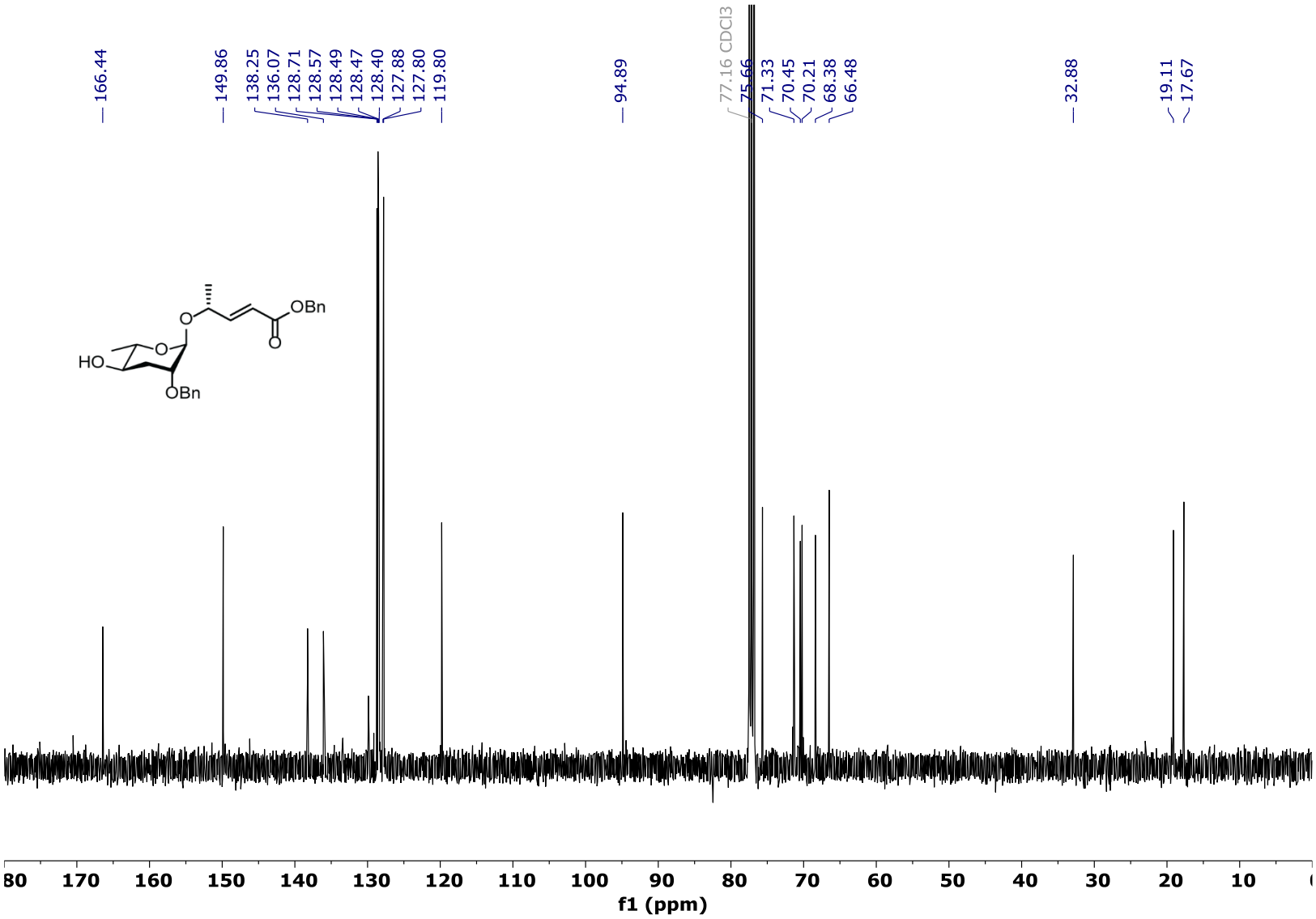

Figure S60: *dqf*-COSY (400 MHz, $CDCl_3$) of benzyl (4*R*)-4-[(2'-*O*-benzyl-3',6'-dideoxy-L-*arabino*-hexopyranosyl)oxy]-2-pentenoate (**24b**).

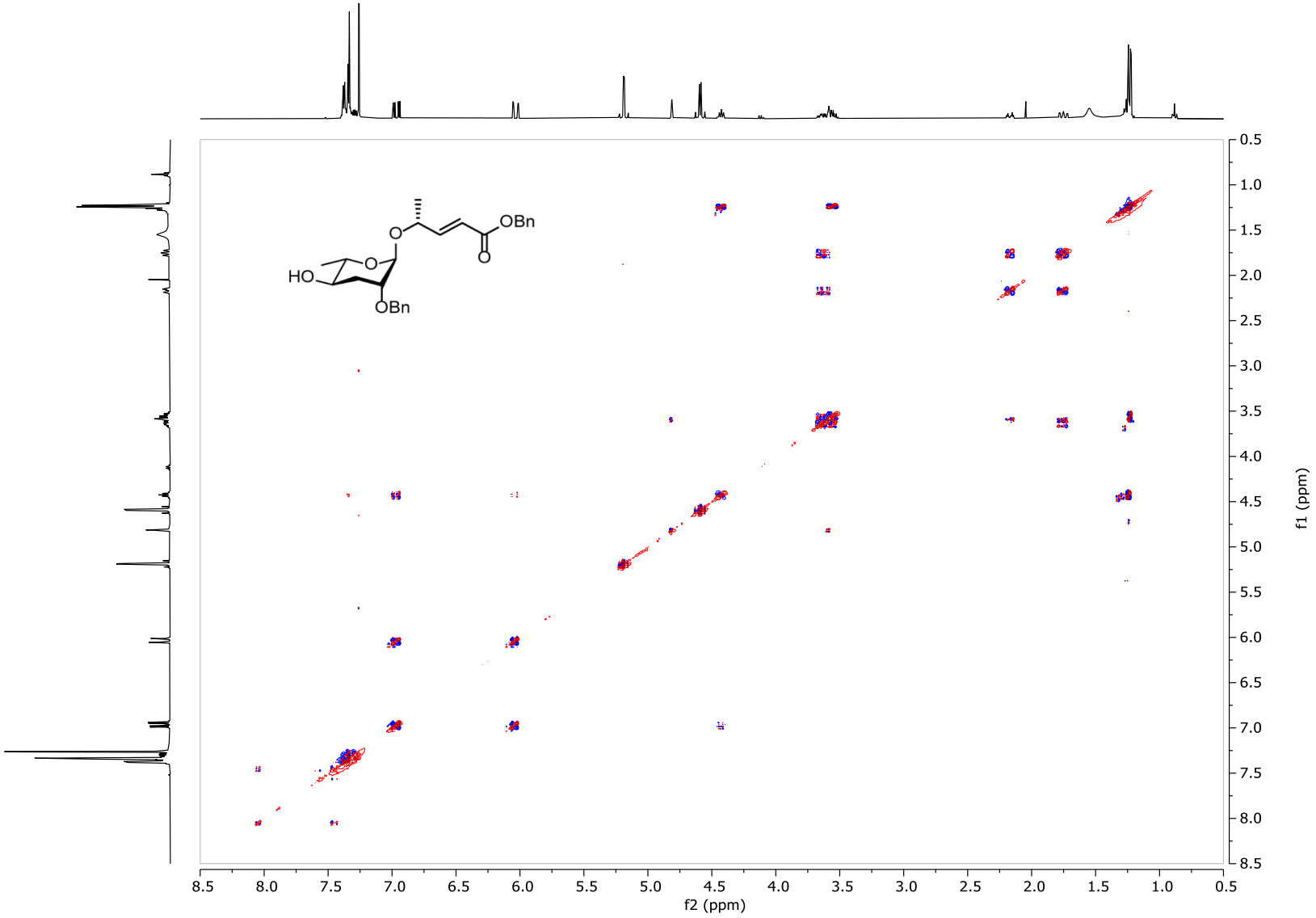

Figure S61: HSQC (400 MHz, $CDCl_3$) of benzyl (4*R*)-4-[(2'-*O*-benzyl-3',6'-dideoxy-L-*arabino*-hexopyranosyl)oxy]-2-pentenoate (**24b**).

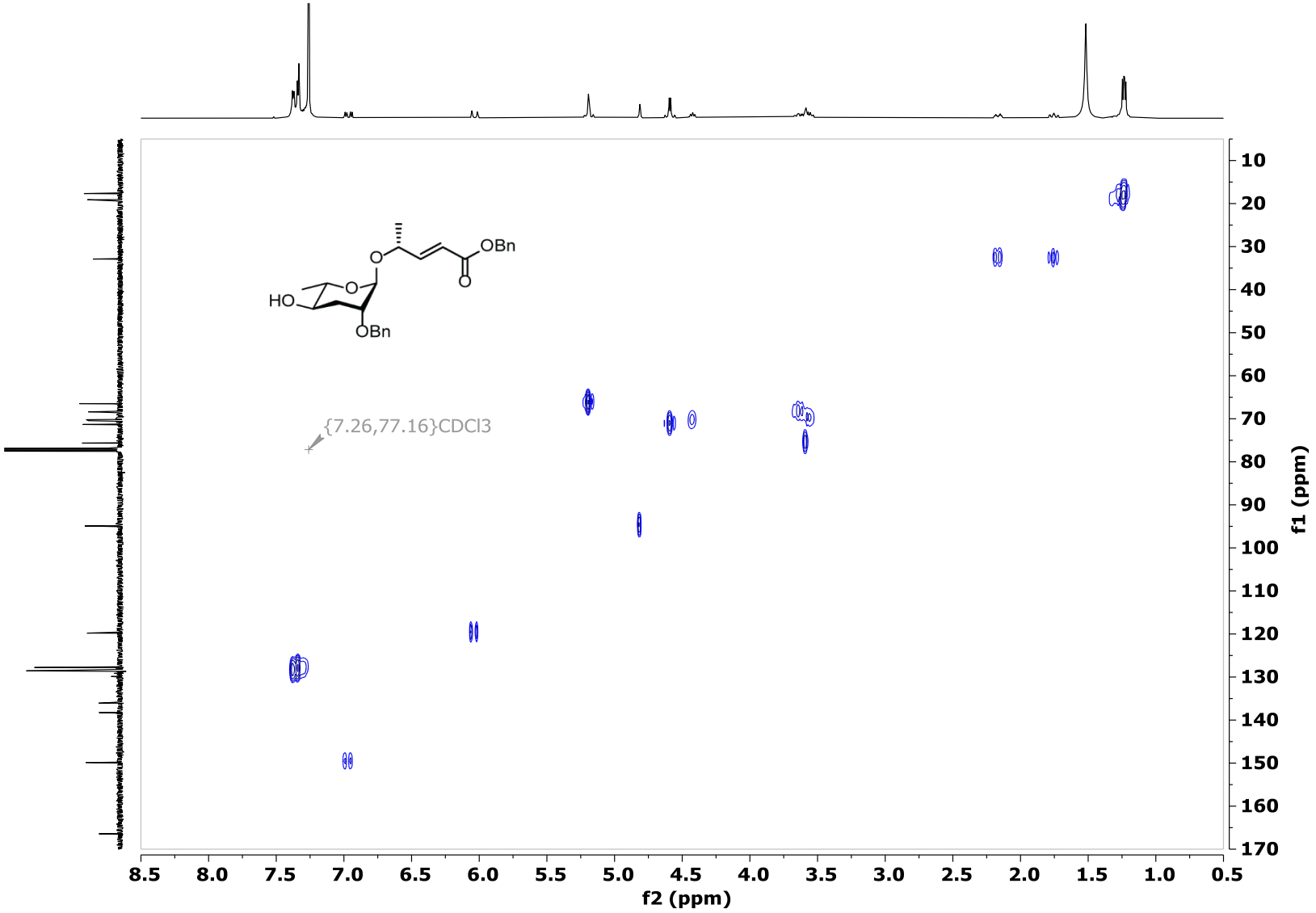

Figure S62: ^{1}H NMR (400 MHz, $CDCl_3$) of (*3R*)-3-[(2'-*O*-benzoyl-4'-*O*-*tert*-butyldiphenylsilyl-3',6'-dideoxy-α-L-*arabino*-hexopyranosyl)oxy]-1-butyne (**25**).

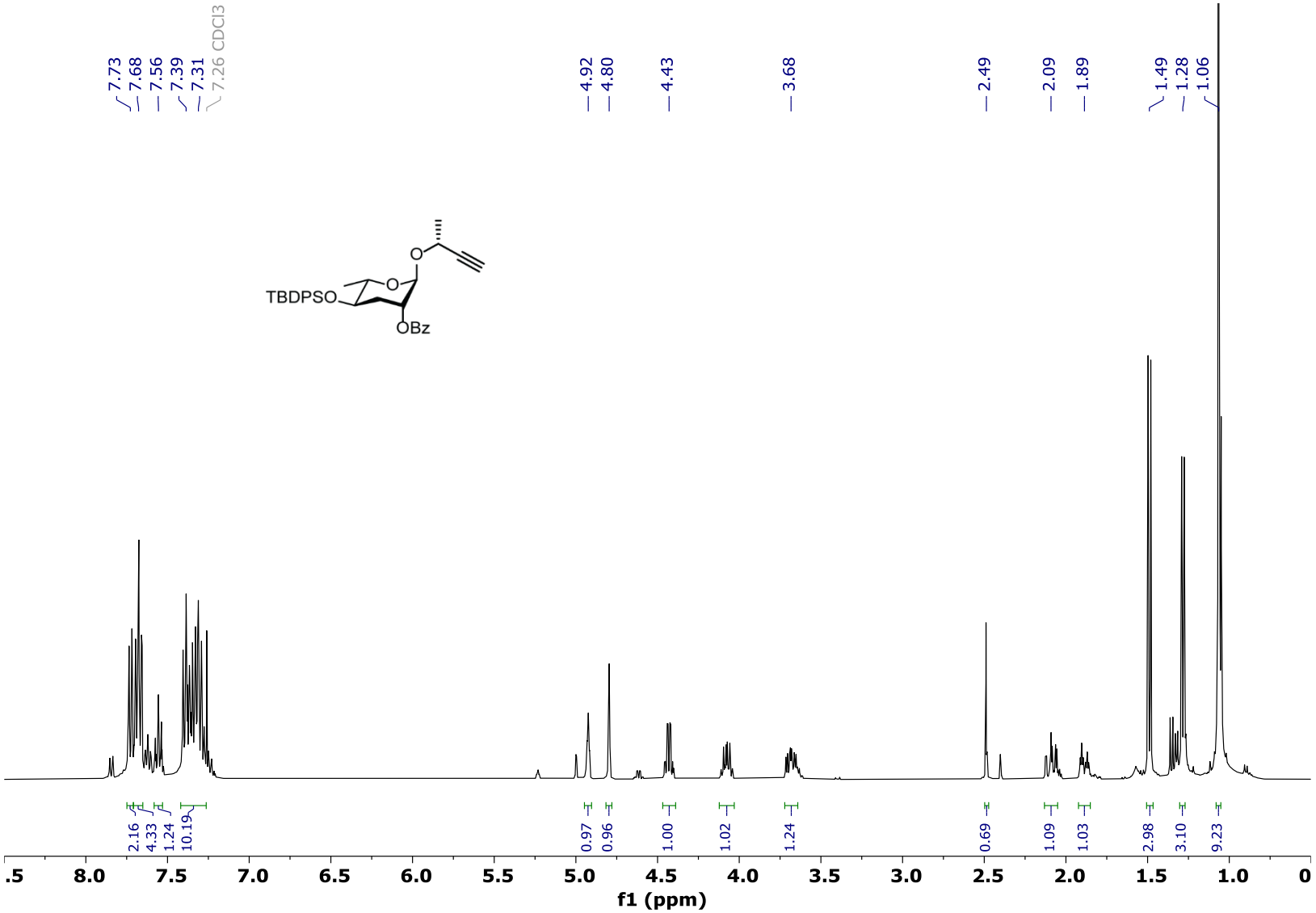

Figure S63: ^{13}C NMR (100 MHz, $CDCl_3$) of (*3R*)-3-[(2'-*O*-benzoyl-4'-*O*-*tert*-butyldiphenylsilyl-3',6'-dideoxy-α-L-*arabino*-hexopyranosyl)oxy]-1-butyne (**25**).

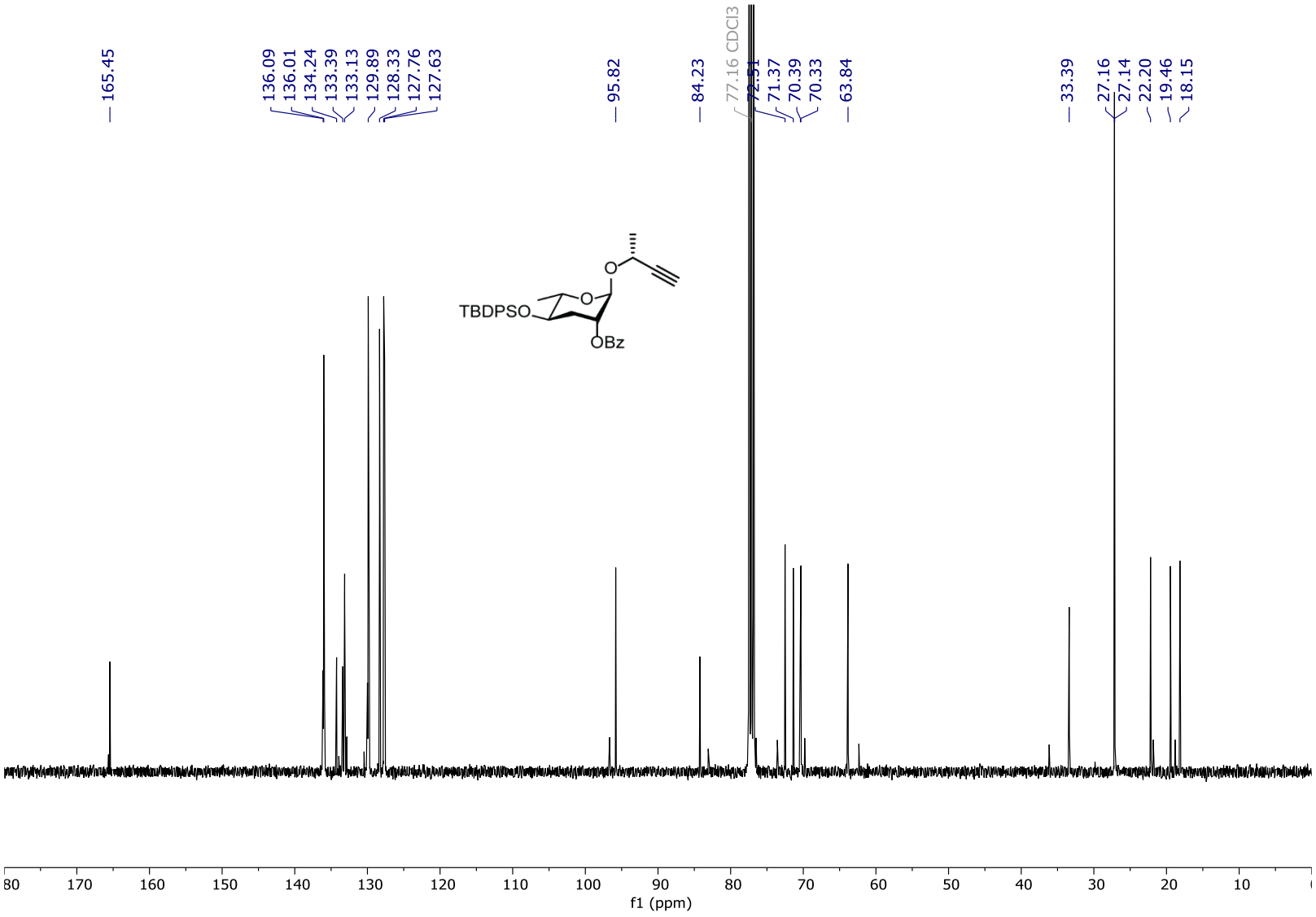

Figure S64: *dqf*-COSY (400 MHz, $CDCl_3$) of (*3R*)-3-[(2'-*O*-benzoyl-4'-*O*-*tert*-butyldiphenylsilyl-3',6'-dideoxy-α-L-*arabino*-hexopyranosyl)oxy]-1-butyne (**25**).

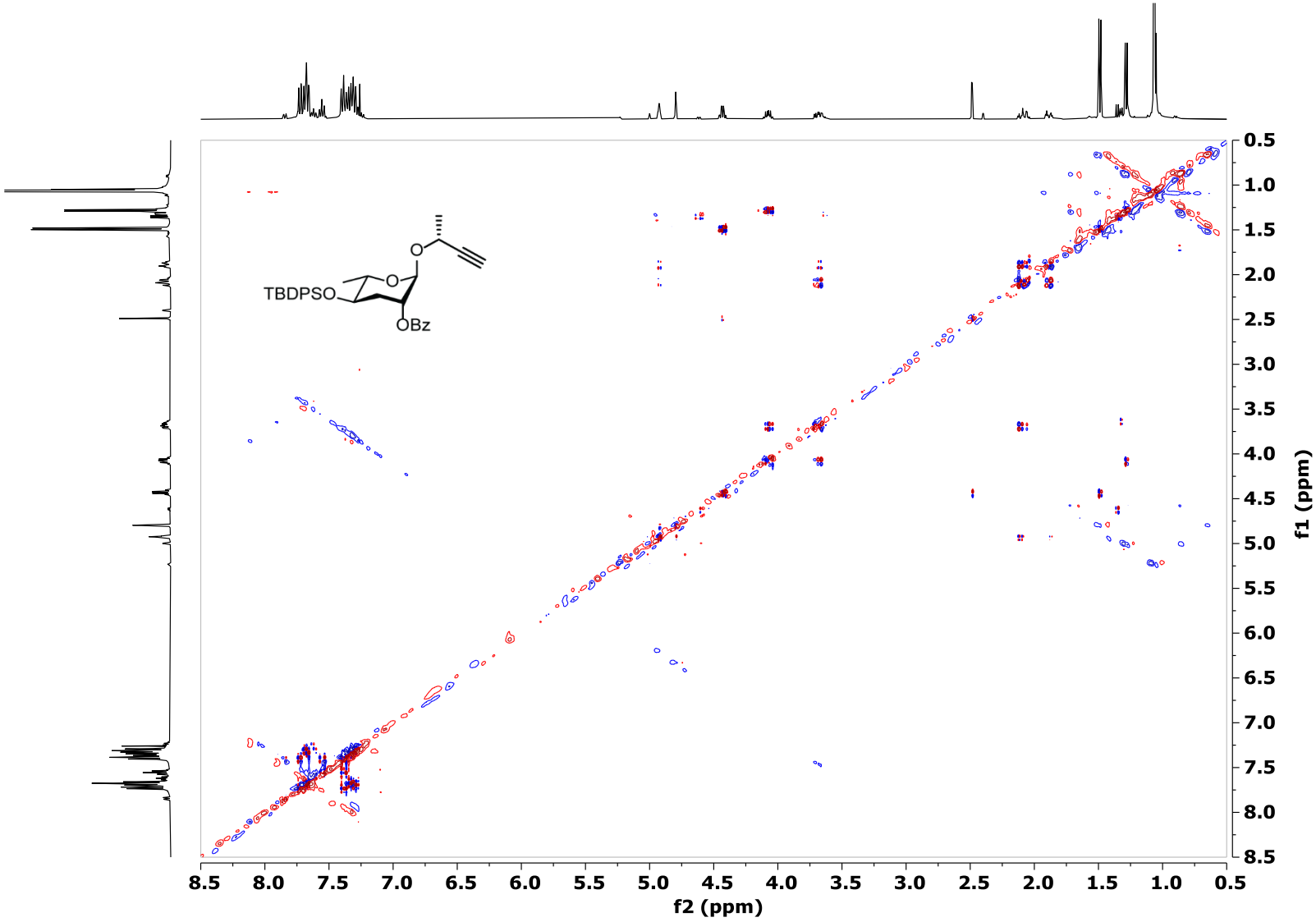

Figure S65: HSQC (400 MHz, $CDCl_3$) of (*3R*)-3-[(2'-*O*-benzoyl-4'-*O*-*tert*-butyldiphenylsilyl-3',6'-dideoxy-α-L-*arabino*-hexopyranosyl)oxy]-1-butyne (**25**).

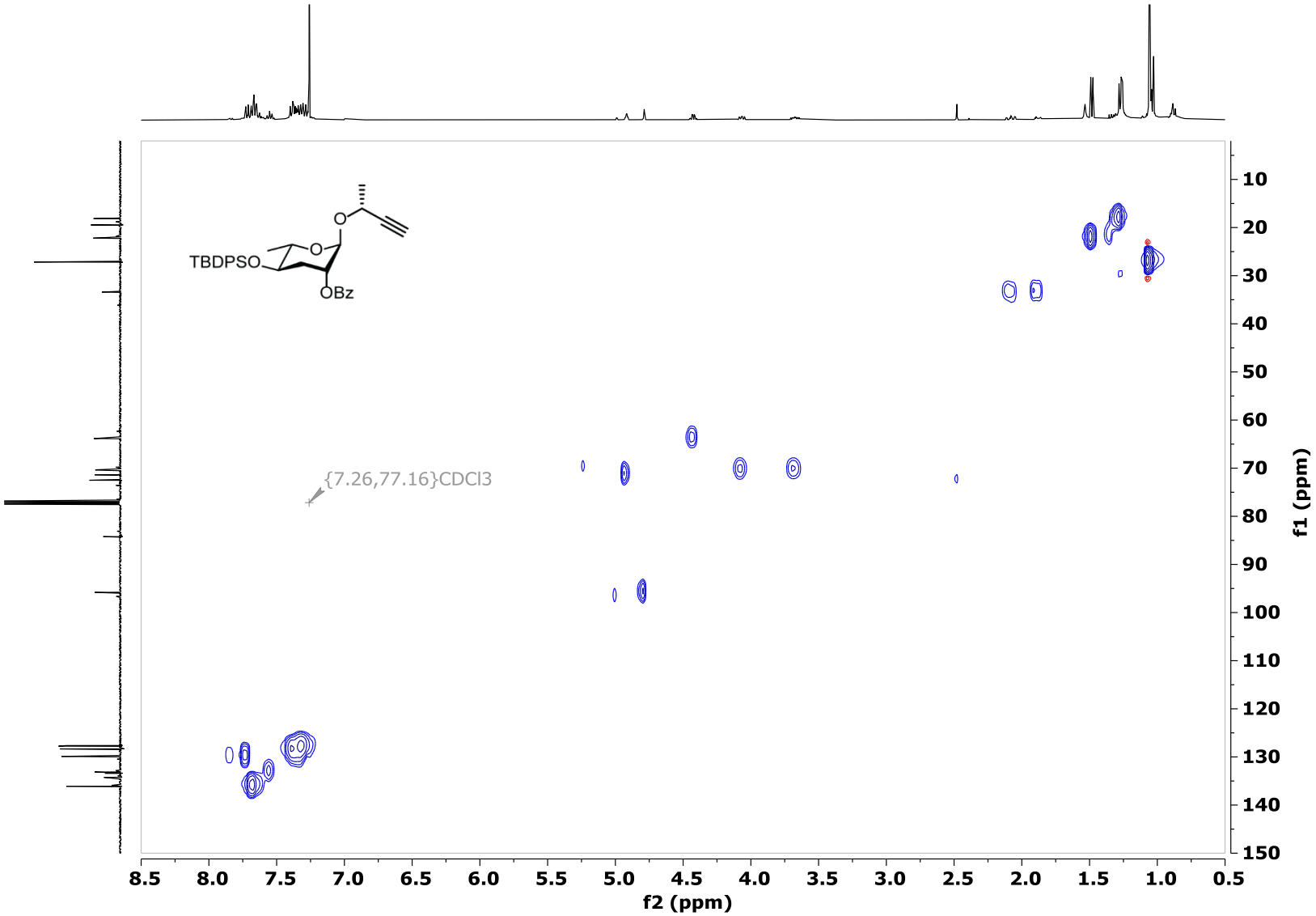

Figure S66: ^{1}H NMR (400 MHz, $CDCl_3$) of (3*R*)-3-[(2'-*O*-benzoyl-4'-*O*-*tert*-butyldiphenylsilyl-3',6'-dideoxy-L-*arabino*-hexopyranosyl)oxy]-1-butene (**26**).

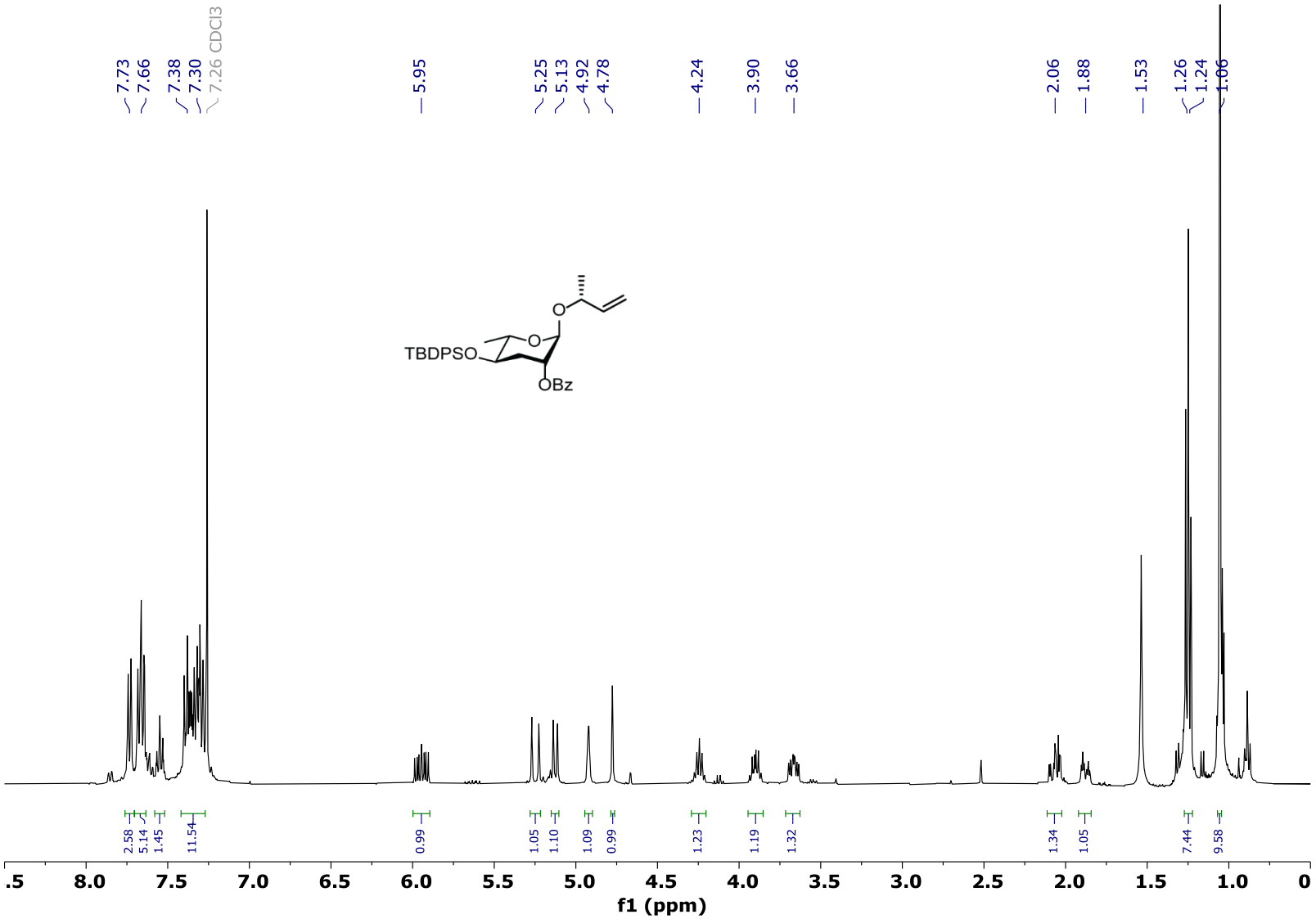

Figure S67: ^{13}C NMR (100 MHz, $CDCl_3$) of (3*R*)-3-[(2'-*O*-benzoyl-4'-*O*-*tert*-butyldiphenylsilyl-3',6'-dideoxy-L-*arabino*-hexopyranosyl)oxy]-1-butene (**26**).

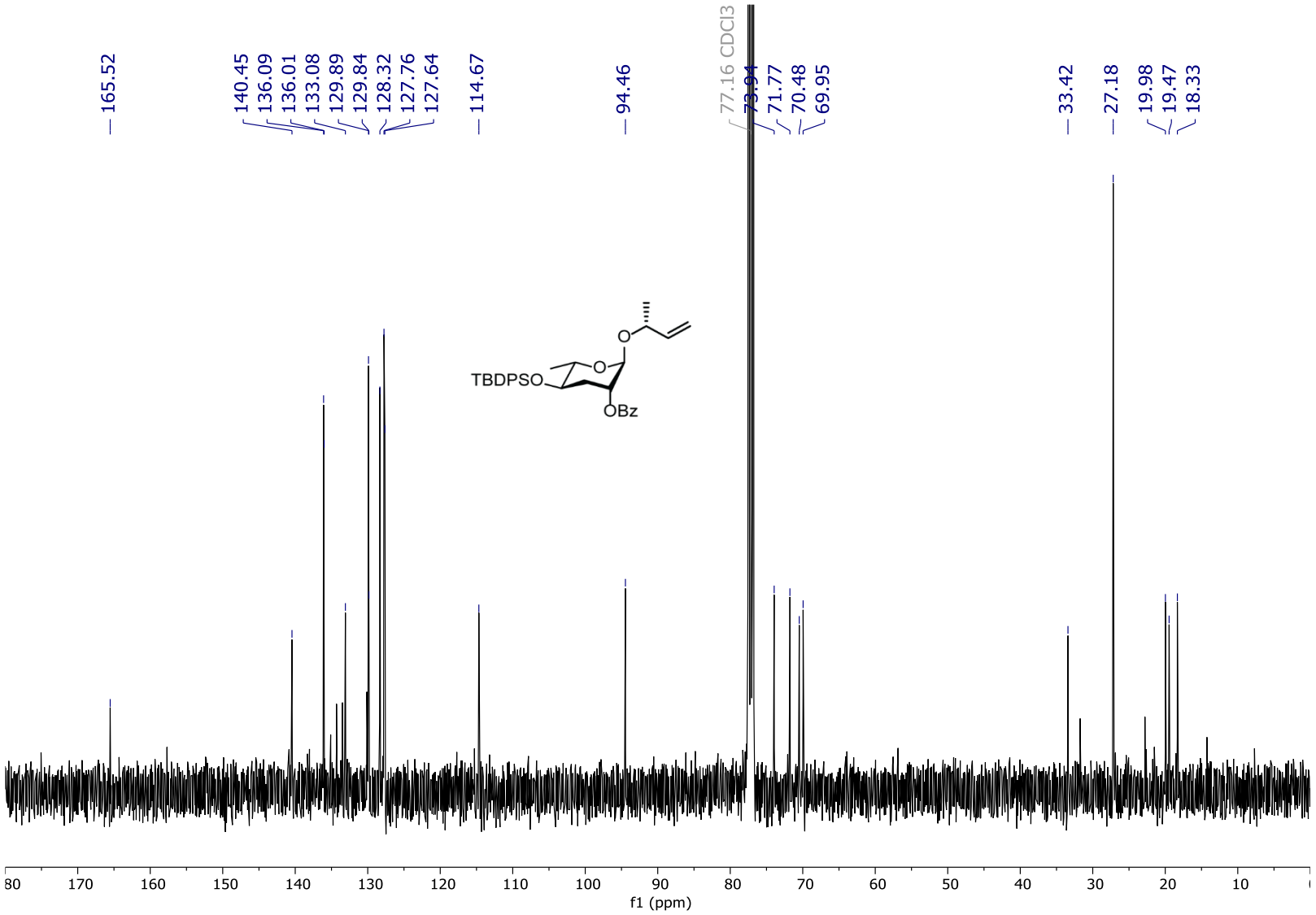

Figure S68: *dqf*-COSY (100 MHz, $CDCl_3$) of (3*R*)-3-[(2'-*O*-benzoyl-4'-*O*-*tert*-butyldiphenylsilyl-3',6'-dideoxy-L-*arabino*-hexopyranosyl)oxy]-1-butene (**26**).

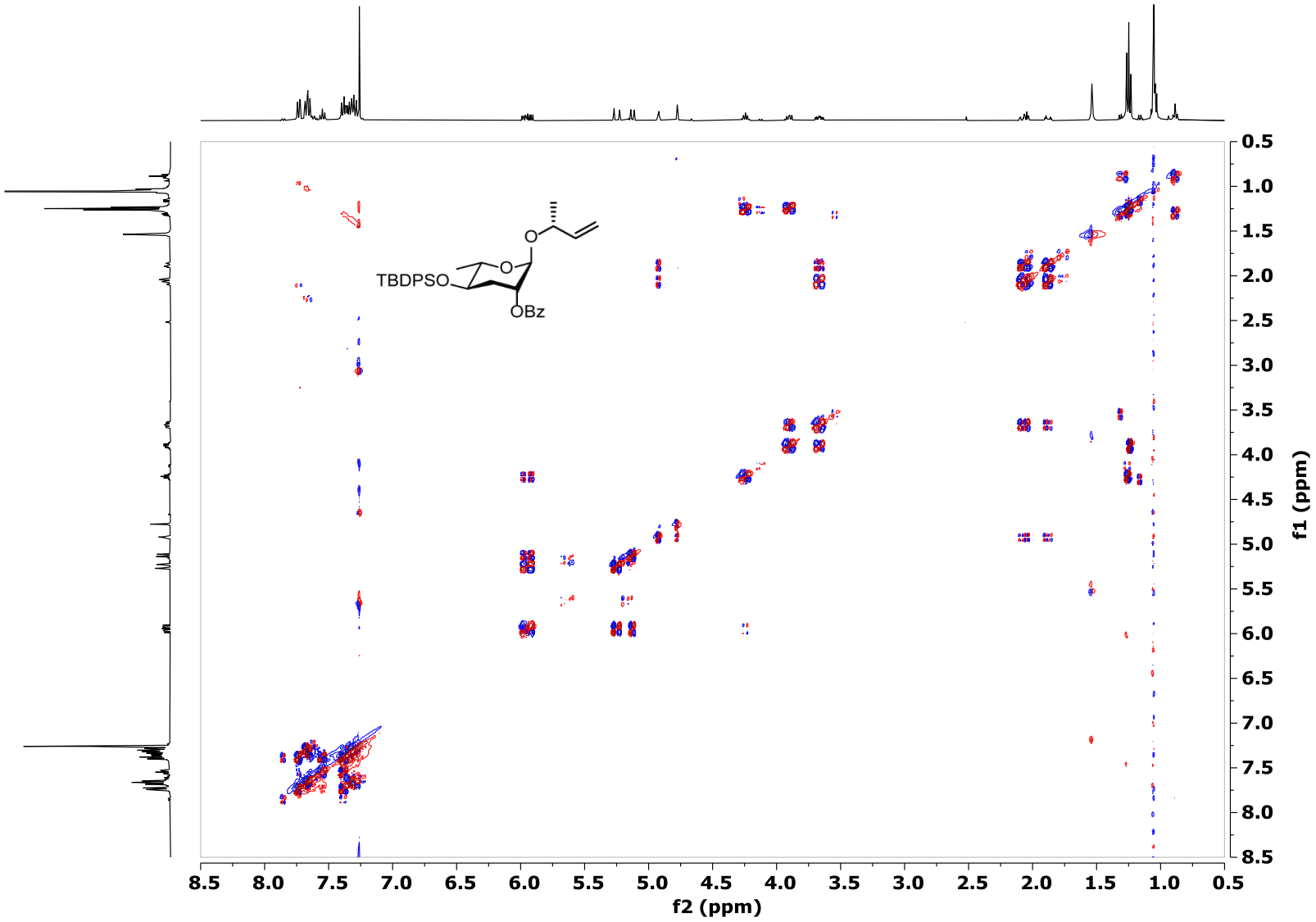

Figure S69: HSQC (400 MHz, $CDCl_3$) of (3*R*)-3-[(2'-*O*-benzoyl-4'-*O*-*tert*-butyldiphenylsilyl-3',6'-dideoxy-L-*arabino*-hexopyranosyl)oxy]-1-butene (**26**).

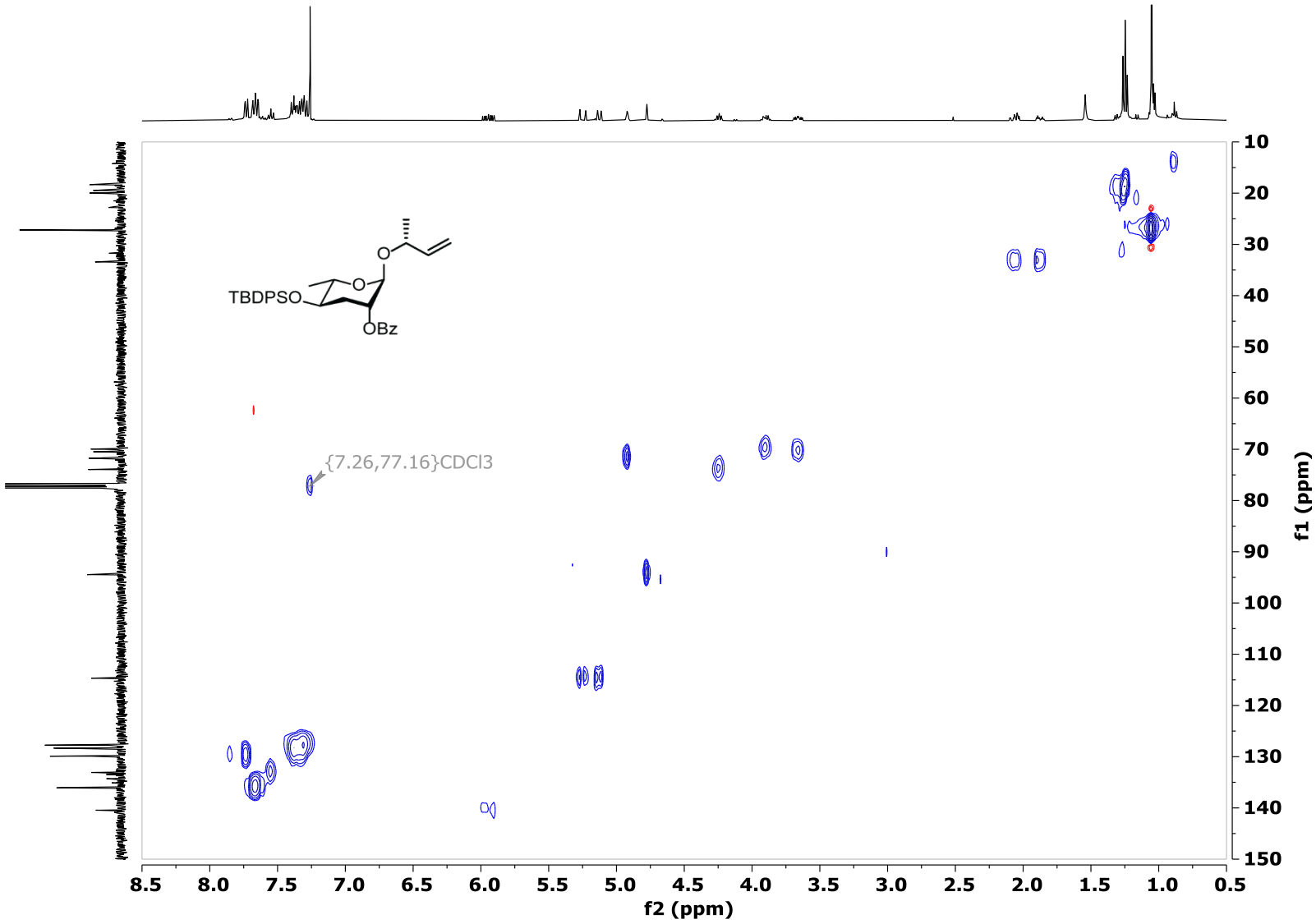

Figure S70: ^{1}H NMR (400 MHz, $CDCl_3$) of (3*R*)-3-[(4'-*O*-*tert*-butyldiphenylsilyl-3',6'-dideoxy-L-*arabino*-hexopyranosyl)oxy]-1-butene (**27**).

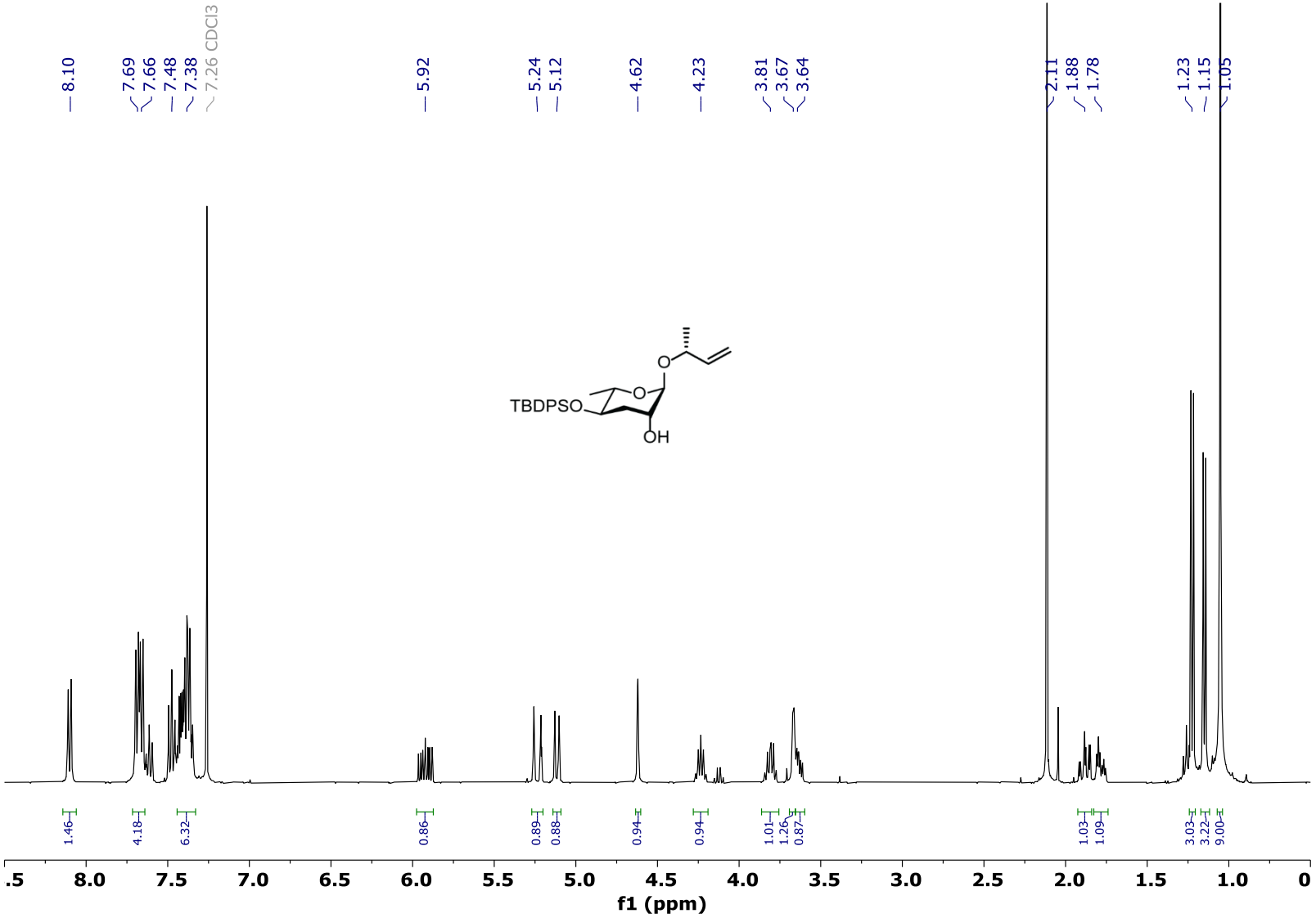

Figure S71: ^{13}C NMR (100 MHz, $CDCl_3$) of (3*R*)-3-[(4'-*O*-*tert*-butyldiphenylsilyl-3',6'-dideoxy-L-*arabino*-hexopyranosyl)oxy]-1-butene (**27**).

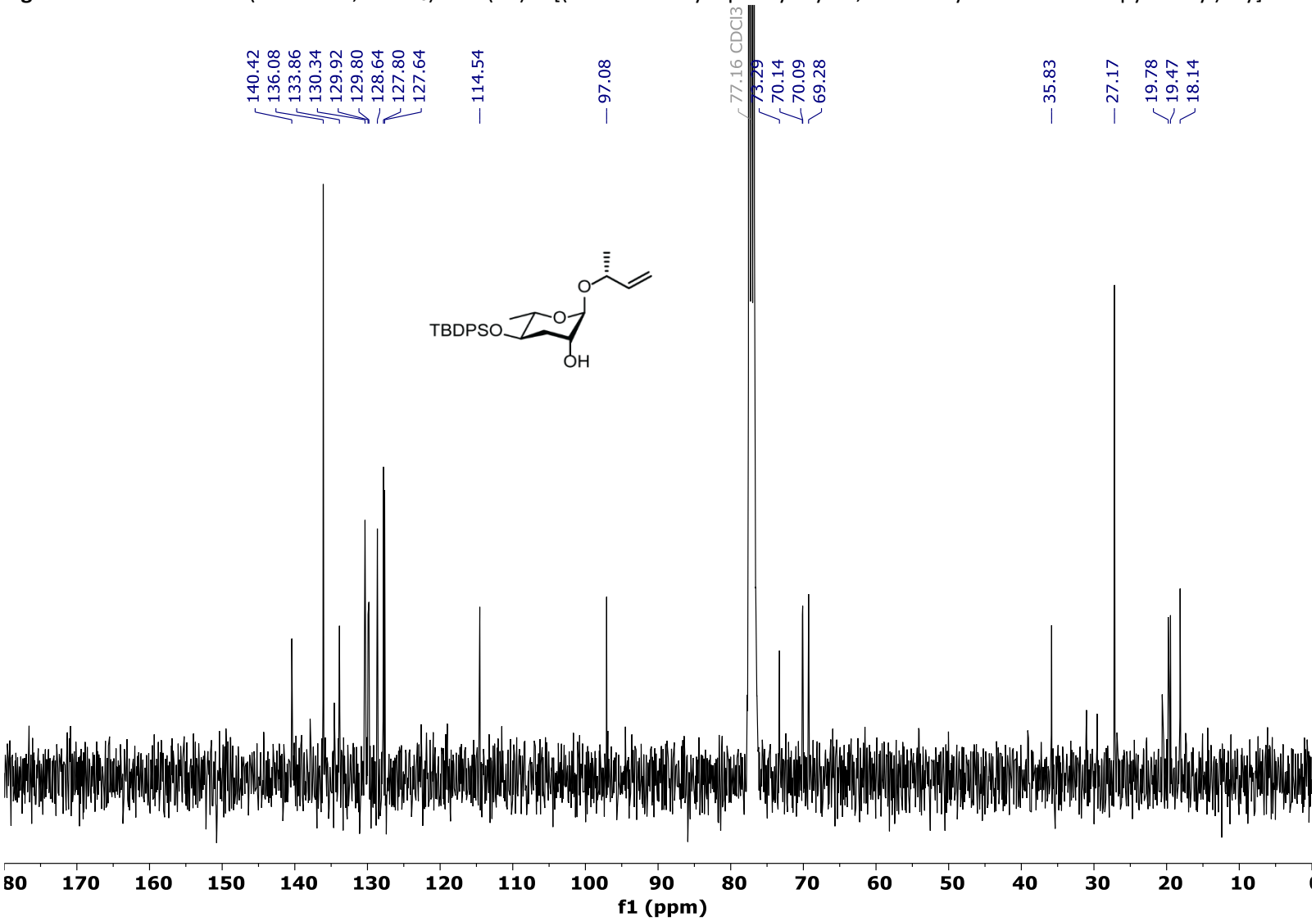

Figure S72: *dqf*-COSY (400 MHz, $CDCl_3$) of (3*R*)-3-[(4'-*O*-*tert*-butyldiphenylsilyl-3',6'-dideoxy-L-*arabino*-hexopyranosyl)oxy]-1-butene (**27**).

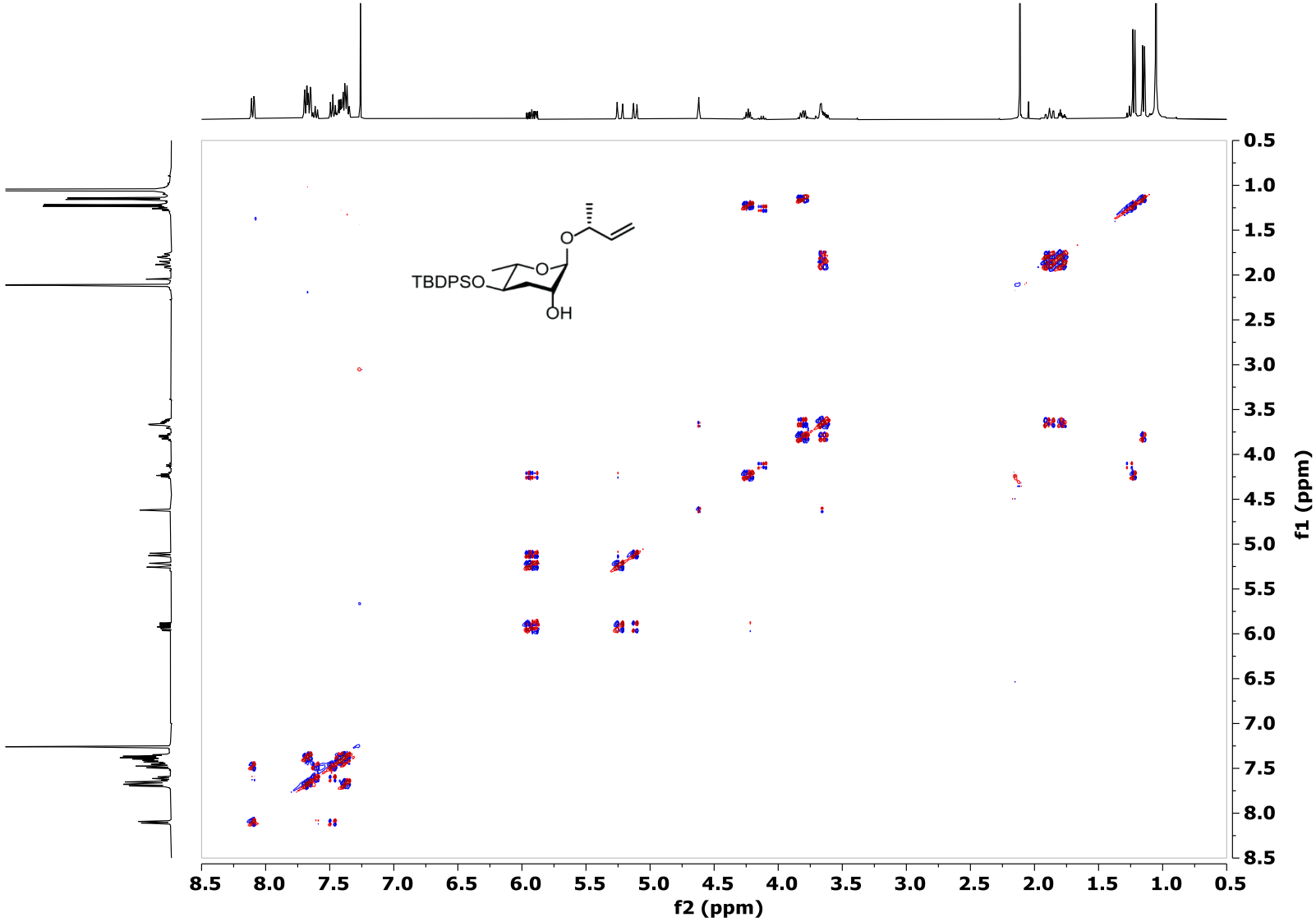

Figure S73: HSQC (400 MHz, $CDCl_3$) of (3*R*)-3-[(4'-*O*-*tert*-butyldiphenylsilyl-3',6'-dideoxy-L-*arabino*-hexopyranosyl)oxy]-1-butene (**27**).

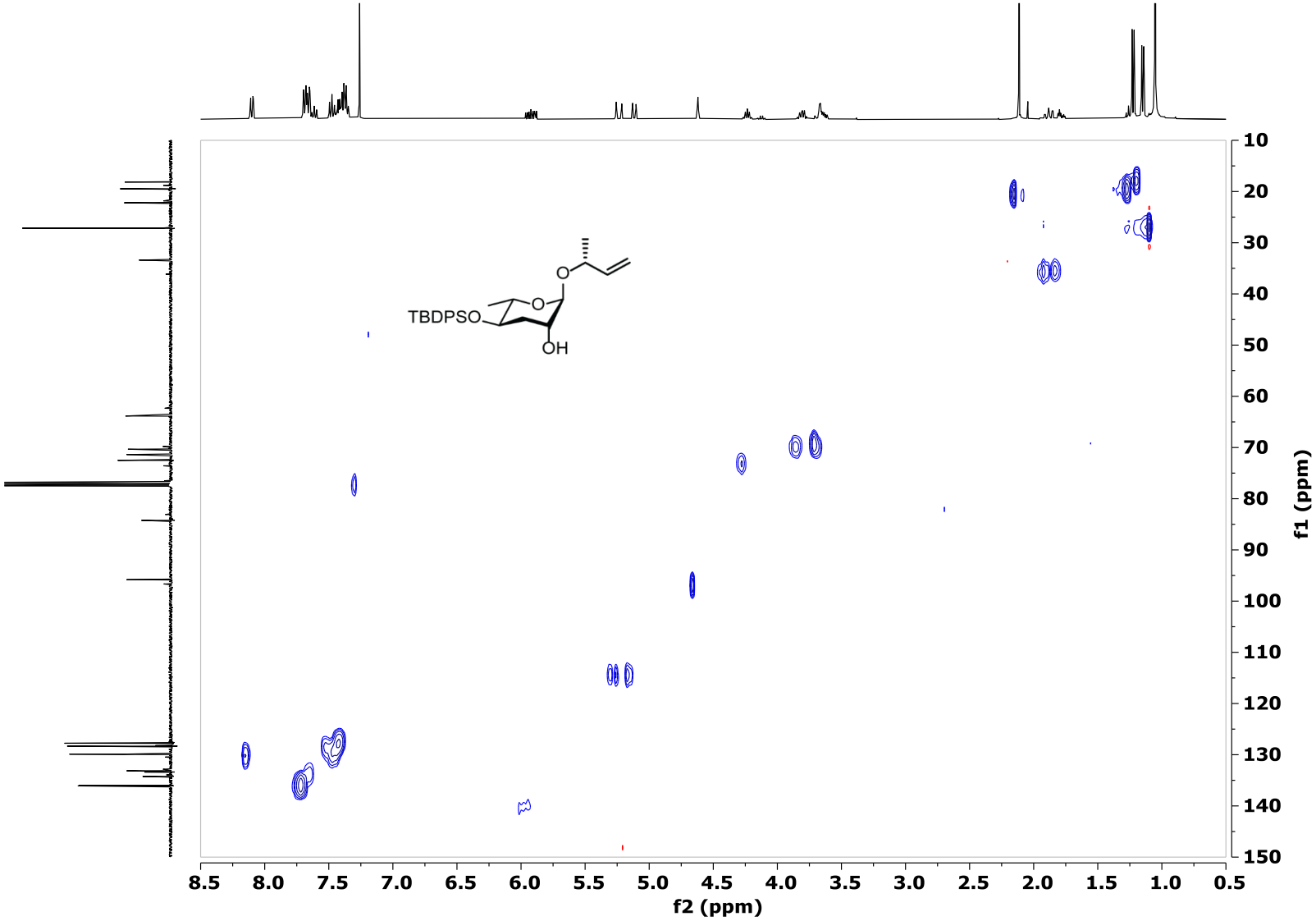

Figure S74: ^{1}H NMR (400 MHz, $CDCl_3$) of (*3R*)-3-[(2'-*O*-benzyl-4'-*O*-*tert*-butyldiphenylsilyl-3',6'-dideoxy-L-*arabino*-hexopyranosyl)oxy]-1-butene (**28**).

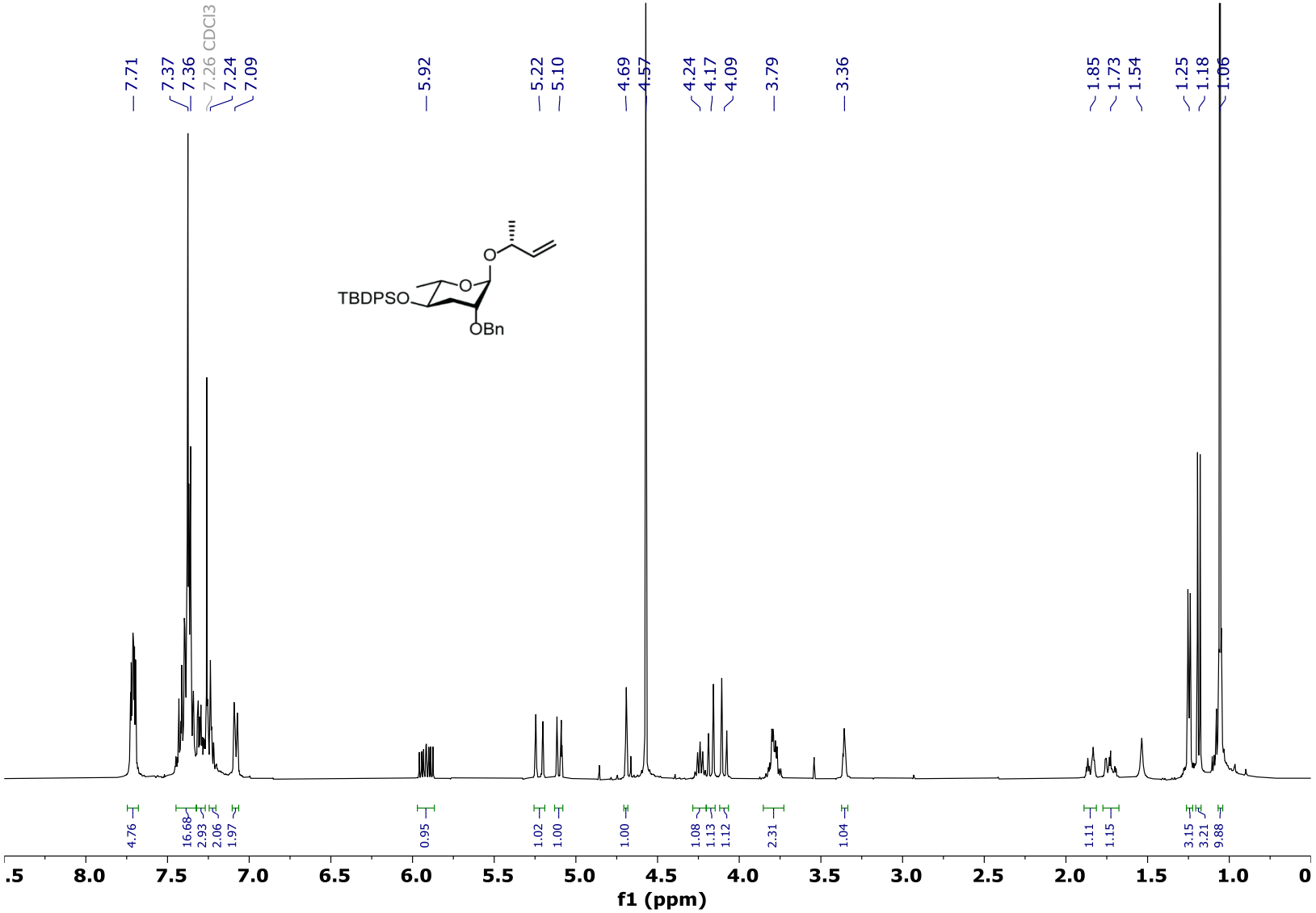

Figure S75: ^{13}C NMR (100 MHz, $CDCl_3$) of (*3R*)-3-[(2'-*O*-benzyl-4'-*O*-*tert*-butyldiphenylsilyl-3',6'-dideoxy-L-*arabino*-hexopyranosyl)oxy]-1-butene (**28**).

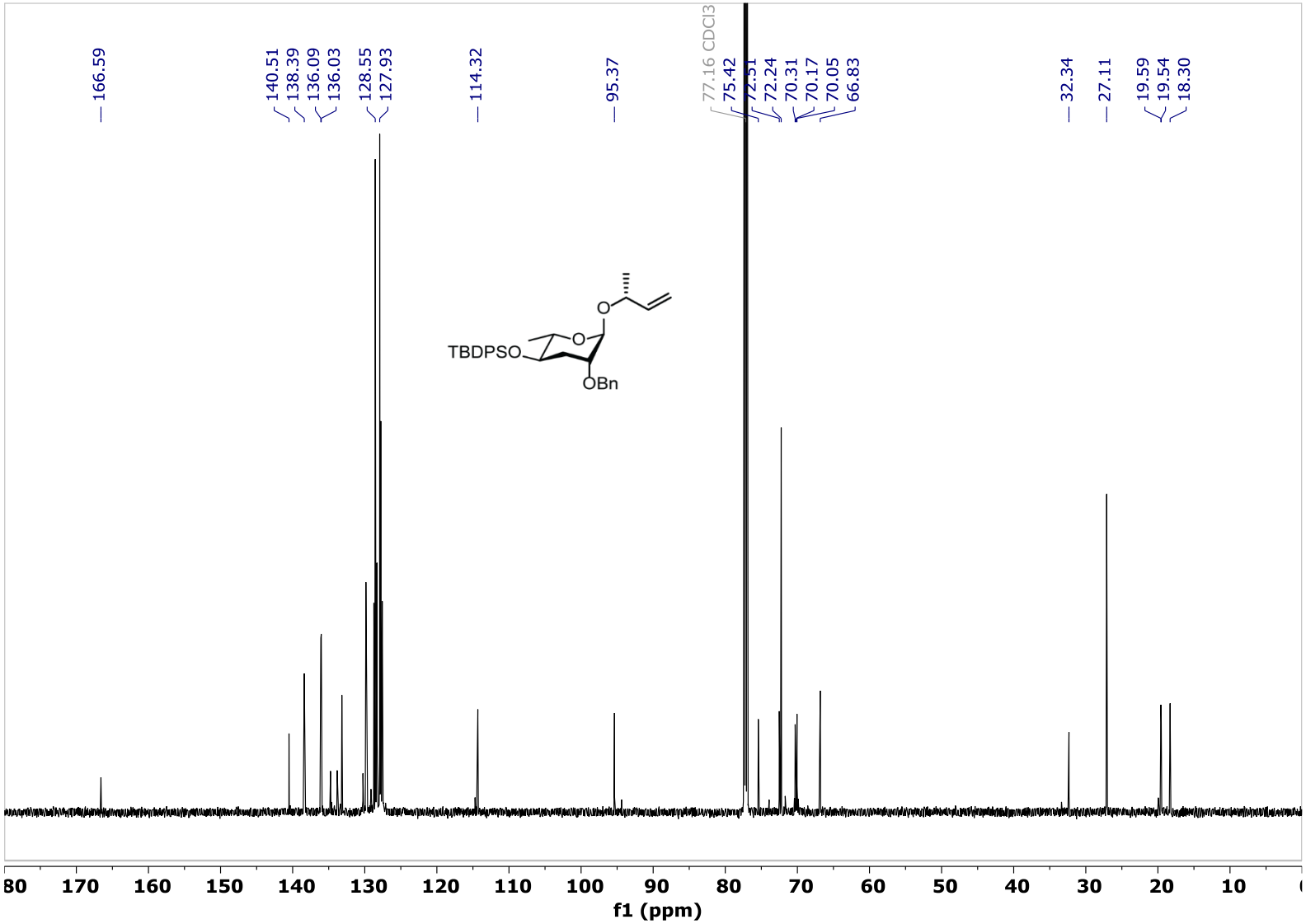

Figure S76: *dqf*-COSY (400 MHz, $CDCl_3$) of (*3R*)-3-[(2'-*O*-benzyl-4'-*O*-*tert*-butyldiphenylsilyl-3',6'-dideoxy-L-*arabino*-hexopyranosyl)oxy]-1-butene (**28**).

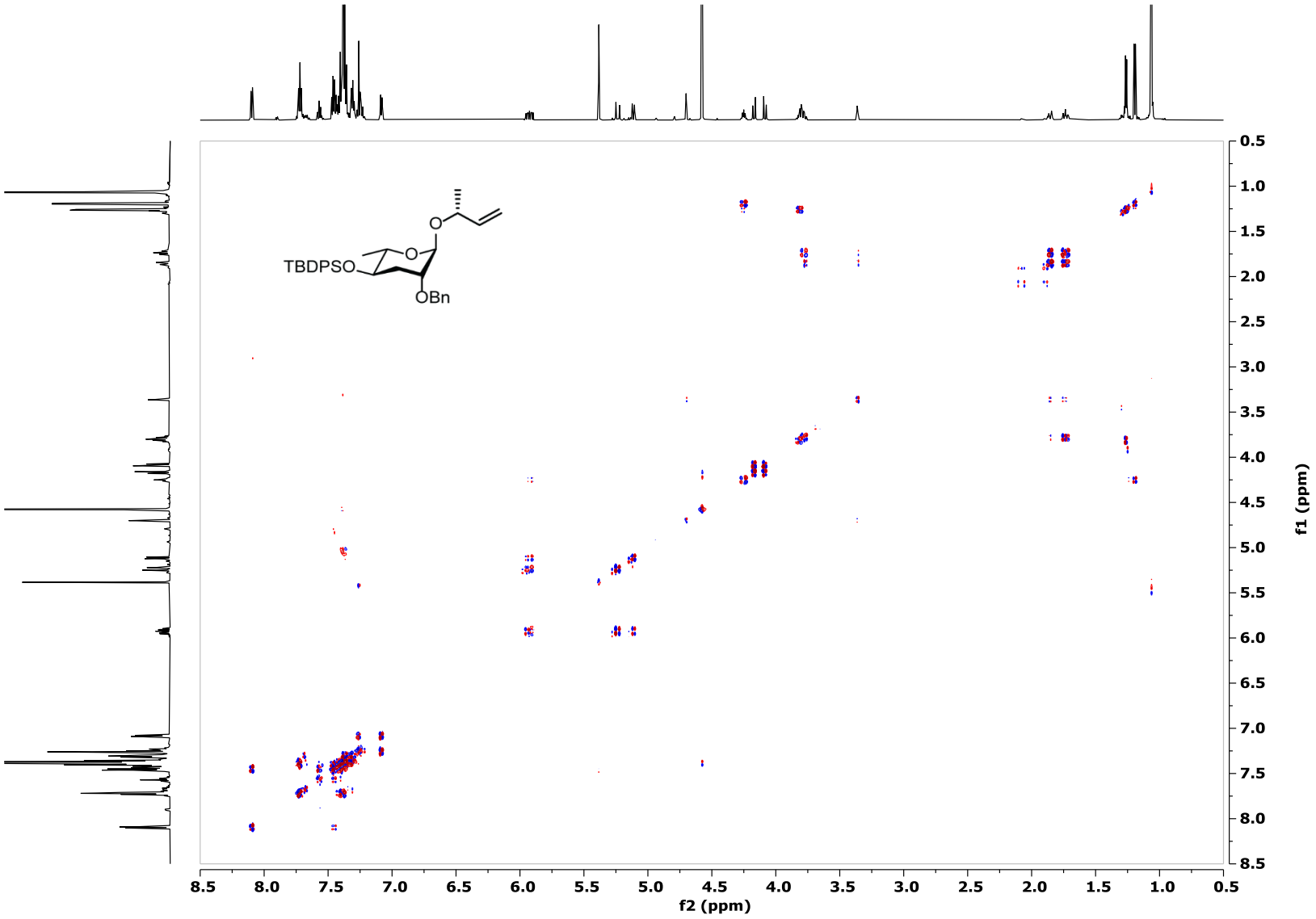

Figure S77: HSQC (400 MHz, $CDCl_3$) of (*3R*)-3-[(2'-*O*-benzyl-4'-*O*-*tert*-butyldiphenylsilyl-3',6'-dideoxy-L-*arabino*-hexopyranosyl)oxy]-1-butene (**28**).

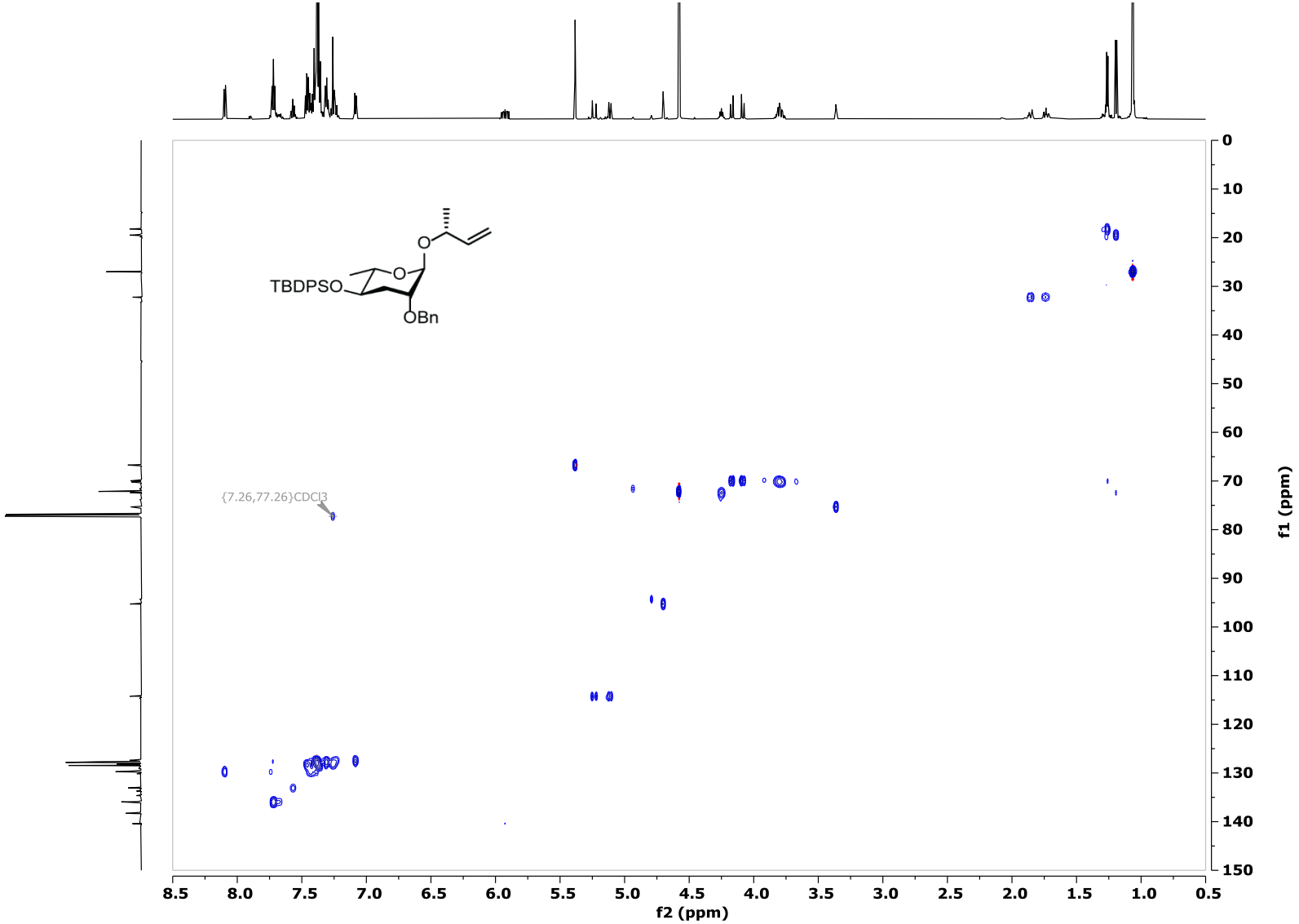

Figure S78: ^{1}H NMR (400 MHz, $CDCl_3$) of (3*R*)-3-[(2'-*O*-benzyl-3',6'-dideoxy-L-*arabino*-hexopyranosyl)oxy]-1-butene (**29**).

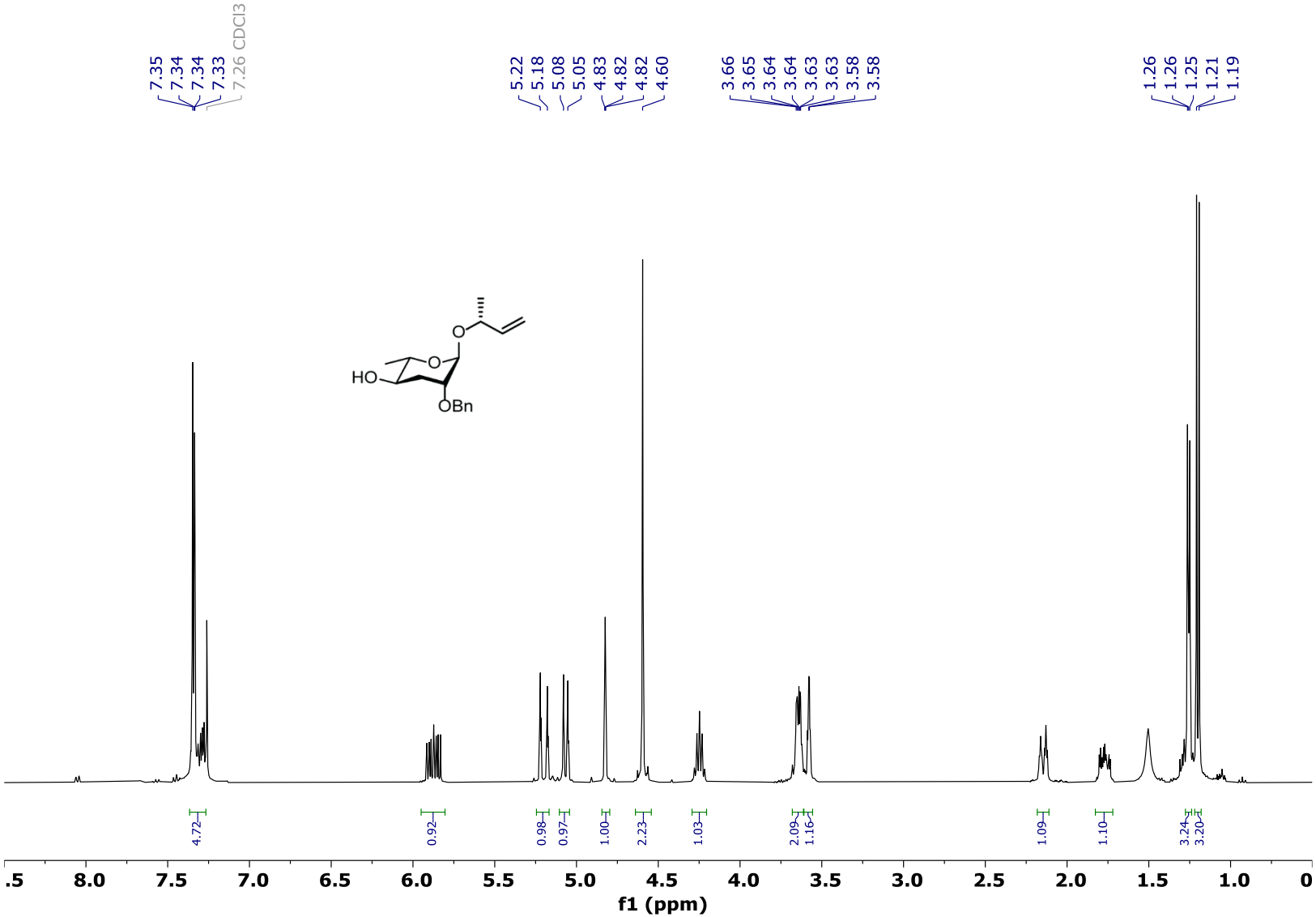

Figure S79: ^{13}C NMR (100 MHz, $CDCl_3$) of (3*R*)-3-[(2'-*O*-benzyl-3',6'-dideoxy-L-*arabino*-hexopyranosyl)oxy]-1-butene (**29**).

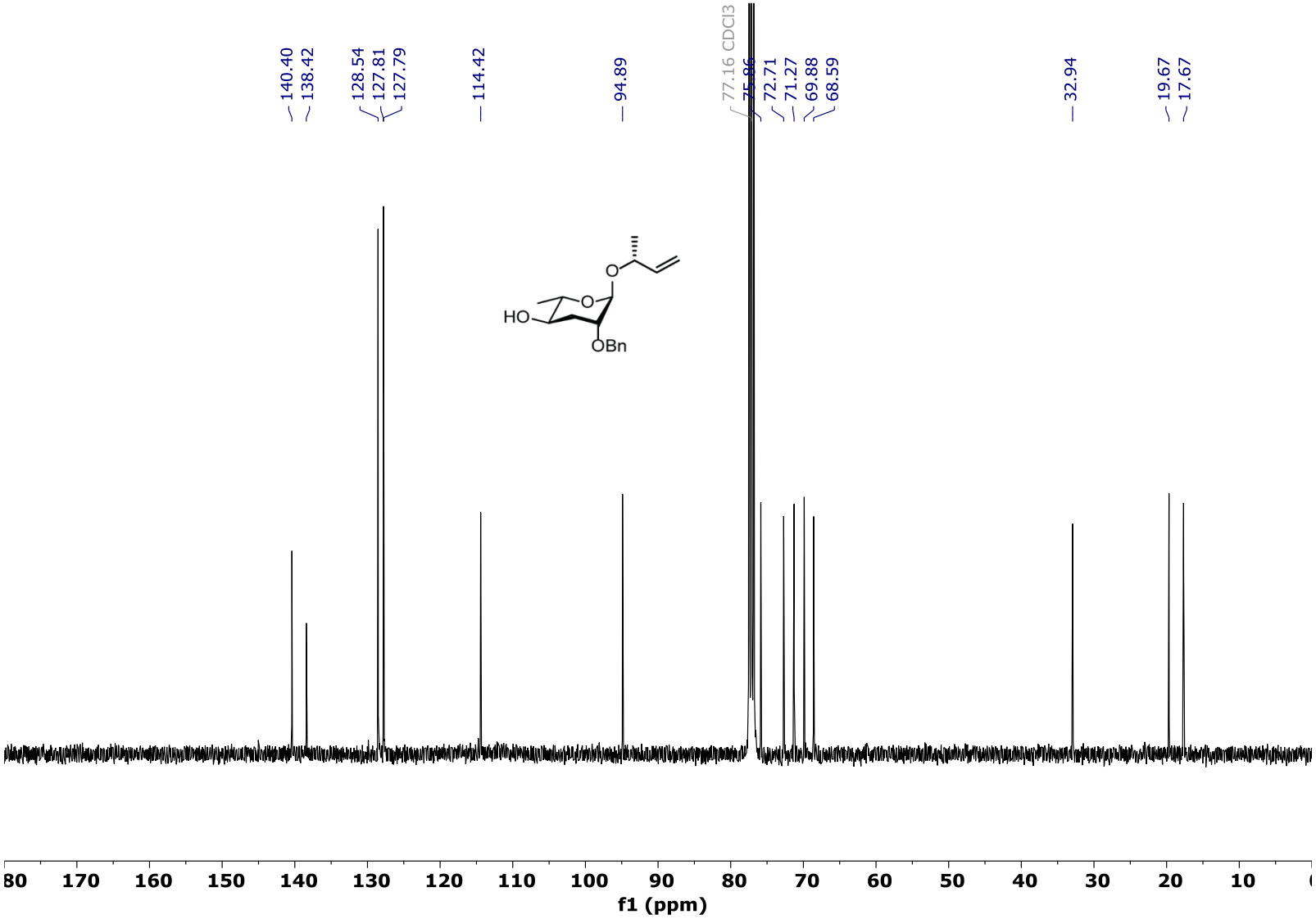

Figure S80: dqf-COSY (400 MHz, $CDCl_3$) of (3*R*)-3-[(2'-*O*-benzyl-3',6'-dideoxy-L-*arabino*-hexopyranosyl)oxy]-1-butene (**29**).

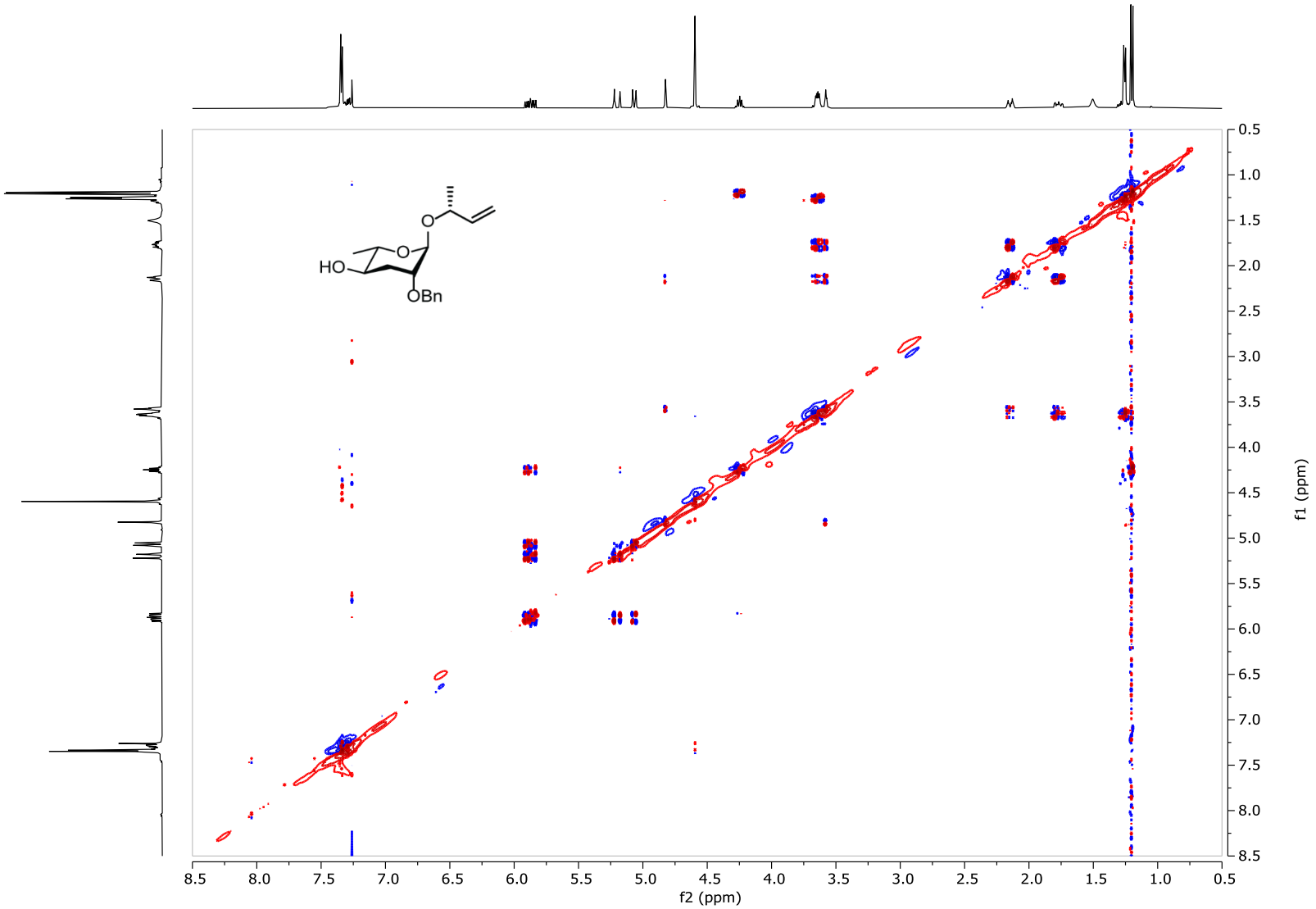

Figure S81: HSQC (400 MHz, $CDCl_3$) of (3*R*)-3-[(2'-*O*-benzyl-3',6'-dideoxy-L-*arabino*-hexopyranosyl)oxy]-1-butene (**29**).

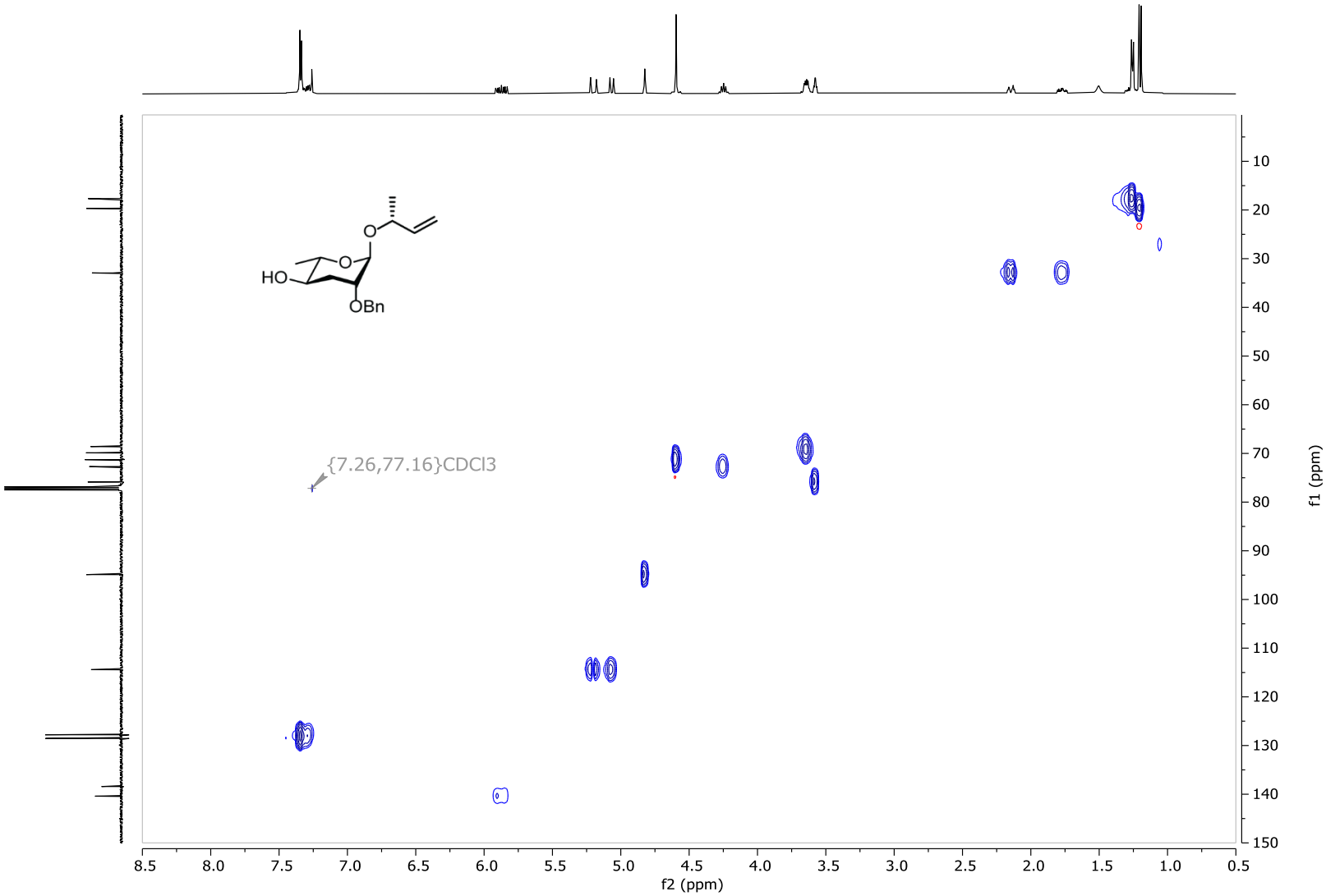

Figure S82: ^{1}H NMR (400 MHz, $CDCl_3$) of benzyl (4*R*)-4-[(2'-*O*-benzyl-4'-(2-(benzyloxy)carbonyl)amino)benzoyl-3',6'-dideoxy-α-L-*arabino*-hexopyranosyl)oxy]-2-pentanoate (**30a**).

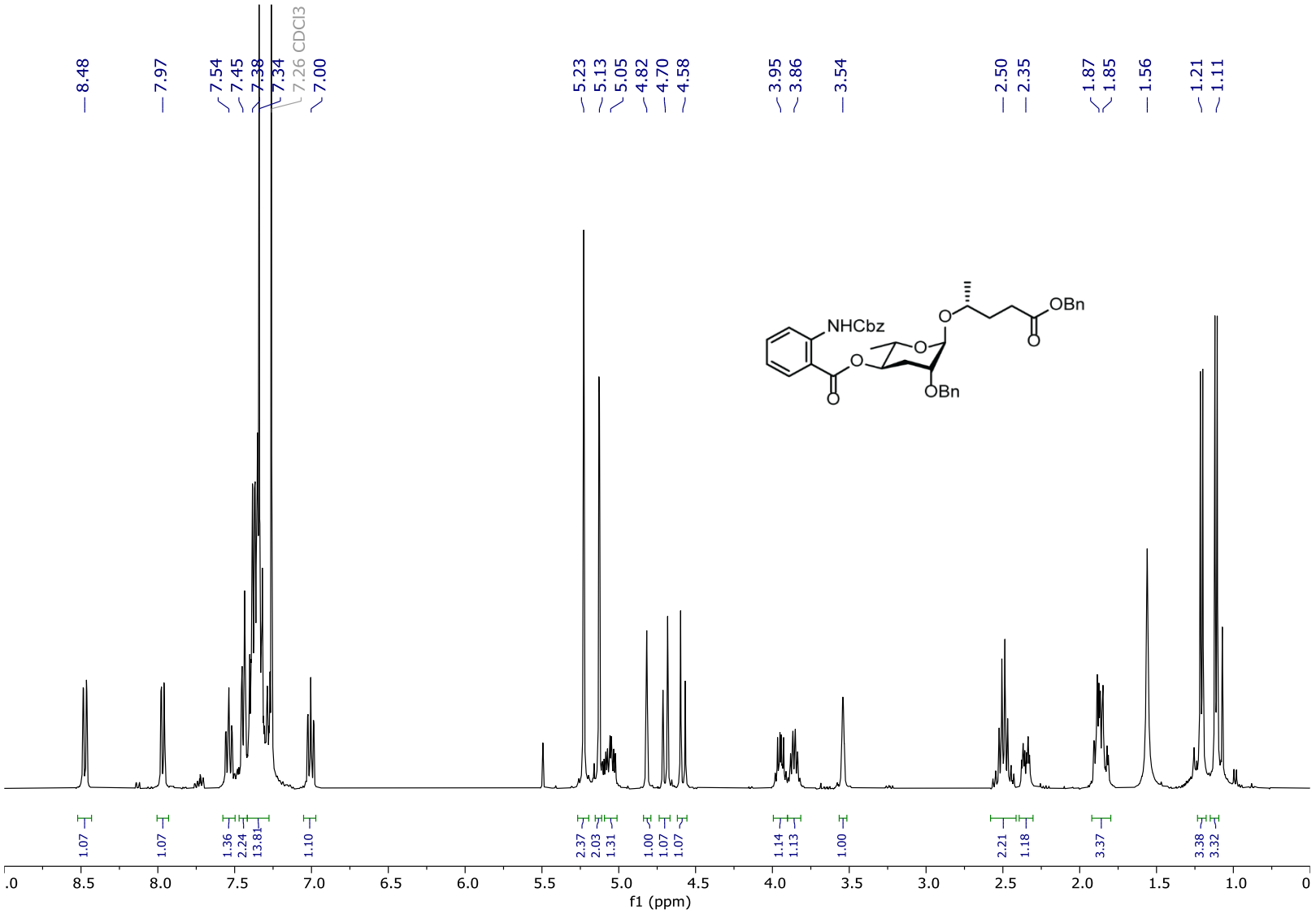

Figure S83: ^{13}C NMR (100 MHz, $CDCl_3$) of benzyl (4*R*)-4-[(2'-*O*-benzyl-4'-(2-(benzyloxy)carbonyl)amino)benzoyl-3',6'-dideoxy-α-L-*arabino*-hexopyranosyl)oxy]-2-pentanoate (**30a**).

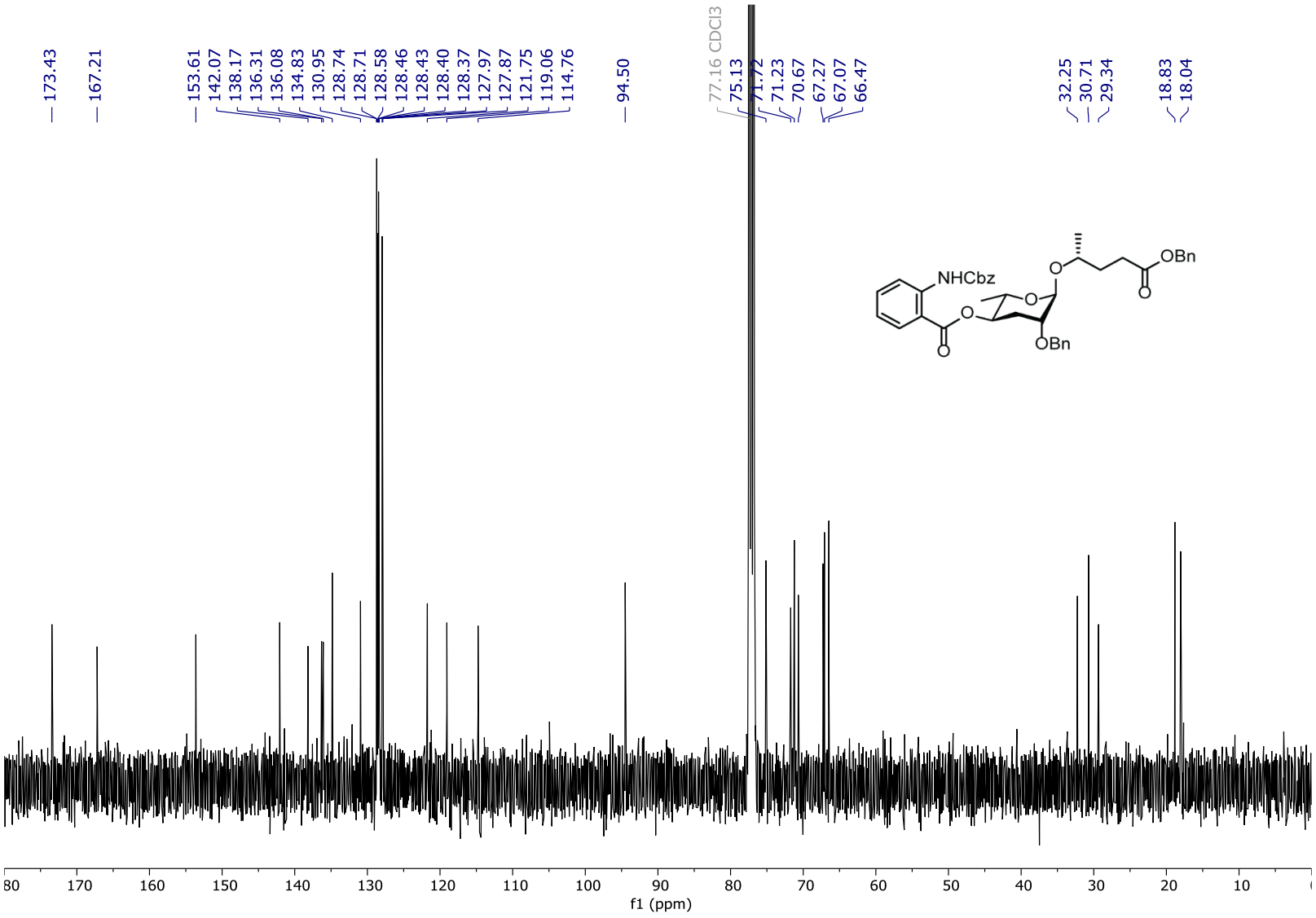

Figure S84: *dqf*-COSY (400 MHz, $CDCl_3$) of benzyl (4*R*)-4-[(2'-*O*-benzyl-4'-(2-(benzyloxy)carbonyl)amino)benzoyl-3',6'-dideoxy-α-L-*arabino*-hexopyranosyl)oxy]-2-pentanoate (**30a**).

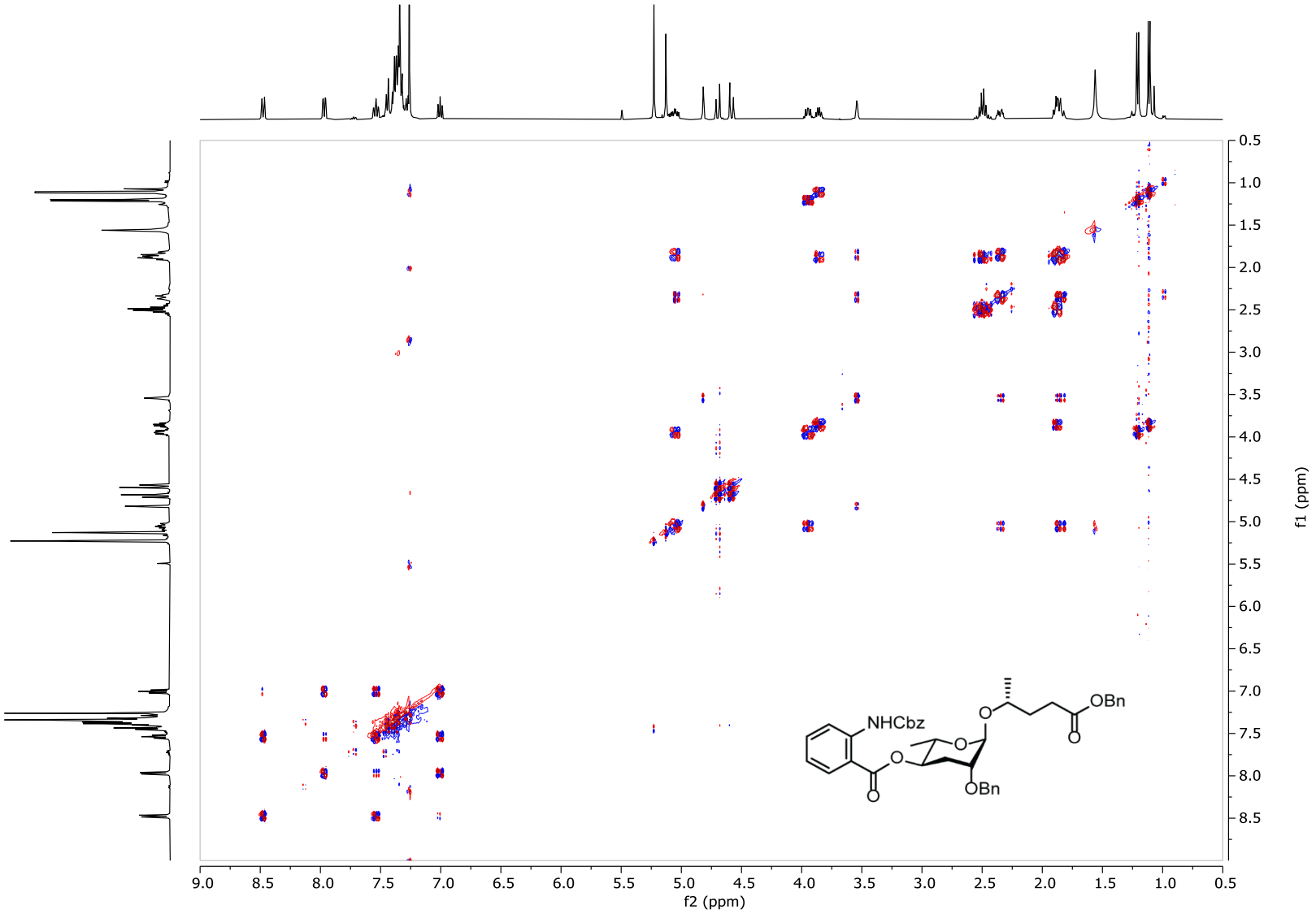

Figure S85: HSQC (400 MHz, $CDCl_3$) of benzyl (4*R*)-4-[(2'-*O*-benzyl-4'-(2-(benzyloxy)carbonyl)amino)benzoyl-3',6'-dideoxy-α-L-*arabino*-hexopyranosyl)oxy]-2-pentanoate (**30a**).

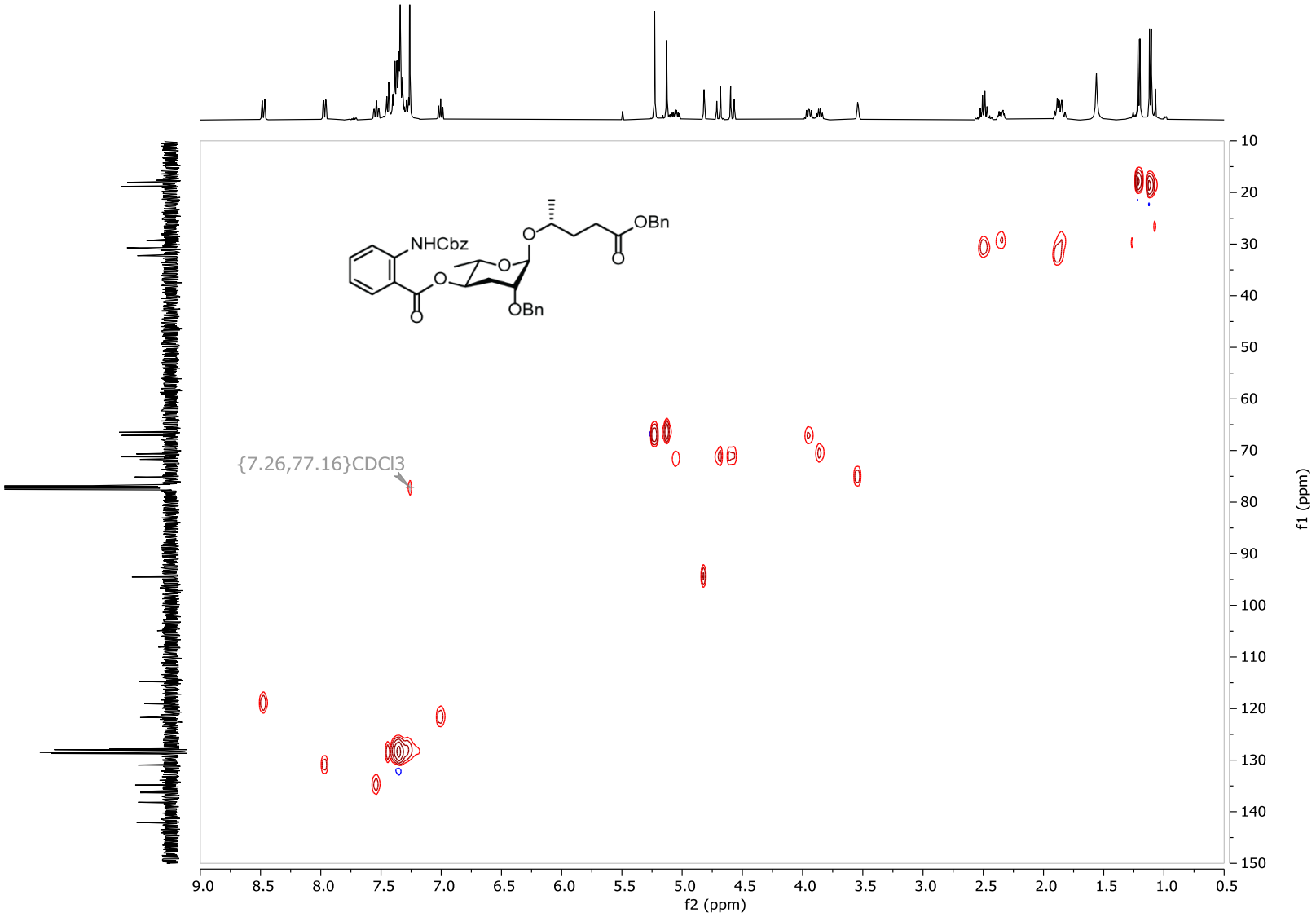

Figure S86: ^{1}H NMR (400 MHz, $CDCl_3$) of benzyl (2*E*,4*R*)-4-[(2'-*O*-benzyl-4'-(2-(benzyloxy)carbonyl)amino)benzoyl-3',6'-dideoxy-α-L-*arabino*-hexopyranosyl)oxy]-2-pentenoate (**30b**).

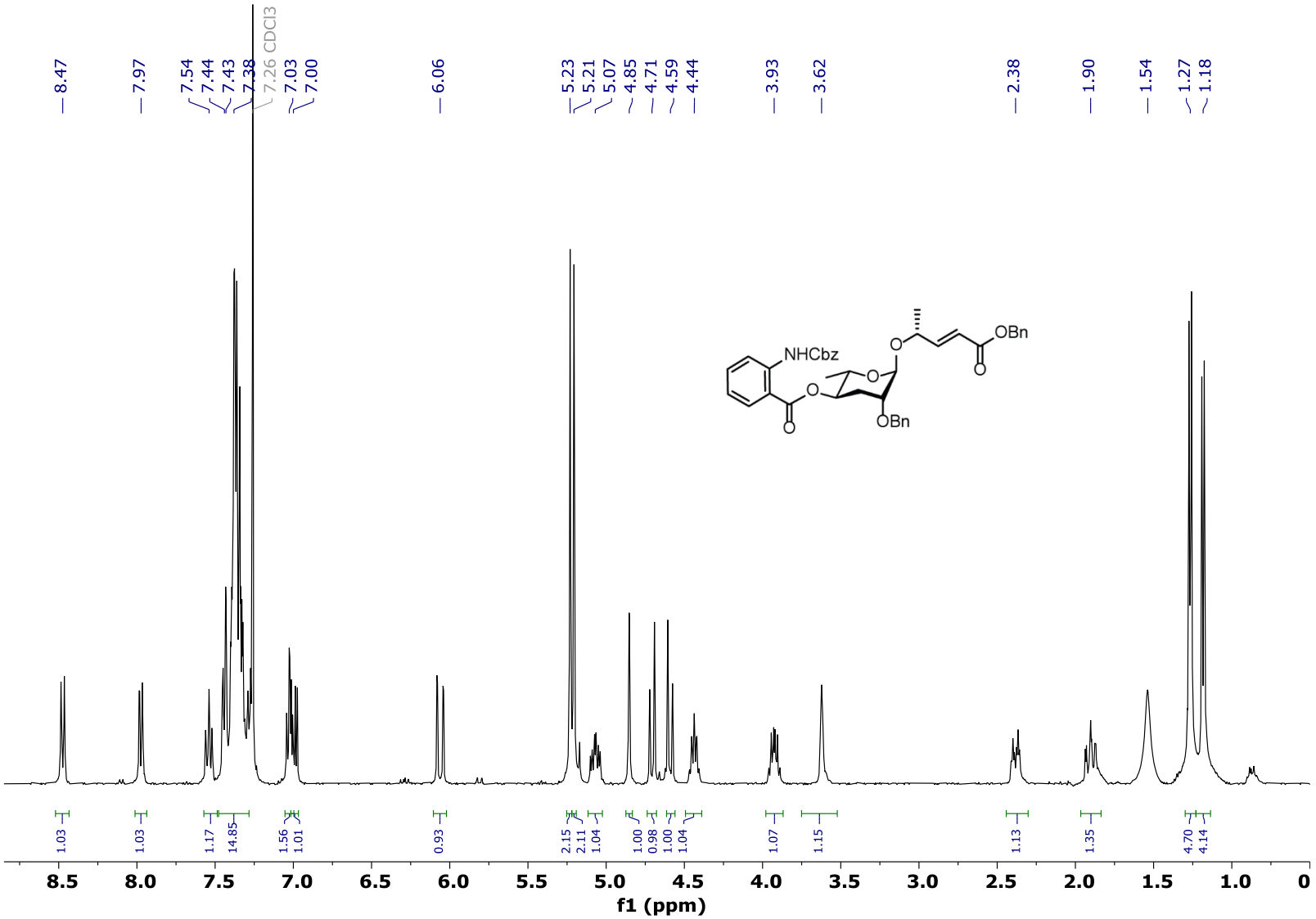

Figure S87: ^{13}C NMR (100 MHz, $CDCl_3$) of benzyl (2*E*,4*R*)-4-[(2'-*O*-benzyl-4'-(2-(benzyloxy)carbonyl)amino)benzoyl-3',6'-dideoxy-α-L-*arabino*-hexopyranosyl)oxy]-2-pentenoate (**30b**).

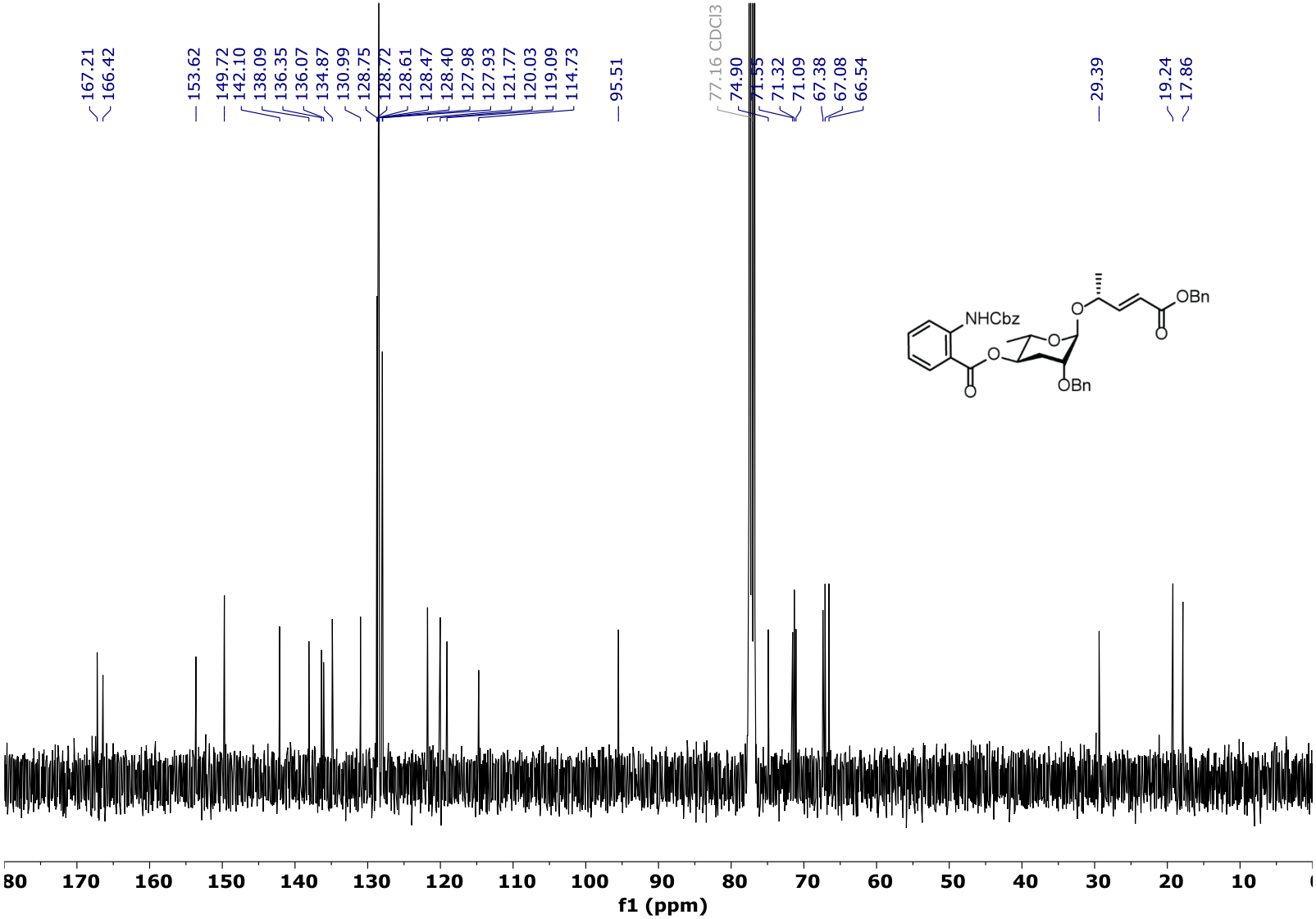

Figure S88: *dqf*-COSY (400 MHz, $CDCl_3$) of benzyl (2*E*,4*R*)-4-[(2'-*O*-benzyl-4'-(2-(benzyloxy)carbonyl)amino)benzoyl-3',6'-dideoxy-α-L-*arabino*-hexopyranosyl)oxy]-2-pentenoate (**30b**).

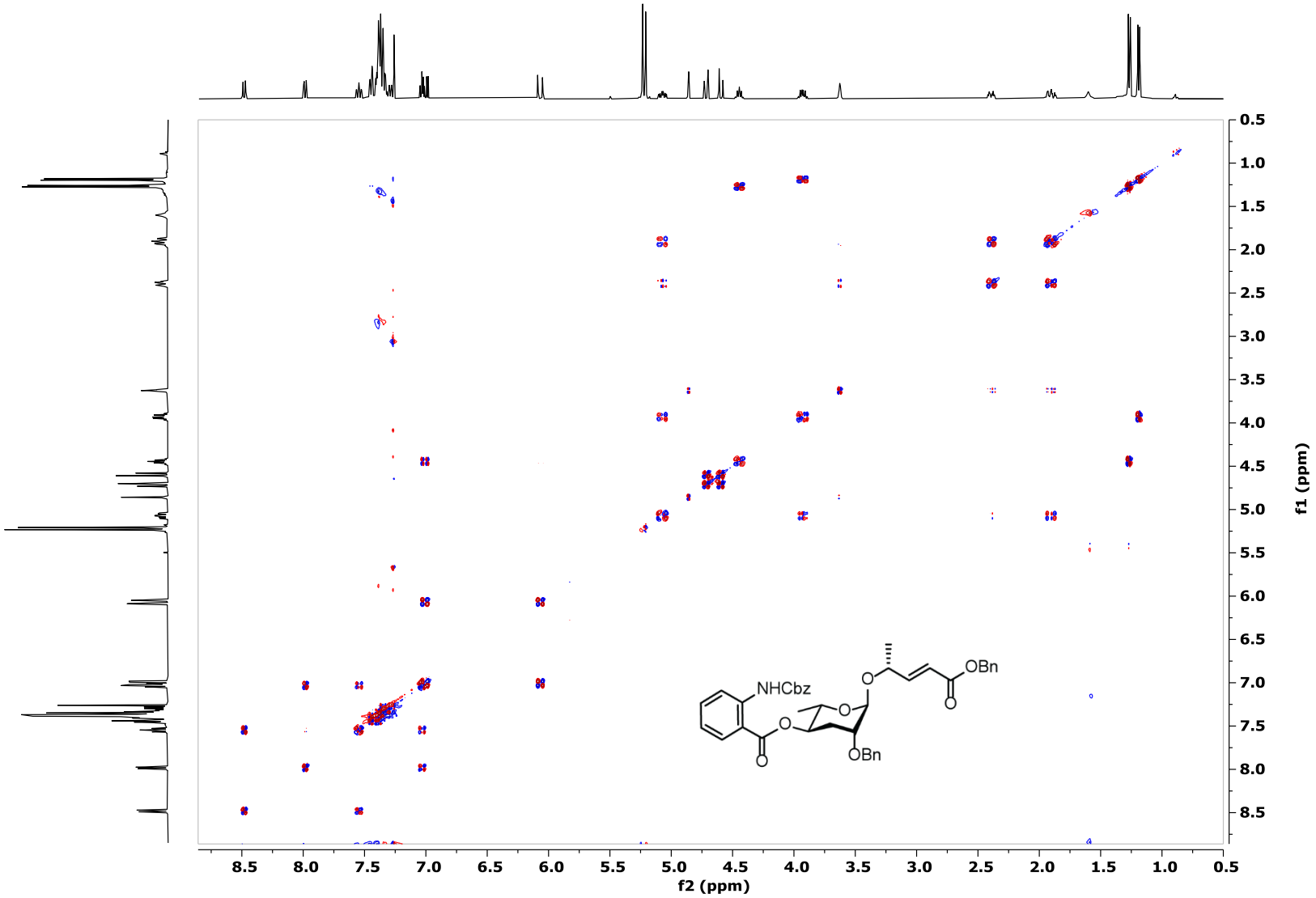

Figure S89: ^{13}C NMR (400 MHz, $CDCl_3$) of benzyl (2*E*,4*R*)-4-[(2'-*O*-benzyl-4'-(2-(benzyloxy)carbonyl)amino)benzoyl-3',6'-dideoxy-α-L-*arabino*-hexopyranosyl)oxy]-2-pentenoate (**30b**).

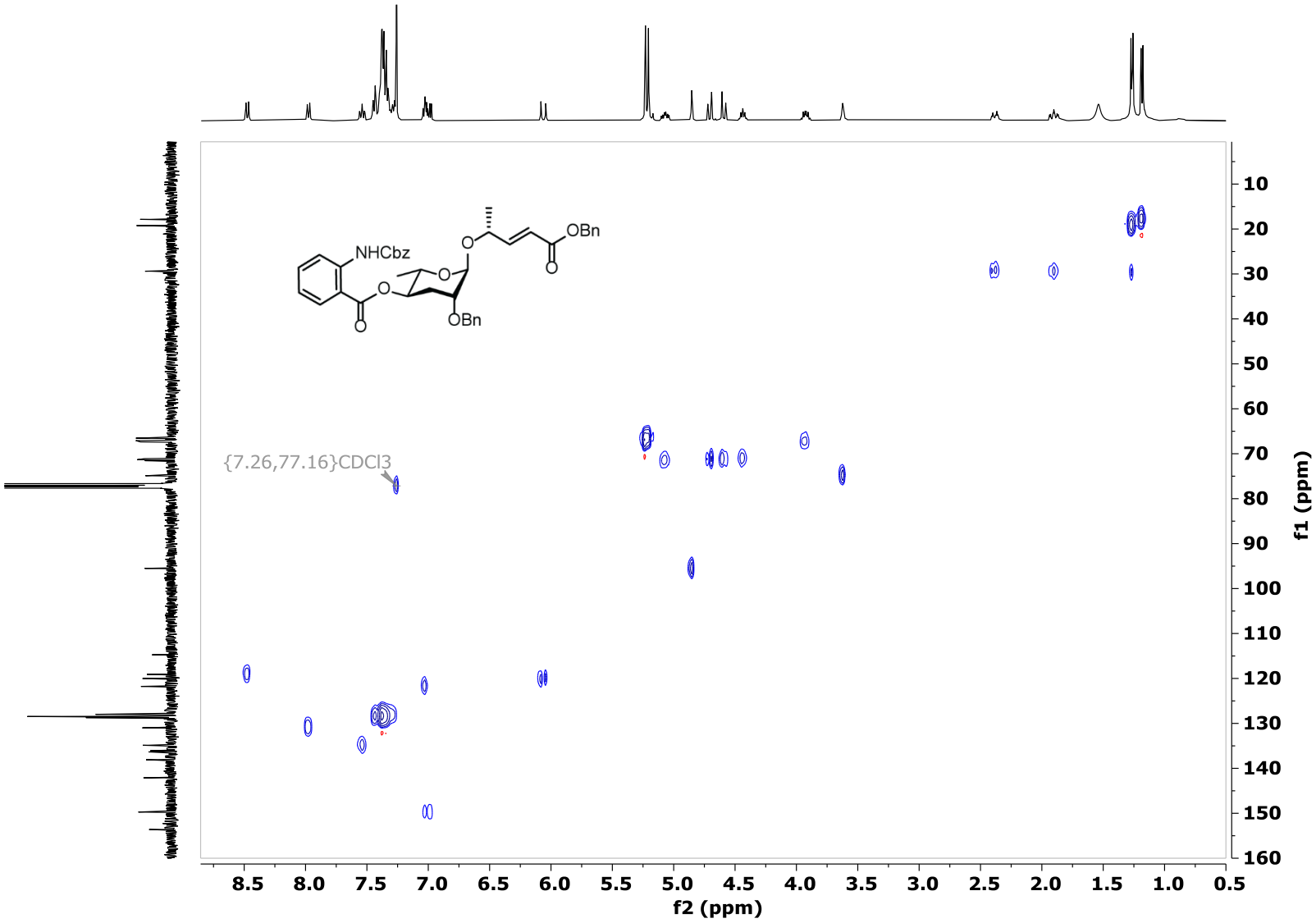

Figure S90: ^{1}H NMR (400 MHz, CD_3OD) of (4*R*)-4-[(4'-*O*-(2-amino-benzoyl)-3',6'-dideoxy-α-L-*arabino*-hexopyranosyl)oxy]-2-pentanoic acid (**6**).

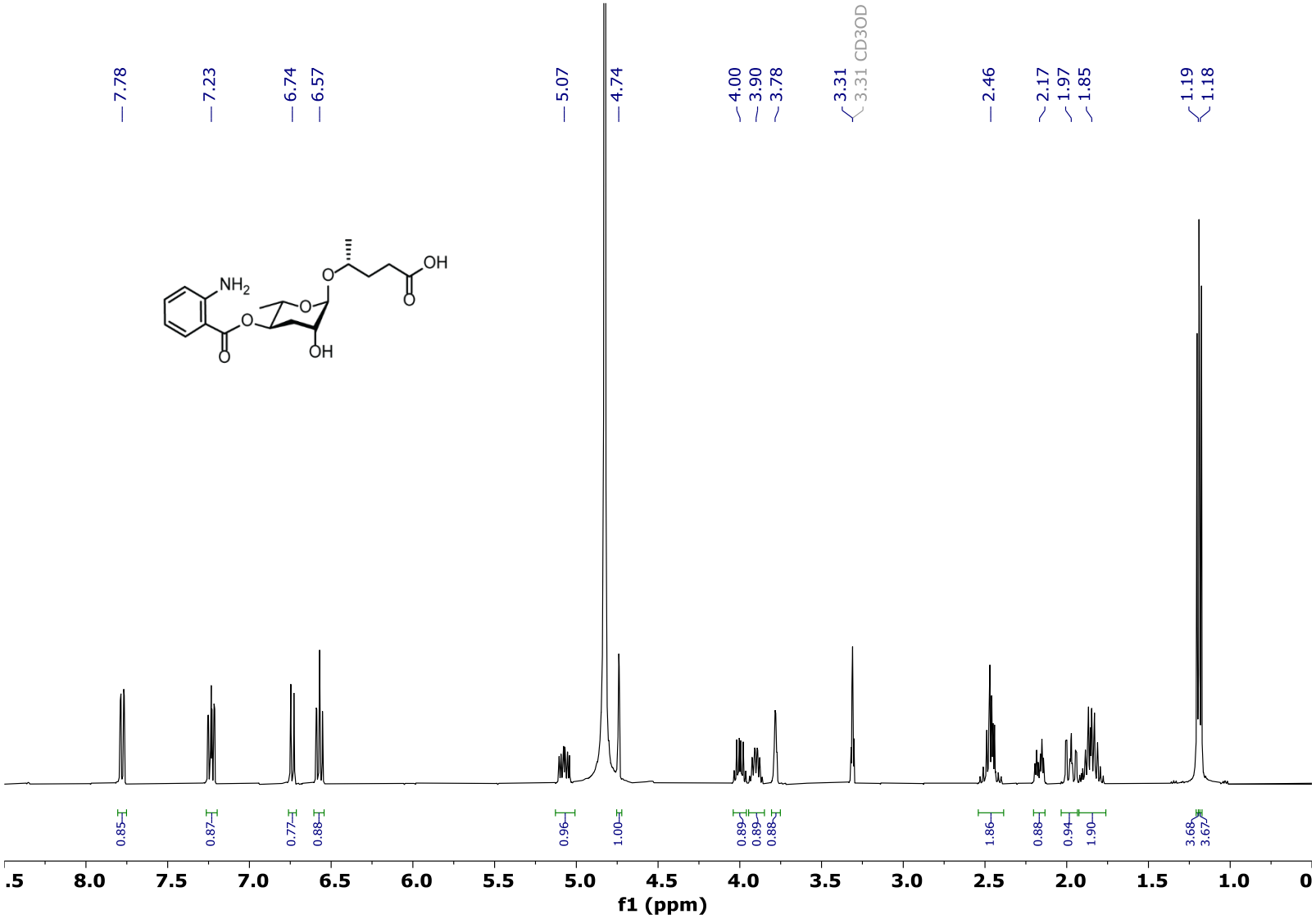

Figure S91: ^{13}C NMR (100 MHz, CD_3OD) of (4*R*)-4-[(4'-*O*-(2-amino-benzoyl)-3',6'-dideoxy-α-L-*arabino*-hexopyranosyl)oxy]-2-pentanoic acid (**6**).

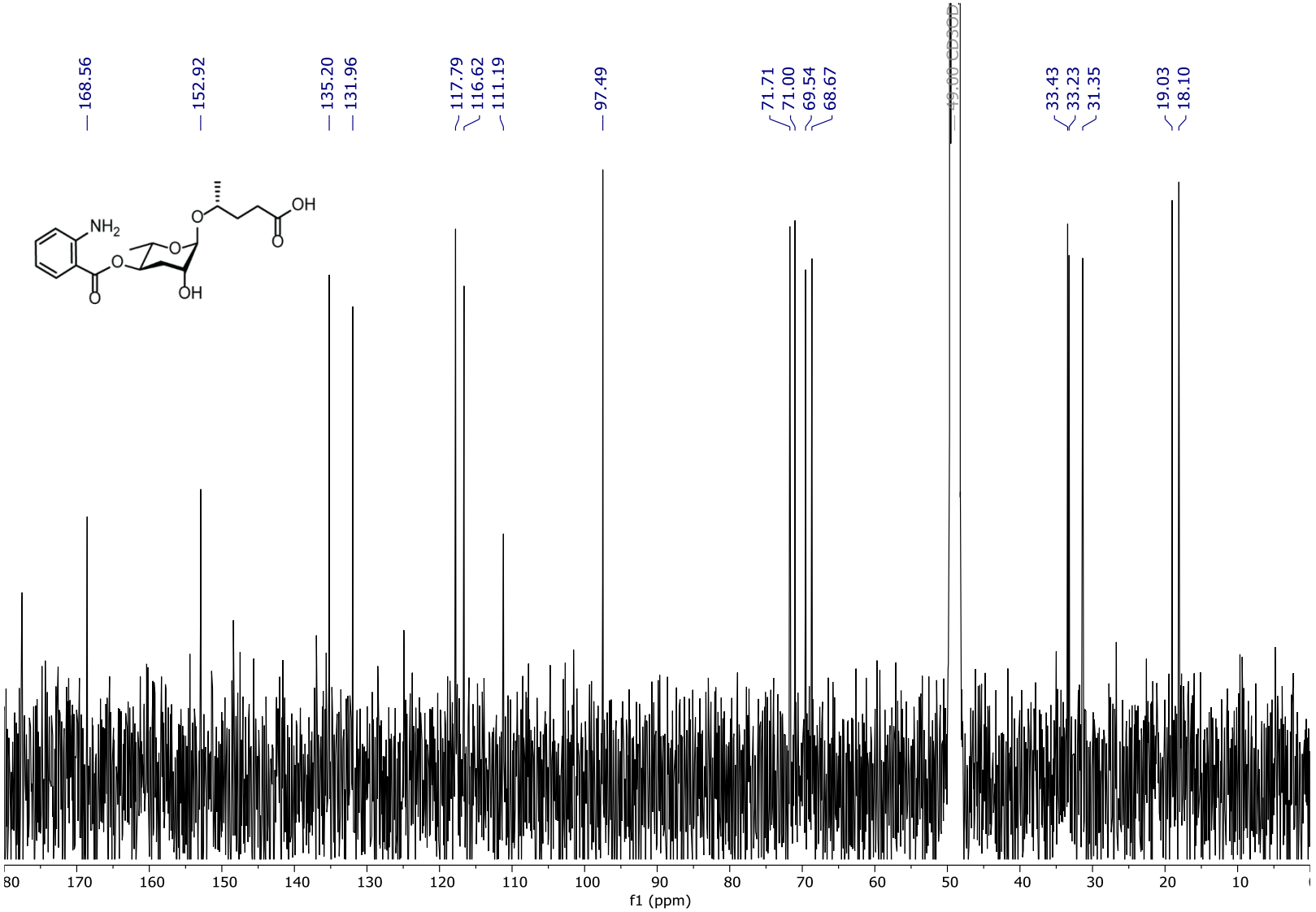

Figure S92: *dqf*-COSY (400 MHz, CD_3OD) of (4*R*)-4-[(4'-*O*-(2-amino-benzoyl)-3',6'-dideoxy-α-L-*arabino*-hexopyranosyl)oxy]-2-pentanoic acid (**6**).

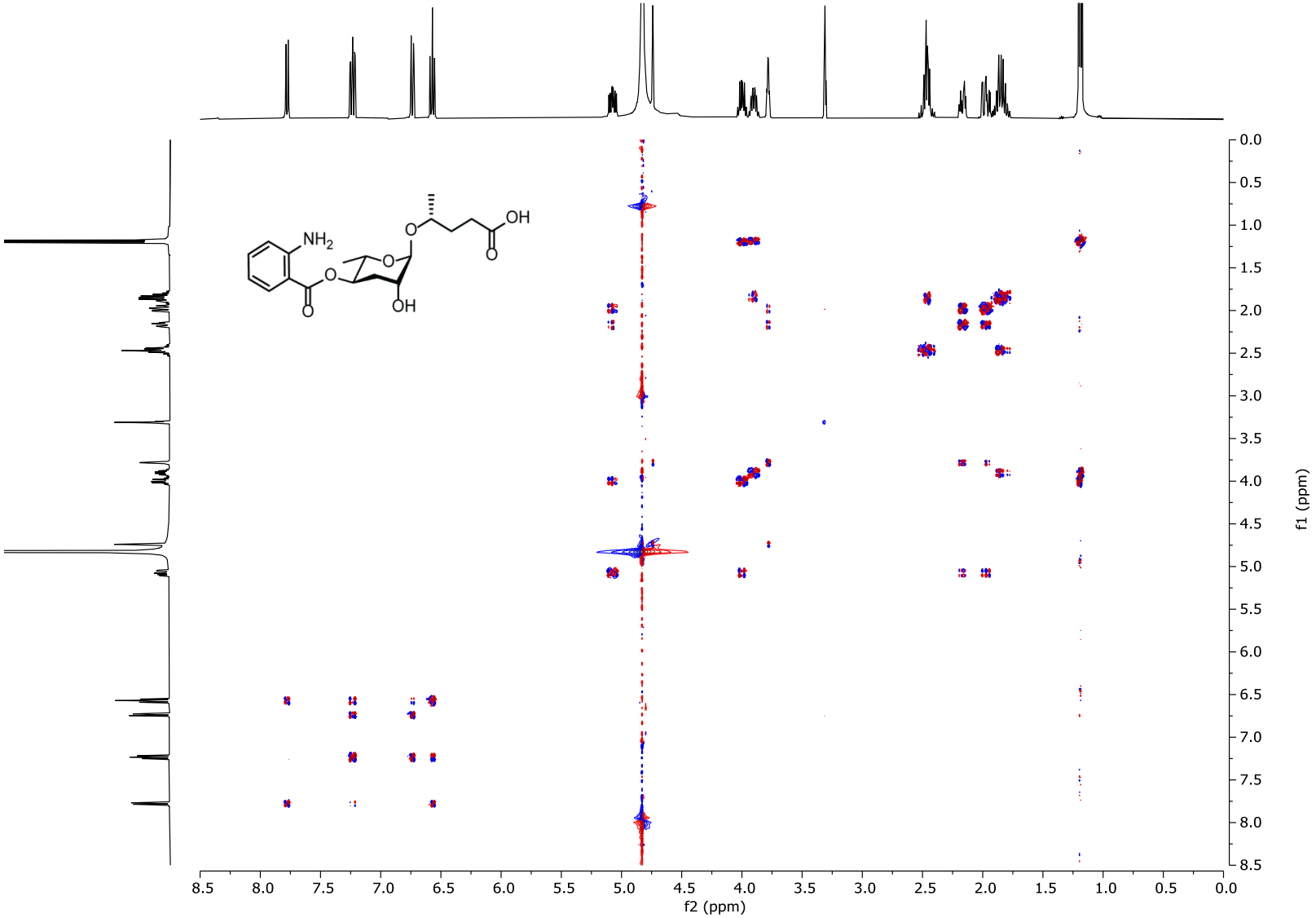

Figure S93: HSQC (400 MHz, CD_3OD) of (4*R*)-4-[(4'-*O*-(2-amino-benzoyl)-3',6'-dideoxy-α-L-*arabino*-hexopyranosyl)oxy]-2-pentanoic acid (**6**).

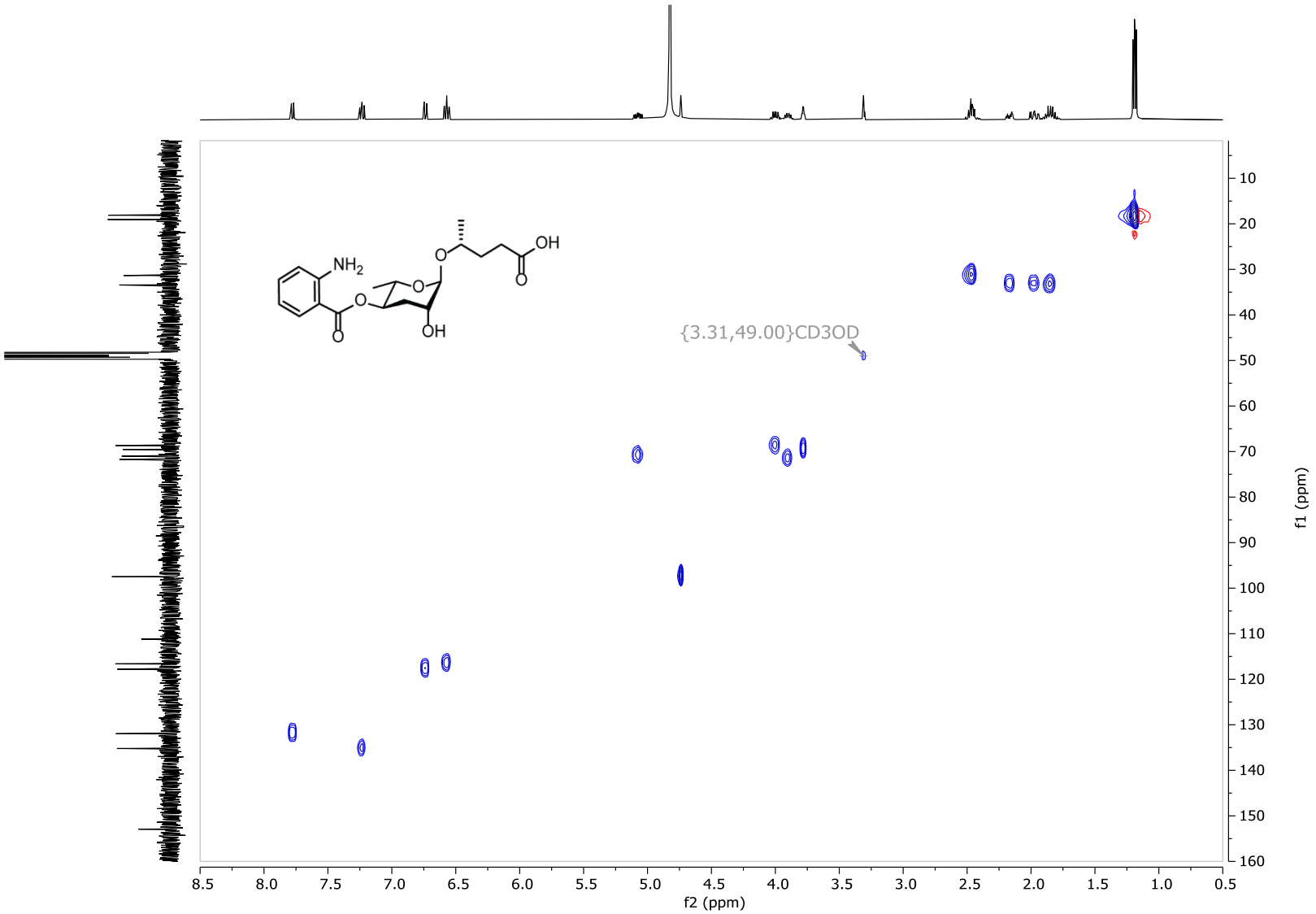

Figure S94: ^{1}H NMR (400 MHz, CD_3OD) of (4*R*)-4-[(4'-*O*-(2-methylamino-benzoyl)-3',6'-dideoxy-α-L-*arabino*-hexopyranosyl)oxy]-2-pentanoic acid (**31**).

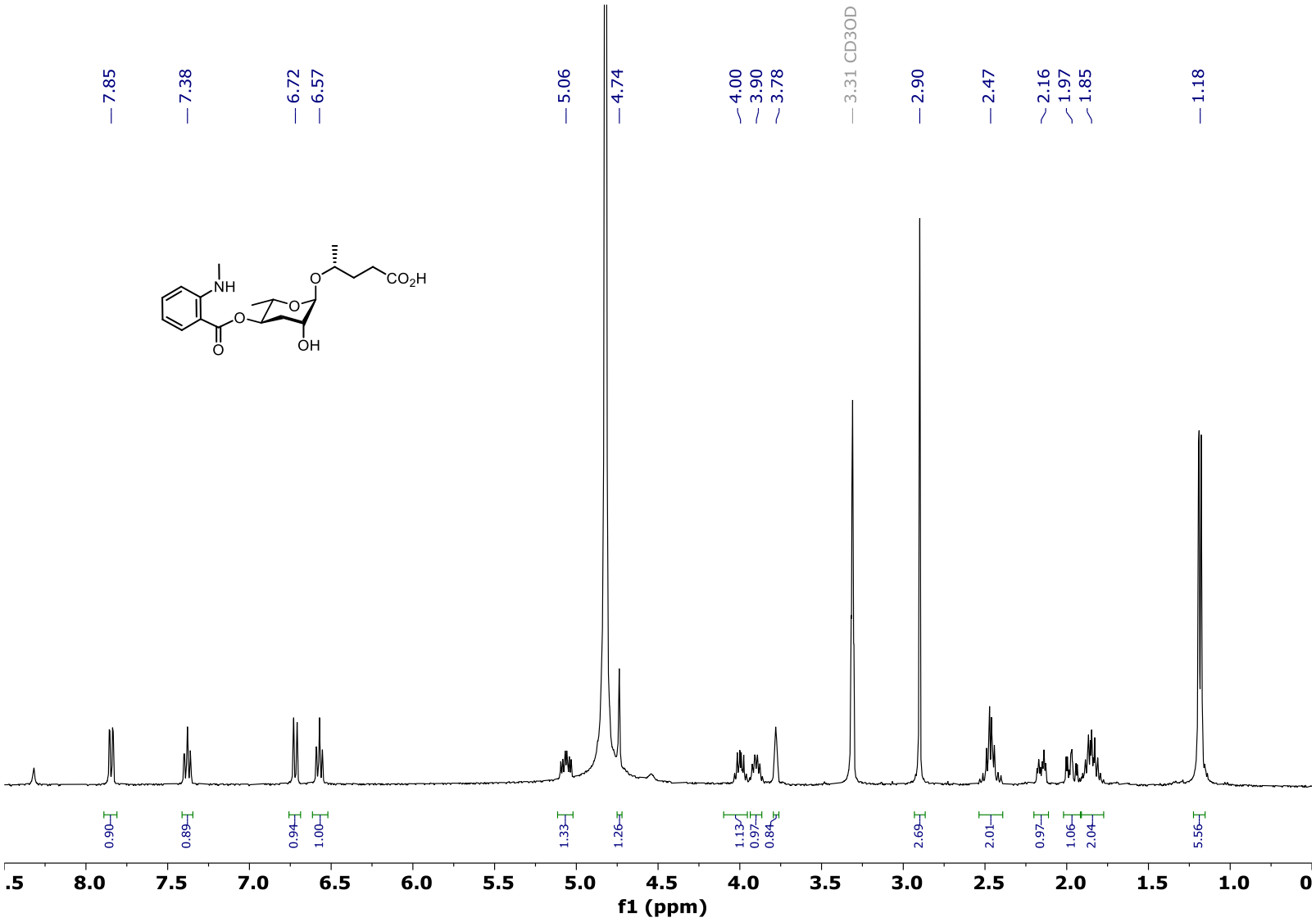

Figure S95: *dqf*-COSY (400 MHz, CD_3OD) of (4*R*)-4-[(4'-*O*-(2-methylamino-benzoyl)-3',6'-dideoxy-α-L-*arabino*-hexopyranosyl)oxy]-2-pentanoic acid (**31**).

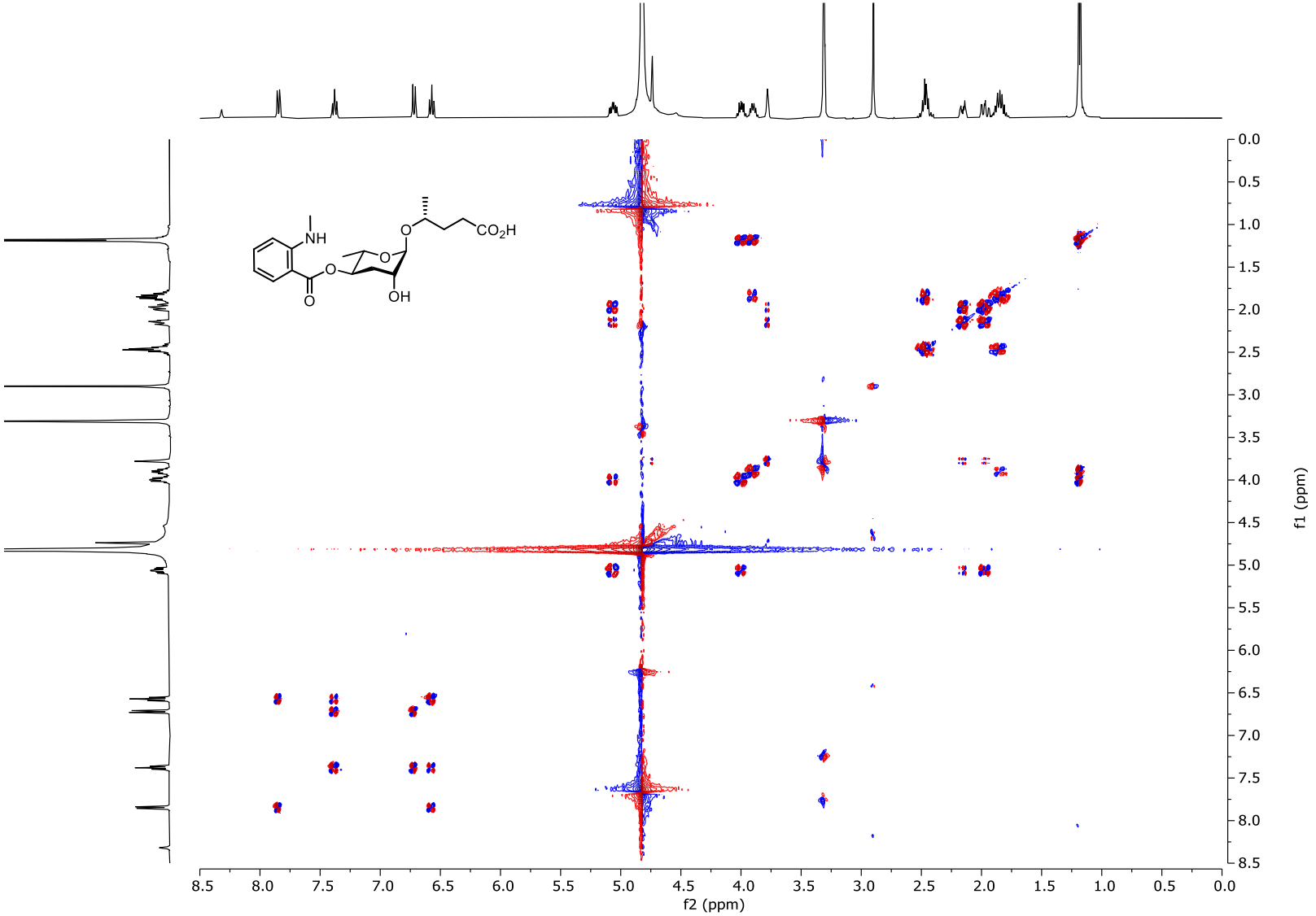

Figure S96: HSQC (400 MHz, CD_3OD) of (4*R*)-4-[(4'-*O*-(2-methylamino-benzoyl)-3',6'-dideoxy-α-L-*arabino*-hexopyranosyl)oxy]-2-pentanoic acid (**31**).

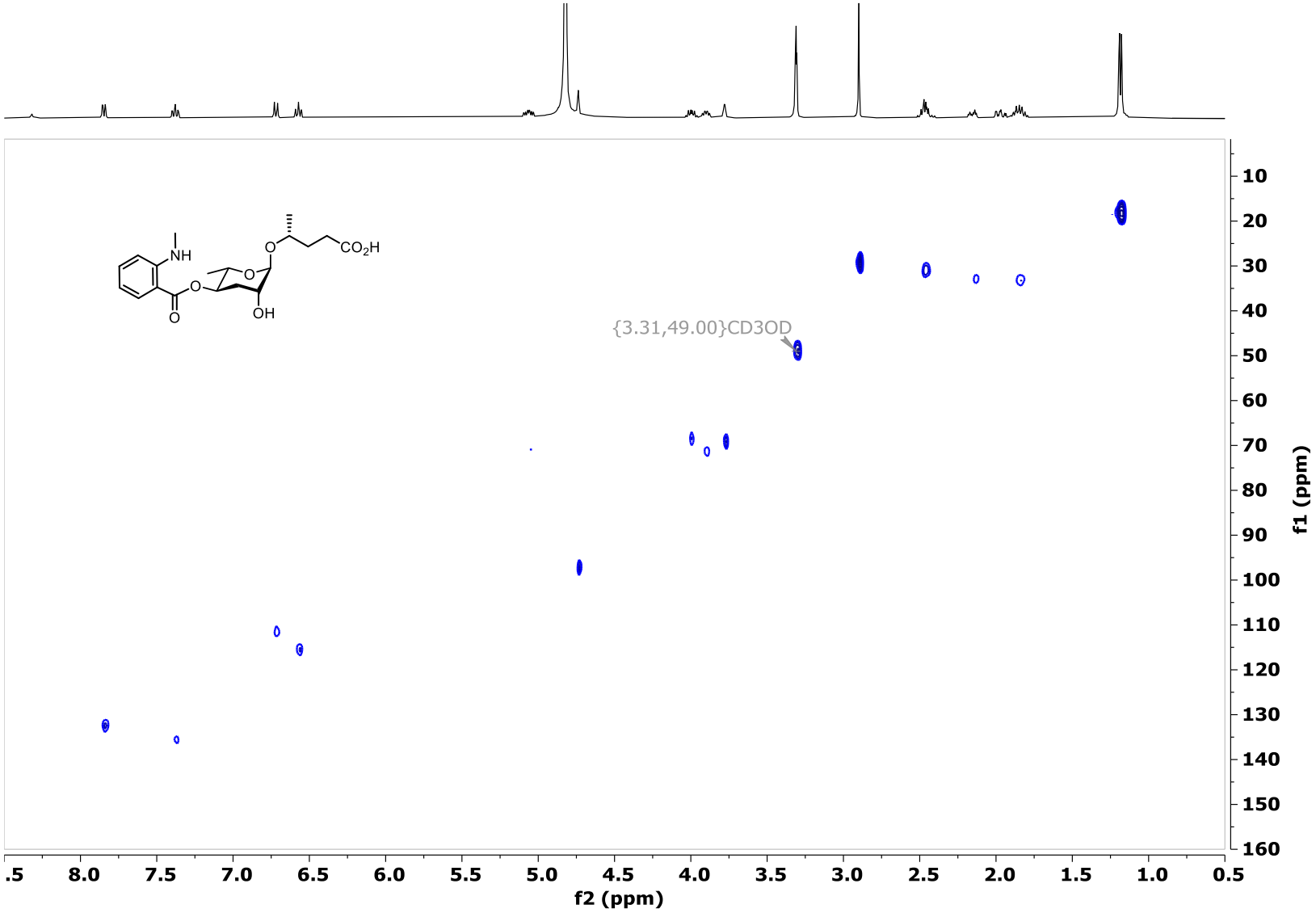

Figure S97: ^{1}H NMR Spectrum (400 MHz, $CDCl_3$) of *N*-Cbz anthranilic acid.

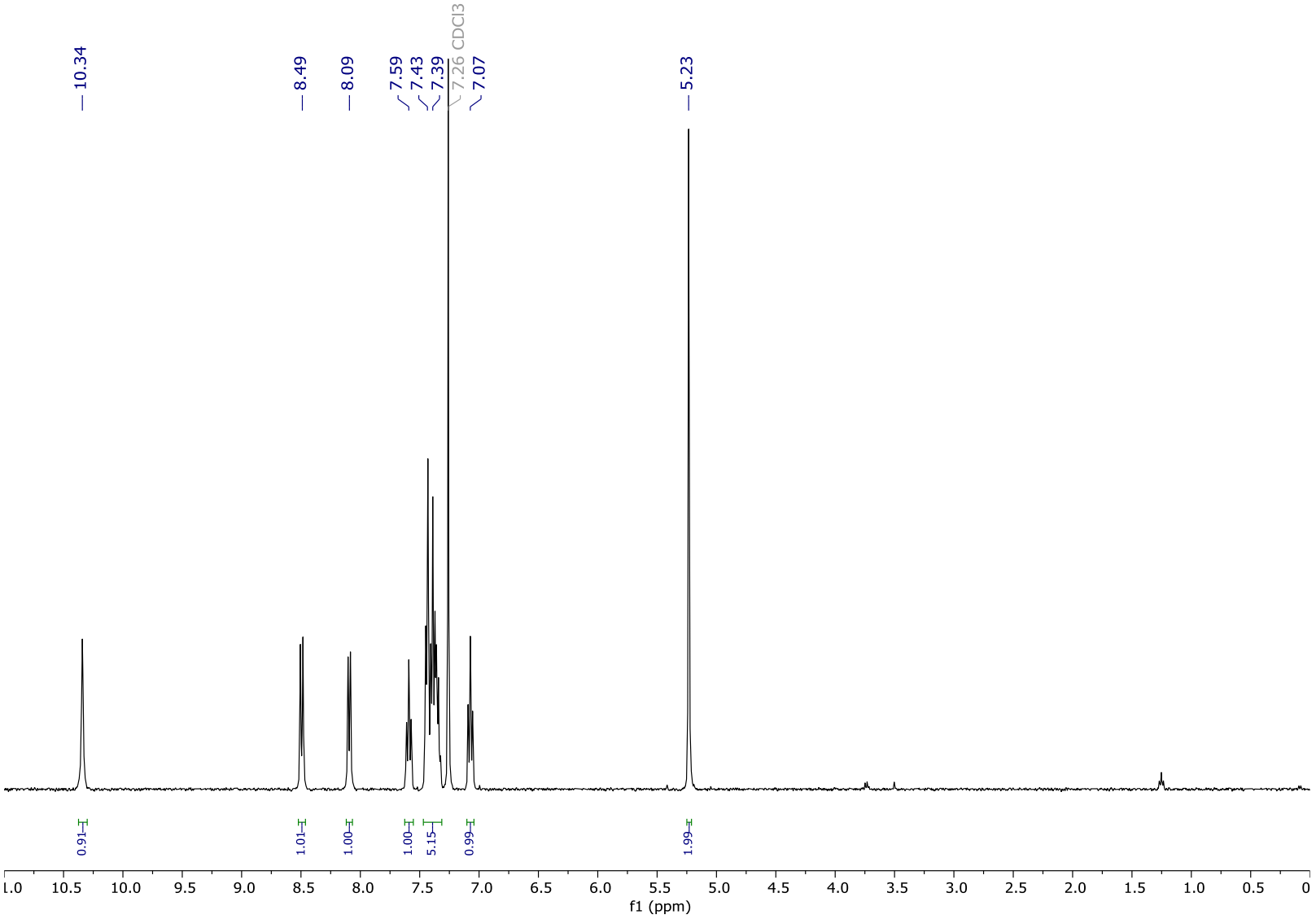

Figure S98: ^{1}H NMR spectrum (400 MHz, CD_3OD) of AB-asc-C5 (**6a**, n = 2) isolated from *C. nigoni* JU1422.

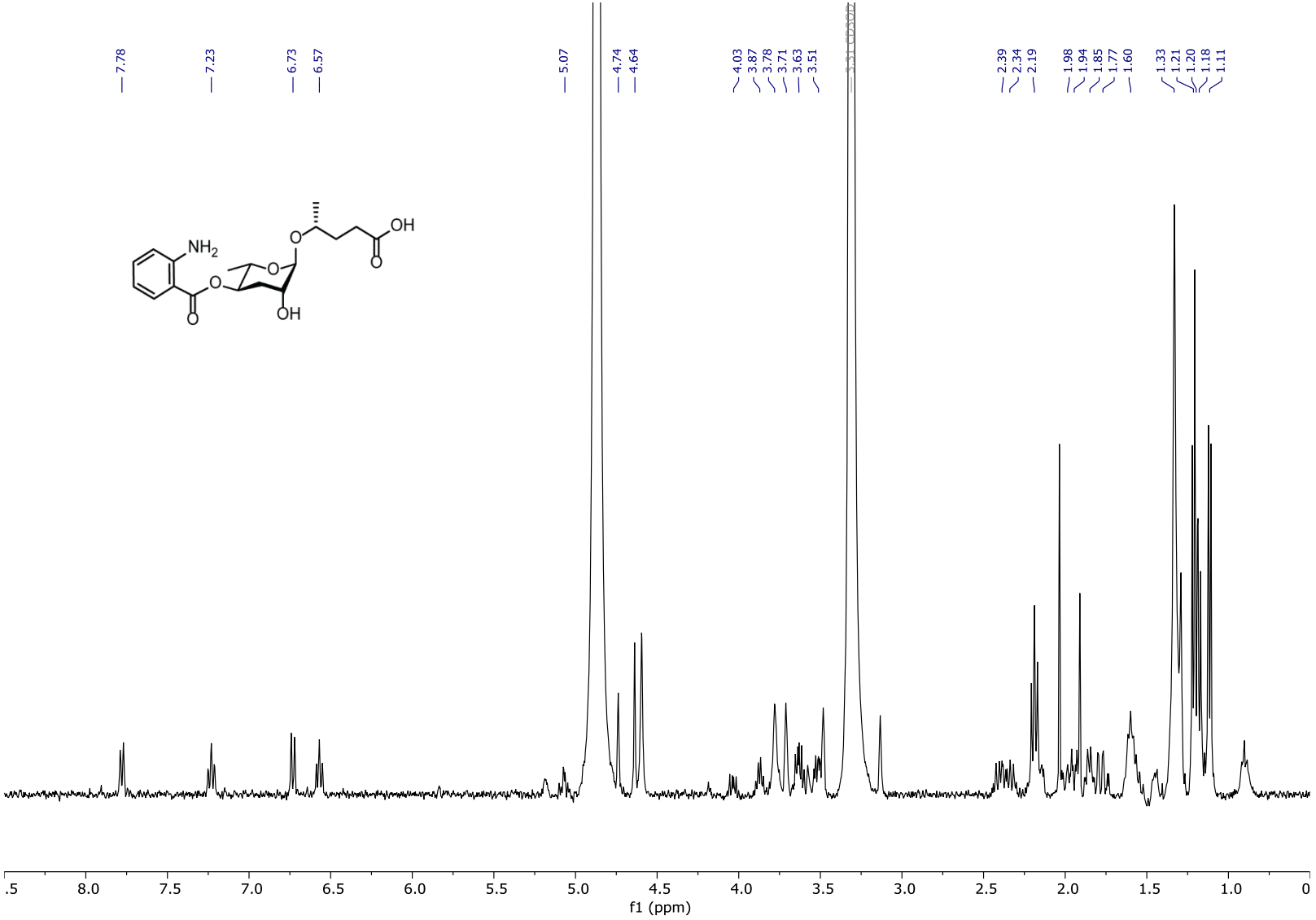

Figure S99: *dqf*-COSY spectrum (400 MHz, CD_3OD) of AB-asc-C5 (**6a**, n = 2) isolated from *C. nigoni* JU1422.

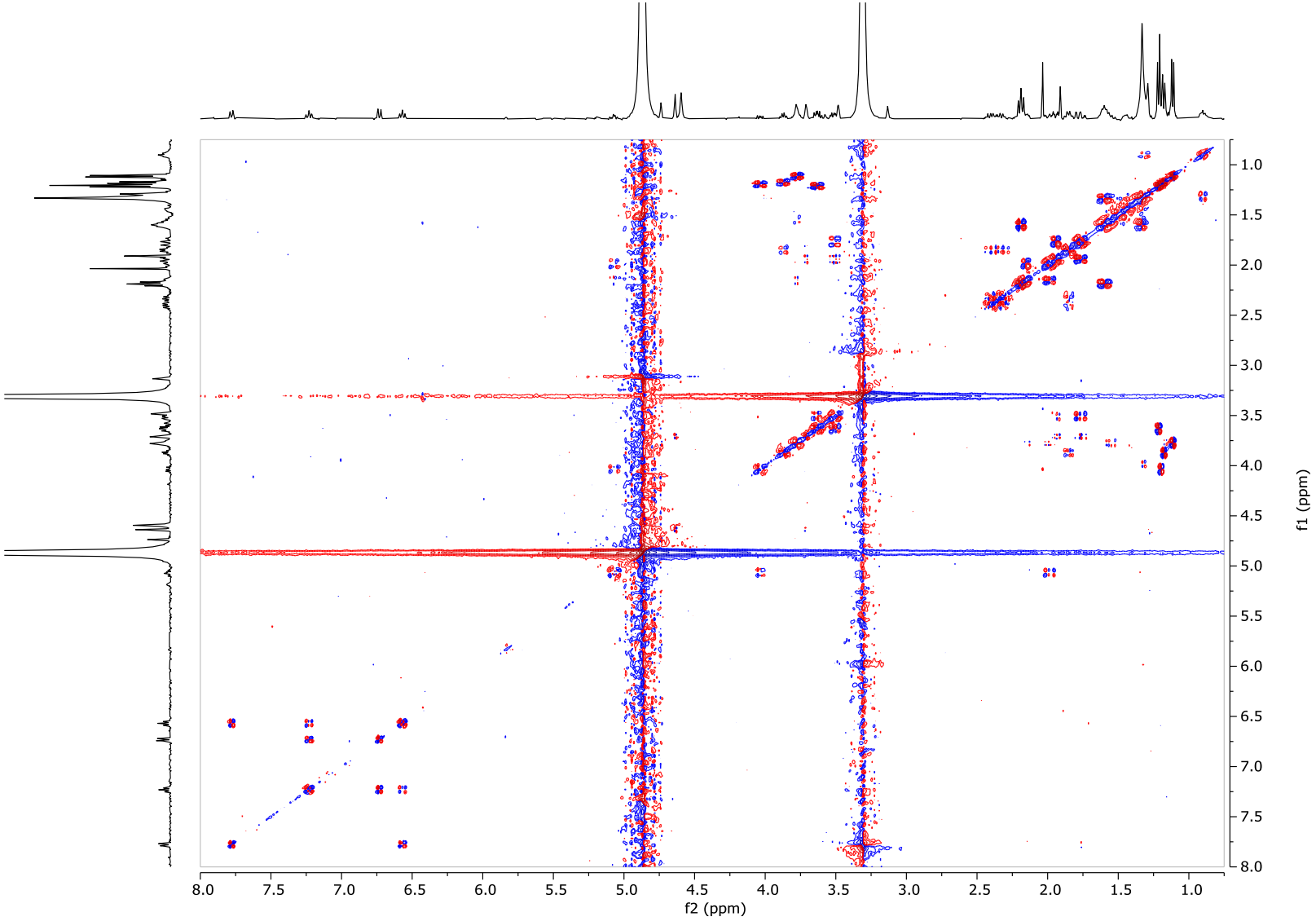
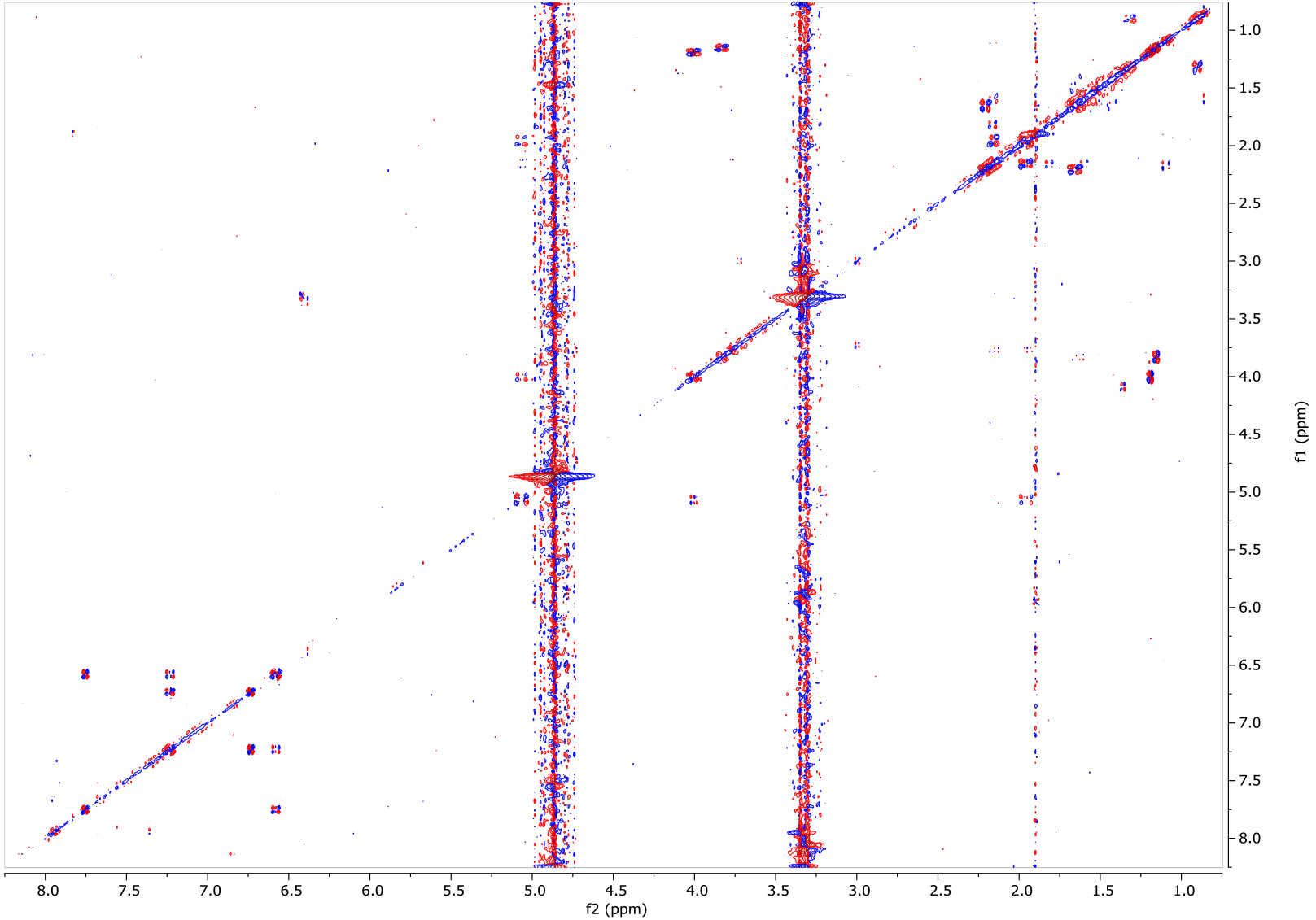
Figure S100: *dqf*-COSY spectrum (400 MHz, CD_3OD) of AB-asc-C6 (**6b**, n = 3) isolated from *C. nigoni* JU1422.